Innovative structural joining for lightweight design

Daniel F. O. Braga

Submitted for the degree of Doctor of Philosophy in Leaders for Technical Industries of the MIT-Portugal Program

Faculty of Engineering of the University of Porto, Portugal

March, 2018

Co-Supervisors:
Lucas F.M. da Silva
Faculdade de Engenharia da Universidade do Porto, Portugal

Virginia Infante
Instituto Superior Técnico, Universidade de Lisboa, Portugal

Marco Pacchione
Airbus Operations GmbH, Germany

Jurgen Silvanus
Airbus Defense and Space GmbH, Germany

Supervisor:
Pedro M.G.P. Moreira
INEGI - Instituto de Ciência e Inovação em Engenharia Mecânica e Engenharia Industrial, Portugal

Abstract

Challenging energy efficiency and pollution emissions goals have been set forth in civil aviation as in other transport sectors. Developing and implementing new manufacturing processes is key to face these challenges. However in load carrying structures, the fulfillment of safety regulations and well established design criteria while simultaneously incorporating new materials, processes and designs presents significant challenges. A multi-disciplinary approach is required to address the complex issues associated with the implementation of new materials and technologies in all product development stages, design, development, manufacturing, operation and maintenance, and finally disposal and recycling.

This thesis aims at advancing the knowledge related to manufacturing technologies of lightweight integral metallic structures. Current fuselage design use differential structures assembled through riveting. The advent of newer joining methods prompt the possibility for new integral structures with reduced weight and easier manufacturing automation. Through the development of manufacturing technologies for integral metallic components, as presented in this study, competitiveness of metallic structures regarding composite structures is kept and with it, the available options of structural designers are increased. Although the emphasis of this PhD project is on aeronautical applications, the proposed technologies may be extrapolated to diverse industries with disruptive potential.

The radical disruptive nature of the adoption of butt joining friction stir welding (FSW) in metallic fuselages, especially at major component assembly level, has hinder its fast adoption, even though the technology potential has been demonstrated in previous works. Geometric tolerance management requirements along with requirements for complete new tooling and quality assurance processes, have pushed fully integral butt-joined FSW fuselages into the future. One variation of FSW that could address the gap between the state of the art riveting process and the disruptive FSW butt-joining is overlap FSW, albeit this methodology results in lower mechanical performance, and lower weight and lead time savings. To overcome these drawbacks a new hybrid joining method, combining overlap FSW and adhesive bonding was developed.

The aim of this thesis is to develop an innovative joining method for fuselage components at major component assembly level. Considering the complexity of technology infusion processes in aerostructures, an initial study was made on technology adoption and product development with special focus on the aeronautical industry. Following this study, a state of the art of relevant joining technologies was made, encompassing issued patents in this field to assess possible future trends. Upon having a well established literary study,

the development of the technology in itself was done. Mechanical performance of the joints was assessed and benchmarking against FSW and adhesive bonding was made throughout the joining process development. The high ductility and fracture toughness of the adhesive associated with the better stress distribution in the hybrid joints overlap led to significant mechanical performance improvements, both in quasi-static loading and cyclic loading. Some scenarios of technology infusion were made and studied for weight and assembly labor time changes. Fatigue testing of a proposed joint design was made and the results were benchmarked against riveted and butt-joined FSW joints. Similar or higher fatigue strength than riveted joints was found, while structural weight of the joints was reduced.

The potential for a new joining methodology for integral metallic structures was demonstrated in this thesis. It aims to serve as a catalyst for future development within this field, expanding the design applications and technology maturity levels.

Resumo

Impõem-se na atualidade metas desafiantes para a eficiência energética e redução de emissões poluentes na aviação civil, bem como noutros meios de transporte. Desenvolver e implementar novos processos de fabrico é crítico para fazer face a estes desafios. Contudo no caso de estruturas dimensionadas para suportar cargas, é fundamental cumprir os requisitos de segurança e os critérios de projeto, ao mesmo tempo que se incorpora novos materiais e designs.

O objetivo desta tese é alargar o conhecimento na área das tecnologias de fabrico de estruturas metálicas integrais aligeiradas. Atualmente estas estruturas seguem uma metodologia de projeto diferencial, sendo assembladas com recurso a rebites. O advento de novas metodologias de ligação, vem permitir o dimensionamento destas estruturas como estruturas integrais, mais leves e com um maior grau de automação no seu fabrico. Através do desenvolvimento de tecnologias produtivas para estruturas metálicas integrais, é mantida a competitividade das estruturas metálicas face às em compósito, desta forma, o leque de opções para os projetistas aumenta. Embora o foco desta tese de doutoramento seja em aplicações na indústria aeronáutica, a tecnologia aqui proposta, poderá ser extrapolada para outras indústrias com um potencial disruptivo.

A natureza radical disruptiva da adoção do processo de soldadura por fricção linear (FSW) na configuração topo a topo em fuselagens metálicas, especialmente ao nível da assemblagem de componentes de larga escala, tem limitado a sua rápida adoção, mesmo tendo sido demonstrado o seu potencial em trabalhos anteriores. Os requisitos de gestão de tolerâncias geométricas, bem como a necessidade de novas ferramentas e processos de controlo de qualidade, não têm permitido evolução das fuselagens completamente integrais soldadas por FSW topo a topo. Uma variante de FSW com o potencial para completar a lacuna entre o estado da arte e as fuselagens completamente integrais soldadas por FSW topo a topo, é a soldadura FSW em sobreposição. Contudo, esta variante resulta num desempenho mecânico inferior às juntas topo a topo, bem como em ganhos mais baixos de redução de peso e tempo de fabrico. De forma a ultrapassar estas limitações, foi estudada uma nova metodologia de ligação híbrida, combinando FSW de sobreposição e adesão estrutural.

O principal objetivo desta tese é o desenvolvimento de tecnologia de ligação para componentes de fuselagem de larga escala. Considerando a complexidade dos processos de infusão de tecnologia em estruturas aeronáuticas, foi realizado um estudo inicial relativo a adoção de novas tecnologias e desenvolvimento do produto, tendo especial foco na indústria aeronáutica. Após este estudo, foi feito um levantamento do estado da arte das tecnologias de ligação

relevantes para o decorrer desta tese, incluindo uma pesquisa de patentes nesta área, de forma determinar futuras tendências. Com a investigação do estado da tecnologia bem estabelecida, foi então desenvolvida a tecnologia proposta. O desempenho das juntas e do processo desenvolvido foram comparados com FSW e adesão estrutural ao longo das várias etapas do desenvolvimento. A elevada ductilidade e tenacidade do adesivo, em conjunto com a melhor distribuição de tensões nas juntas hibridas levou a melhorias significativas do desempenho mecânico, tanto em carregamentos quási-estáticos, como em carregamentos cíclicos. Alguns cenários de infusão da tecnologia desenvolvida em fuselagens metálicas foram propostos e estudados no que diz respeito à redução de peso e de tempo de assemblagem. Foi determinado o comportamento à fadiga de juntas híbridas com geometria semelhante ao caso de aplicação e comparado com juntas rebitadas e soldadas por FSW topo a topo. Foi determinada uma resistência à fadiga, igual ou superior às juntas rebitadas, ao mesmo tempo que foi reduzido o peso das juntas.

Esta tese demonstrou o potencial para uma nova metodologia de ligação para estruturas metálicas integrais. Pretende-se que este estudo seja um catalisador para desenvolvimentos futuros neste campo, expandindo não só as aplicações, mas também o nível de maturidade da tecnologia.

Zusammenfassung

Herausfordernde Energieeffizienz- und Emissionsziele wurden, wie auch für andere Sparten, für die zivile Luftfahrt gesetzt. Neue Fertigungstechnologien zu entwickeln und einzuführen ist der Schlüssel um solche Herausforderungen zu meistern. Im Hinblick auf lasttragende Strukturen ist jedoch die Erfüllung der Sicherheitsvorschriften und bekannten Konstruktionsrichtlinien unter Einbeziehung neuer Materialien, Prozesse und Designs anspruchsvoll. Ein multidisziplinärer Ansatz ist erforderlich, um die komplexen Probleme zu bewältigen, die mit der Einführung neuer Materialien und Technologien in allen Produktphasen verbunden sind: Design, Entwicklung, Fertigung, Betrieb, Wartung und schließlich Entsorgung und Recycling.

Diese Arbeit zielt darauf ab, das Wissen in Bezug auf Herstellungstechnologien von integralen metallischen Leichtbaustrukturen zu verbessern. Das derzeitige Rumpfdesign basiert meist auf differentiellen Bauteilen, die durch Nieten verbunden werden. Das Aufkommen neuartiger Fügeverfahren eröffnet die Möglichkeit neue integrale Strukturen mit reduziertem Gewicht und vereinfachter Fertigungsautomatisierung zu entwickeln. Durch die Entwicklung von Fertigungstechnologien für integrale metallische Komponenten, wie sie in dieser Studie vorgestellt werden, wird die Wettbewerbsfähigkeit von metallischen Strukturen in Bezug auf Verbundwerkstoffstrukturen erhalten und damit die Auswahl für Konstrukteure erweitert. Obwohl der Schwerpunkt dieses Promotionsvorhabens auf luftfahrttechnischen Anwendungen liegt, birgt die vorgeschlagene Technologie auch für verschiedene andere Branchen großes Potential.

Die disruptive Natur von reibrührgeschweißten (FSW) Stumpfstößen in metallischen Rümpfen, insbesondere auch im Bereich der Großkomponentenmontage, hat eine schnelle Einführung behindert, obwohl das Technologiepotential schon in früheren Arbeiten demonstriert wurde. Die Anforderungen an das Toleranzmanagement sowie an komplett neue Werkzeuge und Qualitätssicherungsprozesse haben integrale Rümpfe basierend auf FSW Stumpfstößen in die Zukunft gedrängt.

Eine Variante, die die Lücke zwischen Nietnähten nach dem Stand der Technik und disruptiven FSW Stumpfstößen überwinden könnte, sind FSW Überlappnähte, wenngleich diese Technologie zu einer geringeren mechanischen Belastbarkeit sowie geringeren Gewichts- und Fertigungszeitersparnissen führt. Um diese Nachteile zu überwinden, wurde ein neues Hybridverbindungsverfahren untersucht, bei dem reibrührgeschweißte Überlappnähte und Klebeverbindung kombiniert werden.

In Anbetracht des Hauptziels dieser Arbeit, die Entwicklung eines Verbindungsver-

fahrens für Rumpfschalen auf Großkomponentenebene voranzutreiben sowie der Komplexität der Einführung von neuen Technologien in Flugzeugstrukturen, wurde eine erste Untersuchung zur Technologieeinführung und Produktentwicklung unter besonderer Berücksichtigung der Luftfahrtindustrie durchgeführt. Im Anschluss an diese Untersuchung wurde der Stand der Technik inklusive erteilter Patente hinsichtlich relevanter Verbindungstechnologien bewertet, um mögliche zukünftige Trends zu erkennen. Nach dieser Literaturrecherche wurde die eigentliche Entwicklung der Technologie vorangetrieben. Eine vergleichende Analyse der entwickelten Technologie mit FSW und Klebeverbindungen wurde in verschiedenen Phasen der Studie durchgeführt. Die hohe Duktilität und Bruchzähigkeit des Klebstoffs, verbunden mit der besseren Spannungsverteilung im Überlappbereich der Hybridverbindung, führten zu signifikanten Verbesserungen der mechanischen Eigenschaften, sowohl bei quasi-statischen als auch bei zyklischen Belastungen. Einige Szenarien möglicher Lösungen für die untersuchten technologischen Bedarfe wurden erstellt und hinsichtlich ihres Gewichts- und Fertigungsszeiteinflusses verglichen. Ermüdungstests einer vorgeschlagenen Verbindungskonstruktion wurden durchgeführt, und die Ergebnisse wurden mit genieteten Nähten sowie FSW-geschweißten Stumpfstoßverbindungen verglichen. Im Vergleich zu Nietverbindungen wurden vergleichbare oder bessere Dauerfestigkeitswerte erreicht, jedoch mit einem reduzierten strukturellen Gewicht.

Die vorliegende Arbeit zeigt das Potenzial einer neuen Fügetechnik für integrale metallische Strukturen auf. Sie soll als Katalysator für zukünftige Entwicklungen in diesem Bereich dienen und sowohl die Anwendungen als auch ihren technologischen Reifegrad vorantreiben.

Acknowledgment

First and foremost, I would like to thank my family, my friends and my girlfriend for their patience, support, encouragement and motivation throughout my entire PhD project. I would have not been able to reached its conclusion without their support.

I acknowledge the immense support from all my co-supervisors, Professor Lucas da Silva, Professor Virginia Infante, Mr. Marco Pacchione and Dr. Juergen Silvanus. Also I would like to give special thanks to my supervisor Dr. Pedro Moreira, for always believing in me and giving me his full support throughout this work. His help was invaluable and I would have not started nor finish this journey without his support and encouragement.

To address the issues that were faced in the execution of this research many interactions occurred with many people that I would like to acknowledge. The support from everyone at Laboratório de Ótica e Mecânica Experimental (LOME) in INEGI, Laboratório de Ensaios Tecnologógicos (LET) at FEUP, The Adhesives Group at FEUP / INEGI, as well as the Solid-state joining group at HZG were crucial too all the developed work in this thesis. From the laboratories and entities mentioned I would like to give a special thank you to Engineer Miguel Figueiredo and Engineer Rui Silva from LET, Dr. Eduardo Marques and Dr. Ricardo Carbas from the Adhesives Group at FEUP / INEGI, Engineer Luciano Bergmann and Dr. Jorge dos Santos at HZG. The support of Engineer Ricardo Maciel at IST in the welding procedures and mechanical testing is also acknowledged.

A thank you is due to Professor Paulo de Castro from FEUP, for kicking off my research career, as the research developed in my master thesis under his supervision, was fundamental to my pursuit of a PhD. My colleague Dr. Sérgio Tavares is duly acknowledged for all his inputs and support throughout my research, which were key to facing some challenges that emerged. A note of appreciation must also be given to Dr. Valentin Richter-Trummer for is support, especially during my stays at foreign laboratories.

I also want to acknowledge Professor Alexopoulos Nikolaos and Engineer Christina Charalampidou from the University of the Aegean for their collaboration in the exfoliation corrosion study.

The Fundação para Ciência e Tecnologia (FCT) funding through the PhD scholarship SFRH/BD/92355/2013 is acknowledged. Funding provided from NORTE-01-0145-FEDER-000022 SciTech – Science and Technology for Competitive and Sustainable Industries is acknowledged. The funding provided by project Sold&Maq - Equipamento integrado de soldadura em estado sólido multimateriais e maquinagem NORTE-01-0247-FEDER-023694 is acknowledged.

Contents

List of Figures

List of Tables

Acronyms and Symbols

Symbols

$\bar{\sigma}$	Equivalent von Mises stress
$\bar{\varepsilon_p}$	Equivalent plastic strain
δ_n	Mode I separation
δ_s	Mode II separation
$\dot{\varepsilon}^{pl}$	Plastic flow
$\dot{\varepsilon}_m^{pl}$	Plastic flow of fully dense matrix
ν	Poisson ratio
σ_0	Yield strenght
σ_h	Hidrostatic pressure
σ_u	Ultimate tensile strenght
σ_y	Axial stress or in the Y direction
τ_u	Ultimate shear stress
τ_{xy}	Shear stress or in the XY plane
ε_s	Transverse shear strain
ε_0	Yield strain
ε_1	Principal strain
ε_n	Normal strain
ε_u	Strain at failure
A_f	Elongation at fracture
E	Young Modulus

f Void volume fraction

f_c Critical void volume fraction

f_F Void volume fraction at failure

G_{II}^c Shear critical fracture toughness

G_I^c Normal critical fracture toughness

N_f Number of cycles at failure

$T_{g\infty}$ Glass Transition Temperature of the Fully Cured Network

T_g Glass Transition Temperature

G Shear elastic modulus

R Ratio between minimum and maximum load in cyclic testing

Acronyms

AB Adhesive Bonding

BM Base Material

CBBM Compliance Based Beam Method

CFRP Carbon Fiber Reinforced Polymer

CZM Cohesive Zone Model

DCB Double Cantilever Beam

DIC Digital Image Correlation

DOC Direct Operation Cost

DoD The United States Department of Defense

DoE Design of Experiments

DSC Differential Scanning Calorimetry

DSM Design Structure Matrix

EASA European Aviation Safety Agency

ENF End Notch Flexure

ESA European Space Agency

EXCO Exfoliation Corrosion

FAA Federal Aviation Association

FEM Finite Element Method

FS Friction Stir

FSSW Friction Stir Spot Welding

FSW Friction Stir Welding

GTN Gurson-Tvergaard-Needleman model

HAZ Heat Affected Zone

HSM High Speed Machining

HZG Helmholtz-Zentrum Geesthacht Centre for Materials and Coastal Research

ICAO International Civil Aviation Organization

IMC Intermetallic Compound

INEGI Institute of Science and Innovation in Mechanical and Industrial Engineering

IST Instituto Superior Tecnico of the Universidade de Lisboa

LBW Laser Beam Welding

MCA Major Component Assembly

MEW Manufacturer's Empty Weight

NASA National Aeronautics and Space Administration

NDT Non-Destructive Testing

NVH Noise Vibration and Harshness

PAA Phosphoric Acid Anodization

PAUT Phased Array Ultrasonic Testing

QFD Quality Function Deployment

rFSSW Refill Friction Stir Spot Welding

SAA Sulfuric Acid Anodization

SEM Scanning Electron Microscopy

SZ Stir Zone

TAST Thick Adherend Shear Test

TGA Thermogravimetric Analysis

TMA Thermal Mechanical Analysis

TMAZ Thermo-Mechanically Affected Zone

TRA Technology Readiness Assessment

TRL Technology Readinesss Level

USAF United States Air Force

Chapter 1

Introduction

The proposed PhD research theme garners know-how within the research group in joining and structural design of lightweight structures to address joining of large fuselage components. A proposed hybrid joining method, combining Friction Stir Welding (FSW) and Adhesive Bonding (AB), is developed and studied for possible application in fuselage longitudinal joints at major component level assembly. This new joining technology harnesses the innovation capacity of FSW and expands its reach by overcoming some of its limitations. The introduction of such technology creates potential for new structural design concepts. The main objective in this research is the development of new design concepts and the understanding of the effects of a new technology, considering the different aspects and implications during product development, manufacturing and product life cycle.

1.1 Motivation

New transport vehicles, such as civil aircraft require higher or, at least, equivalent reliability than previous products, while at the same time being more efficient and less expensive. Efficiency is correlated with operational costs, where the major variable is fuel consumption; therefore all weight reductions have significant effect in this variable. The structural weight is a considerable part of the total aircraft weight and each kilogram saved in the structure corresponds to a large cost saving at the end of the product life cycle. New structural concepts which integrate new technologies and materials are then crucial to achieve these goals.

This push towards lightweight efficient structural design has led to an increasing use of composite materials in critical structures, such as aircraft primary structures [1]. The increasing adoption of composite materials is evident in Figure 1.1, where it is possible to see the increasing share of these materials in Boeing aircraft.

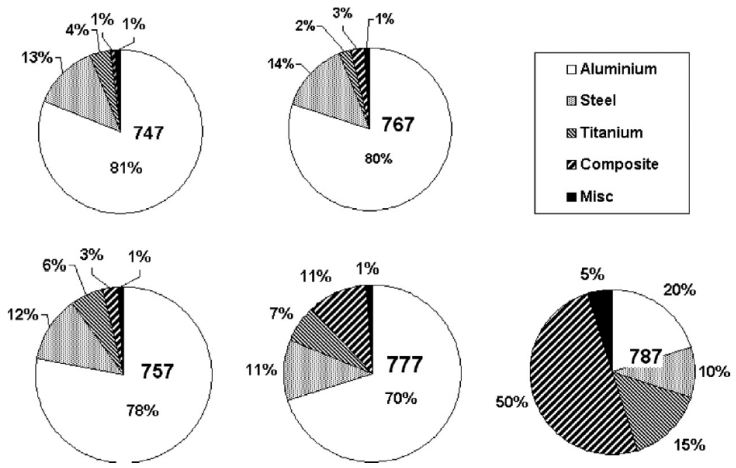

Figure 1.1: Combination of materials used in Boeing Aircrafts [1].

Although composites present several benefits, their higher certification and production costs, low impact resistance and complex mechanical behavior when faced with changing environmental conditions (moisture absorption, becoming soft/brittle when exposed to hot/-cold environments) makes them not the ideal solution for all applications.

Lightweight metallic alloys still have a fundamental role to fill in structural design and new manufacturing and assembly technologies are key in the pursuit of optimized structural designs. The topic of this thesis relates to this increasing interest in joining lightweight alloys and is linked to the application of new advanced manufacturing processes that originate new design concepts and are capable of optimizing the way joints between structural parts are made.

The replacement of riveted structural connections by welded and weld-bonded joints is not straightforward due to the complexity of the industrialization of welding processes for aluminum alloys, avoiding defects, and due to structural issues that can compromise structural integrity.

The advances in new structural joining processes aiming to replace riveting in metallic structures of transport vehicles (e.g. civil aircraft), and their disruptive potential are the main motivation of this thesis. Special focus is on Friction Stir Welding (FSW), since this is the most promising welding process for light metals, and Adhesive Bonding (AB), which is an evolving technology capable of being combined together with FSW in order to fulfill the requirements of safety critical structures.

Several topics regarding the infusion of these processes were chosen for the present research taking into account the critical aspects that can compromise or restrict its application in primary structures. Even though research efforts concerning the application of Friction Stir Welding in aeronautical structures have been made in the past, a number of important aspects regarding the impact of technology replacement (e.g. riveting for FSW) were not yet exhaustively treated. As such, an extra motivation for this work is found in this topic.

1.2 Problem Statement and Research Questions

In the case of products with large product life spans, such as commercial airliners (Airbus A320 is produced since 1986 [2]), process selection will impact greatly the success of the product, with such decisions being kept for the major part of the product life. Production and maintenance costs and complexity is heavily impacted by process selection, which is performed relatively early in process development. This makes it very difficult to correctly assess these costs at this stage.

As mentioned, adoption of new manufacturing processes in industrial environments face challenges. Such is the case dealt within the present thesis, affecting the primary civil aircraft structures design. Any change in material and manufacturing process has many repercussions that require a nearly full product development, or at least, re-engineering of different parts. As aircraft have become increasingly complex the evaluation of all advantages and disadvantages should be scrutinized in detail in order to avoid not well-grounded or uncompleted conclusions. The main question this thesis aims to answer is:

- ***Can Friction Stir Weld-Bonding be a valid alternative to riveting in lightweight structures?***

Due to the broad nature of this research question, a large number of multidisciplinary topics needs to be addressed. In addition, any design change requires large numbers of interactions between different stakeholders relating to airframe design, development and operation. The safety critical nature of these structures demands adherence to strict regulations and a high level of confidence in the effects of any design change in all aspects of the structure life. As such, a set of secondary research questions must be addressed to answer the main research question. These are:

- *How do the mechanical properties of Friction Stir Weld-Bonding compare with other conventional joining methods, such as riveting, Friction Stir Welding and adhesive bonding?*
- *How to manufacture these hybrid joints and how does the welding temperature affect the behavior of the adhesive? Also, how does the adhesive affect the quality of the weld?*
- *What does the adoption of the hybrid joining process affect structural weight and manufacturing lead time?*

1.3 Research Sites and Industrial Liaisons

The complexity and multidisciplinary nature of the problem addressed was only capable of being addressed through the interaction between universities, research institutes and industrial collaborations. The major intervenients in this research are:

INEGI *Institute of Science and Innovation in Mechanical and Industrial Engineering* is a Research and Technology Organization (RTO), bridging the University – Industry gap and focused on applied Research and Development, Innovation and Technology Transfer activities for the industry. It is located inside the campus of the Faculty of Engineering of the University of Porto (FEUP). Most of the research activities were done here, from specimens manufacturing, to testing and analysis. All activities regarding adhesive bonding, fatigue testing, numerical modeling and most of the remaining experimental activities were made here.

IST - IDMEC *Instituto Superior Tecnico of the Universidade de Lisboa* is a university located in Lisbon, Portugal with focus on science and engineering. Friction stir welding equipment from the Mechanical Technology Laboratory of IST was used in welding trials and in the manufacturing of specimens. Some mechanical tests and metalographic studies, were also made here.

Airbus Operations is a market leader in civil aircraft manufacturing. In order to keep competitiveness it has been following the development of FSW and has been performing research regarding to the application of this process in its products. A six months internship took place in its Hamburg site in Germany, where the viability of the technology for application in its products was assessed.

Airbus Group Innovations is a highly reputable research institute within the Airbus Group dedicated to researching technologies deemed of interest for present or future products commercialized by the Airbus Group. A six months internship at its Ottobrunn site near Munich, Germany were the state of the development of new assembly technologies for metallic fuselages within airframe manufactures was assessed.

HZG *Helmholtz-Zentrum Geesthacht - Zentrum für Material- und Küstenforschung* formerly known as *GKSS*, is one of the largest research institutes in Germany. Within it, there is the *Solid State Joining Processes* department which has large technical capabilities and know-how in the field of welding, especially in solid state welding. Welding trials, specimens production and mechanical and metallographic characterization were performed during a six month period stay. Manufacturing of fuselage butt-joint specimens was performed, taking advantage of this institute capabilities.

Internships in several of these organizations allowed a better contact with the development and production of aircraft structures and led to an understanding of how a process can be implemented in aircraft structures and how the advantages of this process implementation can be measured. The research locations are shown in Figure 1.2.

Figure 1.2: Research locations.

1.4 Thesis Synopsis

The research carried out throughout this PhD project aimed at answering the research questions stated in this chapter and encompassed in the field of technology development for aeronautical structures applications. The overall scheme of the conducted research is presents in Fig. 1.3. Squares in blue mark the literary research steps, while the yellow ones relate to experimental activities.

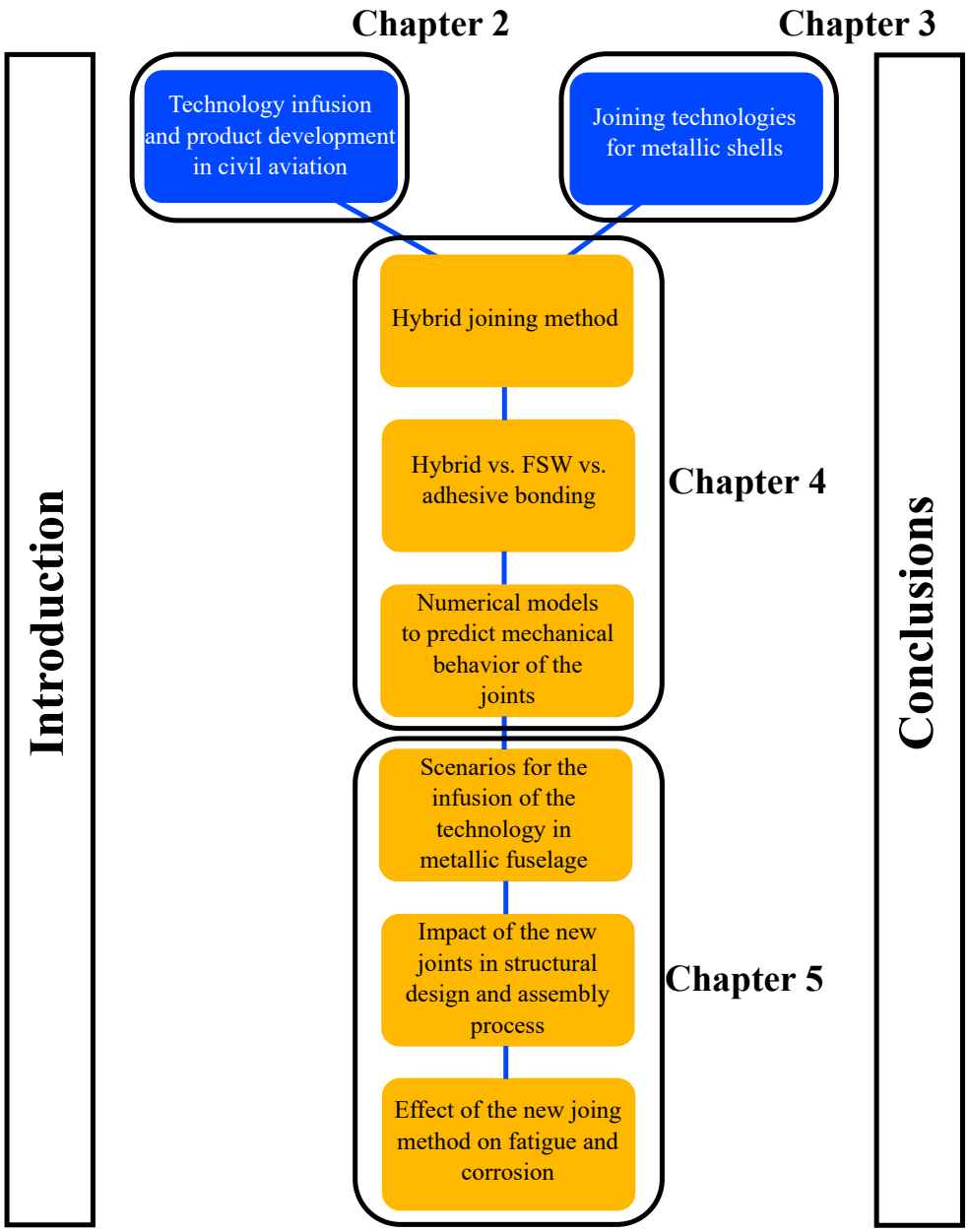

Figure 1.3: Synopsis diagram.

This Dissertation is organized in six chapters, including the introduction and conclusion. This first chapter introduces the work develop in the context of this thesis and that will be described in the following chapters. The motivation, problem statement, main and secondary research questions, involved institutions and published results are also presented in this chapter.

Chapter 2 describes how innovation and adoption of new technologies take place particularly in civil aviation. Technology assessment was reviewed here, and technology adoption was also discussed in this chapter, focusing in the particular case of civil aviation and in technology infusion in structural components.

The third chapter reviews joining methods for metallic thin structures. Special focus is given to technologies that will integrate the solution to be developed, i.e., welding and adhe-

sive bonding. The review also encompassed hybridization of joining processes. This review set the state of the art of these joining technologies, set the limitations and potentials of them and helped defined experimental activities that are latter described in following chapters.

In chapter 4, it is presented the development of Friction Stir Weld-bonding, encompassing the experimental activities and numerical modeling steps. The manufacturing process of the hybrid joint was set and benchmarks were made against adhesive bonding and FSW. The numerical models developed attempt to describe the mechanical behavior of the joints, to serve as future design tools.

Chapter 5, builds on the previous chapter by focusing on the application case of metallic fuselages. More particularly, the study case was fuselage longitudinal joints at major component level assembly. The effect of the adoption of the hybrid joining method on structural design, weigh savings and manufacturing lead time, through labor time was assessed in this chapter. Performance of the joints relating to critical requirements, such as fatigue and corrosion resistance was also studied in chapter 5.

Chapter 6 presents the overall concluding remarks of the conducted research and presents some possible future developments and lines of research within the topics addressed throughout this thesis.

1.5 Published Results

The research presented in this thesis has already been partially published by the author in scientific journals and conferences. Part of the results presented here may, among others, be found also in the references listed below:

Chapter 2: Daniel F.O. Braga, S.M.O. Tavares, Lucas F.M. da Silva, P.M.G.P. Moreira, Paulo M.S.T. de Castro, Advanced design for lightweight structures: Review and prospects, Progress in Aerospace Sciences, 69, pp. 29-39 (2014), doi:10.1016/j.paerosci.2014.03.003.

Chapter 3: Daniel F.O. Braga, Ana C.F. Silva, P.M.G.P. Moreira, Chapter 4 Mechanical Properties in Besharati-Givi, M-K., and Parviz Asadi. *Advances in friction-stir welding and processing*. (p.p. 147-191), Oxford, UK: Woodhead Publishing Elsevier, 2014

Chapter 4: Ana C.F. Silva, Daniel F.O. Braga, M.A.V. de Figueiredo, P.M.G.P. Moreira, Friction stir welded T-joints optimization, Materials & Design, 55, p.p. 120-127 (2014), doi:10.1016/j.matdes.2013.09.016.

Chapter 4: Ana C.F. Silva, Daniel F.O. Braga, M.A.V. de Figueiredo, P.M.G.P. Moreira, Friction stir welded butt joints optimization, Materialwissenschaft und Werkstofftechnik, 45(11), p.p. 1010-1017 (2014), doi:10.1002/mawe.201400299.

Chapter 4: Daniel F.O. Braga, L.M.C. de Sousa, V. Infante, Lucas F.M. da Silva, P.M.G.P. Moreira, Aluminum friction stir weldbonding, Procedia Engineering, 114, p.p. 223-231 (2015). doi:10.1016/j.proeng.2015.08.062.

Chapter 4: Ana C.F. Silva, Daniel F.O. Braga, M.A.V. de Figueiredo, P.M.G.P. Moreira, Ultimate tensile strength optimization of different FSW aluminium alloy joints, The International Journal of Advanced Manufacturing Technology, 79(5-8), p.p. 805-814 (2015), doi:10.1007/s00170-015-6871-2.

Chapter 4: V. Infante, Daniel F.O. Braga, F. Duarte, P.M.G.P. Moreira, M. de Freitas, P.M.S.T. de Castro, Study of the fatigue behaviour of dissimilar aluminium joints produced by friction stir welding, International Journal of Fatigue, 82, p.p. 310-316 (2016), doi:10.1016/j.ijfatigue.2015.06.020.

Chapter 4: Daniel F.O. Braga, L.M.C. de Sousa, V. Infante, Lucas F.M. da Silva, P.M.G.P. Moreira, Aluminium friction-stir weld-bonded joints, The Journal of Adhesion, 92(7-9), p.p. 665-678 (2016), doi:10.1080/00218464.2015.1085860.

Chapter 4: J. Fortunato, Chirag Anand, Daniel F.O. Braga, R.M. Groves, P.M.G.P. Moreira, V. Infante, Friction stir weld-bonding defect inspection using phased array ultrasonic testing, The International Journal of Advanced Manufacturing Technology, 93(9-12), p.p. 3125-3134 (2017), doi:10.1007/s00170-017-0770-7.

Chapter 5: Daniel F.O. Braga, Ricardo Maciel, L. Bergmann, Lucas F.M. da Silva, V. Infante, J. F. dos Santos, P.M.G.P. Moreira, Overlap friction stir weld-bonding of an Al-Mg-Cu alloy, Fatigue & Fracture of Engineering Materials & Structures, (submitted and under review).

Chapter 2

Technology Adoption and Product Development

Product development in high complexity systems (e.g. new aircraft fuselage) is constrained by engineering design capabilities. As such, engineering design is one of the most important phases in product development, especially when new product's requirements are simultaneously extensive and highly detailed, such as the case of safety-critical systems. For this reason, accurate technology assessment is critically important as to guarantee the integration of innovation in these systems without risking important attributes.

A traditional way of analyzing technology adoption is through the "S-curve" model [3]. Through this empirical model, three distinct phases are observed, early development, fast adoption and saturation (see Fig. 2.1). The speed of adoption varies between these three phases. Initially high costs and technology uncertainty limit the adoption (emerging technology), but as research and development of the technology increases, uncertainty and adoption costs decrease leading to a faster proliferation (developing technology). Research and development continues, but as the physical limits are approached, these efforts have diminishing returns which eventually leads to a reduction in adoption rate (mature technology).

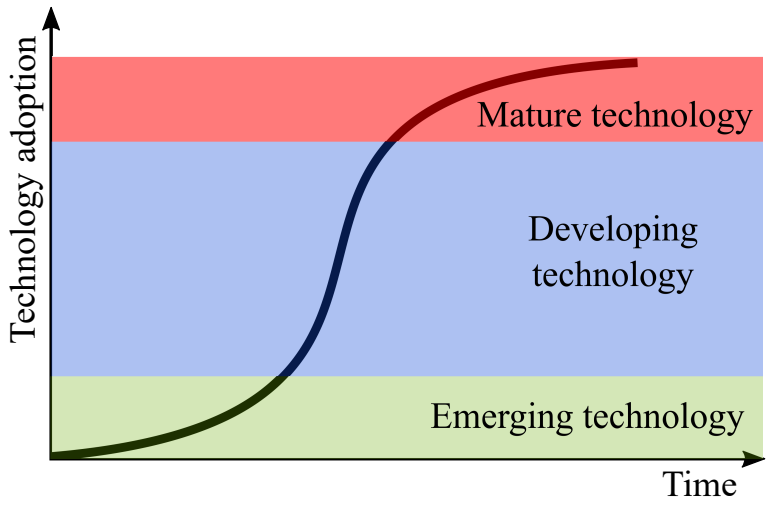

Figure 2.1: S-curve model of technology adoption.

Even though the S-curve model for technology adoption is very simple and intuitive, it has limited application in practical terms, for two main reasons, according to Smaling and de Weck [4]. Since most authors that refer to this model do not populate the curves with quantitative data, it becomes more of a mental model and not an evaluation tool. Also, if the data is available to plot the curve, it is only *a posteriori*, which makes the model unsuited as decision helping tool. The model only considers the adoption as a function of a performance metric, while in practical terms, the difference between relative performance improvements and the relative cost difference of both acquisition and operations is the driving force behind technology adoption.

This chapter will review the relevant processes associated with the integration of technology in complex products. Special interest is taken in the aeronautical industry, as it was the main industry of focus of the developed research in this PhD project.

2.1 Technology Assessment

As technology systems increased in complexity and integration, product design and development has become itself more complex. In order to achieve the intended goals in product design and development programs, multi-disciplinary teams are required to work towards common goals in parallel and in-sync with the various stakeholders. In the case of extreme complex systems, such as the nuclear fusion device ITER [5], multi-disciplinary, multi-organization teams are required to cooperate, overcoming linguistic, culture and organizational barriers among others in order to achieve the intended result. With these high levels of complexity, the risk levels are also very high and as such strategies are required to keep track of progress and assess decision making. One methodology that has been employed for this purposed is the Technology Readiness Assessment (TRA), based on the concept of technology readiness levels (TRL) introduced in 1970s by the National Aeronautics and Space Administration (NASA) [6]. At the time of its creation and implementation at NASA, the system was composed of 7 levels as a way of providing a base of mutual understanding of one technology between research and management. The technology Readiness Levels scale was later expanded from 7 to the current 9 levels as presented by Mankins in 1995 [7]. The usefulness of the system led to its adoption by other organizations and agencies with similar requirements (large governing structures, dealing with technology development in high complexity systems). The United States Department of Defense (DoD) and the European Space Agency (ESA) are two such examples [8].

As defined in [8], TRLs are a set of management metrics that in the context of a specific system, application and operational environment allow for the assessment of the maturity of a technology and its comparison against others within a type of technology. As such, a lower TRL relates to lower maturity state of a technology, while a higher TRL means the technology is either in service or close to that stage. A commonly used representation of the TRL's scale is the "thermometer diagram" shown in Fig. 2.2, where the progression between the various maturity levels may be observed as well as the general description of each level.

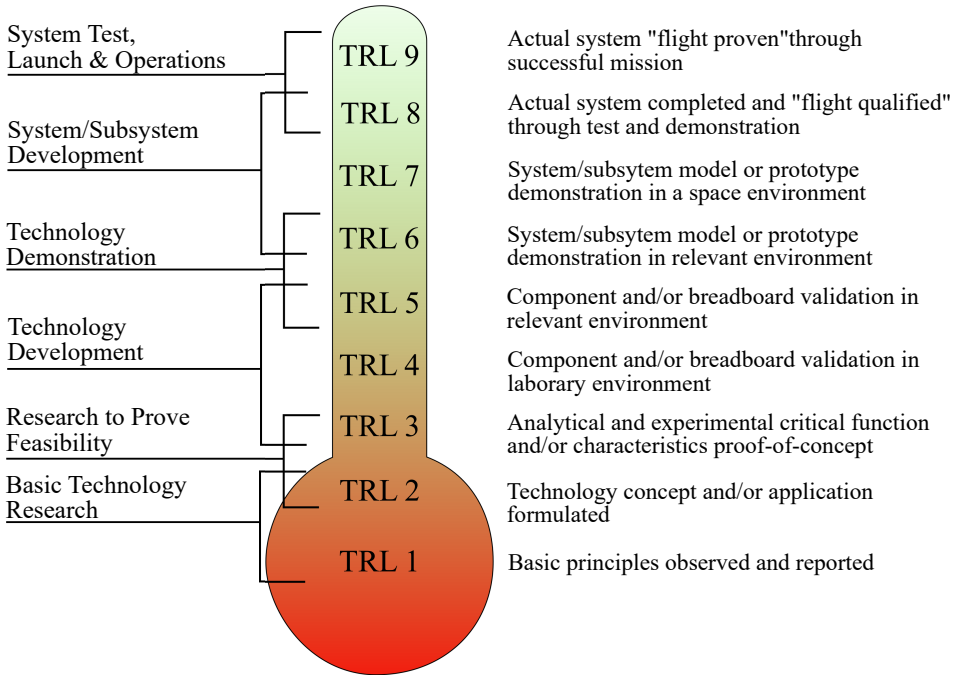

Figure 2.2: Technology Readiness Levels - Thermometer Diagram (adapted from [6]).

Although TRLs are an useful tool when analyzing the maturity of technologies by itself, the successful implementation of new technologies is dependent on correct evaluation of their risks and opportunities when integrated into their parent systems. In [4], Smaling and de Weck propose a framework for technology infusion assessment capable of quantifying the potential performance benefits of a new technology through a multi-objective Pareto analysis. The costs of infusion of new technologies are considered using the concept of architectural invasiveness regarding a baseline system. Fig. 2.3 showcases the proposed methodology. The process starts with the definition of the baseline system in which the technology is to be infused. This baseline system is "mapped" through a Design Structure Matrix (DSM) . A computer model is then used to simulate the performance of the system with varying inputs (design variables). Different concepts are then created with varying architecture, meaning varying methods of integrating the technology in the baseline system. Monte Carlo simulations are then carried out to assess the performance of each architecture, generating large set of alternatives which have to be selected. Fuzzy Pareto filtering is then used to reduce the dataset. Next the changes required to the base system by each architecture are quantified in a change Design Structure Matrix (ΔDSM). The level of changes is summarized in the Technology Invasiveness index, accounting for the amount of redesign cost and effort along with the internal risk (level of uncertainty associated with the technology to be infused). External risks, resulting from changes in regulations among other factors are integrated in the analysis in the form of breakpoints in utility functions (step 5 in Fig. 2.3). The risks and opportunities for each architecture is estimated and can be plotted as an aid to decision making. The advantage of the proposed framework is that although a complex analysis is made regarding infusion of new technologies is performed, including technical analysis that require expertise in specific fields, the outcome is perceptible by non-experts

in each analyzed field. These non-experts are usually who decide on the commitment to the technology, making it important that they have a clear understanding of its benefits and risks.

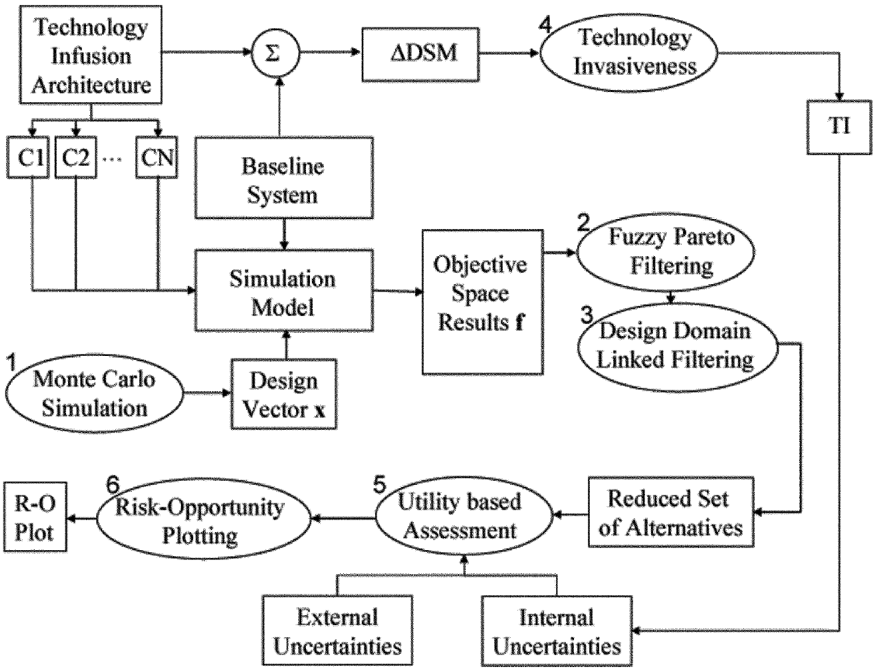

Figure 2.3: Technology Infusion Assessment method (processes are shown in oval; objects shown as rectangles) [4].

In [4], the framework is applied to a hydrogen enhanced combustion engine concept, where the infused technology is plasma fuel reformer technology. The integration of the technology in an internal combustion engine required extensive modifications resulting in various concepts (architectures). The framework resulted in an opportunity-risk plot demonstrating which concept would provide better overall outcome. In [9] Shuh *et al.* revised the Technology Infusion Analysis proposed in [4], taking into consideration deficiencies observed in the methodology. It was observed in the original methodology that the use of piecewise linear utility curves, ultimately leading to a measure of risk and opportunity, may lead to arbitrary weighting factors and subjective adjustments, influencing the risk-opportunity positioning of a technology or technology infusion process. As such, in the revised methodology an attempt is made at linking the efforts of technology infusion, estimated by DSM and ΔDSM on expected net present value and return on investment estimations. The alterations to the framework are better visualized in Fig. 2.4. It may be observed that one of the more significant changes is that “risk” and “opportunity” are replaced by the expected marginal net present value and standard deviation of the expected marginal net present value.

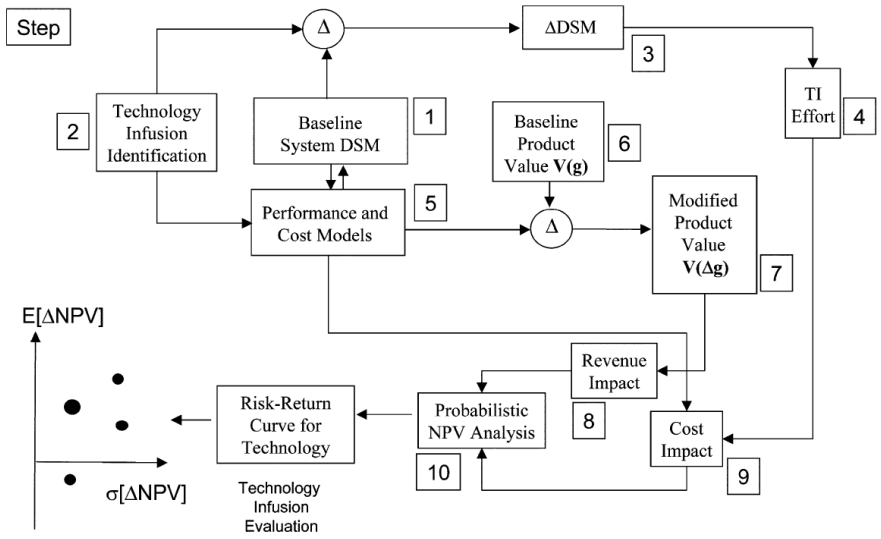

Figure 2.4: Modified Technology Infusion Assessment framework [9].

To demonstrate the methodology, a technology infusion process in a digital production printing system was used as a case study. The analysis showed that despite the required non-recurring engineering effort to infuse the technology, a positive marginal net present value would result over a 12-year time horizon. Even though a complex analysis was required to achieve this result, the result itself is of relative ease of understanding for decision makers and includes relevant estimations to assess the likelihood of success of a technology infusion process. Nonetheless, a limitation present in this framework is that only one technology infusion is assessed at a time, instead of a set of technologies which more commonly occurs when transition between product generations in high complexity systems. In that regard, further study is required to include the effect of the interaction between multiple new technologies infused in the same system, in order to improve the analysis.

2.2 Technology Adoption in Aeronautics

Considering the high number of components and interconnections in civil aircraft, with these interactions or interdependecies being difficult to describe, design change and technology adoption is challenging and costly. These characteristics make civil aircraft complex systems by definition [10]. The complexity is present both in civil aircraft systems and structures, with examples of systems including, electronic, hydraulic and propulsion sub-systems and as examples of structures, the wings, fuselage, landing gears, among others. Within civil aircraft structures, various subdivisions may be made. One that is comprehensive and relevant to the theme of technology adoption, is based on the repercussion of the structure in the aircraft safety. The aircraft battle damage repair manual of the United States Air Force (USAF) presents a detailed description of 5 categories based on the reparability in defense contexts [11]. Considering this division, a general description of each of these structural groups may be as follows:

Primary structures are the safety critical structures of an aircraft. They support the majority of flight and weight loads and without them the aircraft does not maintain structural integrity. Due to transfer of critical loading, the loss of any structure of this category could lead to the failure of subsequent primary structures. Examples of such structures are: main longerons, bulkheads, and wingbox components.

Secondary structures encompasses the structures that although carry significant flight or weight loads, their loss does not equate to a loss of structural integrity. A failure in these structures would affect the performance of the aircraft but would not cause its loss. The repair of these structures is not as critical as the previous category and the aircraft may operate with a certain level of damage in them, making them more damage tolerant. Examples of these structures are stringers/stiffeners, and frames/formers.

Tertiary structures do not carry any load nor do they serve any aerodynamic purpose and as such are superfluous structures. They are not safety critical. Examples are tail cones, landing gear pods and pylons.

Aerodynamic components do not serve load carrying purpose but are responsible for maintaining aerodynamic qualities. These structures are essential to the aircraft performance and controllability. Radomes and nacelles are examples of aerodynamic components.

Non reparable structures are structures where it is unfeasible to repair and that require complete replacement when damage occurs. These components are complex forgings, machined parts, or special extrusions.

As each structure category serves different purposes and affects the safety of the aircraft in varying levels, the amount of design change and technology adoptions vary between them, as well as the effort required to implement new technologies in them. Design changes and adoption of new technologies in civil aircraft structures must adhere to strict regulations to guarantee the airworthiness. In the field of international aviation, the International Civil Aviation Organization (ICAO), ensures safe and orderly growth of international air transport, by establishing directives that all member states are obliged to follow. In addition to the ICAO directives, members established local transport safety authorities, which issue their standards and regulations, although in the accordance with the ICAO Annexes [12]. The Federal Aviation Association (FAA) and the European Aviation Safety Agency (EASA) are two such authorities. The issued regulations by this authorities encompass the various activities related to air transportation and are divided accordingly. As example, the EASA CS-25 [13] comprises the airworthiness standards for large aircraft, such as the case of commercial airliners, and more specifically in the case of these aircraft structures the EASA CS-25 Book 1 Subpart C should be taken into account. This certificate is a requirement for all transport aircraft operating within the member states of EASA. To issue the certificate, the regulatory body may require inspection and testing of the aircraft [14]. Subsequent design modifications and technology integration will require amendments to the certificate [15].

Given the complexity of the various systems and structures and their interdependencies, the transition of new technologies from the lab to full-scale production is challenging. A successful technology scale-up process requires the analysis and fulfillment of two critical topics [16]:

1. Requirements – based on the state of the art and is the minimum required to be fulfilled.
2. Opportunities – improvements added on top of the requirements: these are usually necessary to get a business case. Thus, the opportunities have to be considered from the beginning.

In [16] two examples of technology scale-up regarding composite components within the aeronautical industry are presented. These examples are based on serial production and are to be improved regarding cost (manufacturing cost saving), quality (leaner production, reduction of rework) and eventually performance (weight saving). For risk minimization, i.e., to enable fall-back-solutions compared to the baseline technology, it is indispensable to fulfill at least the state-of-the-art quality requirements of the current, more or less manual production. For investment in additional automation, it is usually not sufficient to only meet the current production requirements. The business case for more automation requires the realization of additional opportunities such as tighter production tolerances (e.g., savings in weight, material, leadtime, non-value adding process steps). If the above stated requirements are checked with the industrial partner(s), the upscaling of manufacturing technologies and the automation toward an industrial production can start. The examples of scale-up given were, a composite pressure bulkhead (scale-up from an existing manual process) and a fully automated application of a lightning strike protection material. In the first example the baseline process is a manual process that is complex, costly and time consuming and through the implementation of more automated processes it is intended to assure the quality of the finished parts, while improving on the drawbacks of the current method. Various automation solutions were proposed for different stages of production, but the authors observed that full automation may not always be the right approach, as added complexity not always equates to improved process and also introduces vulnerabilities. The authors also found that the perspective of the whole process chain and its interfaces between process steps must never be neglected. The second example presented was motivated by the need to ramp-up production of the lightning strike protection material to keep up with production demands from new long range aircraft that make extensive use of composite materials, such as the Airbus A350. The fully automated process achieved an elevated TRL level, with significant improvements over the original process. Both examples showed the complexity of scale-up of technology from lab to production in aircraft manufacturing, requiring efforts in many varied fields and with uncertain final results. The authors also show that even though at the beginning of research and development processes, the introduction of complex full automation processes may seem beneficial but the vulnerabilities these systems bring are sometimes to significant to justify their implementation.

In [17] technology assessment for managing innovative technology development in aeronautics is studied, and examples of its use are given. These assessments use two methods,

scenario techniques and technology vector. In scenario techniques, all of the repercussions of a technology in a virtual environment are listed in a cross-impact matrix. The data is weighed by specific functions and then reduced to just a few macro scenarios. The calculation of the benefits and penalties of the technology is performed on the basis of each scenario, such as a 'green' scenario or a 'low-cost' scenario. This technique helps in understanding the outcome of modifications at an aircraft level, even with future uncertainties. The technology vector defines the performance of an aircraft, making a comparison with a reference aircraft that can be plotted at the origin of a coordinate system. The repercussions of a technology can be drawn as a vector, with the manufacturer's internal rate of return on the x axis and the operator's internal rate of return on the y axis. Depending on the position or quadrant, it can immediately be seen whether the new aircraft or the aircraft with a new technology is beneficial for the manufacturer, the operator, both, or neither. Although technology assessment in aeronautics is shown to be a powerful tool to rate new technologies, it may risk stopping valuable research if its results are taken to literally or taken just as a single digit instead of as sensitivities. The issue comes from the fact that technology assessment always addresses future developments, and boundary conditions are set in the current context of the evaluation. An example given is when boundary-layer suction devices for laminar flow control were under investigation in the early 1990s, laser beam drilling was the only technology available at that time and today the tiny holes required can also be drilled by electron beam drilling, with major implications for cost and quality. As such, boundary conditions of changed, demonstrating the limited reliability of technology assessment when it comes to future forecasts.

One structure rife for innovation in aeronautical structural design is the fuselage, as the increasing maturity of the composite technologies for manufacturing structures at competitive costs creates a growing competition between metal and composite design solutions. Facing stiff competition from composite structures, new innovations are required to maintain the competitiveness of metallic structures. This way, both design solutions (metallic and composite) are pushed to their limit. In [18], the challenges and future developments of metallic fuselage are discussed. The authors point out three main aspects guiding the future development of metal technologies for fuselage:

- Increase of structure performance by means of the latest generation materials tailored for the specific structural applications;
- Reduction of manufacturing and assembly costs increasing the application of integral structure concepts;
- Development of minimum weight design principles with extreme material tailoring including selective reinforcements.

The authors listed the ongoing developments at the time at Airbus regarding metallic fuselage structures. Two families of aluminum alloys have been developed with potential application here, aluminum-lithium and aluminum-magnesium-scandium. Aluminum-lithium offer high static strength, combined with a lower density than currently used 7000 series

aluminum alloys, making them relevant for stringers. Aluminum-magnesium-scandium, have good fatigue strength and damage tolerance properties, with lower density than current aluminum-copper alloys used as skin materials. These lower density materials are also weldable, making them capable of being integrated in designs encompassing new welding technologies. Welding procedures are also in development at Airbus, with special interest on laser beam welding (LBW) and friction stir welding (FSW). The combination of metallic materials with composites in fiber metal laminates is another area of development and bridges both metallic and composite material technological development. These technologies and others mentioned by the authors will be key to assuring the competitiveness of metallic materials for this application. In [1], a review of recent developments in aluminum alloys for use in aircraft design is made, listing also the alloys mentioned previously, as current focus of development by the airframe manufacturers and material suppliers.

Current structural design of aircraft fuselages makes use of differential structures, with skins, stringers and frames joined together, mainly through riveting. The adoption of welding processes would result in a change of design philosophy, from differential to integral structures, shown in Fig. 2.5. These new design concepts are attractive as they allow simplifying and optimizing the design for manufacturing and assembly process. However, the crack arrest capability may be compromised. In [19], an introductory quality function deployment (QFD) analysis, based on [20] is performed aiming at the identification of the opportunities associated to this process when applied in aeronautical structures with several design goals. Two welding techniques, along with high speed machining (HSM) were considered to manufacture integral structures, replacing riveting. The fasteners and overlap areas used in rivet joining are considered non-value added parts in these structures, and by employing welding techniques, producing integral structures, these non-value added parts are reduced. Design goals for the partial QFD analysis were selected based in the main requirements of reinforced panels in critical aeronautical parts. The QFD analysis made use of the method of Cross, correlating the design goals based in the experience of experts, ranking their importance in the specific scope of aeronautical reinforced panels. The benchmarking among the different manufacturing processes was based in these design goals. The resultant table from the method of Cross and resulting benchmark are shown in Table 2.1. The results allowed to demonstrate the potential of application of one of the joining technologies for producing integral structures, but also highlighted the challenge of guaranteeing structural integrity with this welding procedure and design change.

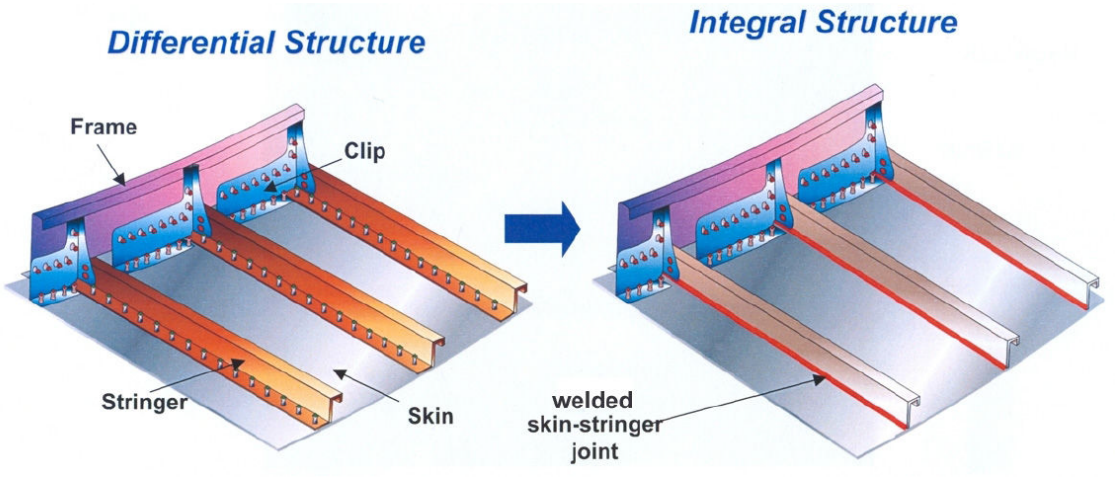

Figure 2.5: Differential *vs.* integral fuselage structure [21].

Table 2.1: Method of Cross used in a generic integral structure of fuselage through welding [19].

	Fatigue behavior	Minimum maintenance	Aerodynamic (& aesthetics)	Minimum fabrication cost	Availability of parts	Minimum weight	Minimum manufacturing time	**Total**
Fatigue behavior		1	1	1	1	1	1	6
Minimum maintenance	0		0	0	1	0	0	1
Aerodynamic (& aesthetics)	0	1		0	1	0	0	2
Minimum fabrication cost	0	1	1		1	0,5	1	4,5
Availability of parts	0	0	0	0		0	0	0
Minimum weight	0	1	1	0,5	1		1	4,5
Minimum manufacturing time	0	1	1	0	1	0		3

Goal along rows is given a score of 1 if more important than the corresponding column goal. The goal along the row is given a score of 0 if perceived as less important than the corresponding column goal; where both column and row goals are perceived as of equal importance, they are given a value of 0.5.

a) rank ordering the design goals

	FSW panel	Riveted panel	LBW	HSM
Fatigue behavior	4	5	4	3
Minimum maintenance	5	3	5	5
Aerodynamic (& aesthetics)	5	3	3	5
Minimum fabrication cost	5	3	5	2
Availability of parts	4	3	4	5
Minimum weight	5	5	3	5
Minimum manufacturing time	5	3	5	5

('5' is higher grade).

b) benchmarking

2.3 Chapter Summary

The research conducted during this PhD, which is described throughout this dissertation, aims at the development of a joining technology with possible application in aircraft fuselage structures. As discussed in this chapter, these are complex structures and the integration of technology in them is a complex issue on itself. The conditions that a material, manufacturing process and component must fulfill are diverse as these structures have many requirements, and are critical from a safety point of view. During technological development,

assessment is required throughout the process, assuring the intended goal is met and avoiding, expensive costs overruns from non performing research. When a technology has been comprehensively studied and demonstrated to have a positive value / risk ratio, integration is performed. This integration must consider the relevant regulatory framework, which needs to be contemplated in the value / risk analysis.

Chapter 3

Joining technologies for metallic structures

New manufacturing and assembly technologies are key to assuring the economic viability of metallic structures and more specifically aluminum airframes when facing the rapid development of composite materials and composite structural design. One approach to face this challenge is to reduce the ratio between supplied material and material in the final product. Using welding techniques, the amount of machining operations may be diminished and less material will be wasted. The use of newer and more automated welding techniques, instead of riveting for large component assemblies, may also allow for lead time savings.

The use of lighter and stronger alloys, that allow for lighter designs and improved vehicle performance and fuel efficiency is also key in assuring the viability of metallic airframes [1]. These alloys are however difficult or even impossible to weld with conventional fusion welding techniques and therefor require alternative joining methods, such as solid state welding, fastening or adhesive bonding. These alternative joining methods present other design opportunities. In the case of adhesive bonding it is possible to eliminate stress concentration due to rivet holes by having a continuous adhesive layer. Another added benefit is the possibility of using smaller overlap lengths than traditionally used with riveting joints, allowing for significant weight savings in the fuselage. FSW in butt joint configuration would also eliminate stress concentration due to riveting holes and would not require overlap, making the weight saving even more significant. The removal of all overlaps in the structure would however present great challenges when it comes to geometric tolerance management. The use of FSW in overlap configuration is normally not desired due to its reduced mechanical performance. The sole use of adhesive bonding in large structures assembly is also limited by curing conditions and inspection, maintainability and reparability concerns. A combination of both FSW and adhesive bonding would alleviate many of these concerns and may be a valid assembly process for large structures (e.g. fuselage).

This chapter will seek to present the state of the art of relevant joining technologies to be further studied in the following chapters. Recent and relevant developments on friction stir welding and adhesive bonding were reviewed, with special focus on aeronautical structures applications. Hybrid joining technologies, specially those involving adhesive bonding are

discussed in this chapter. The state of the art research showed an existing gap in literature relating to hybrid friction stir weld-bonding and its application in aeronautical structures assembly. However, the patent search performed in this chapter shows interest from industrial partners in the subject.

3.1 Friction Stir Welding

The aeronautical industry has been shy of welding processes in primary structures due to the related loss of mechanical properties from large heat inputs, weld quality control (process reliability) and the impossibility of welding precipitated hardened alloys (e.g. AA2024 aluminum alloy). Solid state welding mitigates some of these concerns, as lower heat inputs result in improved mechanical performance and easier process control improves process reliability. Friction stir welding has shown to produce sound quality, high performing joints and as such is the most appealing welding technology for aeronautical structures [1, 22]. In its most basic form, FSW is performed with a tool composed of shoulder and pin. The tool is inserted while in rotation into the pieces to be welded and transverses along the weld line, as shown in Fig. 3.1 a). The shoulder is mainly responsible for providing heat from friction onto the sheets or plates to be welded, while the pin's main job is mixing the materials to be joined. The combination of heat and resultant material softening and recrystallization along with material flow during the process result in a modified metallographic structure in the joint cross-section. The resultant material zones have different physical and mechanical properties. Generally these areas can be subdivided in 4 zones, see Fig. 3.2. These are, the base material (BM) where heating is not sufficient to cause metallographic changes and the material keeps the original morphology, heat affected zone (HAZ) where heating is sufficient to cause softening, the thermo-mechanically affected zone (TMAZ) is softened and material plastic flow is noticeable here by the elongated and reorientated grains, and in the center of the weld is the recrystalization zone, usually called stir zone (SZ), where the combination of heating and mixing of the tool causes grain breakage resulting in small equiaxed grains. The potential of this joining technology has led many researchers to study the diverse fields associated with it and currently encompassing reviews on the matter may be found [23, 24, 25]. Magalhães *et al.* in [26] reviewed FSW with the perspective of industrialization of the process, listing the main areas of industry/research where the FSW technology is being applied/explored and the geographical distribution of the main players in its implementation/research. It is concluded that, although FSW technology was born in Europe, the largest number of patents published on the process are from Asia and America. The main industry making use of FSW and advancing the state of the art was found to be the transportation industry, and within this, the automotive industry. The authors conclude that the technology has reached maturity, as the number of patents slightly diminished since 2009.

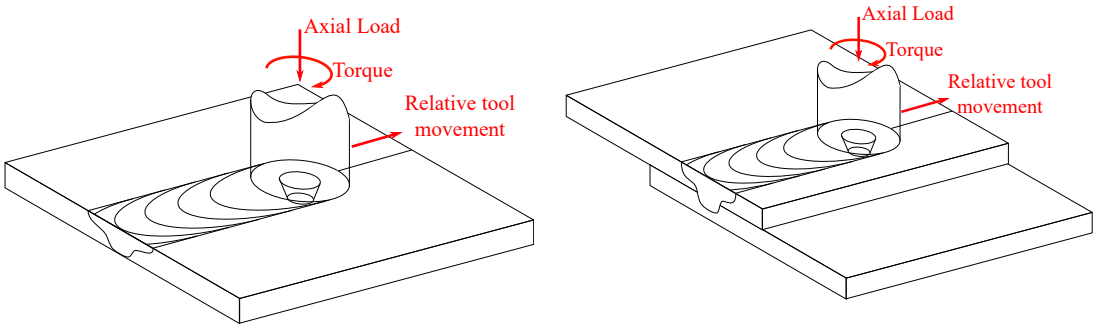

Figure 3.1: Scheme of Friction Stir Welding in a) butt-joint configuration and b) overlap configuration

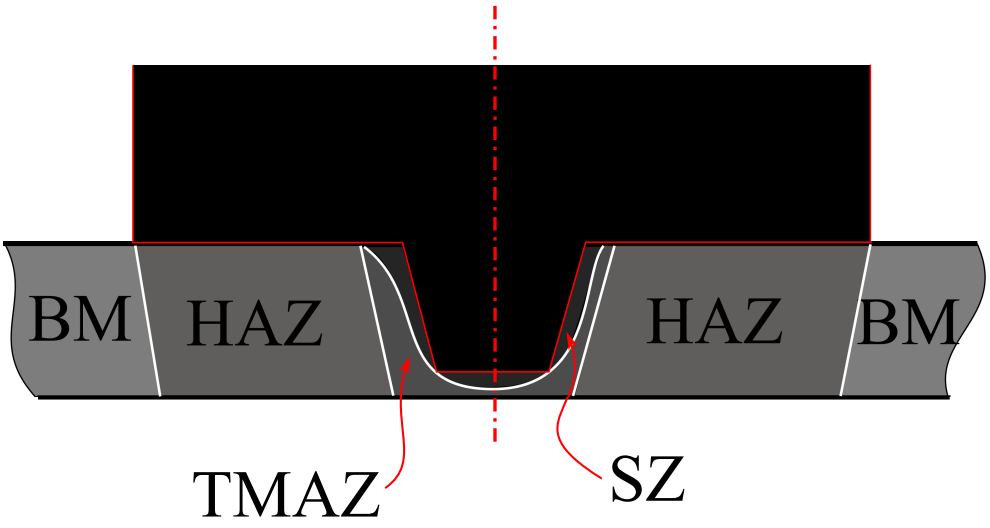

Figure 3.2: Resulting weld zones from FSW

The excellent mechanical properties resultant from FSW and the potential to reduce weight of metallic structures by eliminating fasteners and overlaps has generated interest for the technique from the aeronautical industry. In [22] an extensive experimental program was performed to study quasi-static mechanical performance, fatigue strength and corrosion strength of two common aeronautical aluminum alloys with two different thicknesses. The welds were performed on AA2024-T3 and AA7075-T73 aluminum alloys with 0.040" (≈1 mm) and 0.125" (3.175 mm). In tensile testing, strength of the welds was found to be between 80-93% of the base material. Fatigue, fatigue crack propagation, and fracture toughness were shown to be comparable to base material. The welds were shown to be susceptible to corrosion and stress corrosion cracking, although the authors mention that these issues may be overcome through post weld treatments.

Although butt-joint configuration is the most common welding configuration used in FSW and also the most reported in the literature, other joining configurations are possible [27, 28, 29]. In overlap configuration, as the name suggests, welding is not performed by joining two sheets or plates through their abutting surfaces but through their superposition, as shown in Fig. 3.1 b). Even though FSW butt-joints have been reported to have mechanical

strength comparable with base material, the appearance of crack-like unwelded regions in overlap configuration means the latter joints strength is greatly diminished [30]. Nevertheless, overlap configuration may be preferable in cases, where tolerance management may be more difficult and a zero gap weld is not assured, as is the case of major component assembly in aeronautical frames. When friction stir welding butt-joints, the existence of gaps between the abutting surfaces will have a significant effect on the weld quality [31].

In [31], Shultz *et al.* studied the effect of gaps in 5 mm thick aluminum alloy AA5083-H111 butt-joints and proposed techniques to mitigate the effect of such gaps. By altering the plunge of the tool and the angle of attack it was possible to mitigate the gap, by trading off a reduction in cross-section thickness for a continuous material fill of the gap area. However, it was noticed that gaps over 0.5 mm caused significant joint efficiency reduction for the material used in the study. It should also be noted that the strategy employed by the authors to mitigate the effect of gaps in the abutting surfaces requires the precise knowledge of the position and size of the gap, which may not be easily achieved in a manufacturing environment, such as the case of major component assembly in aeronautical structures. In [32], Richter-Trummer *et al.* studied the influence of clamping forces during the welding process, including gaps in the material to be welded. The authors used a specially made clamping system capable of measuring both the axial clamping loads, as well as horizontal clamping loads. This measurements were then related with distortion and residual stress measurements in the welds. The authors also found that even welds that initially had 0 mm gap when welded with low clamping forces resulted in a measurable gap at the end of the weld. Higher clamping forces not only allowed to maintain the intended gap, but also resulted in lower distortion and residual stress. Wanjara *et al.* in [33] studied the effect of gaps in weld defects, micro hardness and weld mechanical performance, in order to study the implementation of load control robotic FSW in an industrial environment. The authors welded 3.18 mm thick aluminum alloy AA6061-T6 with various predetermined gaps and found that a wormhole defect appears and increases with increasing gap but has no significant effect in hardness or weld performance up to 0.5 mm gap. Between 0.5 mm and 0.8 mm gap a drop in hardness in the stir zone was measured but still no change in mechanical performance was found in the bending tests. Beyond this gap level deterioration of the mechanical performance was observed. Even though between 0.5 and 0.8 mm gap no performance reduction was observed, the forge force measured during the welding process showed a decrease, meaning that the tool had started to plunge into the sheets. As such, the authors proposed that a limit of 0.5 mm or 16% of thickness should be established for gaps in FSW butt-joints. With increasing weld sizes there is also an increasing need for complex and robust clamping systems. For these cases the effect of small degrees of misalignment before welding may lead to large gaps and severely influence the quality of the welds. Schulze *et al.* in [34] used a pentapod FSW machine and a clamping system with movable clamping bars and load cells to study the effect of initial gaps in misalignment and residual gaps. By measuring transverse loads during the welding process, the authors were able to verify that the load shifts direction during the process. During tool plunge the sheets face pressure from the tool, but as the welding starts and progresses the loads shift sign leading to a residual shrinkage. An initial gap of

0.6 mm or 30% of sheet thickness was found to lead to the lower residual gaps.

However, in the case of long welds, such as the case of longitudinal joints in major component assembly (MCA) in an aeronautical metallic fuselage, guaranteeing initial gap levels will be extremely challenging and could prove to be economically unviable. One solution for these types of welds, as mentioned above would be to opt for overlap weld configurations, similar to the current state of the art with riveted joints. Inconveniently this configuration results in reduced mechanical performance, specially when it comes to fatigue strength, due to the shape of the unwelded tips at the extremities of the weld bead, as well as the more complex loading of these joints. Ericsson *et al.* in [35] fabricated and tested 2 mm thick AA6082-T6 aluminum alloy overlap welds, with varying tool configuration in quasi-static and fatigue loading. A joint efficiency (joint ultimate load compared to base material ultimate tensile strength) of about 55% was observed in the quasi-static loading. An even more drastic reduction in performance was observed when cyclic loading these joints. At 10^5 cycles the fatigue strength is about 20-30% of the quasi-static lap strength of the joints. The fracture was observed to initiate at the unwelded tip on the advancing side, where the vertical material flow outside the pin resulted in a "hook" like shape, pointing to the top of the weld. Fersini and Pirondi in [36] studied the fatigue strength of 1.6 mm thick aluminum alloy AA2024-T3 overlap welds, using an experimental and numeric approach. As a way of studying the effect the secondary bending has on quasi-static and fatigue strength, the authors used additional tests where the specimens were constrained in the out of plane direction. In quasi-static loading a joint efficiency of 70% was achieved and by employing the antibending system, this efficiency was increased to 75%. The Wöhler curve obtained was comparable with the ones reported in [37] and [35] but fatigue strength was lower than the specified design curve of bolted joints proposed in Eurocode 9 [38]. At 10^5 cycles the efficiency was only about 14% of the quasi-static strength of the joint. The antibending system also resulted in an improvement in fatigue strength, showing that the out of plane bending is responsible for roughly half of the joint strength decrease. The authors also found that correctly predicting fatigue life with numeric models was challenging due to the early stage shear-dominated (mode II) crack propagation which occurs experimentally but cannot be accounted in the numerical model. In order to study the use of overlap FSW for stringer-skin connections, Letora in [39] compared aluminum alloy AA2024-T3 riveted overlap joints with overlap friction stir welding, through cyclic pressurization tests as indicated by the FAR rules on a scale model. Even though an improvement in quasi-static overlap shear ultimate load was achieved with FSW when compared to riveted joints, the presence of unwelded tips on the sides of the weld, the micro-structural heterogeneity and the excessive rigidity from having continuous joints led to severe decrease in fatigue strength. In the cyclic pressurization test, while the panels with riveted stringers showed no cracking until the established infinite life (60000 cycles), cracks appeared on the FSW panels after about 30% of the number of cycles in the test. The cracks appeared beneath the weld bead and grows always in the skin, not transitioning into the stringer. In an attempt to diminish the degree of constrain in the panels during pressurization, shorter (50 mm) welds spaced between each other were used in each stringer. This modification resulted in similar results to the riveted panels, although it must be added that

at end of each short weld a small hole is left by the tool extraction. These small holes were not determinant in crack nucleation, but may become critical in other loading cases or may be detrimental in terms of corrosion resistance.

One way of addressing the lower mechanical performance of overlap welds, especially when it comes to fatigue is to use multiple-pass welds. In [40] Dubourg *et al.* studied the use of single pass and double pass welding in AA2024-T3 skin and AA7075-T6 stringer overlap joints. By increasing the feed ratio (welding speed / rotational speed) in single pass welds it was possible to reduce the size of the hook in the advancing side and the top plate thinning in the retreating side, although it was not possible to completely eliminate these defects. An inversion of the hook direction was also observed when increasing the feed ratio which improved the performance of these joints. Having defined the optimum parameters for the single pass welds, they were then used to manufacture also double pass clock wise (retreating side always facing outwards) and counter clock wise (advancing side always facing outwards) joints. It was verified that by using the double pass welding with retreating side always facing outwards, the hook defect was avoided, but the top plate thinning was still present and now on both sides, which led to failure in bending tests through these defects, as seen in Fig. 3.3 e). The double pass counter clock wise configuration was able to pass the bending test by avoiding the top plate thinning. This configuration was then assessed in quasi-static and cyclic tensile loading, and its performance was compared to single pass welding and riveted joints. It was verified that the use of this configuration not only improved average ultimate tensile strength (σ_u) but also reduced the scattering in these tests. Single pass welds showed significantly lower fatigue strength than the riveted joints. Double pass welds improved the fatigue strength but were still not able to match riveted joints. To surpass the fatigue strength of the riveted joints, the authors employed double pass discontinuous welds, similarly to the strategy mentioned above in [39].

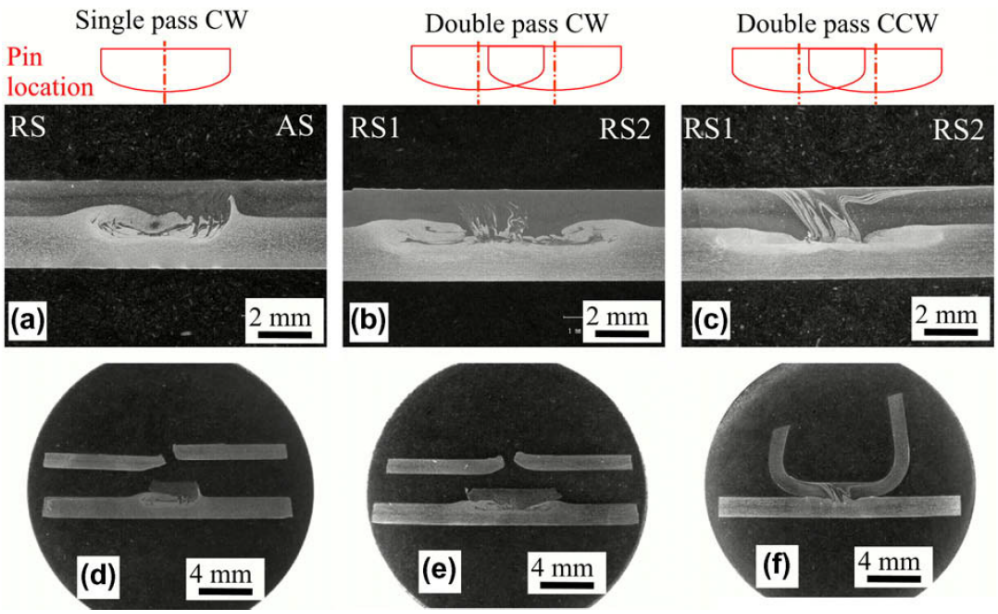

Figure 3.3: Cross section of skin / stringer joints after welding (above) and after bending tests (below) [40]

He *et al.* in [41] also focused on the skin-stringer connection using overlap FSW in single and double pass configuration. Equilateral L stringers made of aluminum alloy AA7150-T77511 with 2.4 mm were joined to 1.8 mm aluminum alloy AA2524-T3 skins and subjected to tensile, peel and metallographic tests. When tensile loaded the defect-free single and double pass welded joints, showed similar performance and fracture location (skin fracture in the advancing side), as in both cases necking was present, showing that the yield point of the skin material was surpassed. In the case of peel tests, an improvement in strength was achieved (80.4 N/mm and 166 N/mm for single and double pass configuration, respectively). This significant difference in peel resistance is most likely due to the increased width of the connection, as in the single pass welds the width is 2.5-3.0 mm (related to the diameter of the pin) while in the double pass it is 7.5-8.0 mm (related to the diameter of the pin plus the distance between passes). This difference causes decreased peak stress during peeling and as such leads to different failure modes. Most single pass welds failed through peel off while the double pass welds mostly failed through fracture of the skin. In [42] Papadopoulos *et al.* studied the mechanical performance of AA2024 overlap friction stir welds. Various configurations, including single pass Fig. 3.4 (a), double pass Fig. 3.4 (b-d) and triple pass Fig. 3.4 (e) were studied. Conventional tool and bobbin tool were also both used in this study. Quasi-static tensile testing showed that increasing the distance between passes improved the strength of the joint, leading to the triple pass weld being the highest strength joint welded with conventional tool. Using bobbin tool in a double pass configuration, a strength close to the material tensile strength was achieved. This configuration also resulted in the highest fatigue strength. The trend observed in quasi-static testing (higher distance between passes equals higher strength) was however not confirmed in fatigue strength as the shape of the cross-section (position of the advancing side and retreating side and corresponding interface

shapes) seems to play a more important role in cyclic loading. The maximum fatigue strength achieved at 10^5cycles in this study was 37.9 MPa of stress amplitude.

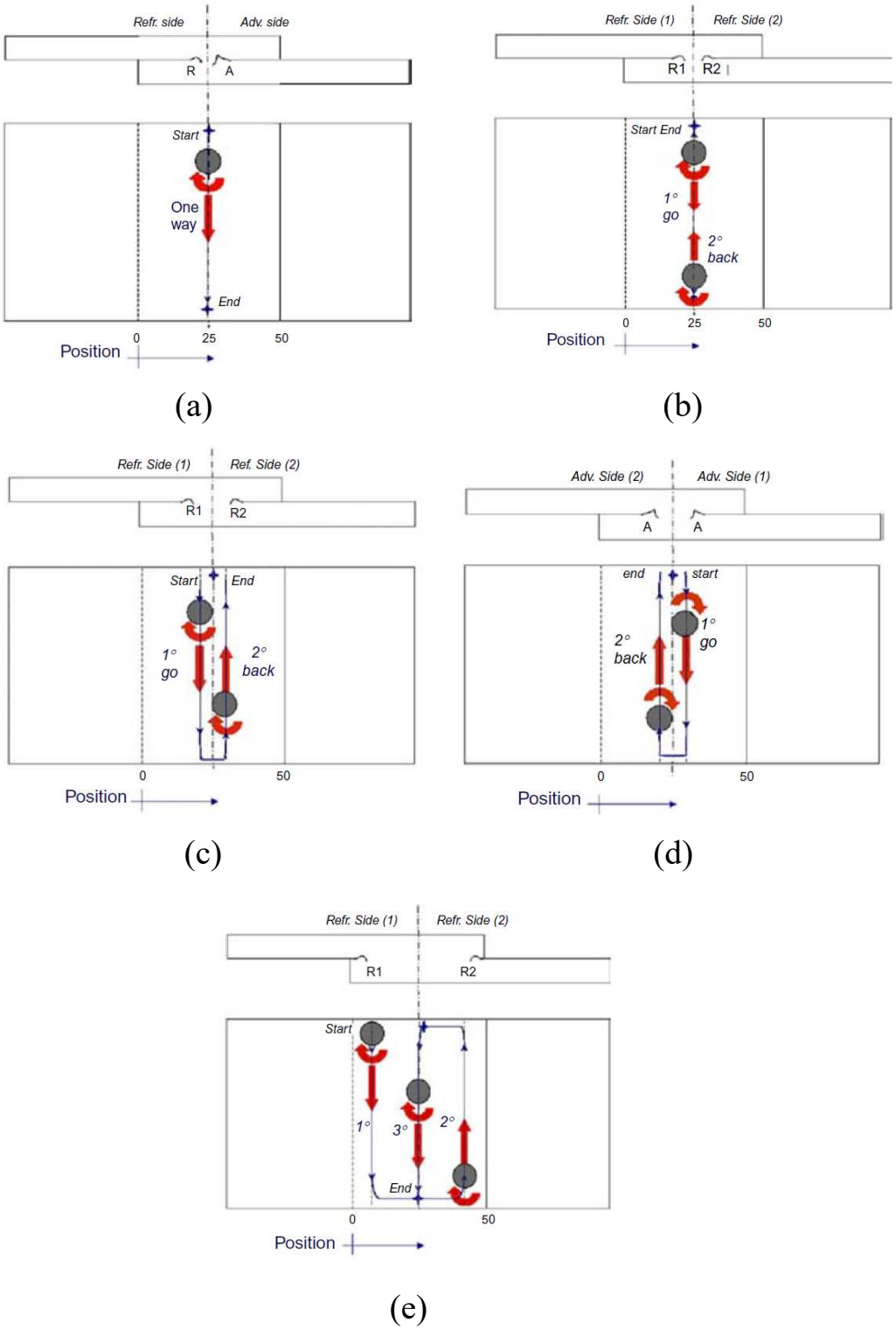

Figure 3.4: Weld configurations in [42] (adapted from [42])

In [43], Leitao *et al.* employed multipass friction stir lap welding for aluminum-steel dissimilar joints. A triple pass configuration was used to weld 3 mm thick aluminum alloy

AA6082-T6 and S355J2 + N steel with 5 mm thickness, where the aluminum plate was always on the top and minimal pin penetration in the bottom plate. By using this configuration the authors aimed to increase the width of the bonded area and as all weld passes were performed in the same direction the position of the advancing side and retreating side remained similar to what would be the case in a single pass weld, as shown in Fig. 3.5 a). The authors then used two different specimen configuration for quasi-static study, as shown in Fig. 3.5 b) and c). The tensile joints were tested in quasi-static condition, as the lap joint configuration and weld set-up used will result in only the advancing side being loaded. The tests with both configurations were made with the use of digital image correlation (DIC). When analyzing the shear-tensile results and corresponding DIC images, it was possible to observe that failure occurred through gradual collapse of the bonded interface, after significant plastic deformation in the aluminum HAZ. The first pass to fail is the 3^{rd} pass due to stress concentration in the weld, leading the load to be transferred to the 1^{st} pass which upon failure transfers the load to the 2^{nd} pass which then fails after minimal load increase. The much weaker behavior found on the 2^{nd} weld pass compared to the other two, led the authors to conclude that bonding was non-uniform between the different weld passes. This non-uniformity may lead to difficulties in predicting the behavior and strength of multi pass welds and is a clear disadvantage in their implementation. In the tensile tests, failure occurred in the HAZ / TMAZ region with low plastic deformation in TMAZ, as this region was constrained by the lower steel plate. The tensile tests were used to plot the real stress / real strain curves for the HAZ and TMAZ and the latter showed much lower yield strength than former. The TMAZ yield strength was then used to define the test loads in cyclic loading test. The results of these tests showed that only when loading with 30% of the TMAZ yield strength was the infinite life achieved (10^6 cycles was chosen as the infinite life threshold). As such, although the use of multi pass welding resulted in wider bonded area and improved quasi-static strength, fatigue performance remained low.

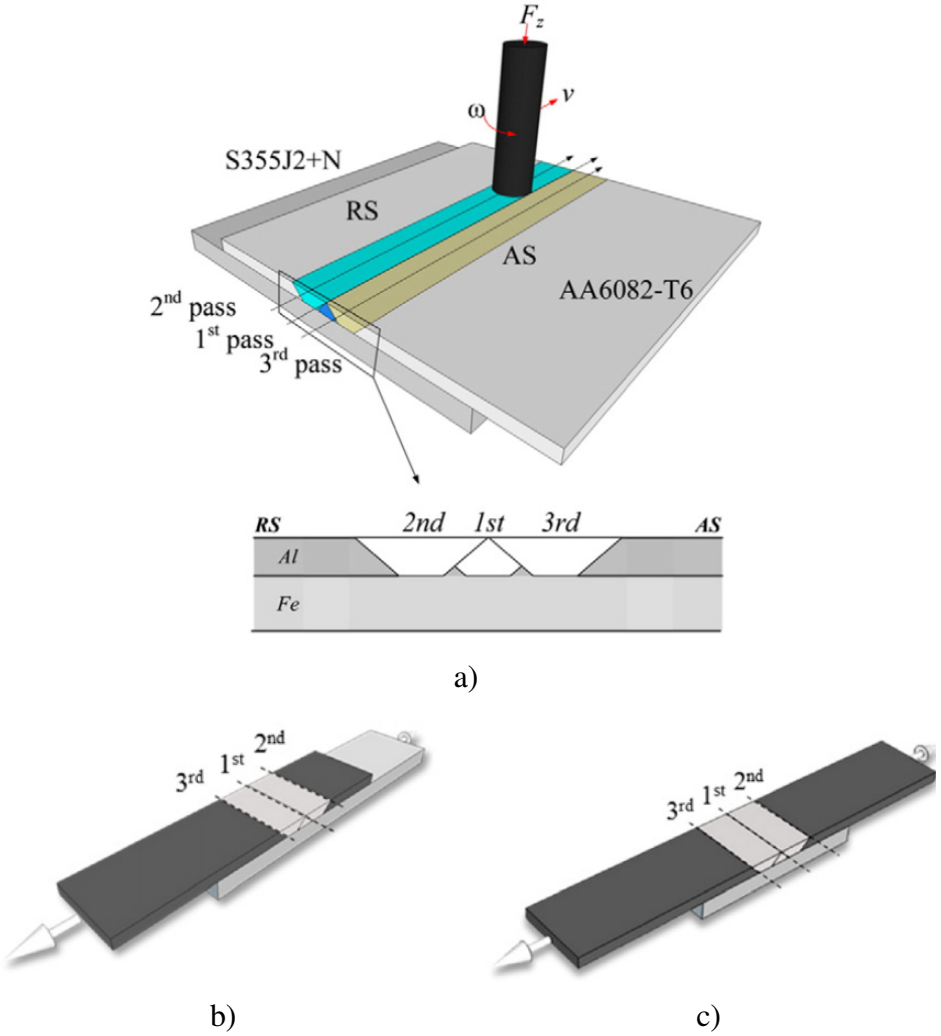

Figure 3.5: Schemes of triple pass joint (a) and shear-tensile (b) and tensile (c) joints used in [43] (adapted from [43]).

Regardless of the FSW joint configuration (butt-joint or overlap joint) to be employed in the assembly of large panels of hollow metallic structures, the absence of a suitable backing bar is a substantial engineering challenge. One concept that has been proposed capable of circumventing this challenge is the bobbin or self reacting tool. In this concept, no backing bar is required as the tool itself has a secondary shoulder capable of providing the backing force required during welding. The concept was first presented in a superficial way in the original patent relating to FSW [44], but was further developed by following inventors, such as in [45] and [46]. The potential application of these tool concepts both for hollow metallic structures as well as large thickness plates resulted in substantial research effort towards them. In [47] Threadgrill *et al.* were able to weld 25 mm thick AA6082-T6 aluminum alloy without defects using a bobbin tool. Huang *et al.* in [48] used a self-support FSW tool (similar to bobbin tool but with different size and shape shoulders) to join hollow AA6005 aluminum alloy hollow extrusions, demonstrating the possibility of welding hollow structures without fixed backing. Welding with these tools is substantially different from conventional tool plus backing bar, has the secondary shoulder will also generate friction heat. As such, Hilgert *et*

al. in [49] proposed three thermal 3D models capable of representing the weld process with these tools. The models were validated with experimental results, showing their potential for application. Bobbin tool is mentioned in [50] where a method for joining fuselage panels is patented.

Besides the lack of proper backing bar, the weld lengths and complex geometries involved in large shell structures, such as aircraft fuselages, are complex challenges to be overcome. Schulze *et al.* in [51] proposed a solution for FSW of large aircraft fuselage panels. The solution consists of a trolley with a welding head that moves along a set of rails that follow the curvature of the panels to be welded as well as the curvature of the weld line. The rails also hold vacuum pads that position the panels to be welded. A scheme of the system is presented in Fig. 3.6. The system proposed also made use of bobbin tool with stationary shoulders.

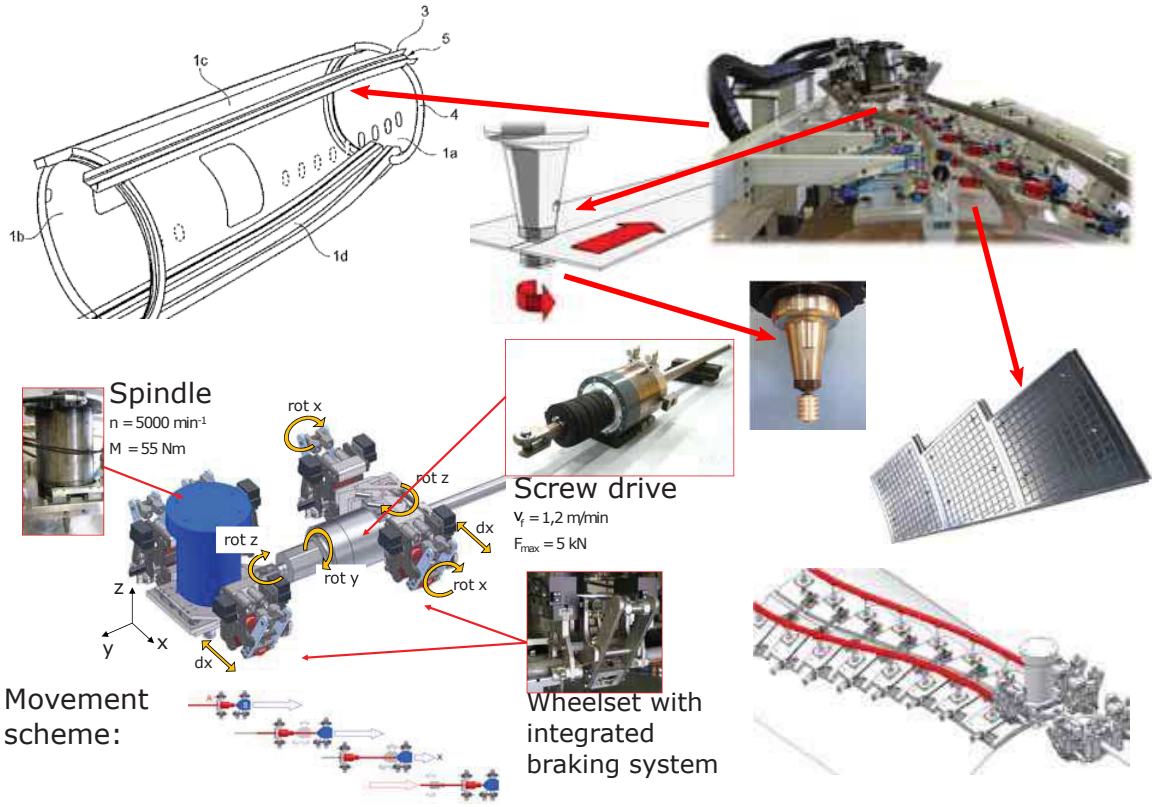

Figure 3.6: Scheme of the MUVAX system for FSW of large panels (adapted from [51]).

3.2 Adhesive Bonding

Beyond solid state welding, another joining technology that has shown high potential for disruptive innovation in structural design is adhesive bonding. Adhesive bonding, as a technique, has been extensively review in [52]. Even though its use in aeronautics dates more than 20 years, it is not extensively applied in this field as its potential would suggest. The reasons behind this are diverse, but in general adhesive bonding is not considered yet a fully reliable joining methodology [53, 54]. The promising potential of adhesive bonding in aero-

nautics is mainly due to the larger adoption of fiber reinforced composite materials, as current joining methods (employed in metallic structures) are not suitable for these materials. The use of bolts and rivets in structures made from these materials damage the continuous reinforcing fibers and as a result, will impact the load-carrying capacity of the structure [55]. Currently, adhesive bonding in fiber reinforced composite aerostructures is limited to non load-critical structures, as shown in Fig. 3.7 [56]. Limiting a more extensive use of adhesive bonding is the difficulty in inspecting bondline quality following manufacturing and during in-service life [57] as well as the sensitivity to environmental attack and physico-chemical conditions of the substrates.

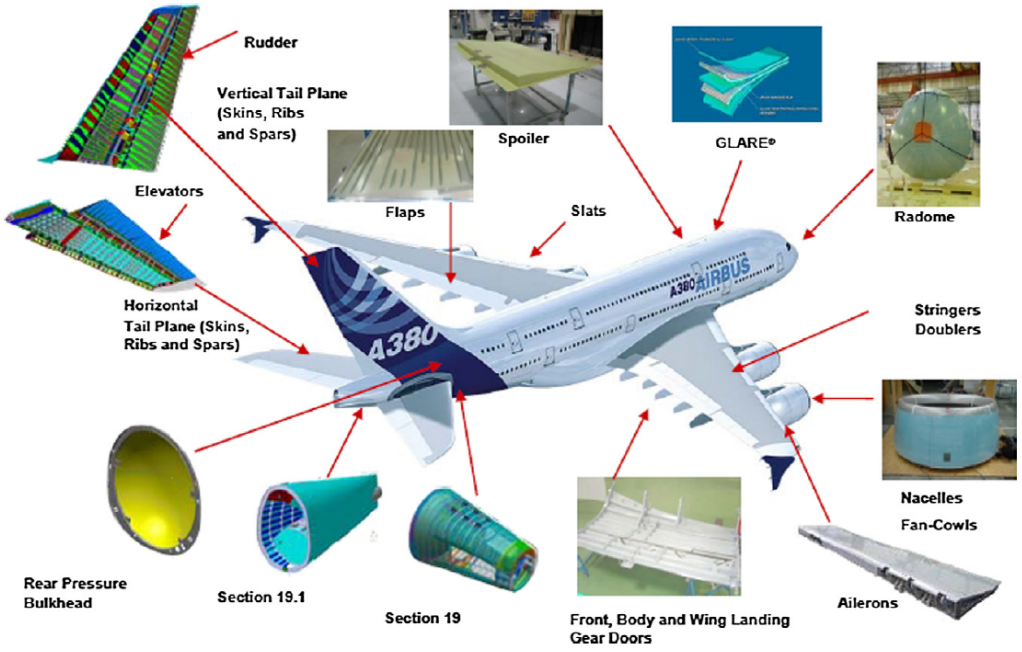

Figure 3.7: Adhesive bonding in the Airbus A380 [56].

Various studies have been performed regarding the effect of various manufacturing defects that may occur during adhesive joints manufacturing, as well as on non-destructive testing (NDT) techniques capable of detecting them. Adhesives, as polymeric materials in both the thermoplastic or thermoset form, require curing in order to transfer loads between substrates. As such, improper cure can compromise the integrity of the bonded joint. Aydin *et al.* in [58] studied the effect of curing pressure on the shear strength of adhesive bonded joints. The manufacturing of adhesive bonded joints requires the use of silicone-containing release agents, as to guarantee complete demolding upon curing. During the manufacturing process, these agents may contaminate the bonded area affecting the performance of the joint. In [59] Jeenjitkaew *et al.* studied the effect of surface contamination with Frekote® 700NC, a silicone-containing release agent, producing kissing bonds on aluminum alloy AA2014-T6 double lap joints with two different adhesives performance. A reduction of 27% in joint strength with the contamination was noted. In [60] Jeenjitkaew *et al.* used an electrically disbonding epoxy adhesive to also study kissing bonds in adhesive bonded joints. Through a constant DC current and the adhesive, the authors were able to reliably induce kissing bonds

in the adhesive joints, which were not detectable by C-Scan NDT analysis. The induced manufacturing defect resulted in a reduction of 57% in failure strength of the steel double lap joints.

High and low temperatures, both in operation and during curing, may also induce residual stress and affect the mechanical performance of bonded joints [61]. This is a particular concern in dissimilar material joints, as mismatch in coefficient of thermal expansion leads materials to expand an contract at different rates. Structural adhesives due to their polymeric material have very different mechanical behavior with different operating temperatures. For instance, if a dissimilar material joint is loaded below glass transition temperature (T_g), high thermal stress may lead the joint to fail prematurely, while if it is cured and loaded always above T_g, there is no generation and accumulation of thermal stresses. As such, adhesives, substrates, and joint geometry must therefore be carefully selected to minimize these effects. Beyond the induced thermal stress issue, structural epoxy adhesives have generally low flash points [62] when compared to metallic materials, which limits their applicability. The advent of new adhesive formulations, capable of operating at enlarged temperature ranges, partially addresses these drawbacks. However, the polymeric nature of structural adhesives will always exclude them from some applications, requiring mechanical fastening methods or welding procedures.

Environmental effects, such as moisture may also be detrimental to the adhesive joint performance, both when the adhesive joint is exposed to it or when it is present as a pre-bond condition. Structural adhesives as polymeric materials can absorb high quantities of water, leading to moisture-induced plasticization of the adhesive, which lowers its yield stress and stiffness and increases its strain to failure [63]. The effect of moisture in the adhesive can vary with temperature, as the absorption of water lowers the adhesive's T_g. When adhesive joints are loaded at low temperatures the effect of moisture is not very significant as temperature is bellow T_g, but when service temperature is higher adhesive's strength and stiffness are reduced and their ductility increases [64]. Performance of adhesive joints when subjected to moisture in cyclic loading may also be affected [65]. Costa el al. in [66] studied the effect of moisture on the fatigue crack growth in mode I through double cantilever beam (DCB) specimens. Although no change in the slope of the Paris Law was observed, a shift in the curves due to water absorption occurred. The lower crack growth threshold will therefore result in lower lifespan of adhesive bonded components when subjected to moisture conditions. When moisture is present before and during the curing process its deleterious effect may be even more severe than during service. In [67] the pre-bond humidity was demonstrated to have a significant effect on the crack growth resistance of joints made of aluminum alloy AA6060-T6 substrates with a one-component epoxy adhesive. Various surface treatments were employed in the study, such as sulfuric acid anodized (SAA) in AC and DC form as well as DC phosphoric acid anodization (PAA). Crack growth resistance decrease with increased humidity during curing process and especially so for the DC-SAA treated specimens. The increase in humidity also resulted in blister formation in the adhesive bondlines, which was correlated to the decrease in crack growth resistance. Water release from the conditioned adhesive and oxide films during curing of the adhesive was pointed to be the cause

for blister formation.

During service adhesive bonded components may be subjected to contaminants resulting from the operation of the equipment itself. In aviation, Skydrol is a phosphate ester used as hydraulic fluid and its leakage may alter the mechanical performance of adhesive joint it enters in contact with. Significant reductions in cleavage strength and tensile strength of adhesive bonded joints due to exposure to hydraulic fluids or kerosene based fuels, which are the main fuel type used in modern day aviation, have been reported in [68, 69].

Taking into consideration the various conditions (during manufacturing or in service) that can affect the performance of adhesive bonded structures, it is not only important to have very controlled manufacturing conditions but also reliable NDT technologies. Conventional NDT methodologies focus on detection of cavities but in the case of adhesive joints, defected joints may result from lack of adhesion and not due to the formation of cavities ("0 thickness defects"). As such, these methods are not suitable for adhesive joints quality control. Markatos *et al.* in [56] performed Ultrasonic and X-ray inspection along with fracture toughness evaluation of adhesive bonded carbon fiber reinforced composite joints with various manufacturing or in service defects. The scenarios studied were: poor curing, release agent contamination, moisture, Skydrol contamination and thermal degradation and they were compared to a reference scenario with no intended defect. All scenarios resulted in a reduced fracture thoughness, with reduced G_I^c and lack of cohesion through the epoxy film, demonstrated by the failure surfaces. The NDT methodologies employed did not identify in an obvious ways the joints defects, with only the Skydrol contamination and moisture scenarios showing apparent defects. In these cases the expanding gas during the bonding process due to water vaporization may be the cause for the formation of the porosity detected in the ultrasonic C-Scans. The unreliability of conventional NDT methods for adhesive bonded joints quality control was further discussed in [70]. More recently extended non-destructive testing, capable of ascertain selected physicochemical properties which are important for the performance of adhesive bonds have been developed. In [71], three extended NDT technologies were proposed for adhesive bonds. These are, optically stimulated electron emission, aerosol wetting test and laser-induced breakdown spectroscopy. These methods were tested for detecting different contamination layers such as release agent, moisture or hydraulic oil as well as thermal degradation of carbon fiber reinforced polymer (CFRP) adherent surfaces before adhesive bonding. These techniques demonstrated high potential as tools for detecting thin layers of a silicone-based release agent on carbon fiber reinforced polymer surfaces. Optically stimulated electron emission was shown to indicate surface states resulting from moisture uptake by the bulk of the composite panels, impact of Skydrol hydraulic oil contamination or thermal degradation. As such, these techniques are able to assess the quality of the surface prior bonding and may be used for quality assurance.

3.3 Hybrid Welding and Bonding

As a way of incorporating the advantages brought forward by adhesive bonding and also to overcome the mentioned difficulties associated with them, adhesive bonding has been

applied in conjunction with other joining methods, resulting in hybrid joining techniques. The broad range of mechanical and chemical characteristics of structural adhesives as well as their ability to bond dissimilar materials as allowed the combination of adhesive bonding with various other joining technologies.

One of the simplest hybrid joining methods developed combined mechanical fastening and adhesive bonding [72]. As mentioned in [73], various situations may justify the use of this joining method. For once the joint may be subjected to a combination of multiple loads. In this case, the adhesive carries shear stresses while the fasteners carry transverse loading. Another reason lies with the survivability of the joint in case of fire. With elevated high temperatures resulting from fire, adhesives soften and loading must be transferred from the adhesive to the fastener for the joint to survive. The use of fasteners to reinforce adhesive joints may also alleviate concerns over long-term performance of the adhesive when subjected to environmental conditions. An extensive review of this joining method is presented in [74]. This technology however is not attractive for high performing lightweight structures as the weight penalties from fastener joints remain as well as the challenging economic viability of large scale manufacturing.

Combining welding methods with adhesive bonding (weld-bonding) has been a more promising field of technology from industrial application perspective as well as from research point of view, with higher number and more recent research performed in this field. The original development of weld-bonding is reported to have been done in the USSR for the type AN-24 aircraft [75]. The method developed, relied in performing resistance spot welding first and then applying a low viscosity adhesive in the overlap interface. This approach is called “flow-in” method. By combining welding and adhesive bonding, structural designers achieved the following benefits when compared to conventional fastening techniques: i) reduced manufacturing costs and adaptability to mechanization; (ii) high static strength; (iii) improved fatigue strength; (iv) improved corrosion resistance; (v) the elimination of sealing operations; and (vi) the elimination of the shop noise of riveting. The “flow-in” method is highly laborious and as such not suitable for mass production. As such, an alternative approach was developed where the adhesive bonding was performed first followed by the welding procedure. This approach is called the “weld-through” method. Both techniques are schematically presented in Fig. 3.8.

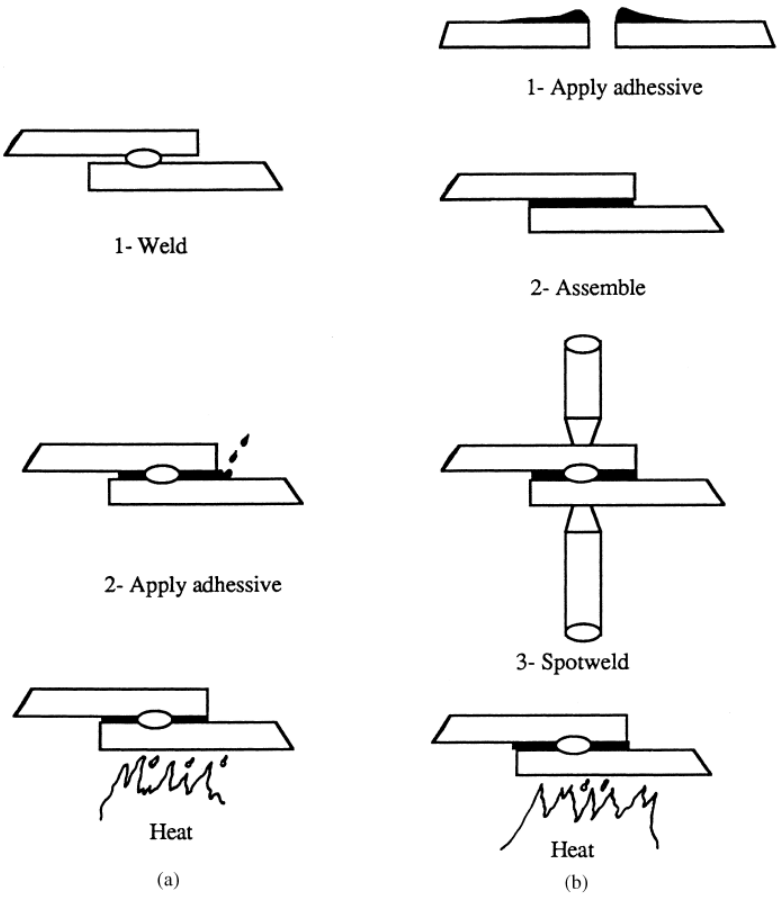

Figure 3.8: Weld-bonding in (a) flow-in method and (b) weld-through technique [76].

The use of weld-bonding based on resistance spot welding has seen adoption in the industry, mainly automotive structures, as this welding technique was already extensively applied. Some special care is required when choosing and adhesive for this purpose, not only related to temperature fields during welding process but also related with electrical conductivity of adhesive required for the welding process. Hybrid resistance spot welding and adhesive bonding has been reviewed in [77].

An experimental campaign was performed to compare the mechanical performance of several hybrid joining methods relative to the original joining technologies in [78]. The joining methods studied were, resistance spot welding, clinching, riveting, self-piercing riveting and adhesive bonding, along with the combinations of these with adhesive bonding. The authors employed a DoE methodology to study the effect of adherend thickness and material, pitch of welding / fastening, temperature and ageing on strength, stiffness and energy absorption in single lap joints. Regarding weld-bonding in this study it was verified that stiffness, strength and fracture energy was higher than in welded or bonded joints, as shown in Fig. 3.9. The use of weld-bonding also resulted in a lowered dependence from temperature and ageing when compared with adhesive bonded joints. Similar mechanical performance improvements were observed for hybrid-fastener joints.

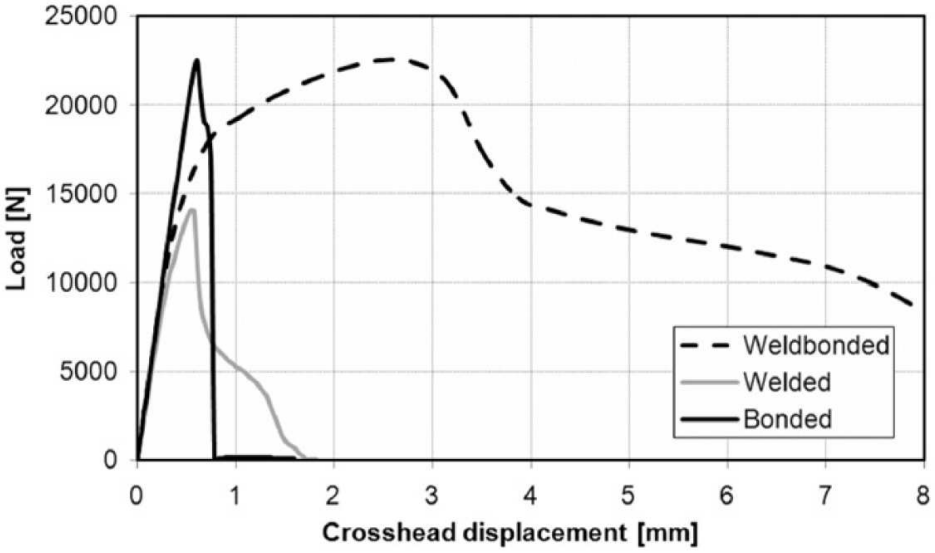

Figure 3.9: Comparison of weld-bonding with resistance spot welding and adhesive bonding of S275 lap joints [78].

Campilho *et al*. in [79] studied the mechanical performance of low carbon steel joints made with resistance spot welding, adhesive bonding and hybrid resistance spot welding and adhesive bonding using both an experimental and numeric approach. Cohesive zone model (CZM) for both adhesive and welding failure modeling was used and good agreement was found between experimental and numeric modeling results. A parametric study on the effect of the overlap length is presented here demonstrating the cases where the use of weld-bonding is beneficial and the ones it is not. For lower overlap lengths a significant improvement in joint strength was observed. This improvement is justified by the presence of singularities due to the stiffness variation between the weld-nugget and adhesive layer of about two orders of magnitude, increasing the tensile stress (σ_y) in the center o overlap (usually lightly loaded) as well as increasing the shear stress (τ_{xy}) in this region, as shown in Fig. 3.10. As the overlap length increases the nugget influence gradually diminishes, as peek shear stress is observed at the periphery of the overlap and not in the weld.

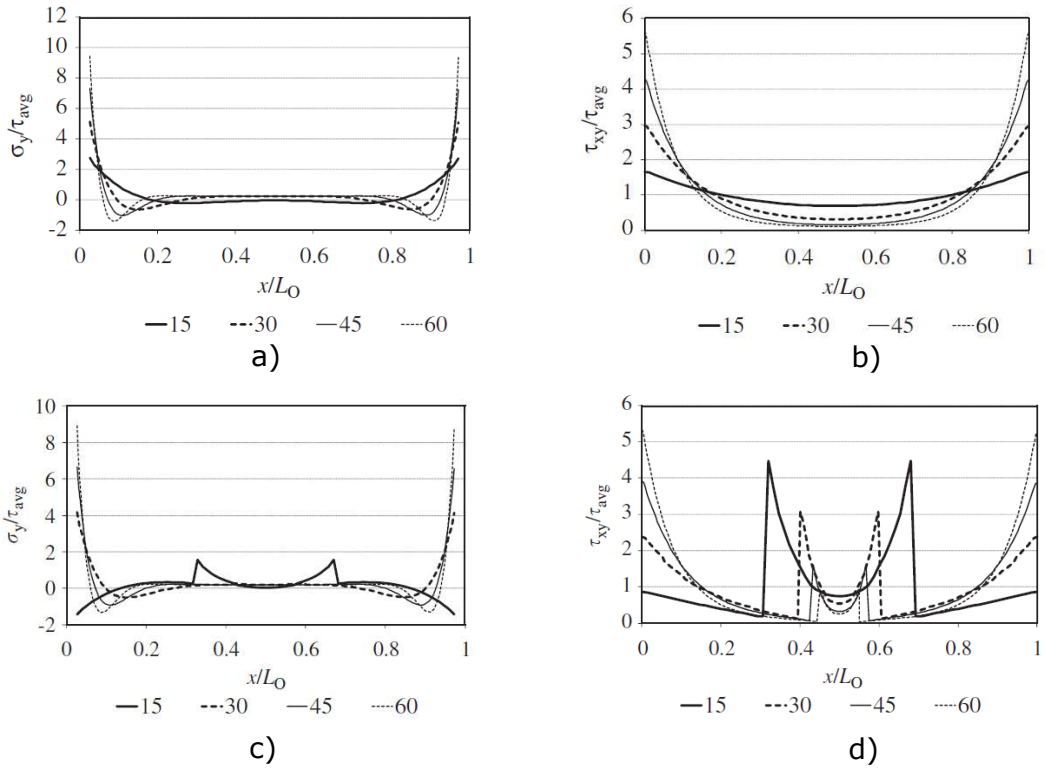

Figure 3.10: Normalized adhesive bonded σ_y (a) and τ_{xy} (b) and hybrid σ_y (c) and τ_{xy} (d) along the overlap length (adapted from [79]).

Other fusion welding technologies have also been combined with adhesive bonding to create hybrid weld-bonding techniques, such as MIG welding [80, 81], TIG welding [82], laser beam welding [83, 84, 85, 86, 87] and ultrasonic welding [88], among others. The general reasons behind the addition of adhesive bonding to welding processes are the following:

- Combining different mechanical properties in one joint (e.g. high ductility and strength);
- Capability of carrying different simultaneous loads in the joint (e.g. shear and peel);
- Damage tolerance (ability to carry load and not fail catastrophically even if part of the joint fails);
- Improved resistance to fatigue loading;
- Reduced noise and vibration dampening (improving noise vibration and harshness (NVH) in vehicles);
- Corrosion resistance (the adhesive serving as a sealant).

Friction stir welding, is a relatively more recent joining technology, and as such the combination of it with adhesive has not yet been as extensively studied as other fusion welding techniques. Studies on friction stir weld-bonding (hybrid friction stir welding and adhesive

bonding) are scarce and recent. Chowdhury *et al.* in [89] studied friction stir spot welding (FSSW a variant of FSW) with adhesive to joint dissimilar magnesium aluminum joints. Two millimeter AZ31B-H24 and AA5754-O were joined together using FSSW in three different combinations, (top)Al/Mg(bottom), Al/Mg with an adhesive interlayer, and Mg/Al with an adhesive interlayer. The adhesive used (Terokal® 5089) was an epoxy based one component adhesive and was cured at 170ºC for 20 minutes before welding. Welding these dissimilar materials resulted in the formation of hard intermetallic compounds (IMC), such as Al_3Mg_2 and $Al_{12}Mg_{17}$. In the case of the Al/Mg weld these IMC covered most of the boundary but the thickness of the interfacial layer varied, while in the Mg/Al with adhesive weld the adhesive was present in the interfacial layer with IMC remnants. The larger presence of these IMC and the increased bonded area from the addition of the adhesive resulted in significantly improved mechanical performance, both in quasi-static lap joint tensile testing as well as in cyclic loading (R=0.2), as shown in Fig. 3.11. The improvement in mechanical performance between Al/Mg with adhesive and Mg/Al with adhesive were due to lower melting point of the Mg when compared to the Al which resulted in the former softening more with the process temperature and as such penetrating further in the lower plate, causing more interlocking. The failure mode also varied between welds without adhesive with nugget debonding and welds with adhesive with nugget pull-out failure. This difference in failure mode was attributed to the IMC layer as it is much more fragile than the base materials. The same trend observed in quasi-static loading was observed in the cyclic loading tests, with the adhesive layer eliminating the stress concentration surrounding the weld along with the less predominant presence of IMC mentioned before. The failure mode was mainly similar to the one observed in quasi-static but some specimens failed perpendicular to the loading direction.

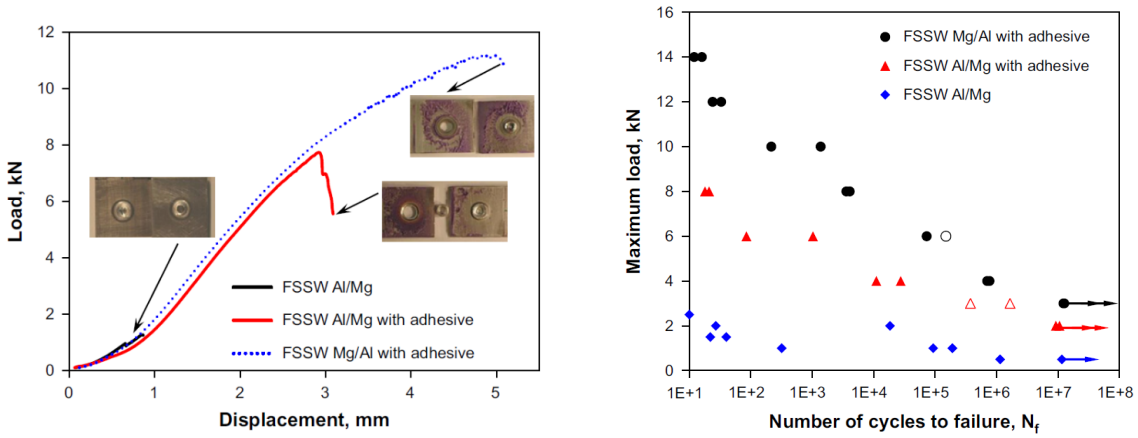

a) b)

Figure 3.11: Comparison of quasi-static lap joint tensile (a) and cyclic lap joint tensile (b) between dissimilar aluminum and magnesium joints with and without adhesive [89].

The use of polymer films as adhesives has also been studied in refill friction stir spot welding (rFSSW) in [90]. A PPS film interlayer was used in rFSSW of 2 mm thick aluminum alloy AA2024-T3 and 2.17 mm thick carbon-fiber-reinforced poly(phenylene sulfide)

laminate. Two parameters set were used, designated as low heat input and high heat input, relating to energy generated in the joint from the friction joining process. The use of the PPS film resulted in an increase of ultimate lap shear strength of about 55% for the low heat input condition. The higher heat input condition resulted in a decrease of the PPS film viscosity an as such allowed the film to be squeezed out as flash and as such not contributing as much to the mechanical performance of the joint. In this case the improvement in strength was of about 20%. The improvements in mechanical performance with the addition of the PPS film were due to larger bonding area (590 $\pm$ 50 mm^2 compared to 355$\pm$ 10 mm^2 with low heat input condition), as well as better load distribution from the hybrid joining mechanism. The failure surfaces also demonstrated improved micro-mechanical interlocking between the CFRP and the aluminum when using a PPS film interlayer.

A different approach to friction stir weld-bonding was presented in [91]. In this study friction stir welding was used to improve mechanical interlocking between adhesive bonded aluminum and carbon fiber reinforced polymer. This approach varies from conventional weld-bonding techniques as in these the goal usually is to improve the mechanical properties of the welded joint by adding adhesive bonding. Joining aluminum sheets and CFRP is challenging as they have very different physical-chemical properties, and as mainly been achieved through adhesive bonding and fastening. As alternative to these joining methods some welding processes were proposed and was found that achieving significant infiltration of aluminum around the fibers in these processes would result in improved mechanical performance. As such, the authors proposed using an FSW tool to promote heating of the bond area and promote softening of the aluminum. With varying parameters (spindle speed, welding speed and pin penetration) the authors found that just outside the destructive zone of stirring there lies a region where plasticized aluminum will infiltrate the carbon fibers, yet leave them intact. Carbon fibers processed in such a region and remaining in the direction they were processed. The resin of the CFRP and the softened aluminum act as an adhesive layer in the interface of the two sheets. An infiltration of about 3 layers of carbon filaments (17μm) was achieved and correlated well with the resin transfer molding model used to predict it.

As mentioned above studies on friction stir weld-bonding (continuous welding instead of spot joining) are scarce to non-existing. However, industrial entities have demonstrated interest in the process, which shows in patent applications. Christner in [92] proposed using a sealant / adhesive within surfaces of components to be friction stir welded, as seen in Fig. 3.12. In this invention the main purpose of the polymer material added in the welding is to protect the welded joints from corrosion. The example of welding stringer to skin using this invention is given in the patent. The effect of sealants in FSSW was also studied in [93]. Mechanical properties and corrosion resistance of joints performed with this technology were evaluated. The PRC-DeSoto PR-1432 GP sealan, a 2 part dichromate polysulfide compoud was used in FSSW of 1 mm thick AA2024-T3. The use of sealants was found to increase the joint strength but at the cost of increased scatter in the results. An improvement in joint strength was also found when compared with riveted coupons, as these only showed to have 44% of the strength of the FSSW with adhesive coupons. Corrosion resistance was

also tested with exposure to a controlled environment followed by lap joint tensile testing. The sealant within the FSSW showed to protect the joint by maintaining the same ultimate strength after corrosion exposure, especially when appropriate surface treatment processes were used.

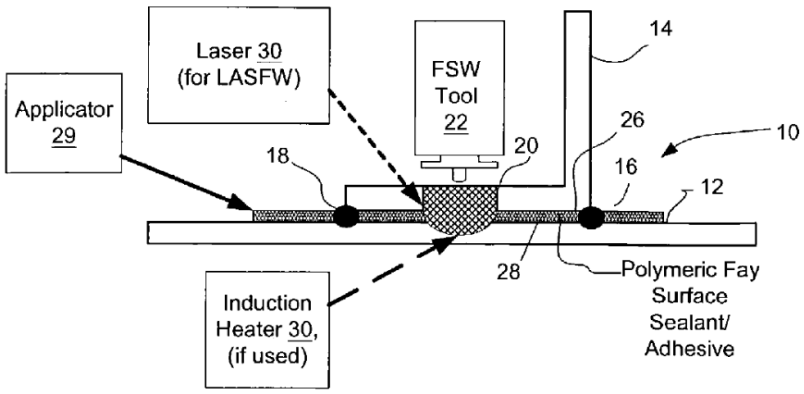

Figure 3.12: Scheme of FSW with sealant proposed in the invention [92].

Talwar in [94], proposed a method to join work-pieced by friction stir welding with and adhesive between at least two workpieces, see Fig. 3.13. The invention comprises both continuous friction stir welding as well as friction stir spot welding with adhesive.

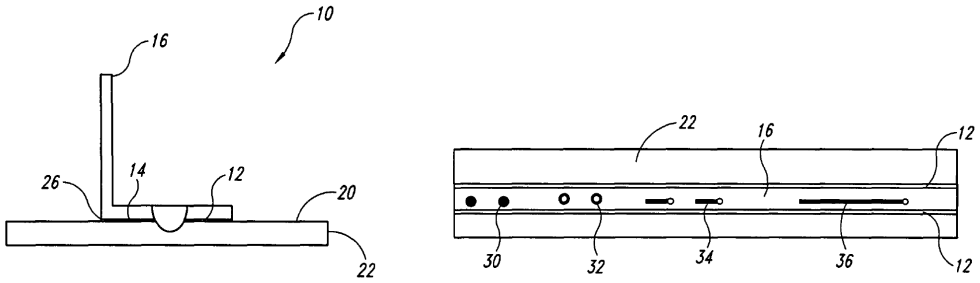

a) b)

Figure 3.13: Cross sectional (a) and top view (b) of join described in the invention [94].

In [95] a method for weld-bonding together metal sheets with an adhesive in between the sheets and with a cooling apparatus to avoid degrading the adhesive bond was developed. An example proposed in the patent where it is possible to see the welding and adhesive bonding along with the tool with the cooling apparatus is shown in Fig. 3.14. The invention proposes a cooling solution implemented in the tool that cools the surrounding material to the weld. This way the high temperatures required for sound welding are contained in the weld region and avoid degradation of the adhesive. Through this method the authors intend to avoid the need for distancing the welds or the increase of adhesive that is used to compensate the effect of the degraded adhesive.

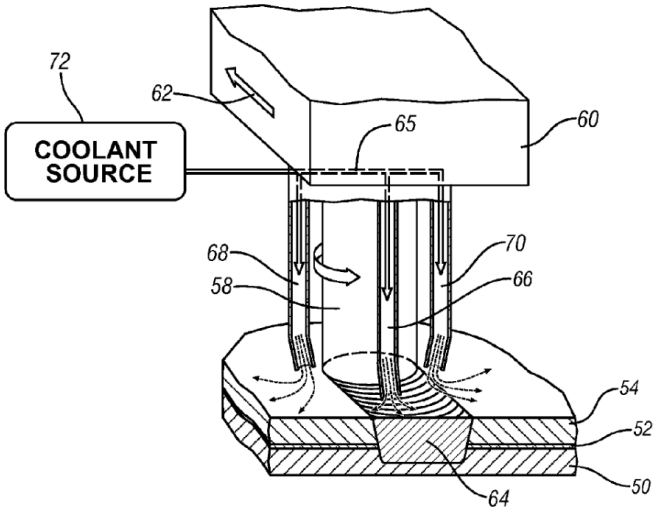

Figure 3.14: Example of weld-bonding as described in the invention [95].

3.4 Chapter Summary

A literature review on joining methods for metallic fuselages was presented in this chapter. Emphasis was given to new technologies and joining methods related to the ones to be studied throughout this PhD research. A significant number of published works on FSW butt-joining were found, given the disruptive potential of the technology. FSW overlap joints were less commonly studied due to the lower mechanical performance of these joints. Methods to mitigate the performance loss due to the joint geometry were studied in the literature, such as multi-pass welding. The combined use of solid state joining and adhesive bonding is not commonly found in the literature, but patent search showed industrial interest and application case of combined adhesive bonding and friction stir welding.

The research conducted during this PhD project and that is presented in the following chapters aims to complete the state of the art, by developing a friction stir weld-bonding technique, benchmarking it against overlap FSW and adhesive bonding, as well as to study its implementation in structural design. As shown in this chapter, few published results on hybrid friction stir welding and adhesive bonding exist. This thesis aims to fill this gap in the literature, by not only developing and benchmarking these joints, but also studying its application to longitudinal fuselage joints.

Chapter 4

Friction Stir Weld-Bonding

In this chapter the research work developed in this PhD project regarding the development of the metal joining technique, friction stir weld-bonding, will be presented. Experimental campaign and numerical models were developed and were used to benchmark the technology with adhesive bonding and friction stir welding. The methodology was developed in a laboratory setting, with intent to be applied in the future in a production environment.

4.1 Single Lap Joints Manufacturing

As mentioned in section 3.3, when discussing weld-bonding methods, two distinct methodologies exist, "flow-in" and "weld-through". The latter was chosen to be adopted in the development of friction stir weld-bonding, as the former would limit the choice of structural adhesive by viscosity and especially because a "weld-through" method, as mentioned previously in the literature review, presents several advantages concerning industrialization.

To develop the joining method it was opted to use AA6082-T6 aluminum alloy for its availability and relative low cost, as well as overall good weld ability and past experience within the work group concerning welding this alloy. The mechanical performance of this alloy and welds made with it will be further discussed in a following section. As part of the 6000 series alloys, the main components are magnesium and silicon, which precipitate in the form of Mg_2Si (β-phase) inside the α-phase aluminum matrix. The chemical composition is presented in Table 4.1. The T6 heat treatment was achieved through solution heating to approximately 530ºC followed by artificial aging at a temperature of approximately 180ºC. Precipitation hardening occurs during the latter stage, with the formation of β" and β' phases [96]. During the welding procedure, temperatures are high enough to change the temper state of the alloy, causing change in mechanical properties.

Table 4.1: Chemical composition of aluminum alloy AA6082-T6 (% mass) [97].

Mn	Fe	Mg	Si	Cu	Zn	Ti	Cr	Others (Total)	Al
0.40 1.00	0.50	0.60 1.20	0.70 1.30	0.10	0.20	0.10	0.25	0.10	Balance

The adhesive chosen was the Araldite 420 from Hunstman® (Salt Lake City, UT, USA). This adhesive, is a two part epoxy (thermoset) capable of cure at room temperature, but temperature will accelerate the curing process and improve its strength. This choice was based on its mechanical performance, resistance to elevated temperatures (important due to the welding process) as well as the previous experience of the work group with this adhesive.

Friction stir (FS) welds were produced on an ESAB® (Gothenburg, Sweden) LEGIO 3UL numeric control machine, shown in Fig. 4.1. The machine is capable of welding both in displacement control, as well as load control. The machine integrates a cooling system for the welding tool.

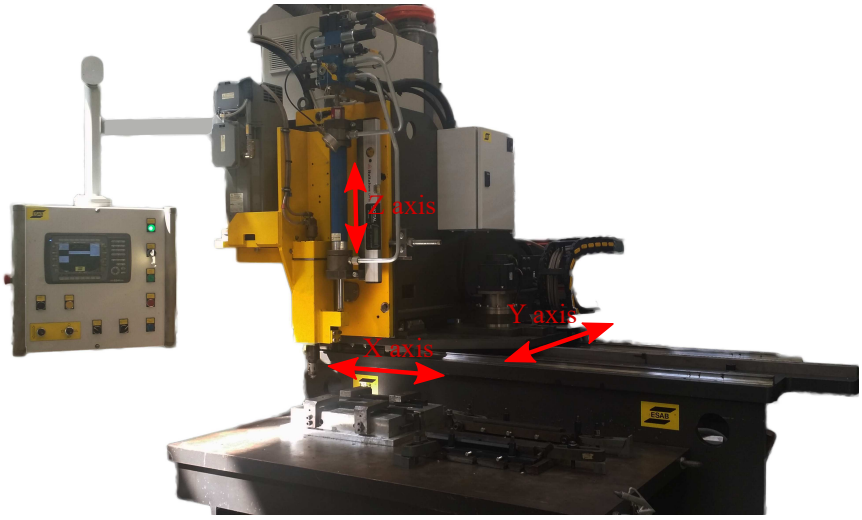

Figure 4.1: FSW machine used for aluminum alloy AA6082 joints.

Adhesive bonded joints and adhesive specimens for mechanical characterization were manufactured in a hot plate hydraulic press, with time, temperature and pressure adhesive curing control. The molds used (shown in Fig. 4.2) were of either steel or aluminum depending on the substrate material. Adhesive thickness was achieved through the use of spacers. Before adhesive deposition all the molds and spacers surfaces were covered with the release agent Frekote® 770-NC from Loctite® in order to allow a proper releasing of the specimens once the adhesives cure is complete.

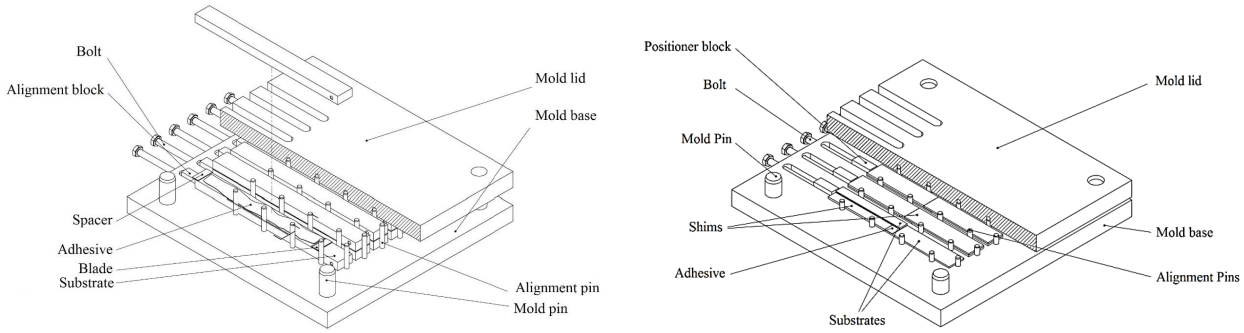

Figure 4.2: Schemes of Mold for a) fracture specimens manufacture and b) single lap joints manufacture. [98].

4.2 Materials and Joints Characterization

4.2.1 Base and FS Welded Material Characterization

As mentioned above, the heat generated during welding causes metallographic transformations and these will cause the material to behave differently from the as supplied material. In [99], the mechanical performance of FSW was assessed and bechmarked against the base material properties through quasi-static (1 mm/min cross-head speed) tensile tests, according to ASTM E8M standard [100]. The welds were made on a 3 mm thick aluminum alloy AA6082–T6 plate with a 6 and 15 mm pin and shoulder diameter tool, respectively. The welding parameters were, 800 mm/min; pitch angle of 2º and rotating speed of 1500 rpm. A 25 mm length clip gauge was used to measure the strain in the center of the specimens. A reduction in strength, both ultimate and yield, as well as ductility was observed in the welded specimens, as shown in Fig. 4.3.

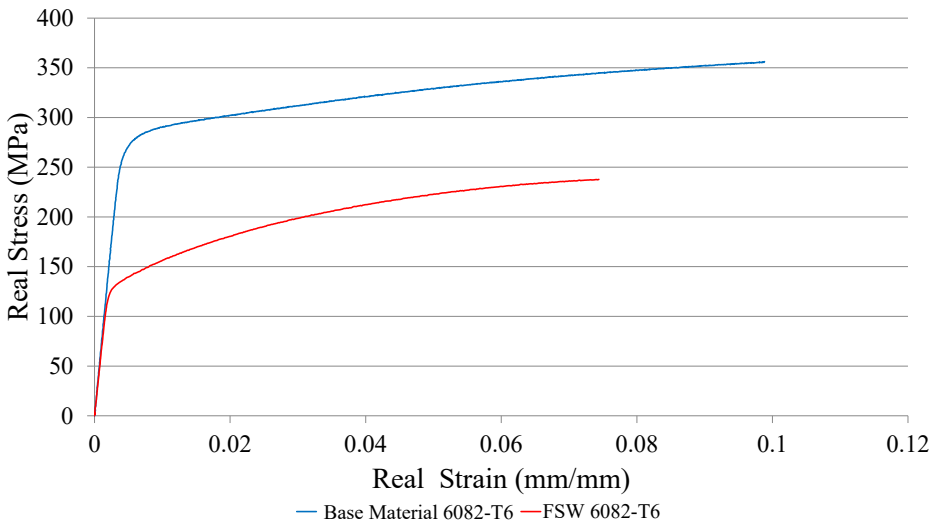

Figure 4.3: Base AA06082-T6 and FSW real stress vs. real strain curve (adapted from [99]).

As various material transformations occur due to heating and material flow in a very localized region in the center of the welded specimen, it was required to use an alternative method to measure strain and to better discretize the material behavior. DIC measurements were used in tensile testing of 3 mm thick welds in order to obtain stress-strain curves of the different regions identified in the weld. The FSW butt-joints were manufactured at 1000 rpm, 290 mm/min and displacement control with a probe length of 2.83 mm (≈94% penetration). These process parameters were obtained through the use of Design of Experiments (DoE), more specifically Taguchi Method and ANOVA analysis for optimization purposes, presented in [101]. Fig. 4.4 shows the identified regions in the weld to be analyzed with DIC.

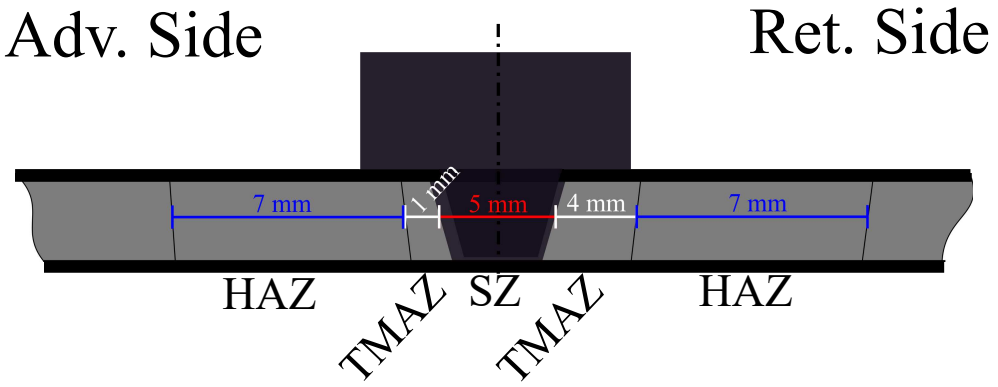

Figure 4.4: Scheme of weld affected material sections.

Tensile testing was performed at cross-head speed of 1 mm/min in the welded specimens, which were previously milled according to specification of ASTM E8M [100]. A VIC-3D workstation from Correlated Solutions® (Irmo, SC, USA) with a 4 MP camera was used for DIC in 2D mode on the side of the specimen to measure the strain in the full plane. Fig. 4.5, shows principal strain (ε_1) measured with this technique in 4 stages, initial (unloaded), elastic threshold, maximum stress and rupture onset.

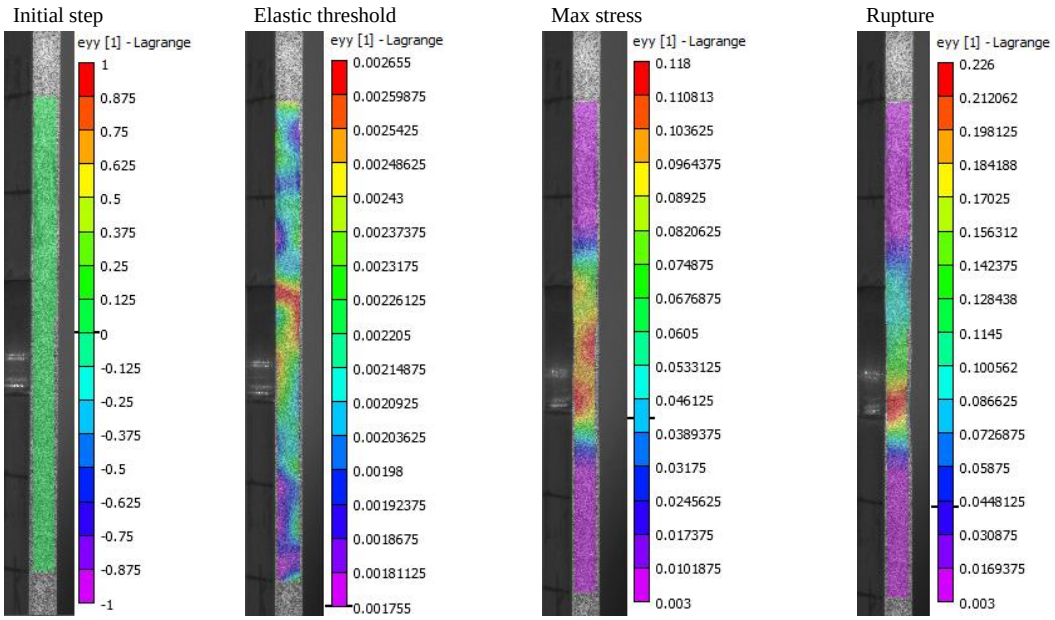

Figure 4.5: DIC measurements in four different time points.

The resulting curves for each material region are shown in Fig. 4.6. The specimens failed in the boundary between HAZ and TMAZ in the retreating side, similarly to what is found in the literature.

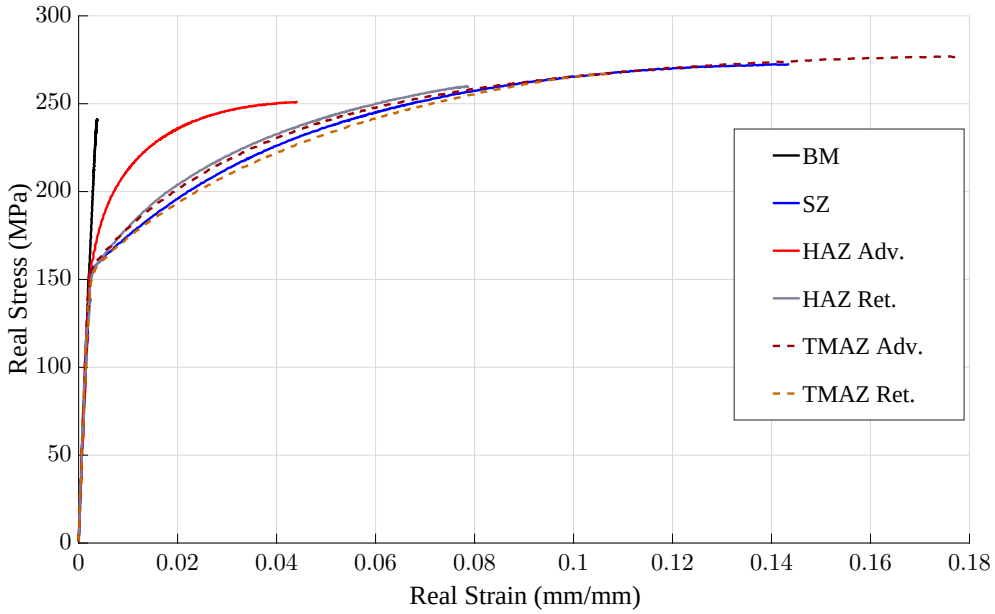

Figure 4.6: Real stress vs. real strain curves for the different material sections in the specimen.

It is possible to observe that different regions of the weld have different hardening behaviors, which should be considered in more detailed FEM models of welded joints. Due to necking, the loading and deformation in the specimen become heterogeneous and as such it is required to use hardening laws as a way of extrapolating the stress-strain curves of each

material region. The Swift and Voce isotropic hardening laws are presented in equations 4.1 and 4.2, respectively.

$$\text{Swift law} \qquad \sigma_s = K\left(\varepsilon_0 + \bar{\varepsilon_p}\right)^n \tag{4.1}$$

$$\text{Voce law} \qquad \sigma_s = \sigma_0 + Q\left(1 - e^{(-\beta\bar{\varepsilon_p})}\right) \tag{4.2}$$

where $\bar{\varepsilon_p}$ is the equivalent plastic strain, ε_0 is the yield strain, K and n are Swift law material constants, σ_0 is the yield stress, and Q and β are Voce law material constants. The relationship between the stress and the strain increments in plasticity can be derived from Hooke's law and the total strain decomposition assumption (total strain = elastic strain + plastic strain), as shown in equation 4.3.

$$\{d\sigma\} = [C]\{d\varepsilon^e\} = [C]\left(\{d\varepsilon\} - \{d\varepsilon^p\}\right) \tag{4.3}$$

where$\{d\sigma\}$ is the stress increment vector, $[C]$ the elastic stiffness matrix and $\{d\varepsilon\}$; $\{d\varepsilon^e\}$; $\{d\varepsilon^p\}$ are the total, elastic and plastic strain increment vector, respectively. The use of the incremental form here, is due to the history dependent characteristic in plasticity.

The extrapolation results are presented in Table 4.2. The high coefficient of determination (R^2) values show that there is good agreement between the extrapolation and the original real stress vs. plastic strain data.

Table 4.2: Hardening law material constants for the different weld regions.

	HAZ Adv.	HAZ Ret.	TMAZ Adv.	TMAZ Ret.	SZ	BM
ε_0	0.0047	0.0043	0.0044	0.0043	0.0043	0.006
σ_0	183.4	161	162.5	159.7	160.4	278.8
K	394.7	412.7	378.8	408.1	385	438.3
n	0.1341	0.1779	0.1561	0.1859	0.1654	0.0934
R^2_{Swift}	0.967	0.999	0.984	0.996	0.979	0.982
Q	67.24	408.2	113.3	123	116.2	91.31
β	109	32.2	26.33	20.44	24.08	19.06
R^2_{Voce}	0.997	0.999	0.998	0.999	0.999	0.993

Although the obtained extrapolated real stress vs. plastic strain data, was measured for the process parameters set mentioned, they will be used in the developed models of FSW and FS weld bonded of aluminum alloy AA6082 joints, as the resulting material zones should be considerably similar, changing only in dimensions between process parameters.

For aluminum alloys it is generally preferred to use the Voce hardening model [102], as aluminum alloys usually present a hardening saturation level, which is present in this hardening model.

4.2.2 Adhesive Mechanical Characterization

In an industrial environment, especially when joining large components, it is not always viable to completely control the adhesive curing conditions. As such the adhesive chosen must be capable of curing at room temperature as well as at elevated temperatures as per indication of the manufacturer. In the weld-bonding procedure, the adhesive layer will be subjected to a varying degree of elevated temperatures, which will result in different cures and mechanical behavior. The thermoset curing is an exothermic reaction and as such may be detected and quantified through differential scanning calorimetry (DSC). DSC analysis was performed on a Netzsch® (Selb, Germany) DSC 200 F3 equipment on specimens with a mass of ≈50 mg, at a constant heating rate of 20 K/min from 21ºC to 320ºC in an atmosphere of constant flow of 20 mL/min of N_2. The resulting DSC curve is presented in Fig. 4.7.

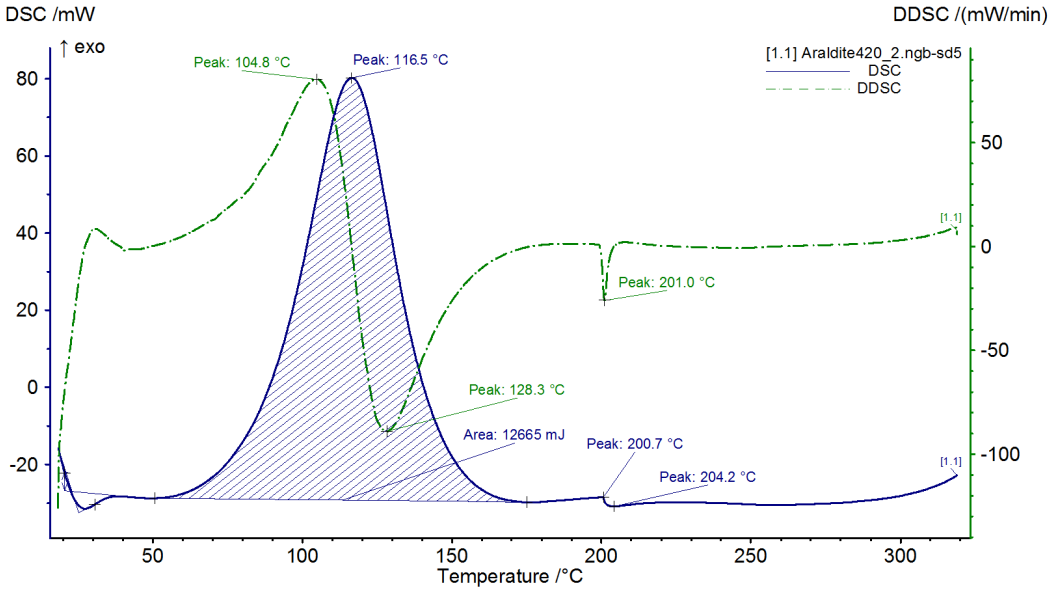

Figure 4.7: Representative curve of DSC analysis of the uncured epoxy resin.

DSC analysis showed that even though the adhesive may cure at room temperature, the majority of the curing process occurs at elevated temperatures, with peek curing at ≈120ºC. An endothermic event is also observed at about 200ºC in all samples tested, which is believed to be evaporation of water, after exceeding the sealing limit of the sample container (water vapor pressure at 200ºC is ≈15 Atm). Glass transition temperature of the uncured resin was not possible to measure as it probably is below the starting temperature of the test.

Glass transition temperature (T_g) is an important physical property of structural adhesives, as the stress-strain behavior of these polymeric based materials changes drastically if mechanically loaded above or below T_g. Polymer chain mobility is significantly smaller be-

low this temperature leading the material to become more brittle. Above it, the high degree of polymer chain mobility results in a "rubbery" behavior. Curing [103] and post-curing [104] conditions have been shown to affect the T_g in epoxy adhesives. To measure the T_g with room temperature cure for more than a week and 120ºC for one hour, an apparatus based on vibration damping measurement during heating and cooling was used. The apparatus presented in [105], is able to measure T_g much faster than DSC or thermo-mechanical analysis (TMA) and as such does not affect significantly the cure and the T_g itself while measuring it. Fig. 4.8 a) presents the measured T_g for both curing conditions and Fig. 4.8 b) shows a typical result from the dynamic mechanical test where it is observable the maximum damping at T_g.

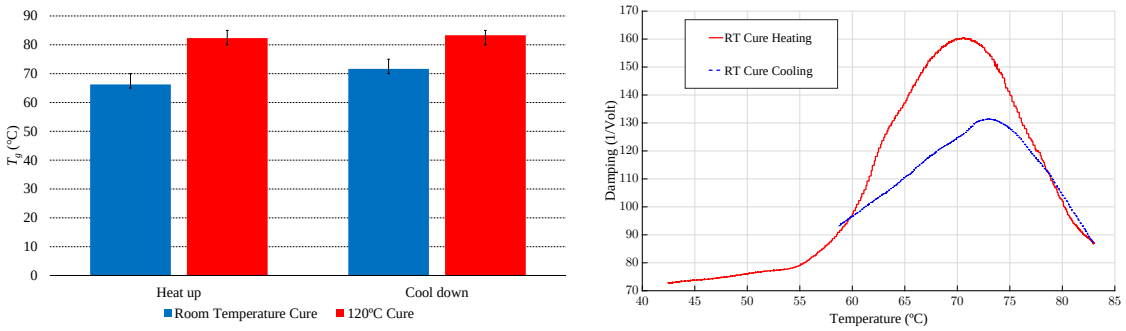

a) b)

Figure 4.8: Glass transition temperature with curing conditions a) and example of dynamic mechanical test for room temperature cure b).

The measurements showed that T_g in both curing conditions is significantly above room temperature which is the test temperature used throughout the rest of this study. It is also observed that between heating and cooling, T_g is kept constant when the adhesive is cured a 120ºC while, it increases slightly in the case of room temperature cure. As in the latter, the cure temperature is below the glass transition temperature of the fully cured network ($T_{g\infty}$), when subjected to temperatures above T_g further cross-linking of the polymer chains will occur increasing the T_g itself.

From the DSC analysis it may be inferred that full curing does not occur at room temperature, leading the adhesive to have different mechanical behavior with different curing conditions. To assess the tensile mechanical properties of the adhesive such as ultimate tensile strength σ_u , yield strength σ_0 and strain at rupture ε_u as well as estimating the Young modulus E, bulk tensile were performed at 1 mm/min cross-head speed in an Instron® (Norwood, Massachusetts, USA) testing machine. The specimens were manufacture in plates using a rigid metal mold with a silicon spacer to assure the specimens 2 mm thickness, in a hot-plate press. The curing conditions used were, room temperature for 7 days (24 hours in the press followed by resting outside the mold), 120ºC for 1 hour as indicated in the adhesive data sheet, 165ºC and 200ºC for 30 minutes. All cures at elevated temperatures were performed by closing the mold at room temperature followed by gradual and slow heating up to the set temperature and were cooled in contact with room temperature air, limiting this way the effect of residual stress in the specimens. The plates were milled into specimens

according to ASTM D638 standard [106]. Representative curves of each cured specimen are presented in Fig. 4.9. It is possible to observe an improvement in σ_0 and σ_u and reduction in ductility which may be associated with increased cross-linking of the polymeric chains with increasing cure temperature.

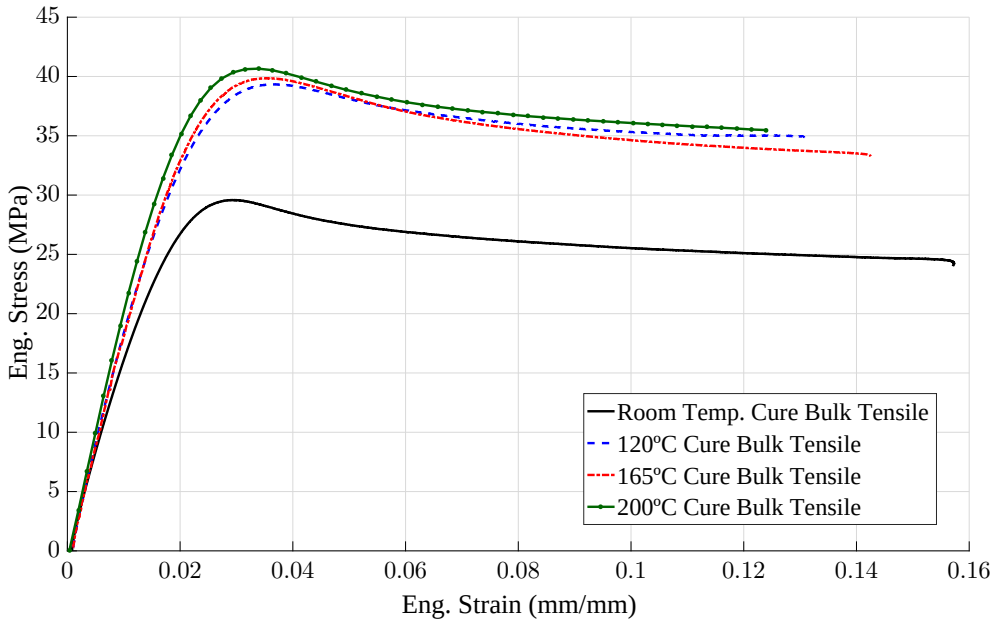

Figure 4.9: Bulk tensile eng. stress vs eng. strain with different curing conditions.

The effect of curing conditions is further confirmed when tensile testing specimens with different post cure procedures. Adhesive bulk plates that were previously cured at room temperature, as mentioned previously, were then subjected to a thermal cycle similar to the ones used for curing at elevated temperatures. The post cures were performed at 195ºC and 235ºC for 30 minutes. Fig. 4.10 presents representative curves of the tensile tests performed, where it is possible to observe that the post cure increases strength and diminishes ductility, demonstrating that the adhesive does not fully cure at room temperature. The increase in strength was not as substantial as the one observed with different curing temperatures, since the mobility of the polymeric chains are not as high as when the adhesive is in its uncured state.

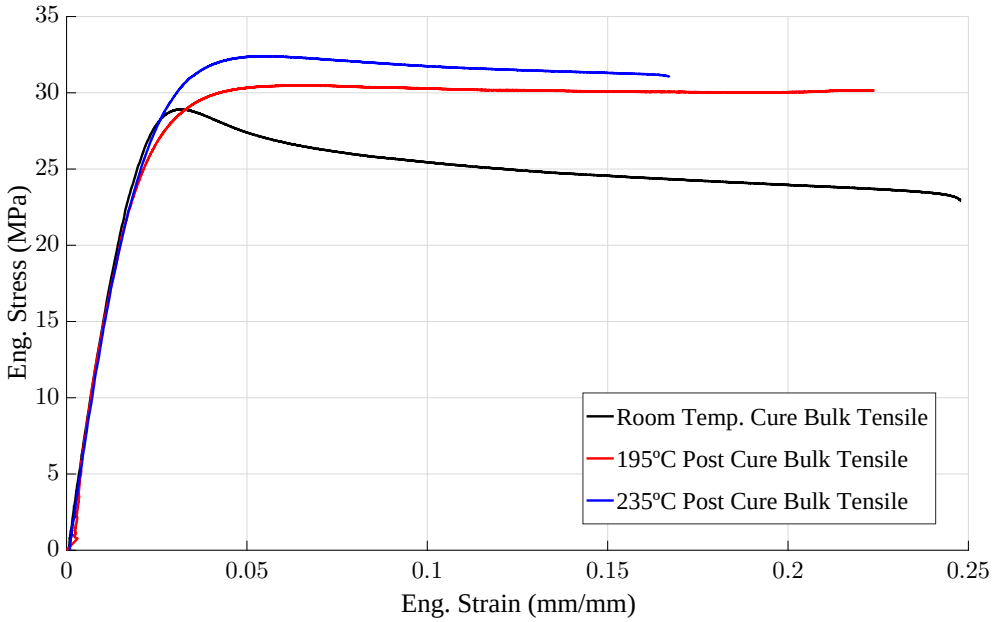

Figure 4.10: Bulk tensile eng. stress vs eng. strain with different post curing conditions.

In overlap joints, the adhesive will be subjected to both peel and shear stress. As such, it is important to account the shear mechanical properties of the adhesive along with the bulk tensile properties. Shear strength was measured through thick adherend shear test (TAST), based on standards ISO 11003-2:2001 [107] and ASTM D5656 - 10 [108]. Given the small axial displacements that occur in this test, a 3D DIC system was used to track the displacement in the specimen. Average shear stress was calculated by dividing the axial load by the overlap bonded area and the shear strain was obtained by dividing the difference in displacement of the substrates by the adhesive thickness. Fig. 4.11 presents a resulting average shear stress versus strain curve, along with the displacement measurement performed with DIC and the resulting failure surface.

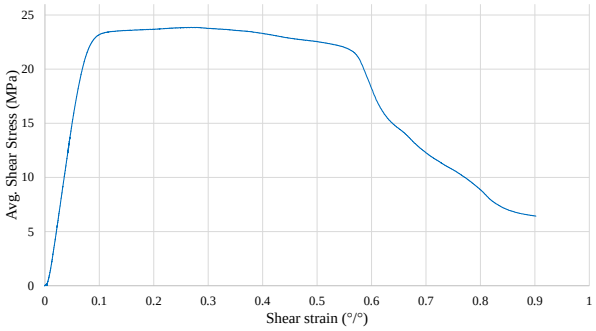

a)

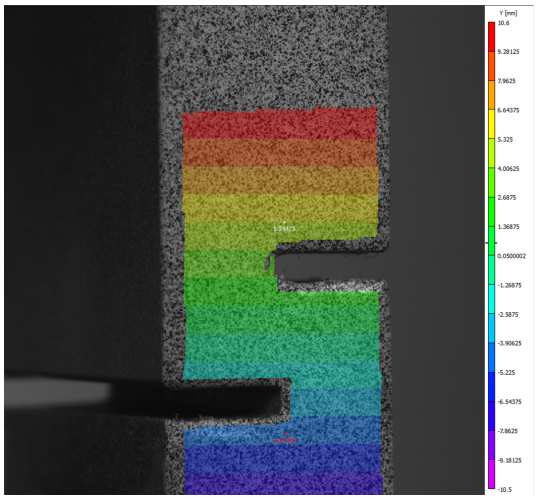

b)

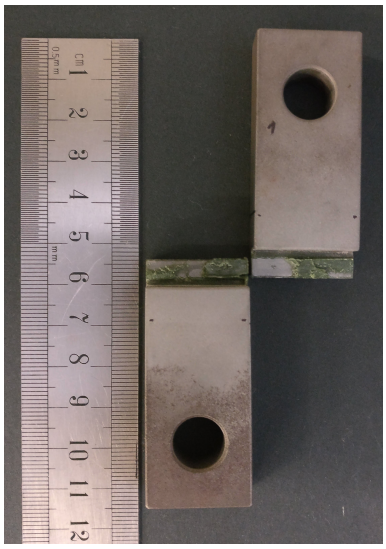

c)

Figure 4.11: Representative stress-strain curve for TAST of 120ºC cured adhesive a), displacement measurement with DIC b) and specimen failure surface c).

When cured at room temperature for 1 week and 120ºC for 1 hour, an ultimate shear stress (τ_u) of 21.3 $^{+0.89}_{-1.04}$ MPa and 27.6$^{+0.66}_{-0.46}$ MPa was measured respectively. The low viscosity of the adhesive when uncured and the fact that the steel substrates used in the TAST specimens were reused led to fillets at the ends of the overlaps, which resulted in scatter in the shear displacement measurement. The limitations of the TAST test have been discussed by some authors [109, 110].

To better assess the elastic properties of the adhesive in shear, the Poisson ratio (ν) was determined through an ASTM E132 - 17 [111] based test. For this purpose bulk specimens (shown in Fig. 4.12) were manufactured with a rectangular face with 150 x 25 mm and 2 mm thickness. Displacement control was used during the test with a constant cross-head speed of 1 mm/ min in an Instrom® E1000 machine. Digital image correlation was used to measure strain in both longitudinal and transverse direction. The resulting Poisson ratio was 0.433 $^{+0.009}_{-0.004}$.

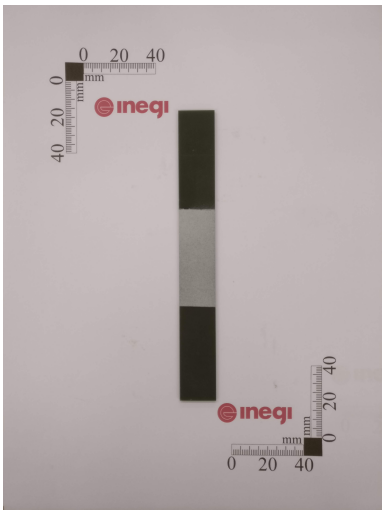

a)

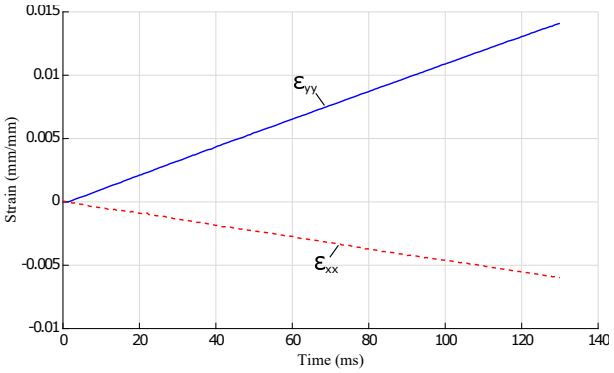

b)

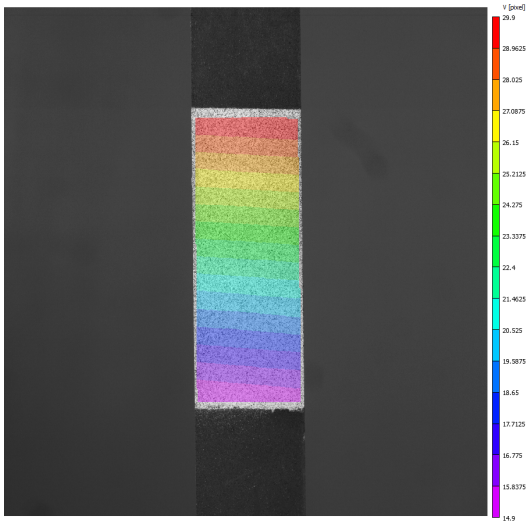

c)

Figure 4.12: ASTM E132 - 17 specimen a), strain in longitudinal and transverse direction b) and longitudinal deformation measurement at maximum load tested c)

One important issue when choosing an adhesive for a weld-bonding procedure is the degradation temperature. Even though friction stir welding results in lower temperatures in the work pieces, as the welding is performed in a solid state, or below the alloy melting point, temperatures are still high enough for a large majority of structural adhesives. Through thermogravimetric analysis (TGA) it is possible to determine the maximum temperature of operation for the adhesive, through the measurement of mass with varying temperature. The degradation of the polymeric material will result in a large loss of mass of the specimen tested. TGA was performed on a Netzsch® (Selb, Germany) Tg209 F3 Tarsus at 20 K/min from 21ºC to 600ºC. As shown in Fig. 4.13 the onset of degradation was found to be at 357^{+2}_{-3} ºC.

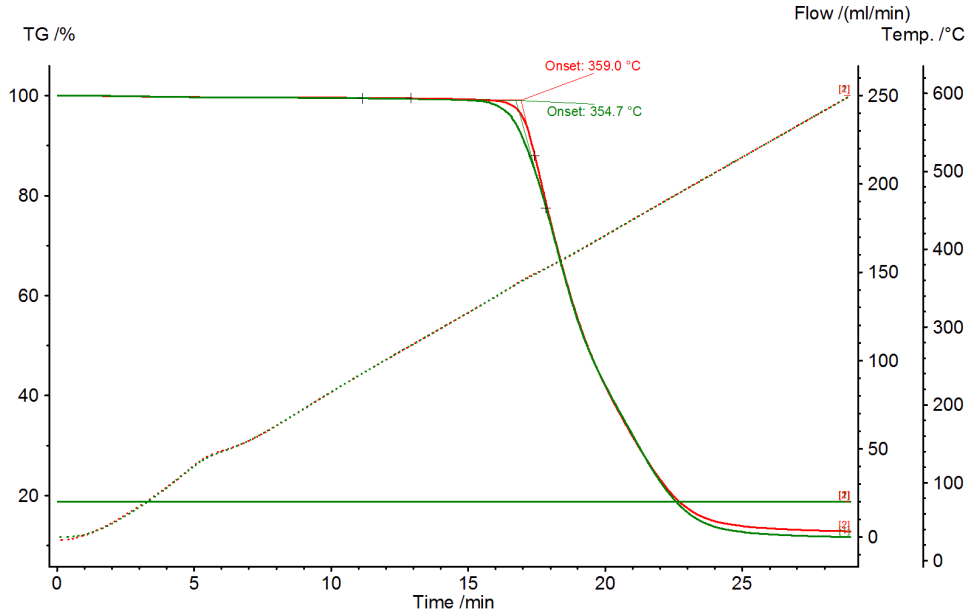

Figure 4.13: TGA of uncured Araldite 420 adhesive.

The strength of adhesive bonded joints will be dependent on the fracture toughness of the chosen adhesive. In order to assess the fracture toughness of the adhesive applied in this research project it was required to manufacture and test double cantilever beam (DCB) specimens and end notch flexure (ENF) specimens. These specimens are manufactured by bonding a 0.2 mm thick adhesive on steel beams with 320 x 25 x 12.7 mm. A notch is introduced in these specimens with a razor blade, from which an initial crack will be formed through pre-testing tensile loading. All fracture toughness specimens were cured at room temperature following the curing procedure mentioned above. DCB specimens were loaded under tension in displacement control with a cross-head speed of 1 mm/min. This loading results in a crack propagation in mode I in the adhesive layer. As measuring the crack length in the adhesive as it propagates is challenging and prone to error, a data treatment scheme relying only on the load displacement curve and the geometry and elastic properties of the specimens was used. Through the compliance based beam method (CBBM) [112], it was possible to plot the R-curves for the specimens tested. One such curve is shown in Fig. 4.14. A critical fracture toughness in mode I (G_{IC}) of 3 N/mm $\pm$ 0.37 N/mm was measured for the structural adhesive to be used in this research.

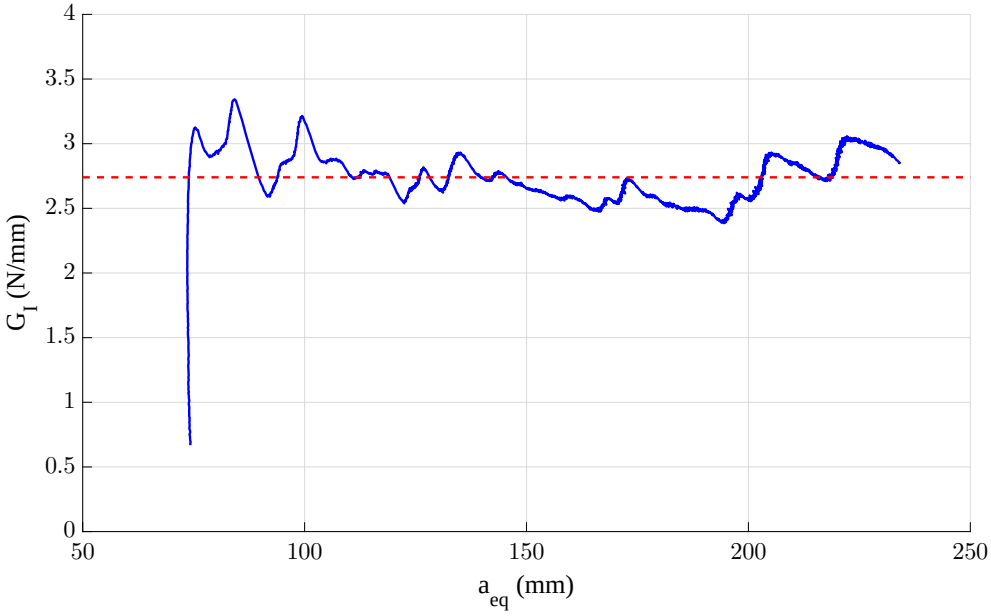

Figure 4.14: Representative Araldite 420 R-curve for mode I.

Mode II fracture toughness was assessed with the ENF specimens which have the same geometry and manufacturing procedure as the DCB specimens but are loaded in a 3-point bending apparatus. ENF testing was performed at 0.2 mm/min cross-head speed. Similarly to the DCB tests in mode I the ENF tests were also analyzed through CBBM method, but in this case for mode II loading [113]. A representative R-curve obtained in the ENF tests is presented in Fig. 4.15. The critical fracture toughness measured in mode II was 11.6 N/mm $\pm$ 0.3 N/mm. However, the maximum bending load was relatively high, which may have induced local plasticity of the substrate, and as such the measured mode II fracture toughness may be artificially high and must be verified through FEM modeling. This verification was made in section 4.3, through comparison of load displacement curves and R-curves of both experimental and numerical results. The suspicion was proven true, and the mode II fracture toughness of the adhesive was estimated to be 9 N/mm.

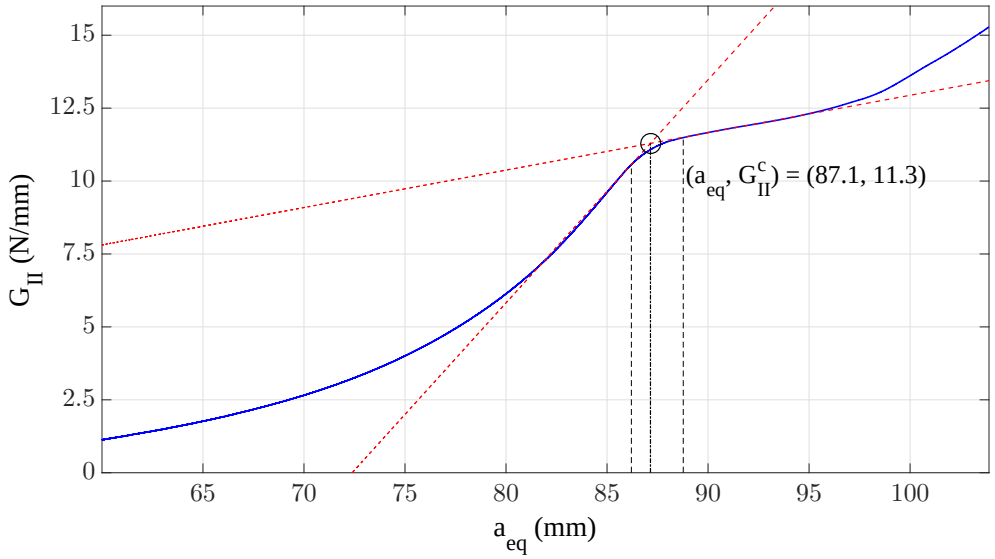

Figure 4.15: Araldite 420 R-curve for mode II.

The adhesive mechanical properties identified will serve as the basis for the numerical models developed and that will be presented in section 4.3. Table 4.3 summarizes the mechanical properties of the structural adhesive, with curing temperature. Mode II fracture toughness is marked with an asterisk, as the value was confirmed through FEM modeling.

Table 4.3: Summary of Araldite 420 mechanical properties.

Cure temperature	E (GPa)	G (MPa)	σ_u (MPa)	τ_u (MPa)	G_I^c (N/mm)	G_{II}^c (N/mm)
Room Temperature	1.57	600	30	22.5	3	9*
120 ºC	1.73	665	40	28	3	9*

4.2.3 Technically Feasibility and Process Parameters and Methodology

In order to study the technical feasibility of the joining process as well choose joint configuration and process parameters, an experimental program was undertaken involving the manufacturing and testing of 60 mm overlap joints. This large overlap length was chosen, as *a priori* the temperature field in the adhesive layer was not known and some adhesive degradation was expected.

FSW overlap joints with single and double pass welds were manufactured as reference. Double pass welding was used as it is a common employed strategy to improve the mechanical performance of overlap FSW joints, as mentioned in 3.1. An initial exploratory set of welds were made in order to set the process parameters window. These initial welds were evaluated in terms of macro defects and weld surface quality, in a qualitative analysis. Having set the process parameter window, the welds listed in Table 4.4 were manufactured for further study. It was observed that due to the proximity of the weld passes in double pass

welds and the heat generated softening of the material, the second pass must be performed under lower plunging force. The double pass welds were manufactured in a way that the advancing side was always facing inwards in the joint. This was achieved by contemplating the rotational direction of the tool and initial and end position of each weld pass. By doing so, the hook defect which originates on the advancing side will be unloaded.

Table 4.4: FSW overlap joints manufactured.

Joint tag	Weld pass	Plunging force (kgf)	Rotational speed (RPM)	Welding speed (mm/min)	Distance between passes (mm)
1-FSW-1	1st	400	1000	200	-
1-FSW-2	1st	450	1000	200	-
2-FSW-1	1st	400	1000	200	12
	2nd	320			
2-FSW-2	1st	450	1000	200	12
	2nd	400			

The hybrid joints manufactured at this stage had the same geometry and were also tested with single and double pass weld configurations. The use of purpose made channels for the adhesive in the overlap or continuous adhesive layer was also tested here. The channels were made by milling two 0.2 mm high and 10 mm wide grooves in the lower plate of the joint, as shown in Fig. 4.16.

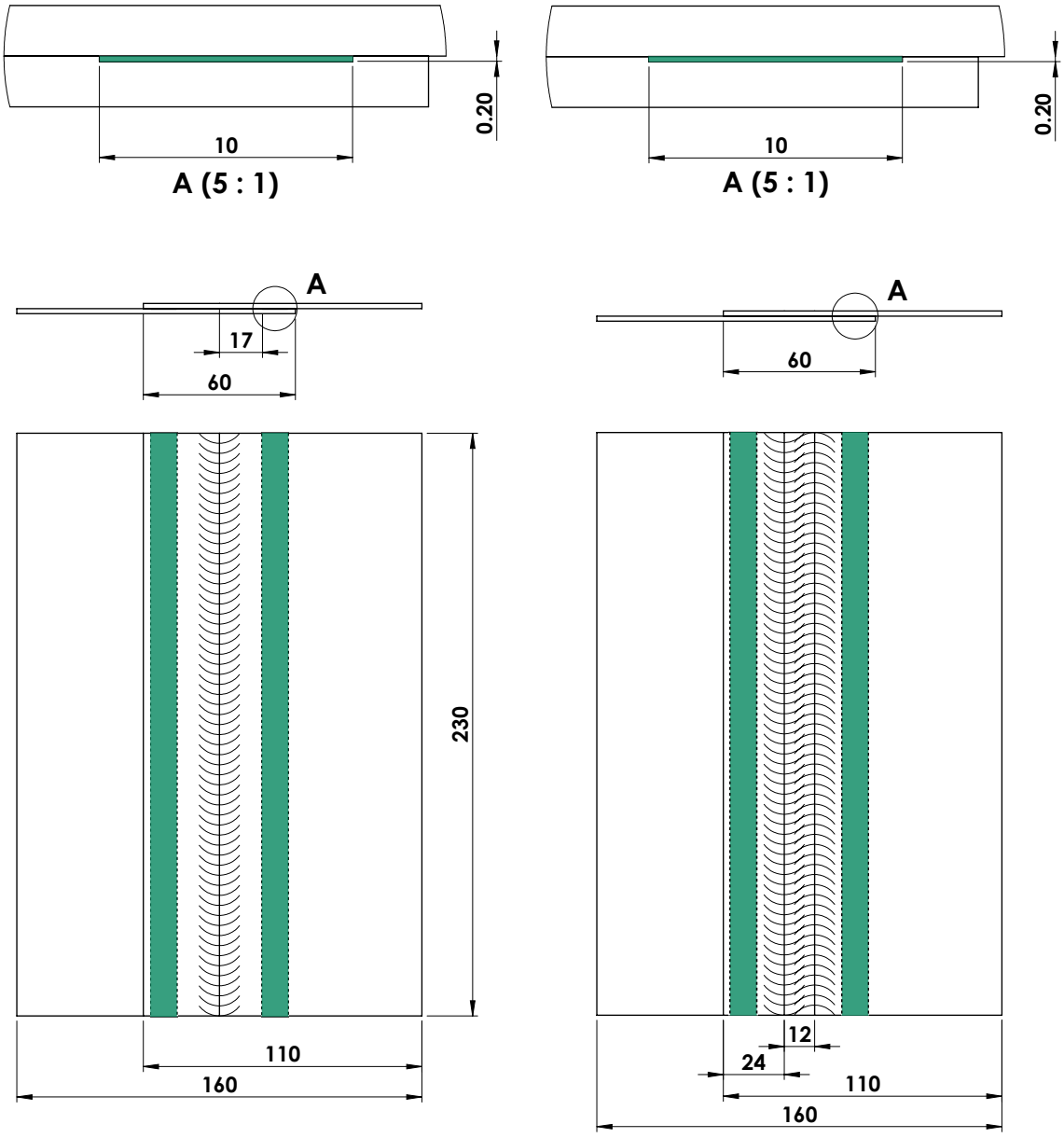

a) b)

Figure 4.16: Single lap joint scheme with channel for adhesive with a) single weld pass and b) double weld pass.

To manufacture the hybrid joints, the adhesive is laid onto the surfaces to be bonded of the lower joint plate and the welding procedure is performed with the adhesive in a non-cured form (welding within 15 minutes after closing the overlap). All of the manufactured hybrid joints at this stage were sandblasted and degreased with acetone before bonding. The list of hybrid joints manufactured and tested are presented in Table 4.5.

Table 4.5: Hybrid overlap joints manufactured.

Joint tag	Weld pass	Plunging force (kgf)	Rotational speed (RPM)	Welding speed (mm/min)	Distance between passes (mm)	Channels for the adhesive
1-Hyb-1	1st	400	1000	200	-	Yes
1-Hyb-2	1st	450	1000	200	-	Yes
1-Hyb-3	1st	400	1000	200	-	No
1-Hyb-4	1st	450	1000	200	-	No
2-Hyb-1	1st	400	1000	200	12	Yes
	2nd	320				
2-Hyb-2	1st	450	1000	200	12	Yes
	2nd	400				
2-Hyb-3	1st	400	1000	200	12	No
	2nd	320				
2-Hyb-4	1st	450	1000	200	12	No
	2nd	400				

The higher temperature in the overlap from double pass welding leading to increased softening, combined with the constant adhesive layer between sheets, which damps the tool loading onto the work pieces, resulted in the tool excessively penetrating the sheets, causing emergency stops of the machine. As such the joints combining these two effects (2-Hyb-3 and 2-Hyb-4) could not be obtained defect free and were disregarded from the analysis.

4.2.3.1 Temperature measurements

Temperature in the adhesive was measured in the 2-Hyb-2 joint as this joint process parameters result in the highest heat input (double pass and higher Plunging forces). Measurement was made with 0.1 mm diameter K-type thermocouples positioned along the joint according to the scheme shown in Fig. 4.17. The positioning of the thermocouples was achieved by drilling 1 mm through holes in the upper plate that were then used to place the thermocouples after closing the joint.

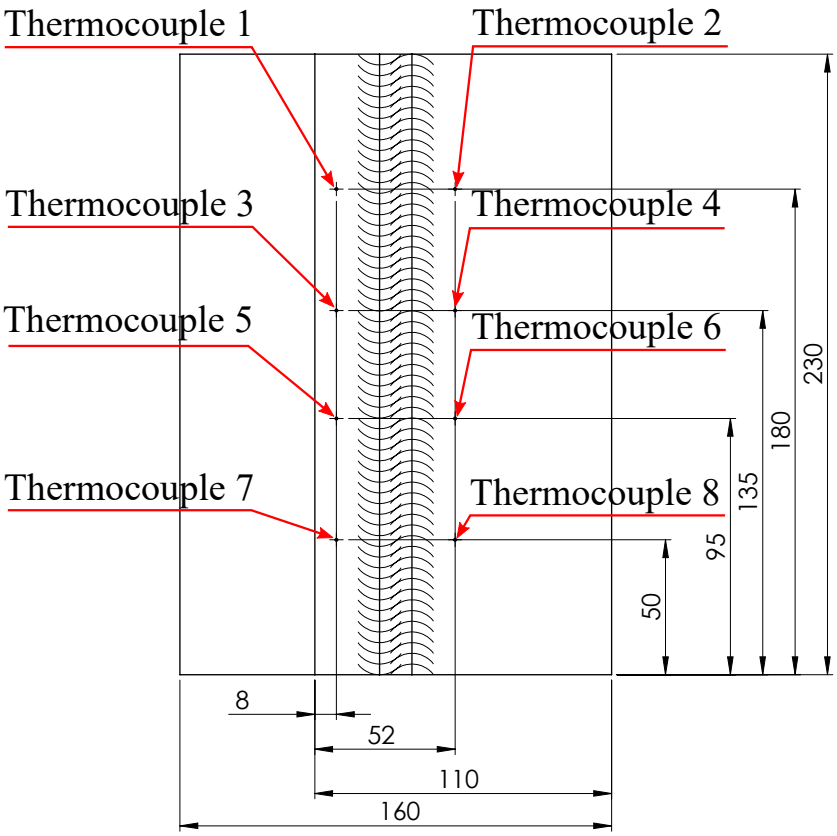

Figure 4.17: Thermocouples positioning in the joint.

Temperatures, shown in Fig. 4.18, measured in the adhesive were found to be below the degradation temperature, which as indicated above is 357ºC. As expected temperature increased from beginning of the weld to the end as the cumulative heat input transfer to the work piece increases. Similarly it was also found that temperatures achieved in the second pass were higher than those measured in the the first one, as the joints do not have enough time to dissipate all the heat.

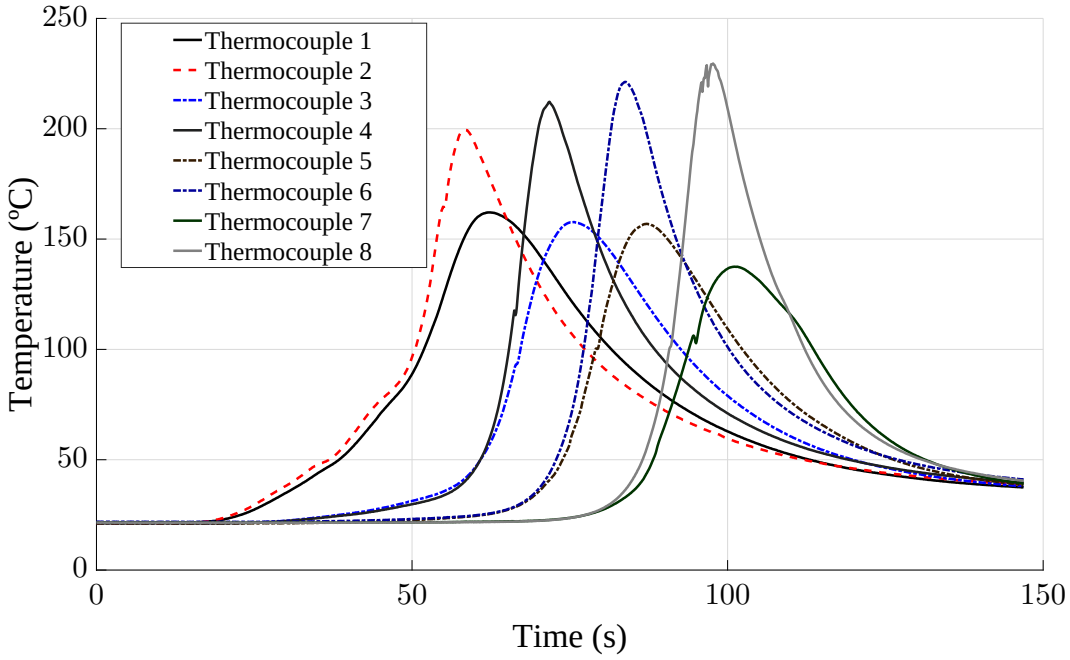

a)

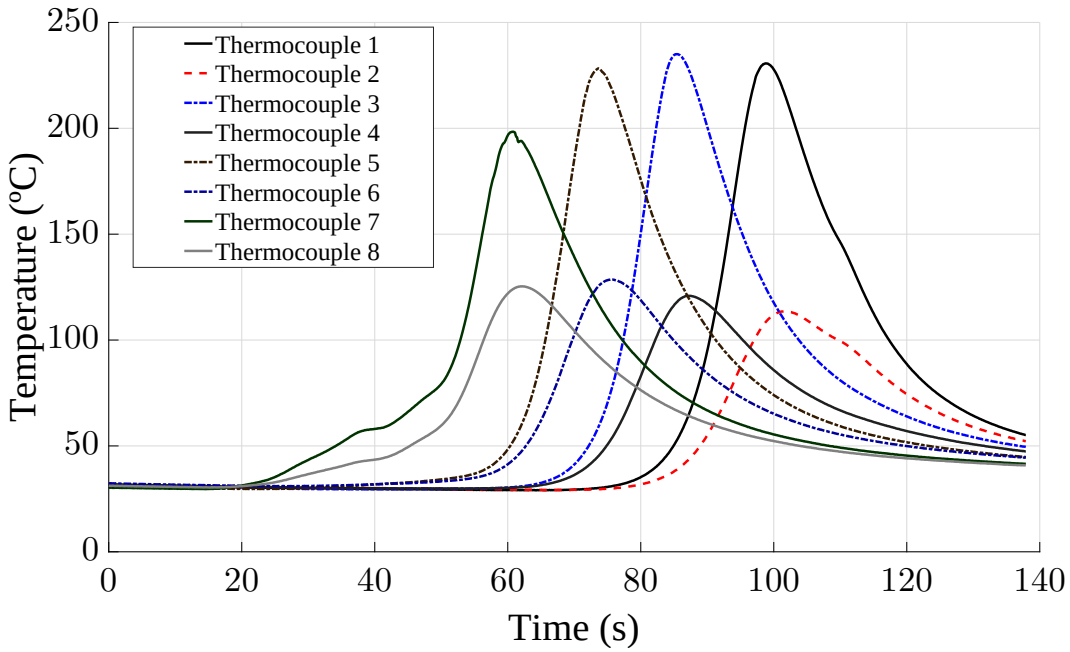

b)

Figure 4.18: Temperature measurement in a) the first welding pass and b) the second welding pass.

4.2.3.2 Distortion measurements

In order to evaluate the effect of the adhesive layer on distortion of the joints, distortion measurements of the FSW and hybrid joints were made. The heat input from the welding process inevitably results in distortion on the final joint, but has epoxy materials generally have lower thermal conduction coefficients than aluminum, the distortions should differ between hybrid and FSW joints. A structured light scanning system (David-3D® scanner), shown in Fig. 4.19 a) and a purpose made Matlab® code, were used to compare the distortion in the joints.

The surface topography was measured always on reverse side of the lower plate as indicated in Fig.4.19 b).

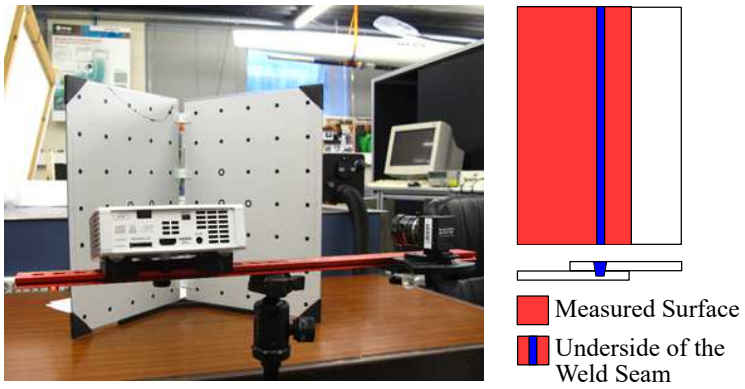

a) b)

Figure 4.19: Structure light scanning set up a) and scheme of the measurement in the joint b).

The Matlab® code uses the topography measurements to calculate a simple numerical value per measured joint for easier comparison. This value is obtained by calculating the average plane of the surface and two additional planes parallel to this average plane. These planes intersect the surface at the two most distant points to the average plane. The distortion value is given as the distance between these tool parallel planes. An example of a measured surface, and the planes used for the calculation is shown in Fig. 4.20.

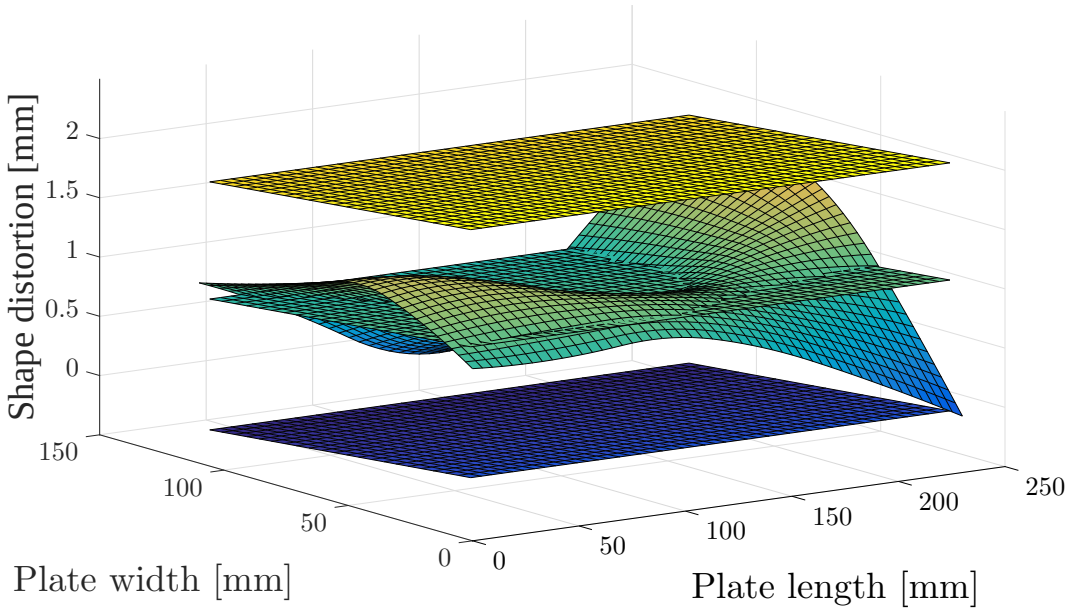

Figure 4.20: Example of distortion measurement (z axis not to scale).

The measured distortion levels in FSW joints are presented in Fig. 4.21. Single pass FSW joints showed to be very sensitive to the heat input (from different Plunging force) during the weld, as distortion increased about 110% from 1-FSW-1 joint to the 1-FSW-2. When using double pass welding this increase was less significant, possibly due to the area being affected

by the heat input being larger than in the case of single pass welds. The distortion measured on the double pass welds was higher than the single pass lower heat input joints, but lower than the single pass higher heat input joints.

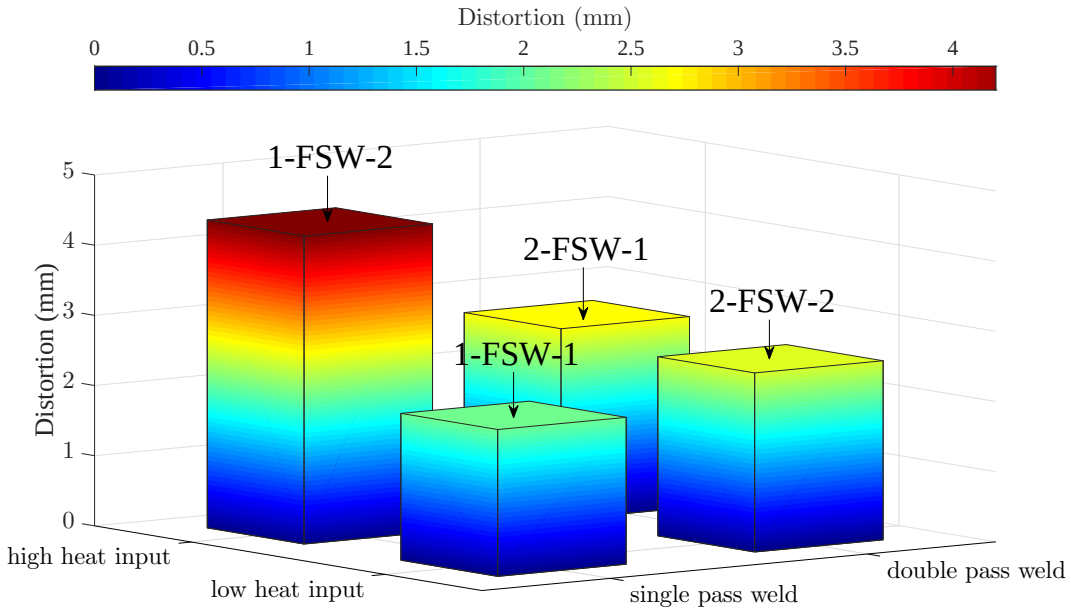

Figure 4.21: Distortion measurement in FSW joints.

In the case of hybrid joints, shown in Fig. 4.22, the plunging force seemed to have little effect on the distortion of the joint. The distortion levels on single pass hybrid joints were similar in all joints and equal or lower to the distortion measured in the FSW joints. This may be explained by the increased constrain level in the overlap as the adhesive decreases the level of free movement of the joint, resulting in lower distortion, albeit possibly increased residual stress. Besides this, the adhesive may also serve as a thermal insulation, leading to a more uniform thermal field which may have reduced thermal gradients. Double pass welds resulted in higher distortion levels and this may be associated with the insulation effect of the adhesive as less heat is conducted away from the overlap from the first weld pass, as the second weld pass introduces more heat in the overlap. The temperature measurement in the adhesive layer, mentioned above may serve to prove this effect as the temperatures in the adhesive were shown to be higher at the moment of the second weld pass, leading to believe that some resistance is found to the heat transfer in the adhesive layer.

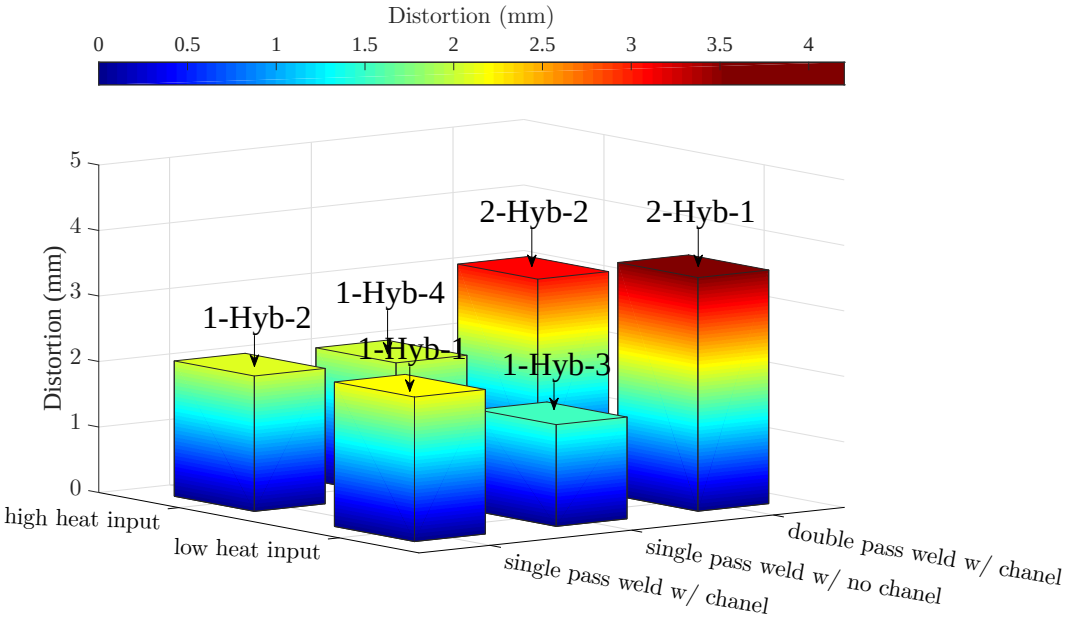

Figure 4.22: Distortion measurement in hybrid joints.

4.2.3.3 Single lap joint tensile testing

After manufacturing the FSW and hybrid joints, these were cut into 20 mm wide specimens based on ASTM D1002 [114] standard. The single lap joint specimens were loaded at a constant 1 mm/min speed up to failure.

Adhesive bonded joints were made with the same geometry as the FSW and hybrid single lap joint specimens. The same surface treatment as in the hybrid joints (sandlbasting and degreasing with acetone) was used initially.

In FSW overlap joints, the use of double pass welding was shown to be beneficial in terms of ultimate strength and ductility as may be observed in Fig. 4.23. This improvement was expected as the use of double pass not only resulted in the advancing side of the weld facing the inside of the joint but also increased the width of the effective overlap as in [42]. The difference in strength within single pass welded joints was not found to be significant as the differences in ultimate strength were within the margin of error. In double pass FSW joints, the higher heat input (higher plunging forces) resulted in an improvement of 17% in ultimate strength. The increase in strength was attributed to a better material flow, as the microscopic observation of the joints cross-section showed a reduction of the unwelded tip in these joints.

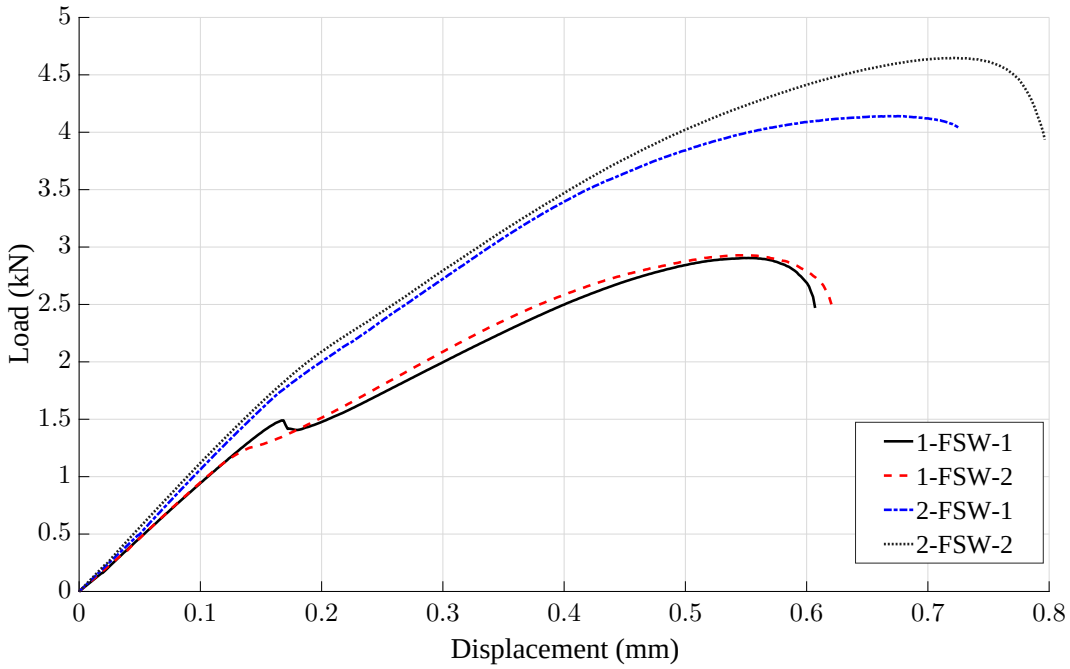

Figure 4.23: Representative load vs. displacement curves of the overlap FSW joints.

Fig. 4.24 presents the load displacement curves for the hybrid joints tested. As it may be observed the use of continuous adhesive layer resulted in significantly increased strength and ductility. The continuous layer of adhesive resulted in a larger adhesive area under shear loading, which led to the increase in mechanical strength. The joints made with purpose made channels for the adhesive resulted in a strength and ductility similar to the FSW overlap joints, not demonstrating any added benefit of hybridization. Regarding the double pass weld hybrid joints, as mentioned above only the ones with channel for the adhesive were defect free. These joints had similar performance to the single pass weld joints as the adhesive showed to be the determinant factor in joint strength. Although most joints had a single failure mechanism, the 1-Hyb-1 joints were able to carry load after the first failure (adhesive failure) occurs. This double failure in the joint would be beneficial in the point of view of damage tolerance if the mechanical performance was acceptable, but as mentioned previously the strength achieved with double pass welds hybrid joints was low and similar to FSW joints. The best performing joint was the 1-Hyb-4, which is a one pass welding with continuous adhesive layer and the higher heat input (higher Plunging force). This joint resulted in an increase of strength and ductility regarding the best performing FSW joint (2-FSW-2) of about 162% and 141% respectively.

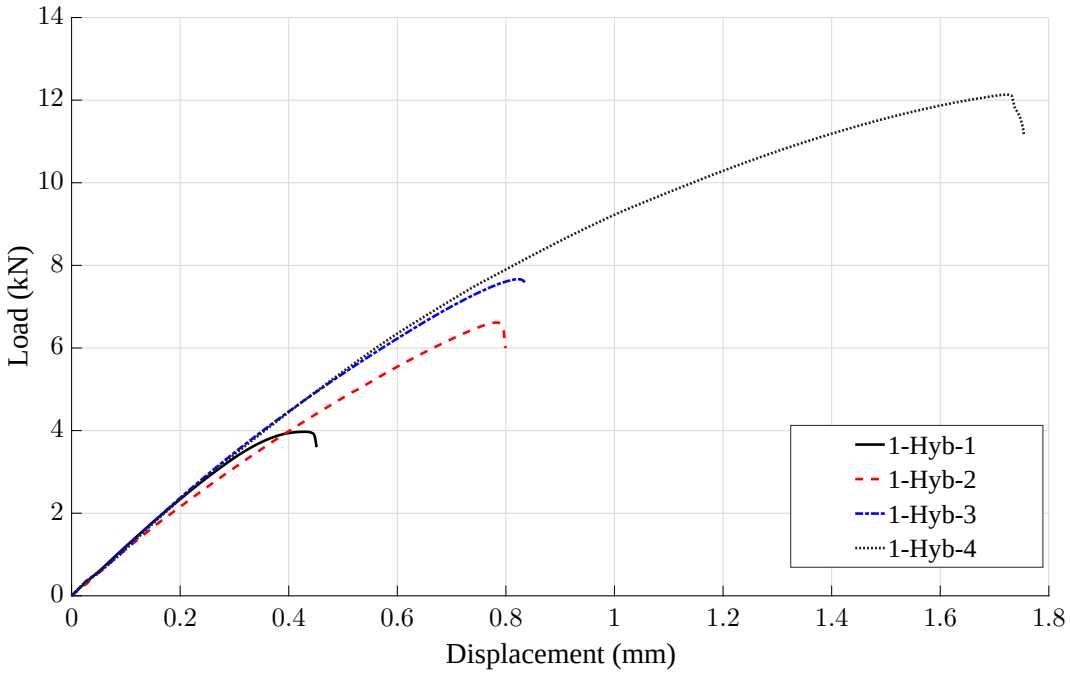

a)

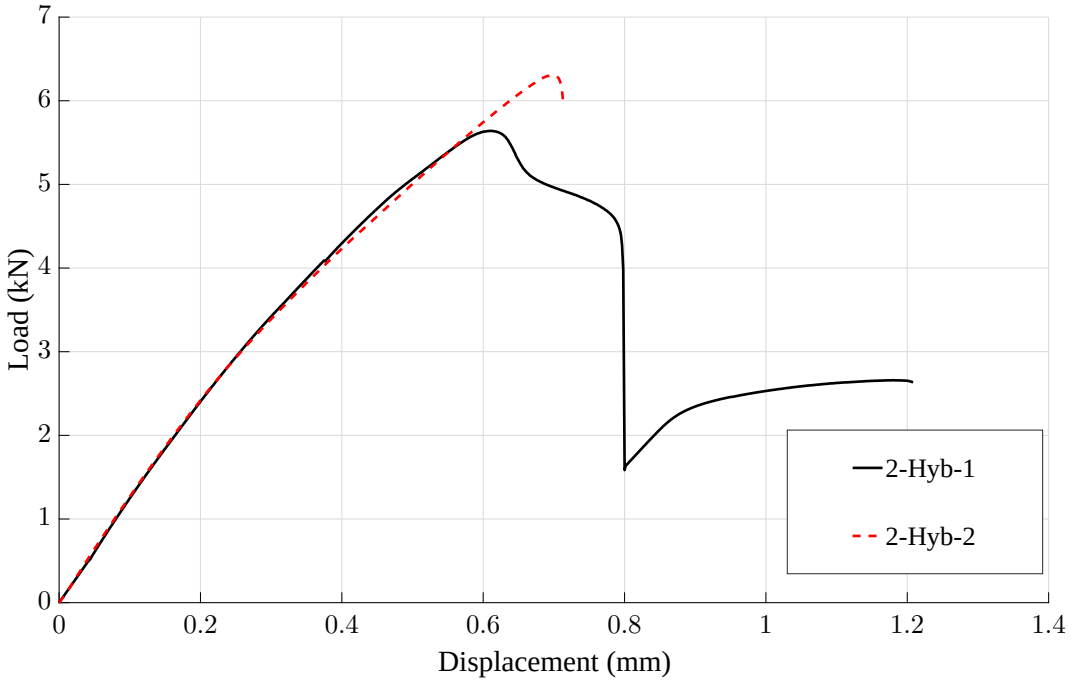

b)

Figure 4.24: Representative load vs. displacement curves of the overlap hybrid joints with a) single pass weld and b) double pass welding.

Failure surfaces of hybrid joints, as well as the adhesive joints (see Fig. 4.25) showed that the failure had been an adhesive failure. As this failure mode demonstrates the adhesive was not performing at its full potential an alternative surface treatment was used to manufacture adhesive bonded joints and the best performing hybrid joint (1-Hyb-4). A phosphoric acid anodization (PAA) according to ASTM D3933 standard [115] was used. Through anodization a aluminum oxide layer is formed with a compact hexagonal cell structure which

improves adhesion [116]. The quality of the surface treatment was assured through scanning electron microscopy (SEM) (e.g. Fig. 4.26).

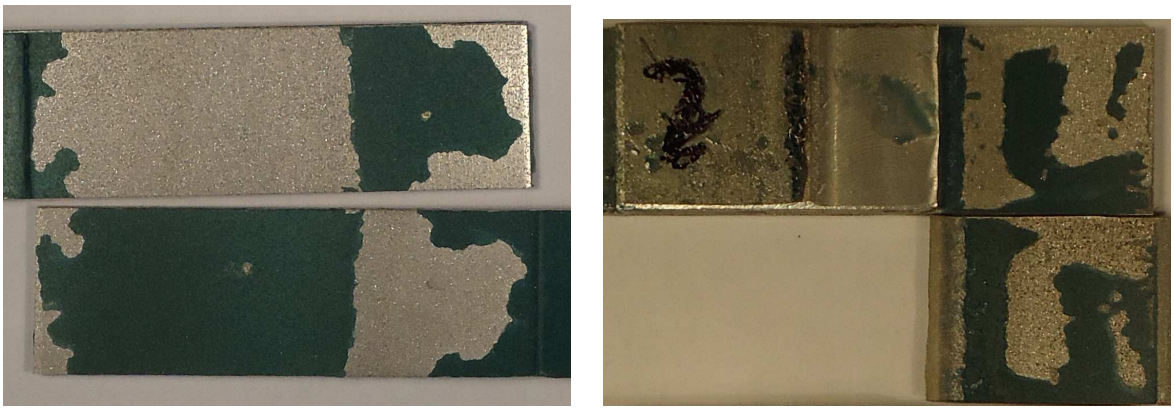

a) b)

Figure 4.25: Failure surface of sandblasted a) adhesive bonded and b) 1-Hyb-4 joint.

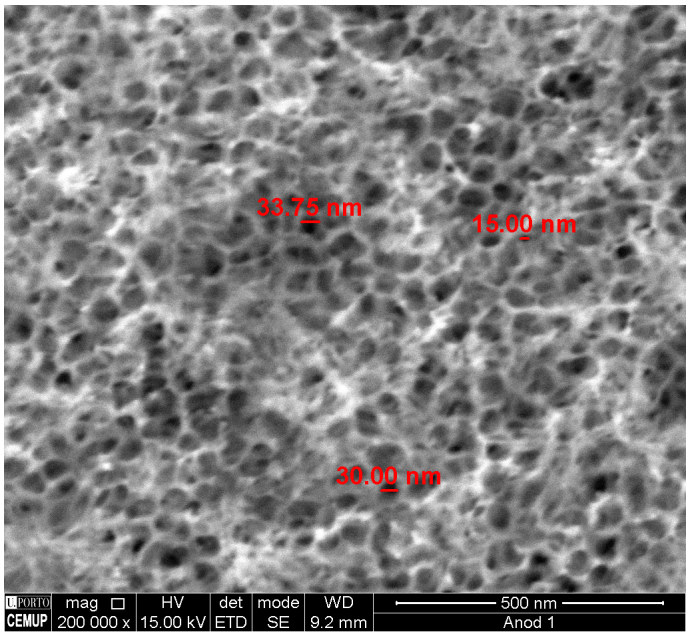

Figure 4.26: SEM image of anodized surface.

The anodization resulted in a small increase in strength but a substantial increase in ductility for both the adhesive bonded joints and the hybrid joints, as seen in Fig. 4.27. This is due to the very large overlap used, which resulted in yielding of the aluminum, with this being the main driver of the mechanical behavior of the joints. The failure in these two types of joints was outside the overlap, where necking led to rupture of the aluminum sheet.

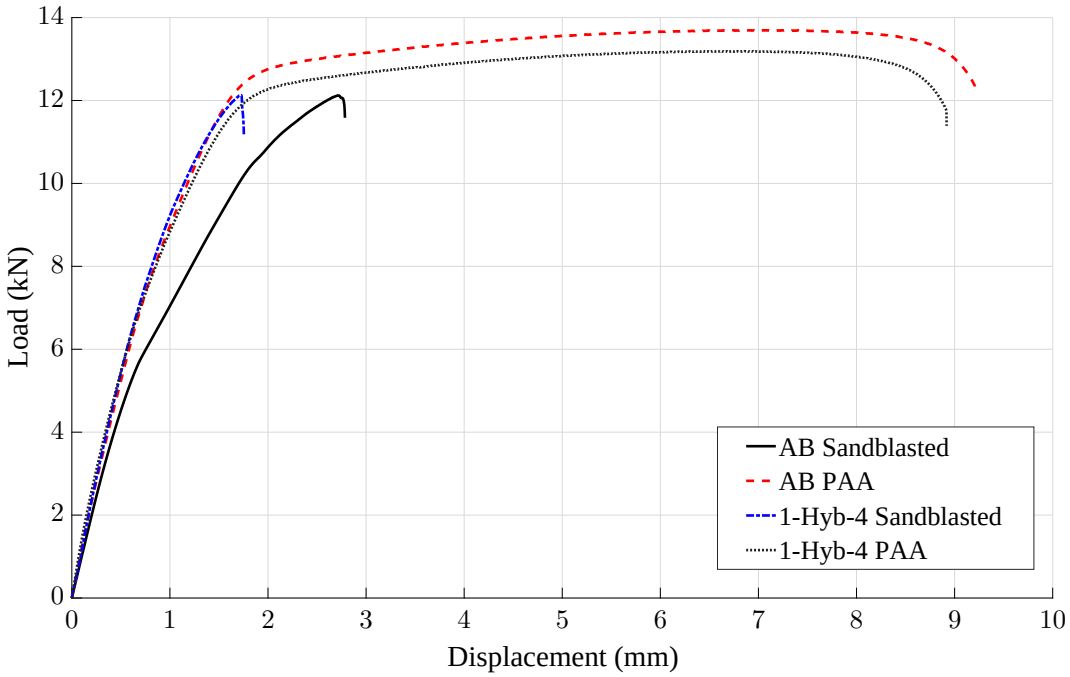

Figure 4.27: Representative load displacement curves of hybrid and adhesive bonded joints, sandblasted and anodized.

When anodized before bonding, the hybrid joints had similar performance to the adhesive bonded joints, with the mechanical behavior and failure of both types of joints being similar. The significant improvement in strength and ductility of hybrid joints towards FSW overlap welds, when correct process method and parameters are used, showed the potential of the technique. The subsequent hybrid joints will use the "weld through" method, with the adhesive non cured when welding and in a continuous layer on the overlap. Single pass welding will be used, as not only resulted in the best mechanical performance, but also results in a more "lean" manufacturing process, as less manufacturing steps are required. In the specific case of 2 mm thick aluminum alloy AA6082-T6 the process parameters to be used are:

- 1000 RPM rotational speed
- 200 mm/min welding speed
- 450 kgf Plunging force
- 0º of tool tilt
- 16 mm diameter grooved shoulder
- 5 mm cylindrical left threaded pin

Although no extensive process parameter optimization was performed at this stage, which would be required for industrialization, the process parameters used resulted in satisfactory performance and as mentioned before, similar performance to the adhesive bonded joints.

4.2.4 Single Lap Joints Benchmark

Having defined the manufacturing method for the hybrid joints and chosen the parameters to use when welding the selected aluminum alloy, a further study benchmarking the performance of the developed joints against established joining methods is required. As the specimens used before showed an excessive overlap, new specimen geometry and subsequently joint geometry were used. To estimate the overlap length of the joints to produce, an equation system may be used, considering the average shear stress in the overlap, for simplicity reasons:

$$\begin{cases} \sigma_u^{aluminum} \geq \frac{P}{b \times t} \\ \tau_u^{adhesive} \leq \frac{P}{b \times l} \end{cases} \tag{4.4}$$

where $\sigma_u^{aluminum}$ is the ultimate tensile strength of the aluminum alloy, $\tau_u^{adhesive}$ is the ultimate shear strength of the adhesive, P the remote tensile load applied to the joint and b, l and t are the width, overlap length, and thickness of the single lap joint, respectively. Through this equation system an overlap of 20 mm is estimated to be the limit for adhesive joints of 2 mm thick aluminum alloy AA6082-T6 before failure occurs outside the overlap. As sufficient and repeatable clamping of 20 mm overlap length FSW and hybrid joints was not feasible, 40 mm overlaps were used instead, but adhesive bonded with both 20 and 40 mm overlaps were used for comparison purposes.

Stress in the joint was calculated contemplating the remote section of the joint as shown in Fig. 4.28. Although the stress field within the joint is complex, with the overlap being loaded in shear and peel simultaneously due secondary bending, for design purposes the joint strength must be related to the stress in the components to be joined. As such, this simplification does not only allow for easier and faster analysis and comparison, but also it is more useful for a structural designer.

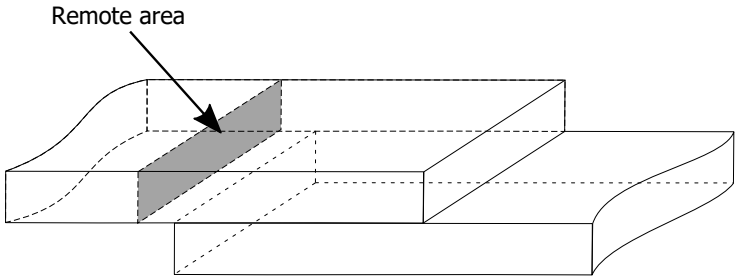

Figure 4.28: Area considered for stress calculation in the joint.

Adhesive bonded joints resulted in a much higher strength and ductility than FSW overlap joints, as shown in Fig. 4.29. The 20 mm adhesive bonded joints had an average ultimate strength of 293 MPa and an average ultimate displacement of 1.92 mm, while FSW overlap joints only had 125 MPa and 0.78 mm of average ultimate strength and ultimate displacement respectively. FSW overlap joints although had much lower strength than the adhesive

bonded joints, they showed an increase of ≈20% regarding the previous 60 mm overlap FSW joints. This strength increase may be a result of lower secondary bending of the joint, due to the lower overlap length. As the effective joined overlap does not significantly change between the two types of joints and is limited by the welding tool geometry and process parameters, the increase in overlap may be detrimental to joint performance.

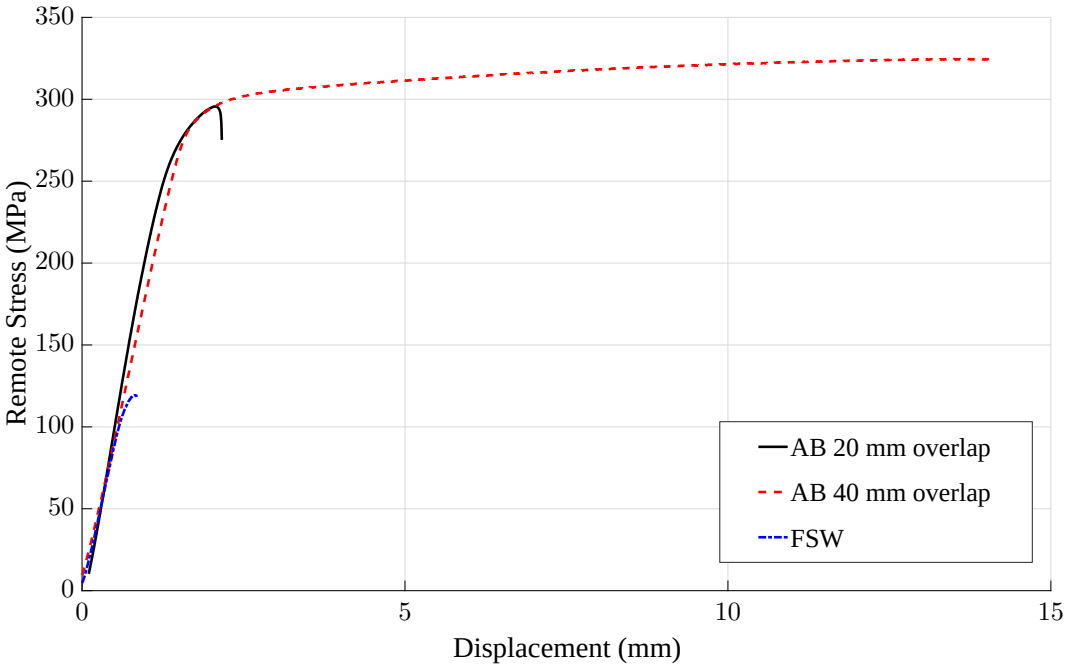

Figure 4.29: Representative stress vs. displacement curves of FSW and adhesive bonded joints.

Failure in the FSW joints occurred through the weld bead, contrary to the joints made in the study mentioned above with 60 mm overlaps, where failure had occurred in the interface between the HAZ and the TMAZ, advancing side on the top sheet. This failure mode indicates that the hook defect became less critical, either because it is of smaller dimension and/or inverted direction (facing downward in the joint instead of upward). The failure location through the weld bead may indicate the presence of a cold lap defect in the joint. This defect may arise from low pin penetration, leading to low mixing between both sheets. Although joints were sanded before welding, a remaining oxide layer may present in the surfaces of the sheets. With low mixing the oxide layer remains continuous through the weld, becoming a point of failure for the joint, due to its lower ductility.

Hybrid joints were able to match the strength of the adhesive bonded joints, although with lower ductility, as shown in Fig. 4.30. The larger effective overlap results in less out-of-plane bending and a more distributed load within the joint. The failure in these joints occurs simultaneously in the adhesive layer, through shear and peel and in the interface between the TMAZ and HAZ in the advancing side. As the adhesive layer loses load carrying capacity the load in the TMAZ and HAZ interface area increases and given the stress concentration in this region, the weld cannot sustain the joint integrity upon failure of the adhesive layer.

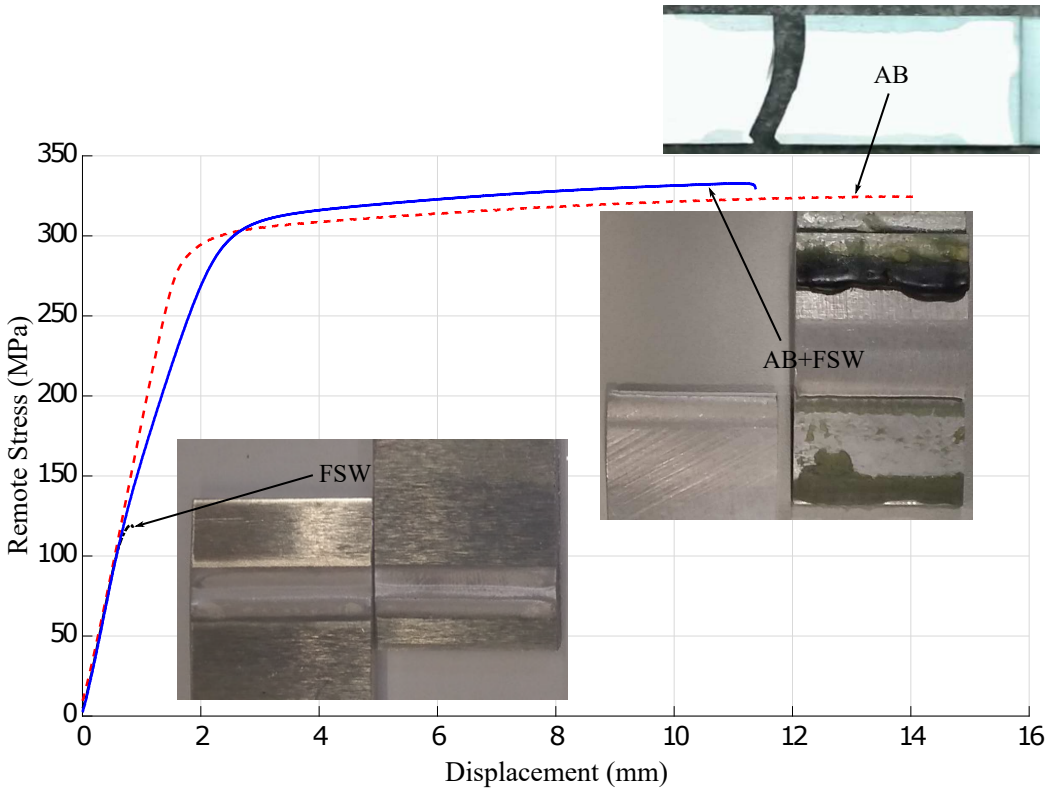

Figure 4.30: Representative stress vs. displacement curves of FSW, adhesive bonded and hybrid joints with failure mechanisms.

4.2.5 Non-Destructive Evaluation

As any joining technique, friction stir weld-bonding requires reliable non-destructive evaluation techniques for quality assurance purposes. NDTs are routinely used to inspect aeronautical structures and are taken into account in early phases of the structure design given the close interplay of actual defects measurement, and damage propagation modeling used in damage tolerant design. Several types of NDTs are available to inspect dierent types of properties. The NDT techniques can be categorized into six main groups [117]: visual, penetrating radiation, magnetic-electrical, mechanical vibration, thermal and chemical-electrochemical. One penetrating radiation technique that has been used in in-line quality control of FSW joints for flaw detection is phased array ultrasonic testing (PAUT) [117].

In order to assess PAUT as a valid NDT for friction stir weld-bonding joints, a preliminary experimental campaign was undertaken on a series of FSW overlap and hybrid joints. Besides the PAUT analysis, optical microscopy and single lap joints tensile testing was performed on the joints. The parameters, listed in Table 4.6, were chosen to be close to the parameters used before in defect free joints. All hybrid joints had much lower strength than expected (joint strength equal or lower than FSW joints), which indicates the presence of manufacturing defects in these joints.

Table 4.6: FSW and hybrid joints used in PAUT analysis.

Joint tag	Plunging force (kgf)	Welding speed (mm/min)	Rotational speed (RPM)	Joint strength (MPa)
FSW-1	400	200	1000	130.4
FSW-2	450	200	1000	119.8
Hyb-1	360	200	1000	71.9
Hyb-2	400	220	1000	57.1
Hyb-3	350	220	900	76.4
Hyb-4	360	190	1000	112.7
Hyb-5	400	200	1000	179.6

The Olympus (Shinjuku, Tokyo, Japan) OmniScan™ SX together with a 10L10-A0-TOP Olympus small-footprint probe, shown in Fig. 4.31, was used for the PAUT scans. A zero-degree wedge was attached to the probe during the inspections. To facilitate the transmission of sound energy from the probe to the workpiece, a water-based couplant was spread on the inspection area before inspection. The inspection was performed on the underside of the welded joints, to avoid the reflections due to the higher surface roughness of the welded top side.

a) b)

Figure 4.31: Olympus OmniScan™ SX a) and probe / wedge assembly b).

Before the PAUT the sound beam focal point was established and the gain adjusted. The gain was adjusted through observation of the front-wall reflection. The focal point was established to be at 2.1 mm deep for the hybrid joints and 2.0 mm for the FSW joints, which are the interface positions of the joints. Table 4.7 presents the input parameters used to perform the analysis. A correct probe frequency is critical, as it trades-off noise levels and resolution of the measurement. Lower frequencies reduce the attenuation effect on sound (such as scattering effects, due to non-homogeneity of the material, causing reflection of the sound wave in the workpiece boundaries), but they also reduce the sensitivity (ability to detect discontinuities) and the resolution (ability to detect defects that are placed close together). As such, both 5 and 10 MHz measurements were made to allow the distinction

between actual defects and other causes of reflection. However for clarity reasons only the 10 MHz measurements will be presented here. The probe was firmly held against the surface in the centerline of the joint. The probe was successively moved along the joint in order inspect the full length of the joint.

Table 4.7: PAUT analysis parameters.

Focal point (mm)	2.0 (FSW) or 2.1 (Hybrid)
Probe frequency (MHz)	5 or 10
Probe type	SAoL
Workpiece thickeness (mm)	4.0 (FSW) or 4.2 (Hybrid)
Wave type	longitudinal
Sound velocity (mm/s)	6400 (based on the workpiece material)

The measurements outputs can be plotted in typical A-scans, where the horizontal axis represents the elapsed time (related to distance from the probe) and the vertical axis indicates signal amplitude. Every peak represents an echo. Two echoes are expected in sound welds, an initial one where the signal reflects on the bottom surface of the specimen, and second one at the top surface. Other echoes are indications of discontinuities in the workpiece. After PAUT analysis, cross section specimens for microscopic inspection were prepared, from the joints tested, by grinding up to 4000 grade paper and polishing up to 1 μm diamond compound. Macroscope images of the joints were made with a Zeiss^{TM} SteREO 95 Discovery. V8 and a Zeiss^{TM} Axiovert 40 MAT microscope was used to analyze joint details. The microscopy images are presented with the underside facing up, as to emulate the PAUT measurements. This was done as the rougher surface caused by the contact between FSW tool and substrate surface would result in more signal reflections.

Both FSW joints tested, did not show any relevant reflections, as shown in Fig. 4.32, indicating that they are defect free. The optical microscopy analysis of the cross section of the FSW joints analyzed with PAUT, shown in Fig. 4.33, also did not show any defects in the joints, confirming the NDT results.

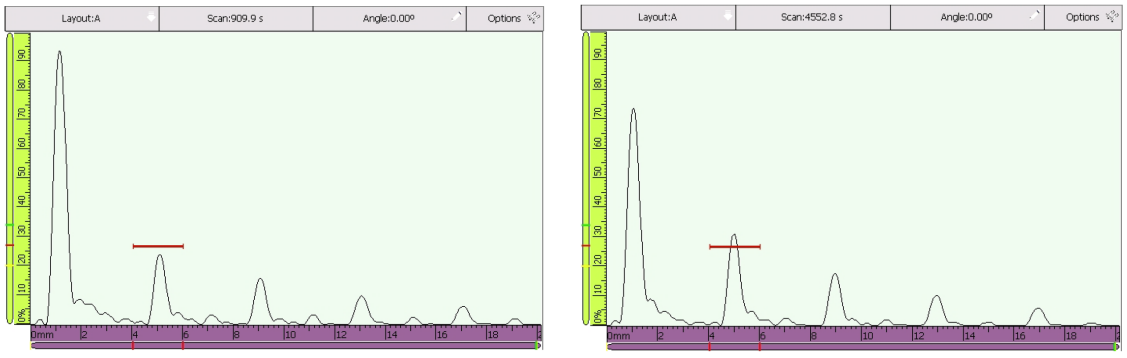

a) FSW-1 b) FSW-2

Figure 4.32: Representative FSW joints A-scans.

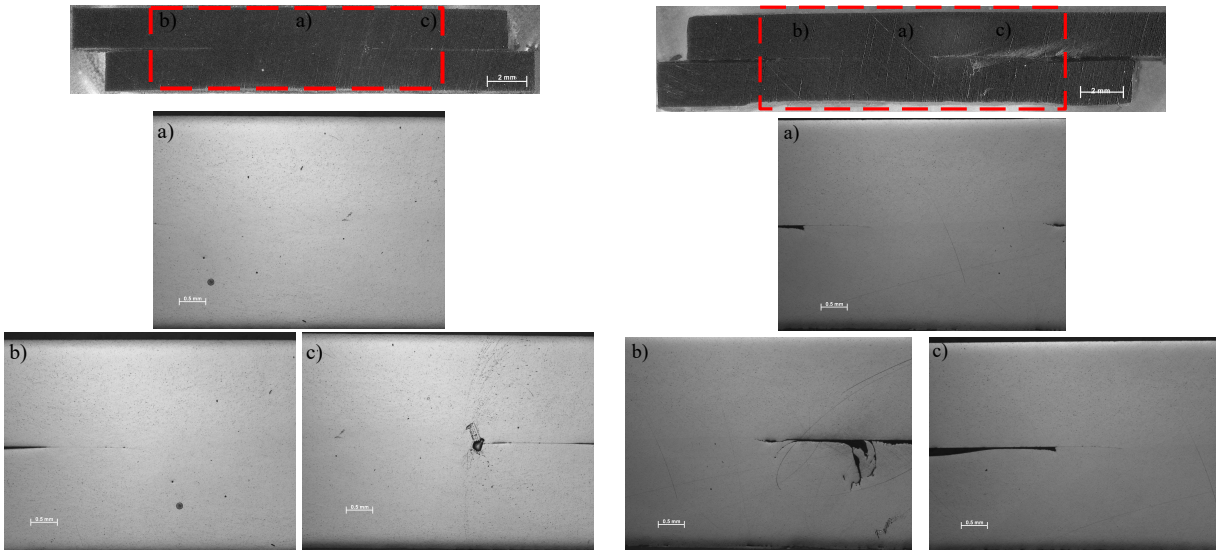

a) FSW-1 b) FSW-2

Figure 4.33: Macroscopic and optical microscopy images of the cross section of the FSW joints.

The PAUT scans of the hybrid joints, allowed to group these joints into two groups. In the first group of joints, which includes joints Hyb-1 and Hyb-3, a reflection peak approximately at the middle of the joints thickness was observed. The PAUT scans for these two joints are shown in Fig. 4.34 and the mentioned reflection is indicated with a red circle. These peaks indicates a material discontinuity along the joints thickness, meaning that an adhesive layer may be present in the joints interface. As such, the FSW production parameters used to produce these joints, may have resulted in low heat input leading to non-welded joints. Both Hyb-1 and Hyb-3 joints were made with lower plunging forces than sound joints mentioned previously (sound joints made with 425 kgf). The Hyb-3 joint was also made with lower rotational force and higher welding speed, resulting in a reduced weld pitch ratio (eq. 4.5), and as such a reduced heat input.

$$\text{Weld Pitch Ratio}[RPM/mm] = \frac{\text{Rotational Speed [RPM]}}{\text{Welding Speed [mm/min]}} \tag{4.5}$$

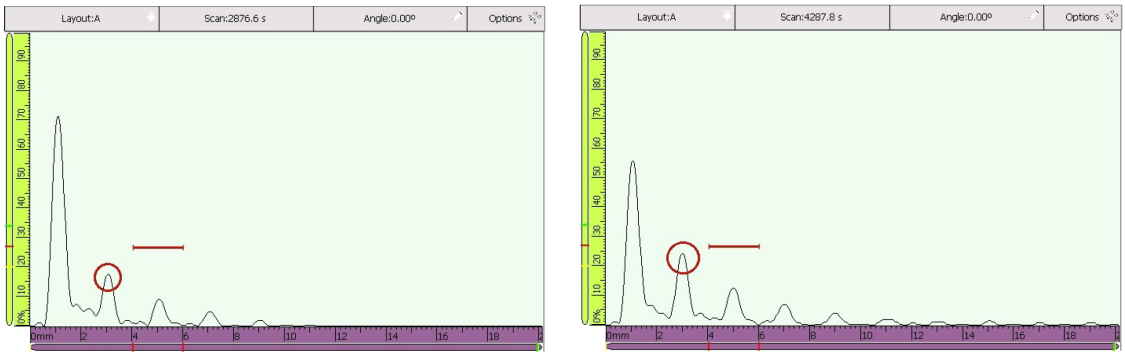

a) Hyb-1 b) Hyb-3

Figure 4.34: Representative A-scans of Hyb-1 a) and Hyb-3 b) joints

Optical microscopy analysis, presented in Fig. 4.35, of the joints confirmed the presence of an adhesive layer in between the two sheets. Hyb-1 joint had a continuous layer of adhesive separating the two sheets, while Hyb-3 which is the weld with lower weld pitch ratio, had inclusions of adhesive within the weld, which are probably result of lack heat generated softening and mixture.

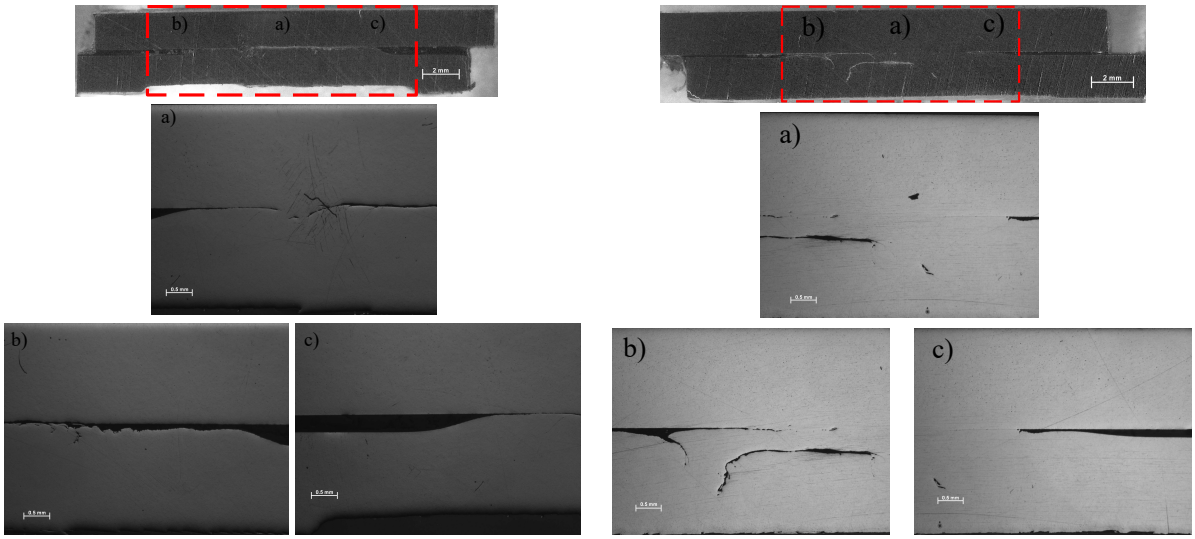

a) Hyb-1 b) Hyb-3

Figure 4.35: Macroscopic and optical microscopy images of the cross section of the Hyb-1 a) and Hyb-3 b) joints.

The second group, including joints Hyb-2, Hyb-4 and Hyb-5, shown in Fig. 4.36, do not show a reflection at the joint interface like the previous mentioned joints, but a small reflection closer to the upper surface of the weld. The small amplitude of the reflected signal indicates that the defect is not a air filled void, as the difference of impedance between air and aluminum is too great and would result in an almost complete reflection of the signal. As such, it is possible to infer that an adhesive interlayer may be present at this location.

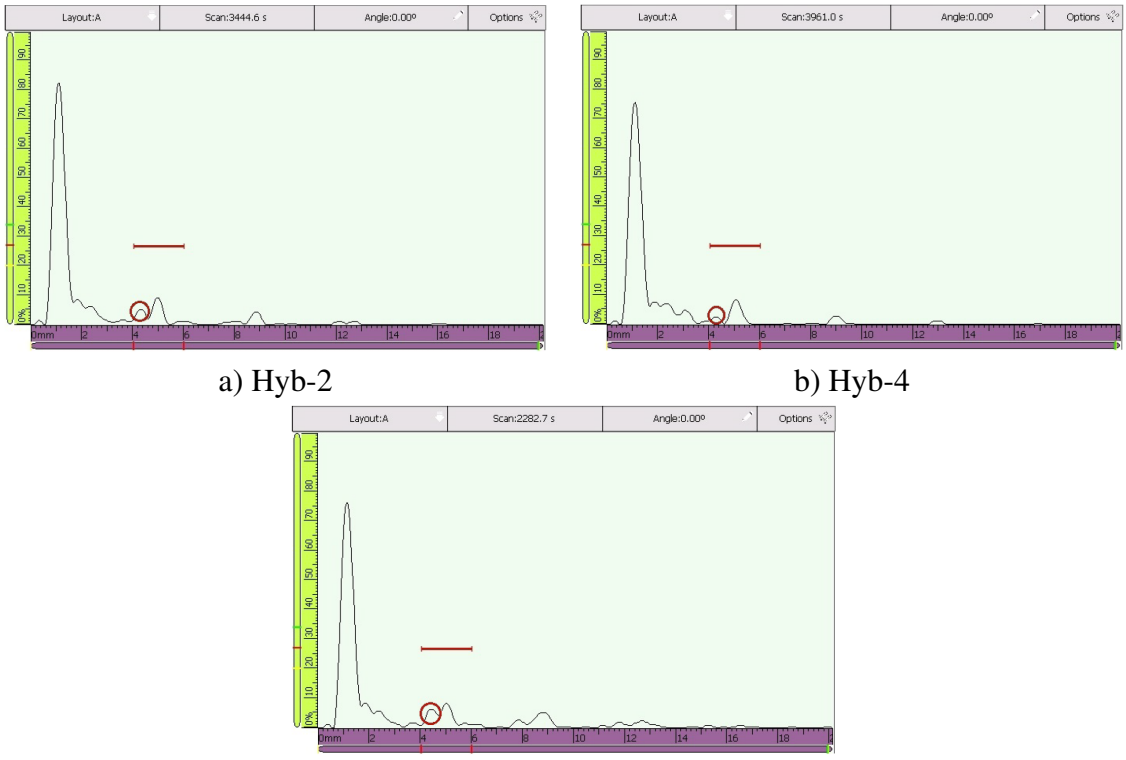

a) Hyb-2 b) Hyb-4

c) Hyb-5

Figure 4.36: Representative A-scans of Hyb-2 a), Hyb-4 b) and Hyb-5 c) joints.

When analyzing the macroscopic and microscopic images of the Hyb-2 and Hyb-4 cross-sections, shown in Fig. 4.37, an adhesive layer was present close to the top surface (microscopic images captured upside down to emulate the PAUT scans), as was indicated by the PAUT scan. It could be observed that the material mixing during FSW caused the adhesive in the periphery of the weld to flow up and create the continuous layer at this location. Although the two PAUT scans were similar between these two joints, it was possible to observe that the Hyb-2 joint had a wider adhesive layer at the indicated thickness of the joint. This may partially justify the significantly lower joint strength of Hyb-2 versus Hyb-4 joint. This wider adhesive layer may be a result of the increased welding speed, which decreased temperature induced softening and mixing time in the joint. The Hyb-4 joint was manufactured at a slower welding speed albeit with a lower plunging force, which also resulted in insufficient mixing.

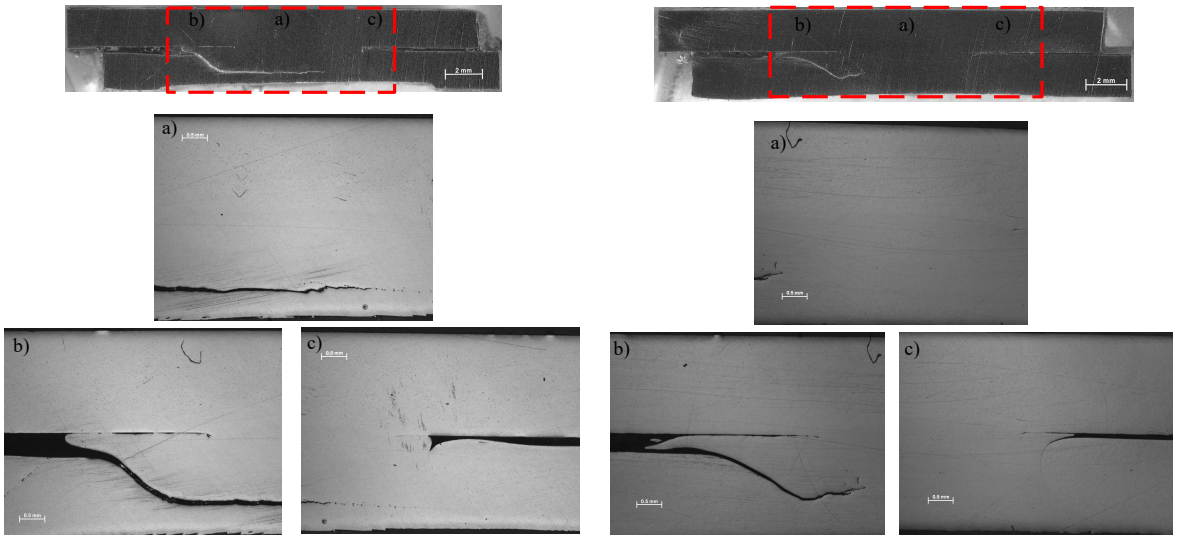

a) Hyb-2 b) Hyb-4

Figure 4.37: Macroscopic and optical microscopy images of the cross section of the Hyb-2 a) and Hyb-4 b) joints.

Even though the Hyb-5 PAUT scan was similar to the two previously mentioned joints, the joint strength was higher than both Hyb-2 and Hyb-4 joints. The cross-section, shown in Fig. 4.38, does not present an incursive adhesive layer of the same proportions as the previous two joints, but only a smaller upwards flow of adhesive in the retreating side of the weld. The retreating side of the weld in a single lap joint with the configuration used, will not be as load critical as the top advancing side due to secondary bending of the overlap.

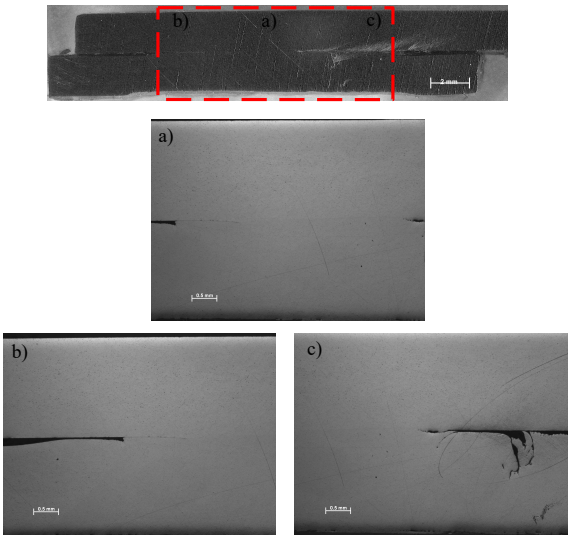

Figure 4.38: Macroscopic and optical microscopy images of the cross section of the Hyb-5 joint.

The Hyb-5 joint was *a priori* expected to have higher strength than the previously discussed hybrid joints, as the weld pitch ratio used was the same as in the sound joints of section 4.2.4 and the plunging force was within the process window which was previously determined. However, even though the Hyb-5 joint did have higher strength than the other

hybrid joints tested, it was still lower than expected. This led to further study the joints physical chemical conditions to determine the reasoning for such mechanical behavior. When analyzing the failure surfaces of the hybrid joints tested here, it was observed that the adhesive had darker and a more "blueish" color, which indicated water absorption. As this water absorption was not initially intended, the presence of other contaminants would also be expected. These failure surfaces were subjected to analysis in SEM, where EDS analysis was also performed. Fig. 4.39 presents these analysis

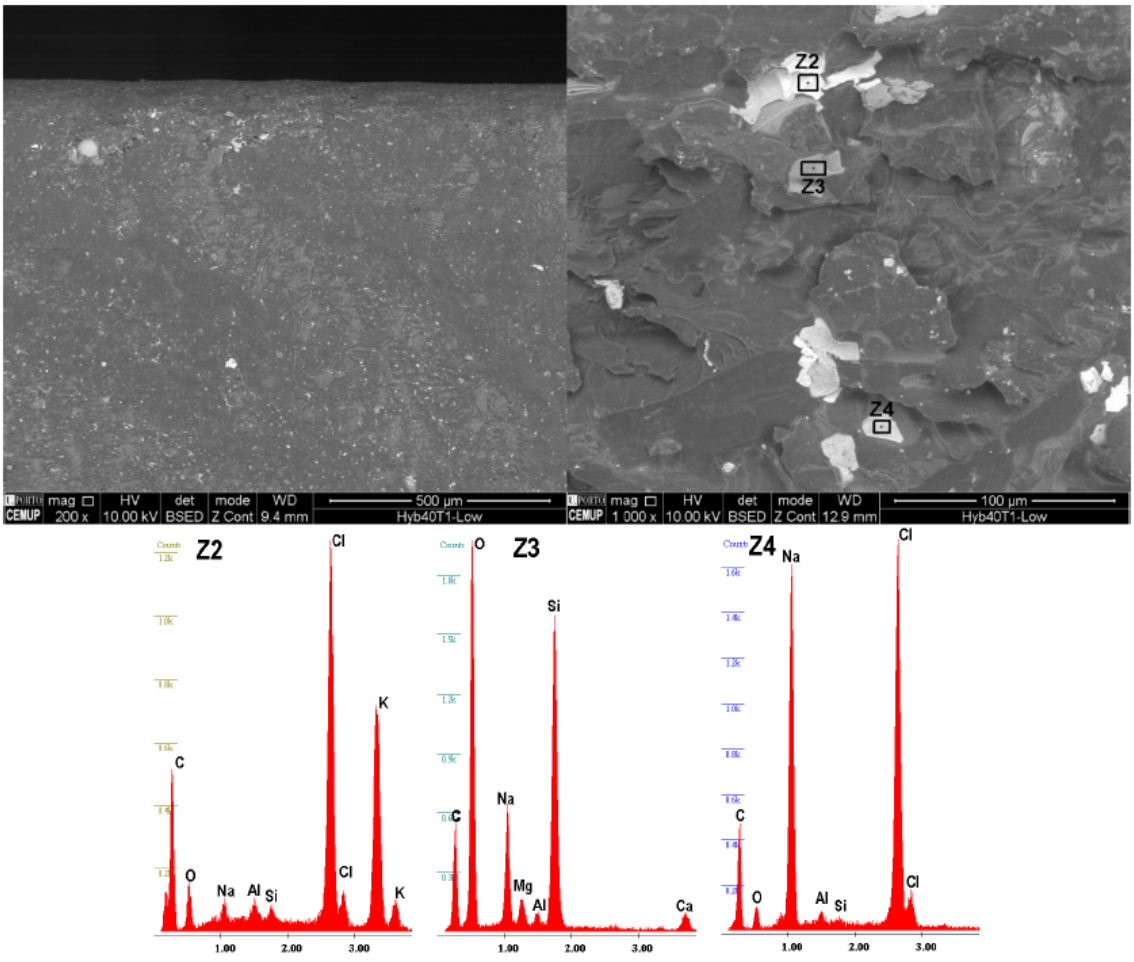

Figure 4.39: SEM and EDS analysis of hybrid joint failure surface with contamination.

Simultaneously to the SEM and EDS analysis, an effort was made to identify the possible cause for the contamination in the adhesive. As water absorption in a cured epoxy is a slow process [118], the contamination had to occur at the time of manufacture when the adhesive is still in its uncured form. Taking this into consideration an inspection of the manufacturing conditions of the joints was made and a possible culprit was found. Due to malfunction in the FSW equipment, the machine coolant was leaking through the FSW tool onto the workpieces.

PAUT scans demonstrated to be capable of indicating the presence of adhesive incursions onto the welds in hybrid joints, but failed to distinguish between severe incursions as in the case of Hyb-2 and minor ones as in the case of Hyb-5. Another limitation is found when

the defect present in the joint does not manifest in a difference of impedance, such as in the case of the contaminations found in the adhesive on the hybrid joints tested. This is to be expected when the mechanism of operation of this NDT is contemplated. As such PAUT could be a NDT method to be used for quality assurance in hybrid joints but will require complementing techniques to validate findings and test other defect types.

4.2.6 Fatigue Benchmark

Metallic structures sustaining varying loads during service may be subjected to fatigue failure. Aircraft fuselages are prime examples of structures where fatigue performance is key. As such, any manufacturing or assembly technology that is proposed for application in them, must be assessed for fatigue strength. One way of assessing the fatigue performance of metallic joints is through the stress-life method or S-N curve. This methodology does not distinguish the beginning or the propagation of a crack, but establishes the relation between the stress range and the number of cycles up to failure, represented in a S-N or Wöhler curve.

The joint and specimen configurations tested in quasi-static lap shear tensile loading, discussed in section 4.2.4 were loaded in cyclic tensile conditions to assess and benchmark their fatigue strength. A stress ration, R= $\sigma_{min}/\sigma_{max}$ of 0.1 was used in all tests and specimens were loaded up to failure or until the stoppage criteria was met. The stoppage criteria was set at 2×10^6 cycles.

Fatigue lifetime analysis has an inherently probabilistic nature, as the scatter of experimental data resultant of cyclic loading tests demonstrates. As such, probabilistic fatigue models are indispensable to take into account the different sources of uncertainty inherent to fatigue lifetime analysis. Castillo and Canteli [119], proposed a unified methodology that merges as the solution of a functional equation, resulting from the necessary compatibility condition to be accomplished along the whole S-N field between both distributions, that of lifetime for given stress (or strain) range and that for stress (or strain) range for given lifetime. The basic probabilistic model accounts the S-N curve, by assuming simple variables, i.e. stress range and strain amplitudes drive the fatigue damage variables. This makes it possible to compare the stress or fatigue data given by the loading conditions and using a hyperbolic field derived from Weibull or Gumbel distribution. Considering the statistical requirements and physical condition for its execution, the probabilistic S-N field might be defined as follows:

$$F\left(log\left(N_f\right); log\left(\Delta\sigma\right)\right) = p = 1 - exp\left[-\left(\frac{V-\lambda}{\delta_{ref}}\right)^{\beta}\right] \tag{4.6}$$

where

$$V = \left(log\left(N_f\right) - B\right)\left(log\left(\Delta\sigma\right) - C\right) \tag{4.7}$$

and

$$V \geq \lambda \tag{4.8}$$

where N_f is the number of cycles at failure; $\Delta\sigma$ is the stress range level; $F()$ is the cumulative probability distribution function of N_f for a given $\Delta\sigma$, V the normalized variable, $B = log(N_0)$, N_0 being a threshold value of lifetime; $C = log\,(\Delta\sigma_0)$, $\Delta\sigma_0$ being the endurance fatigue limit; and β, δ_{ref} and λ are non-dimensional model parameters. β being the Weibull shape parameter, δ_{ref} the Weibull scale parameter and λ the Weibull location parameter defining the position of the zero-percentile curve. ProFatigue® software was used to estimate the parameters in the tested specimens.

Adhesive bonded, FSW and FS weld-bonded joints were tested, and results were compared with the aluminum alloy AA6082-T6 base material from [99]. As the base material specimens are made from a base material sheet, and are milled to a dogbone shape, the stress concentration level in them is much lower than in the overlap joints. As such, fatigue strength of the joints will be significantly lower than base material. Nonetheless the base material Wöhler curve serves as a benchmark for the joints performance, allowing to assess the strength loss from the base material values.

The probabilistic S-N fields and corresponding probabilistic papers and Weibull cumulative distributions for the adhesive bonded 20 mm joint, adhesive bonded 40 mm overlap joints and FSW 20 mm overlap joints are presented from Fig. 4.40 to Fig. 4.42.

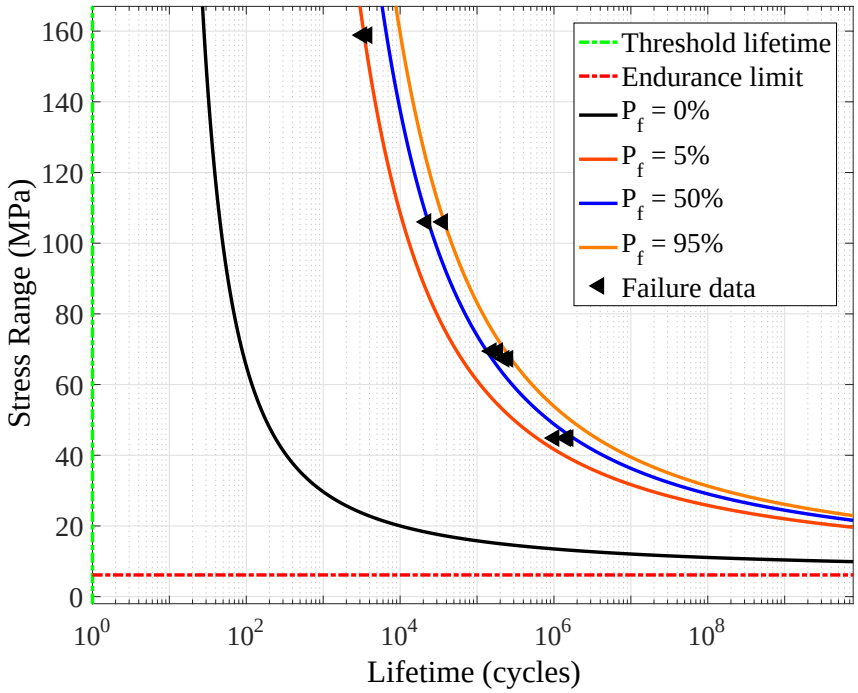

a)

Figure 4.40: Probabilistic S-N field of the 20 mm overlap adhesive bonded joints a) and corresponding probabilistic paper b) and Weibull cumulative distribution c).

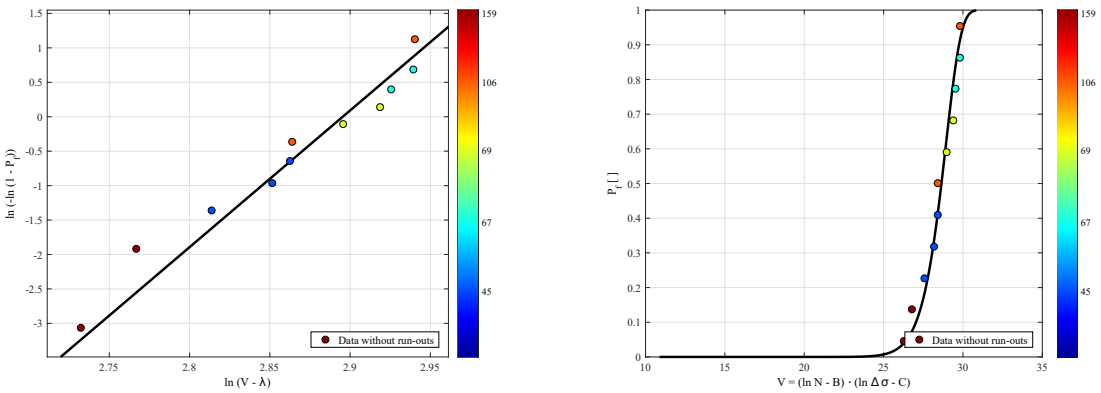

b) c)

Fig. 4.40 (cont.): Probabilistic S-N field of the 20 mm overlap adhesive bonded joints a) and corresponding probabilistic paper b) and Weibull cumulative distribution c).

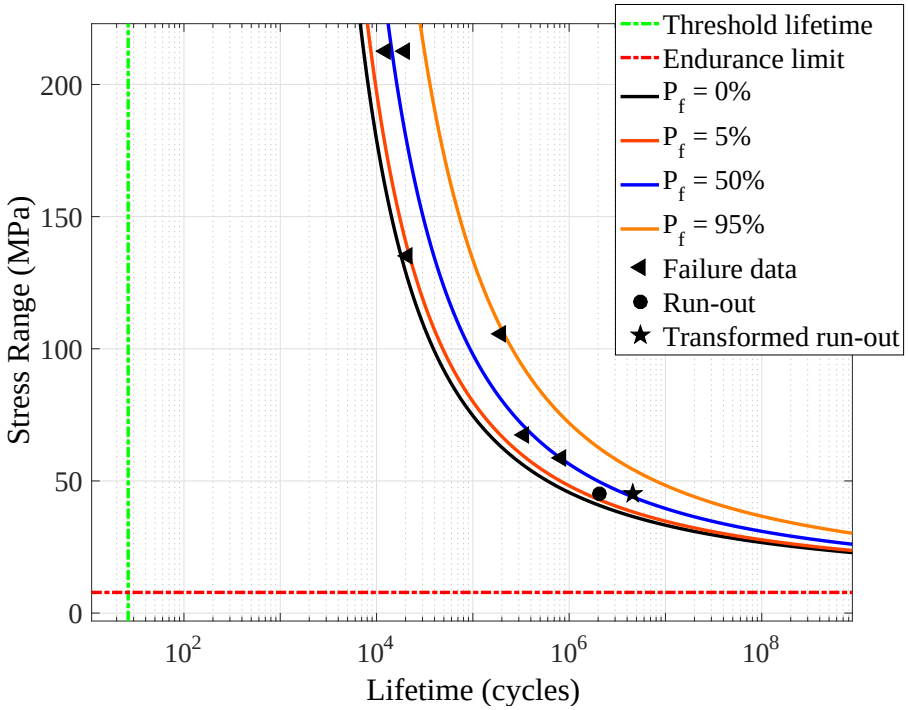

a)

Figure 4.41: Probabilistic S-N field of the 40 mm overlap adhesive bonded joints a) and corresponding probabilistic paper b) and Weibull cumulative distribution c).

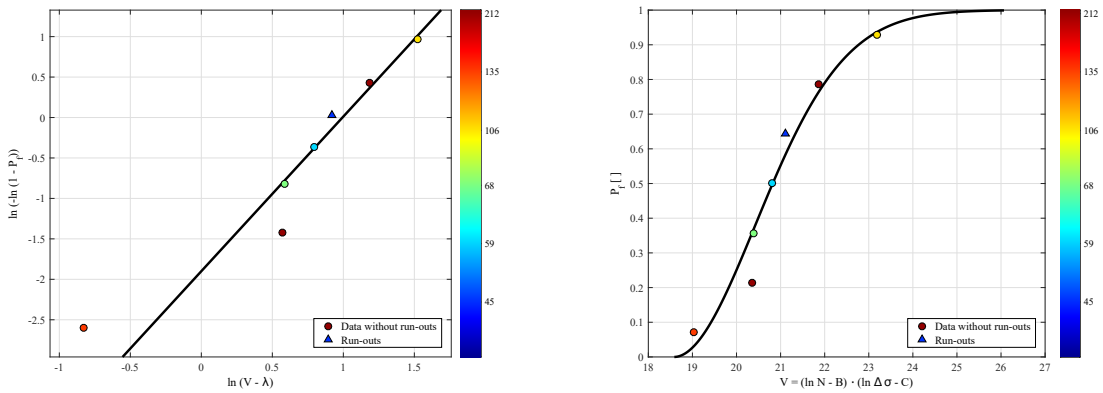

b) c)

Fig. 4.41 (cont.): Probabilistic S-N field of the 40 mm overlap adhesive bonded joints a) and corresponding probabilistic paper b) and Weibull cumulative distribution c).

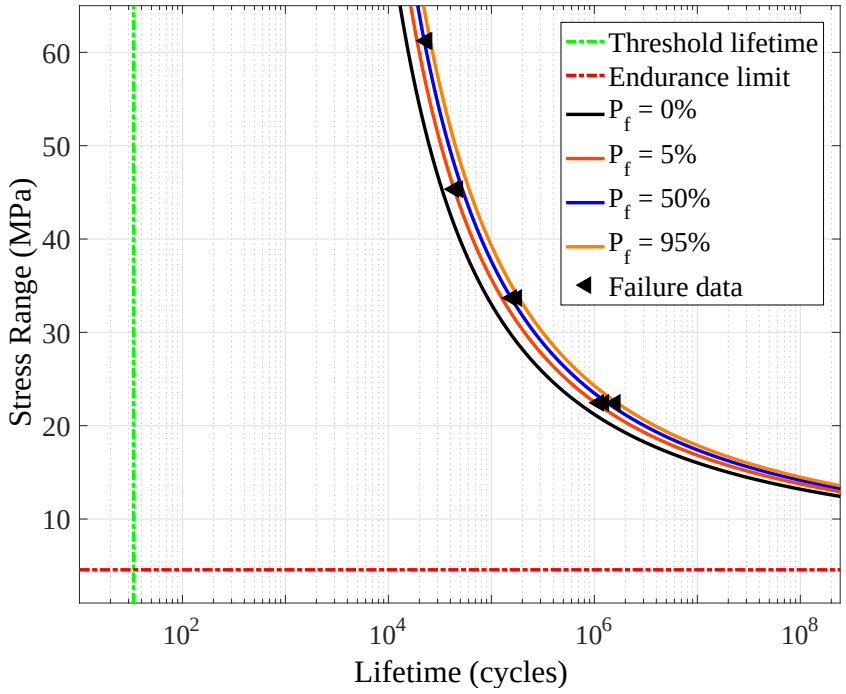

a)

Figure 4.42: Probabilistic S-N field of the 20 mm overlap FSW joints a) and corresponding probabilistic paper b) and Weibull cumulative distribution c).

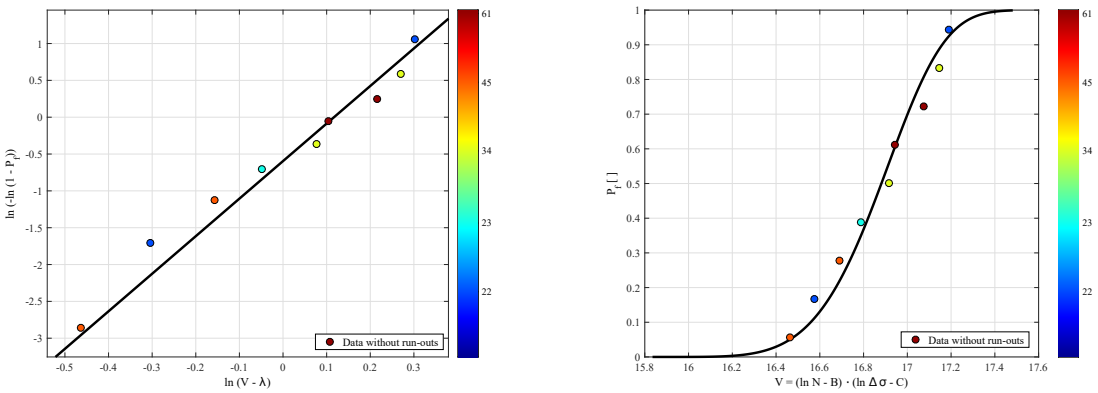

b) c)

Fig. 4.42 (cont.): Probabilistic S-N field of the 20 mm overlap FSW joints a) and corresponding probabilistic paper b) and Weibull cumulative distribution c).

Although the original goal was to assess the fatigue performance of the hybrid joints regarding adhesive bonded and overlap FSW joints, issues with unavailability of the FSW equipment and late delivery of consumables for hybrid joints manufacturing, delayed the manufacture of these joints and as such these results are currently missing and will be completed in following work to be published.

The resulting Weibull distribution parameters from the ProFatigue® analysis on the joints tested are presented in Table 4.8. It must be noted that the threshold value of lifetime (B) estimated, must be considered with care, as the $p - \Delta\sigma - N$ model considered is only valid for high cycle fatigue.

Table 4.8: Weibull distribution parameters of the joints tested.

	β	B	C	δ	λ
AB 20 mm	19.85	0 (1 cycle)	1.81 (6.14 MPa)	18.09	10.89
AB 40 mm	1.91	3.27 (26 cycles)	2.06 (7.83 MPa)	2.70	18.59
FSW	5.10	3.51 (33 cycles)	1.52 (4.56 MPa)	1.12	15.84

Taking the value from Table 4.8 and applying them to equations 4.6 to 4.8, the stress range versus number of cycles relations for each probability level may be established. As example the stress versus number of cycles relation for the adhesive bonded joint with 20 mm overlap for a probability of failure of 5% may be presented as:

$$\text{AB 20 mm: } \Delta\sigma = 6.11045e^{\frac{26.4706}{log(N)}} \tag{4.9}$$

By juxtaposing the Wöhler curves of all joints with the base material, Fig. 4.43 is plotted.

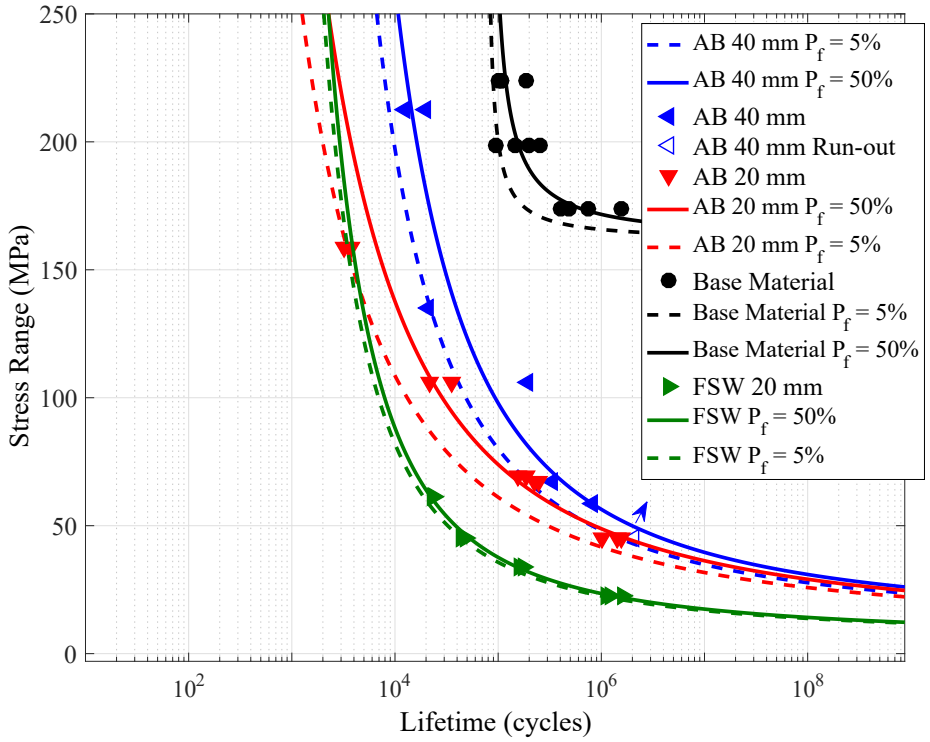

Figure 4.43: S-N curves of all tested joints versus aluminum alloy AA6082-T6 base material.

Although the Wöhler curve for the hybrid friction stir weld-bonded joints is missing, some general remarks may be made regarding the performance of overlap joints. As in quasi-static loading adhesive bonded joints showed higher strength than FSW overlap joints and the increase in overlap length in adhesive bonded joints, also resulted in a slight increase in strength. However, as the number of cycles increase, the difference in strength becomes smaller. This may be due to the lower loads resulting in smaller difference in out of plane bending. Given the shape of the unwelded tip, the out of plane bending is crucial regarding joint strength and failure mode, as it acts as pre-existing crack. Both adhesive bonding and FSW overlap result in high decrease of strength at high number cycles regarding base material, even though in quasi-static this difference is not as significant, especially in the case of adhesive bonded joints. This is due to the stress concentration within the joint due to the overlap and the already mentioned out of plane bending, due to the misalignment of this type of joint.

The higher fatigue strength of adhesive bonded joints regarding other overlap joints, is due to the larger effective bonded overlap and resulting better stress distribution. Another contributing factor to the high fatigue strength of the adhesive bonded joints is the high fracture toughness, as was shown in the adhesive mechanical characterization.

4.3 Numerical Modeling

Given the complex loading scenario in overlap welds, especially with hybrid joining methods, structural designers require FEM models capable of predicting the behavior of joints during service. This section will present the numerical modeling efforts made to predict the experimental tests through FEM models.

4.3.1 Adhesive Bonded Joints Models

Cohesive zone modeling (CZM) is a common employed modeling technique in adhesive bonding, as it is capable of accurately predicting failure in adhesive joints through traction separation laws established on the failure paths [120]. Elastic damage, damage initiation and damage propagation are modeled in CZM through a relationship between stresses and relative displacements in tension or shear, connecting paired nodes of the cohesive elements. All experimental joints tested and numerically modeled had very small thickness and much lower stiffness than the corresponding substrates. As such, the cohesive layer is assumed to be under one direct component of strain (through-thickness) (ε_n) and one transverse shear strain (ε_s), which are computed directly from the element kinematics and the membrane strains are assumed as zero. Elasticity is defined by an elastic constitutive matrix relating the current stresses and strains in tension and shear across the interface (subscripts n and s, respectively).

$$t = \left\{ \begin{array}{c} t_n \\ t_s \end{array} \right\} = \left[\begin{array}{cc} K_{nn} & K_{ns} \\ K_{ns} & K_{ss} \end{array} \right] . \left\{ \begin{array}{c} \varepsilon_n \\ \varepsilon_s \end{array} \right\} \tag{4.10}$$

The matrix $\mathbf{K}$ contains the stiffness parameters of the adhesive layer. Using a a continuum-based approach, a suitable approximation for thin adhesive layers is provided with $K_{nn} = E$, $K_{ss} = G$, $K_{ns} = 0$. Assuming only normal or only shear behavior, the cohesive elements will deform in a linear elastic way until the normal and shear stress limits (t_n^0 and t_s^0 respectively) are achieved. As damage initiation criteria, the quadratic nominal stress criterion was used, which contemplates the effect of both mode I and mode II simultaneously:

$$\left\{ \frac{\langle t_n \rangle}{t_n^0} \right\}^2 + \left\{ \frac{t_s}{t_s^0} \right\}^2 = 1 \tag{4.11}$$

This damage initiation criteria was previously shown to be accurate [121]. Compressive normal stresses are assumed to not cause damage initiation, therefore the use of the Macaulay brackets $\langle\rangle$. After the onset of damage, damage propagation, softening occurs:

$$t_n = \left\{ \begin{array}{ll} (1-D)T_n & T_n > 0 \\ T_n & T_n \leq 0 \end{array} \right. \tag{4.12}$$

$$t_s = (1-D)T_s \tag{4.13}$$

where D is scalar stiffness degradation which varies between 0 and 1 from undamaged to fully damaged and T_n and T_s are the undamaged normal and shear traction respectively. Compressive normal stress will not result in damage propagation. A linear power law form of the required energies for failure in the pure modes is used to predict the complete separation and mixed mode failure displacement:

$$\frac{G_n}{G_n^c} + \frac{G_s}{G_s^c} = 1 \tag{4.14}$$

where G_n and G_s are the normal and shear fracture toughness and G_n^c and G_s^c are the critical normal and shear energy release, determined through the adhesive fracture tests.

Given the adhesive characterization discussed in section 4.2.2 it was required to establish the traction separation laws to be used throughout all models involving adhesive bonding. For this purpose FEM models of the mode I and mode II fracture tests performed before, were made with both triangular and trapezoidal laws. Numerical results were compared with the experimental data adding confidence to the traction separation laws selected. Initially 2D plane stress models were made, as these have lower computational cost which allows them to be run faster and provide results sooner. These were then followed up with 3D models for a more accurate comparison with the experimental results.

Trapezoidal traction separation laws resulted in more accurate models for both the room temperature and 120ºC cured adhesive, which given the relatively high ductility of the adhesive (≈12% elongation at break in bulk tensile when cured at 120ºC), is to be expected. Fig. 4.44 presents the traction separation laws for mode I and II used in the modeling of the adhesive bonds.

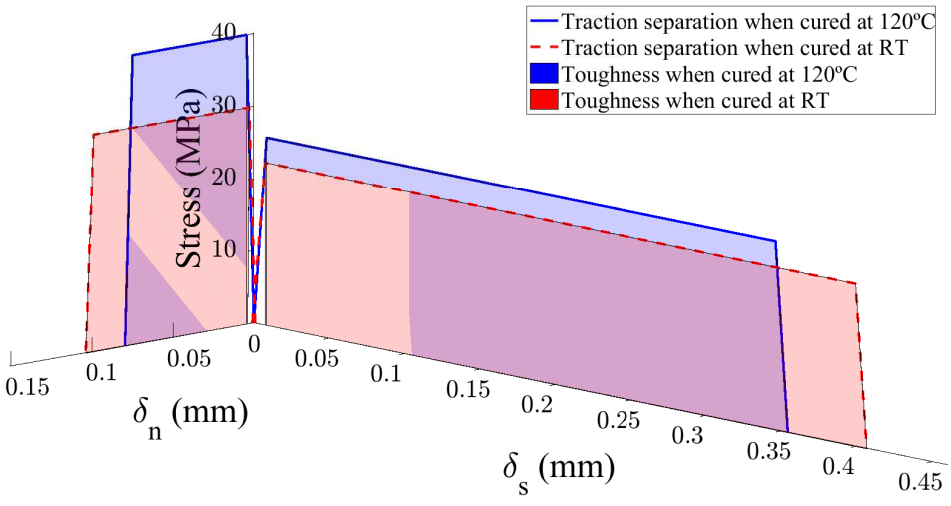

Figure 4.44: Trapezoidal cohesive law for Araldite 420.

As an example of this good agreement, Fig. 4.45 presents both numeric and experimental

load versus displacement curves for the mode I fracture DCB test. Peek load and stiffness degradation (load decrease with increasing displacement after peek load) agrees well with the experimental results.The numerical model showed slightly higher displacement at failure, albeit this value showed some scatter in the experimental tests, which may be due to a final abrupt failure. This value may also be affected by the viscosity damping coefficient used. This coefficient was set to a very low value (1×10^{-5}) in order to allow the model to reach final failure in a time efficient manner. The dissipated energy in cohesive stabilization was monitored throughout the model run and it never surpassed 5% of the total kinetic energy (up until the onset of final failure this ratio was inferior to 0.04%). As such, it can be inferred that this stabilization did not altered the numerical results in a meaningful way.

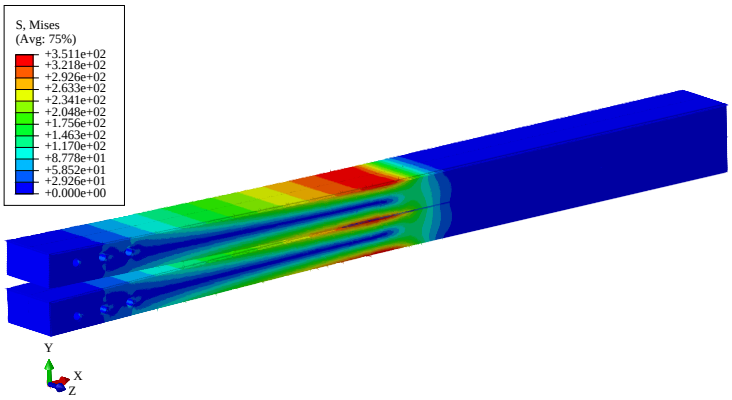

a)

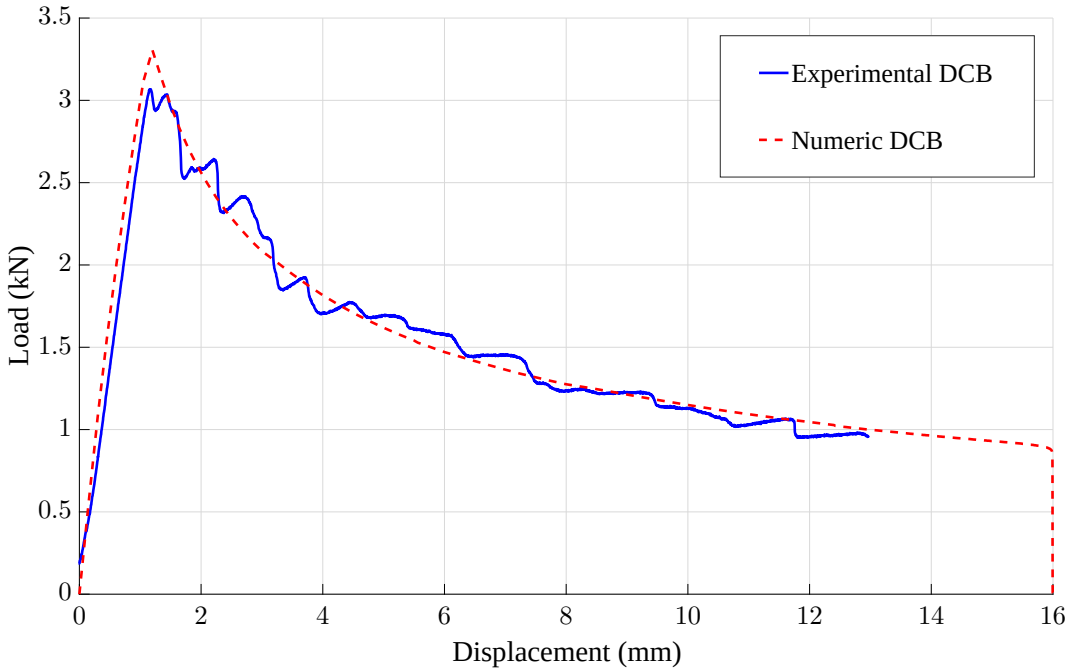

b)

Figure 4.45: a) von Mises stress in 3D DCB Abaqus model at 5 mm displacement and b) load displacement curve comparison between numeric and experimental.

As the DCB test is a mode I fracture test, the DCB numerical model is not very sensitive to the adhesive shear properties and as such a similar procedure was done for the ENF test.

Fig. 4.46 presents the comparison between the experimental and numeric results of the ENF test, where it is possible to observe the good agreement achieved. The ENF FEM model also allowed the verification of the mode II fracture toughness of the adhesive, as the bending load achieved during testing was high and possibly led to local plasticization of the substrates.

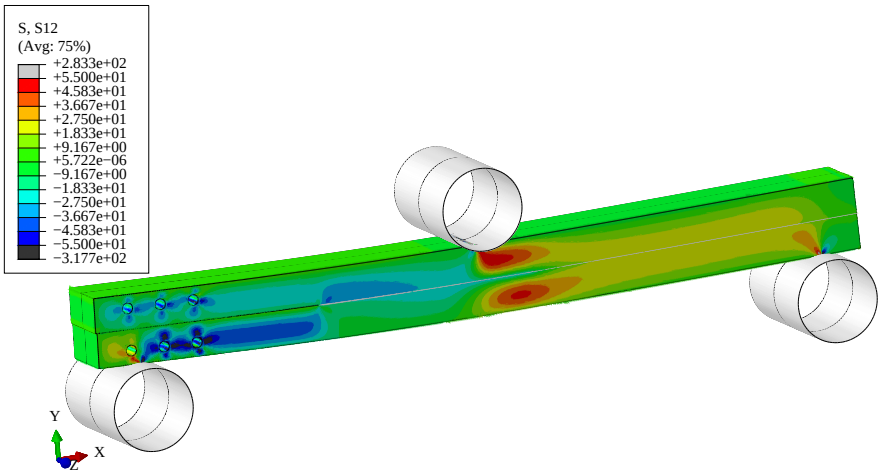

a)

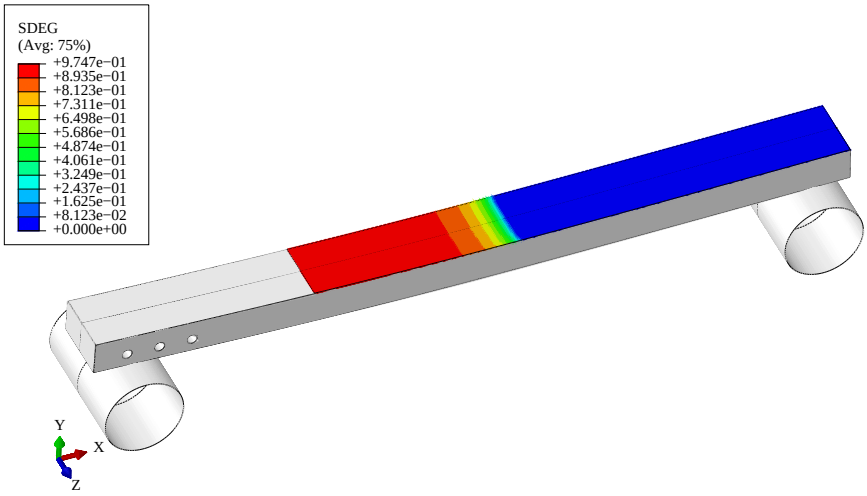

b)

Figure 4.46: a) Shear stress in 3D ENF Abaqus model at the onset of damage, b) scalar stiffness degradation and c) load displacement curve comparison between numeric and experimental.

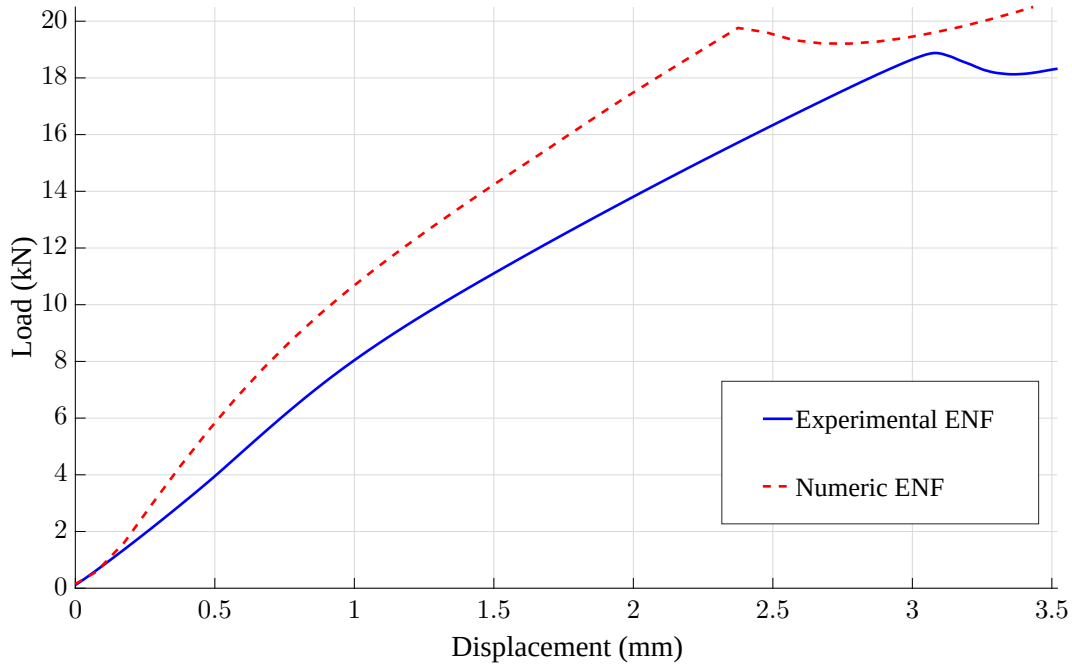

c)

Fig. 4.46 (cont.): a) S
scalar stiffness degradat
and experimental.

Given the good agreement between numeric models and experimental tests for mode I and II fracture tests, a high confidence degree in the chosen traction separation law is achieved. Models for the 20 mm and 40 mm overlap adhesive bonded joints were then constructed. Plasticity in the substrates was modeled as isotropic hardening with by the stress versus plastic strain relation for the unwelded material specified in section 4.2.1. Fig. 4.47 compares the experimental load versus displacement curves with the numeric models. However given that in the case of the 40 mm overlap adhesive bonded joint, the failure was through the substrate and away from the overlap, the numeric model will over estimate the ductility even while correctly estimating maximum load. The numeric models also showed higher levels of stiffness than the experimental tests, although this may be attributed to the way the displacement is measured in the experimental procedure. Since in single lap joints the out of plane bending does not allow for a conventional clip gauge to be used to measure displacement within the specimen, the cross-head displacement was used and as such this displacement will include mechanical slack within the system. This justifies also the difference in stiffness between experimental 20 and 40 mm overlap joints, as in order to keep the distance from the overlap to the grips constant the latter specimens are longer, requiring a higher position of the tensile machine cross-head which results in higher slack (lower stiffness).

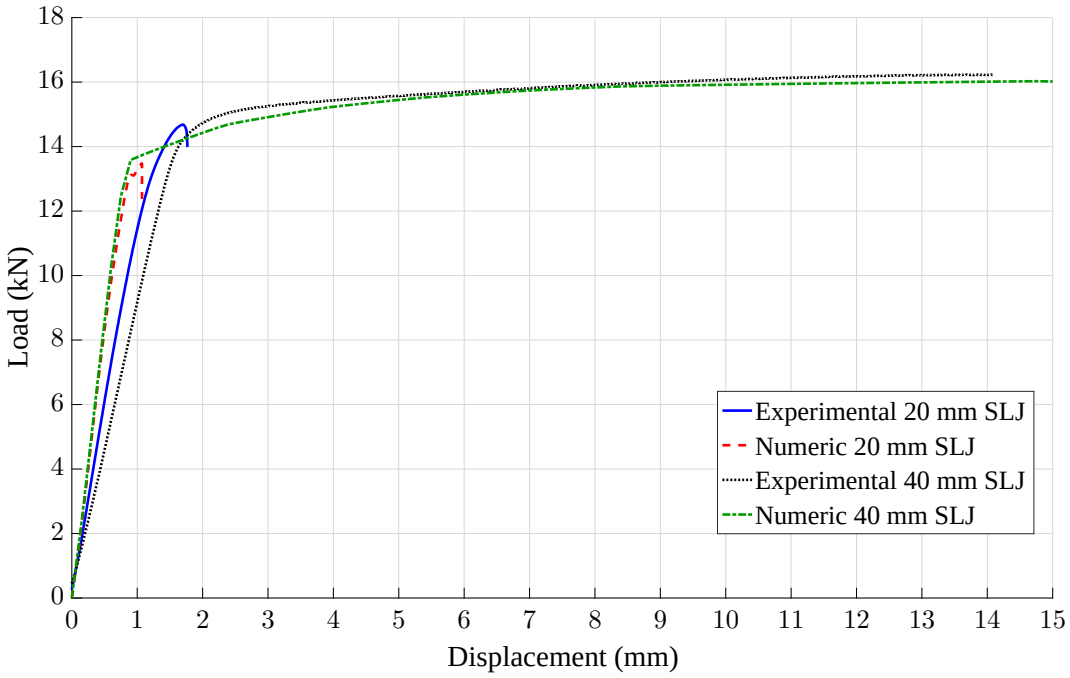

Figure 4.47: Experimental and implicit numeric SLJ load versus displacement.

In order to more accurately model the 40 mm overlap joints a ductile damage criterion is required to account for the failure of the aluminum substrate. Ductile fracture as a result of void nucleation, growth and coalescence, originating from microvoids and second-phase particles is the main failure mechanism. The general modeling strategy involves a damage variable or porosity that progressively affects the strength and stiffness of the material until failure. As these models include plasticity and failure simultaneously they are said to be coupled. One such example is the Gurson-Tvergaard-Needleman (GTN) poroplasticity model originally proposed by Gurson in [122] and modified by Tvergaard [123] and Tvergaard & Needleman [124].

As presented in [124], the GTN model describes the yield function as:

$$\Phi = \left(\frac{\bar{\sigma}}{\sigma_0}\right) + 2q_1 f^* cosh\left(-q_2\frac{\sigma_h}{\sigma_0}\right) - \left(1 + q_3 f^{*2}\right) \tag{4.15}$$

where $\bar{\sigma}$ is the von Mises equivalent stress, σ_0 the undamaged or fully dense matrix yield stress and the σ_h is the hidrostatic pressure. The constants q_1, q_2 and q_3 are material parameters accounting for the interaction of microvoids. The relation $q_3 = {q_1}^2$ is assumed with $q_1 = 1.5$ and $q_2 = 1$ as proposed in [124] and applicable to most metal materials. The void volume fraction f is the ratio of the volume of voids to the total volume of the material and as such $f = 0$ equates to a fully dense matrix and $f = 1$ implies that the material is completely voided and has no stress carrying capacity. Void coalescence will cause the void volume fraction to evolve as a function of the void volume fraction $f^*(f)$. This function accounting for rapid loss of stress carrying capacity from void coalescence is described as:

$$f^* = \begin{cases} f & f \leqq f_c \\ f_c + \frac{\bar{f_F} - f_c}{f_F - f_c}(f - f_c) & f_c < f > f_F \\ \bar{f_F} & f \geqq f_F \end{cases} \tag{4.16}$$

where f_c is the critical void volume fraction, f_F is the value of void volume fraction upon which complete loss of stress carrying capacity in the material occurs. The relation $\bar{f_F}$ is given by:

$$\bar{f_F} = \frac{q_1 + \sqrt{{q_1}^2 + q_3}}{q_3} \tag{4.17}$$

The parameters f_c and f_F were taken from [125], where ductile failure of aluminum alloy AA6082 weldments was studied. Base material f_c and f_F are 0.012 and 0.15 respectively. Hvall *et al.* in [125] states that the particles responsible for the void formation in this alloy are AlFeSi primary particles formed during the soldification process and large unsolved Mg_2Si constituent particles approximately 1 μm in size. The initial void volume fraction f_0 was set to 0, i.e. fully dense matrix was assumed, as in [125].

At last, to complete the constitutive model, it is required to establish void volume fraction as a function of time. The void volume fraction will be dependent on the growth of existing voids along with the nucleation of new ones, as given by:

$$\dot{f} = \dot{f}_{growth} + \dot{f}_{nucleation} \tag{4.18}$$

where $\dot{f}_{growth}$ and $\dot{f}_{nucleation}$ are the void volume fraction growth and void volume fraction nucleation rates, respectively. Growth of the existing voids is based on the law of conservation of mass and is expressed in terms of the void volume fraction as:

$$\dot{f}_{growth} = (1 - f)\,\dot{\varepsilon}^{pl} \tag{4.19}$$

with $\dot{\varepsilon}^{pl}$ being the plastic strain rate. Nucleation of voids is given by a strain-controlled relationship. The nucleation function is assumed to have a normal distribution, with a mean nucleation strain, ε_N and a standard deviation, S_N:

$$\dot{f}_{nucleation} = \frac{f_N}{S_N\sqrt{2\pi}} exp\left\{-0.5\left[\frac{\bar{\varepsilon}^{pl}_m - \varepsilon_N}{S_N}\right]^2\right\}\dot{\varepsilon}^{pl}_m \tag{4.20}$$

the $\dot{\varepsilon}^{pl}_m$ is the plastic strain rate of the fully dense matrix and f_N is the volume fraction of the nucleated voids. The values of ε_N, S_N and f_N, where also taken from [125], as 0.15, 0.10 and 0.01 respectively.

As the void volume fraction growth and nucleation are dependent of strain rate, it is required to solve for the true dynamic equilibrium, i.e. explicit solver is required. Since the explicit solver is computationally inefficient for longer time steps, as in quasi-static tensile loading, the model must be run at higher speeds. However, inertia effects must be kept to a minimum, in order not to distort the results [126].

A first model of a flat specimen tensile test was made to assess the constitutive model and the results were compared to the ones mention in section 4.2.1. Isotropic hardening, with Voce law extrapolation was used in specimens with half symmetry. Fig. 4.48, presents the comparison between numeric and experimental results for the base material tensile dogbone test.

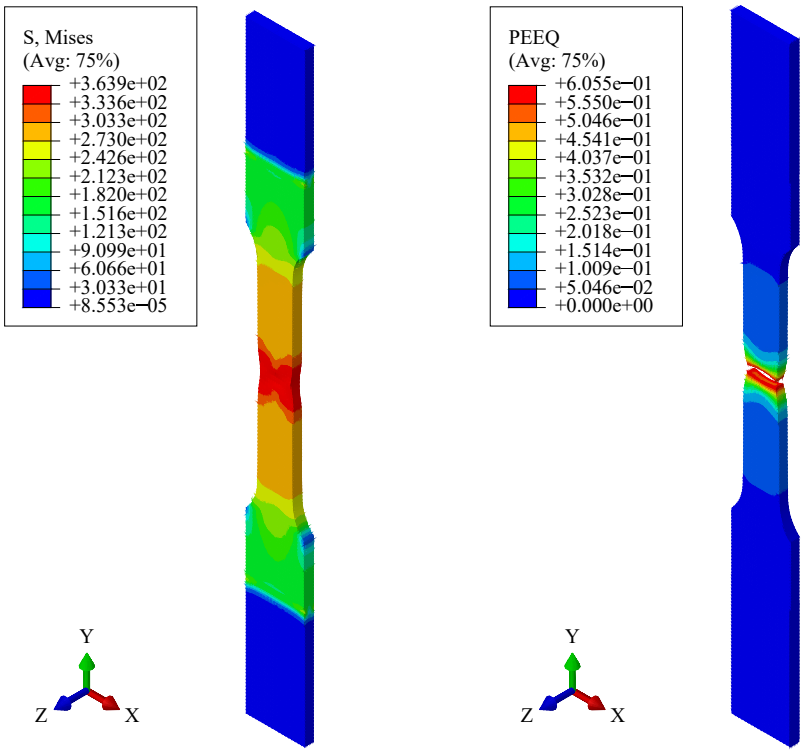

a) b)

Figure 4.48: a) von Mises stress at the onset of failure, b) equivalent plastic strain after failure and c) engineering stress versus engineering strain of both numeric and experimental tensile tests.

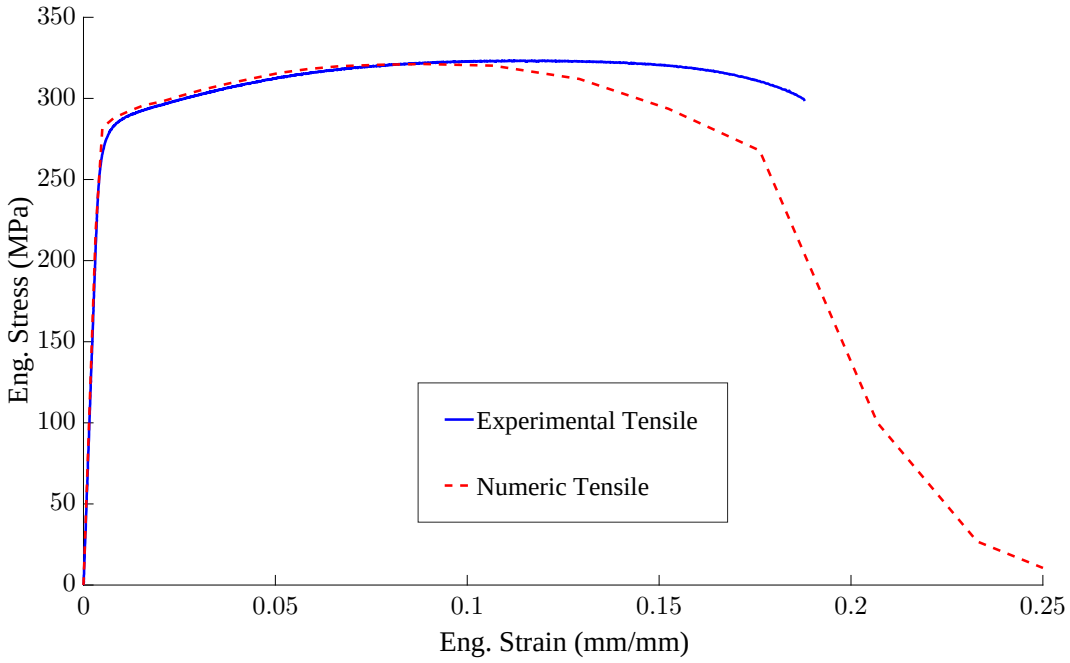

c)

Figure 4.48: a) von Mises stress at the onset of failure, b) equivalent plastic strain after failure and c) engineering stress versus engineering strain of both numeric and experimental tensile tests. (cont.)

The model correlates well up to necking, where the residual strength decreases faster than in the experimental case. This may be explained by the complex strain field after necking, where the material hardening becomes less isotropic. In Fig. 4.49, it is possible to verify that the load case differs from the uniaxial tensile load case (stress triaxiality = 1/3), demonstrating the more complex load case after necking. The experimental curves, also showed some dispersion after necking, as small variation in distribution of precipitates may lead to a different behavior after necking occurs. Some authors have proposed modifications to the classic GTN model to account for the more complex behavior after necking, such as for example, Gao *et al.* [127], Nahshon and Xue [128], Jackiewicz [129] and Malcher *et al.* [130].

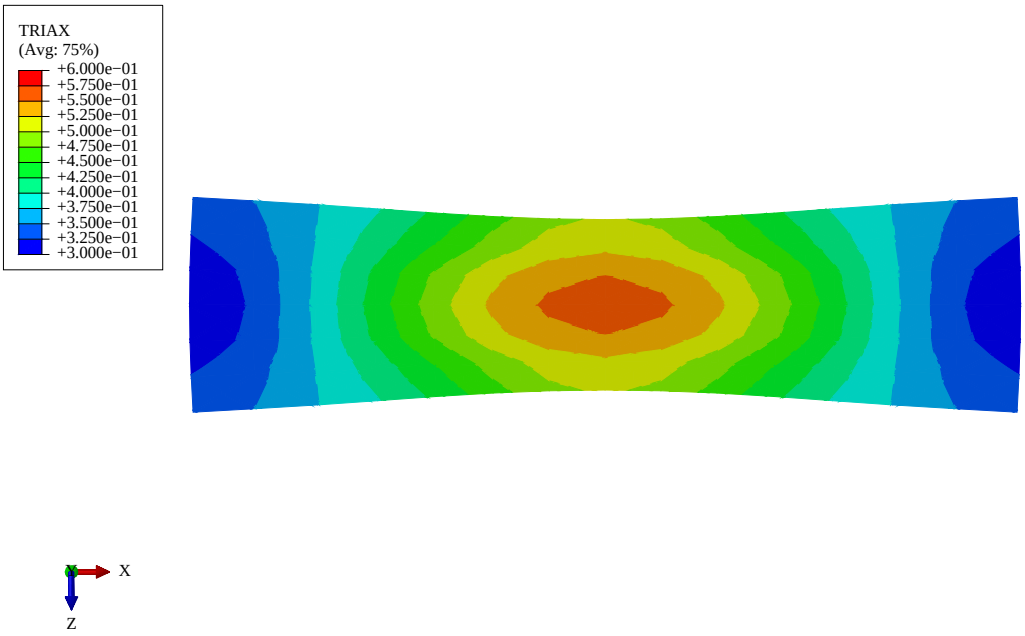

Figure 4.49: Stress triaxiality at the onset of failure in the failure surface.

However maximum stress and strain at maximum stress, as well as strain at failure correlate well with the experimental curves and as such the model is suited for the single lap joints with large overlap.

This ductile metal failure model was then applied to the base AA6082-T6 aluminum alloy substrates in the 40 mm overlap joints to account for the competing failure mechanisms of the adhesive bond (through cohesive zone modeling) and the failure in the substrate (through GTN). As in the experimental procedure, the model failed in the substrate away from the overlap and the load versus displacement curve showed good agreement, as shown in Fig. 4.50. Again the stiffness in the model is higher than obtained experimentally due to the experimental procedure used to measure displacement. The model overestimates the ductility of the joint, which may be related to the limitations of the GTN model for triaxiality states that differ from the uniaxial tensile load case, as discussed above.

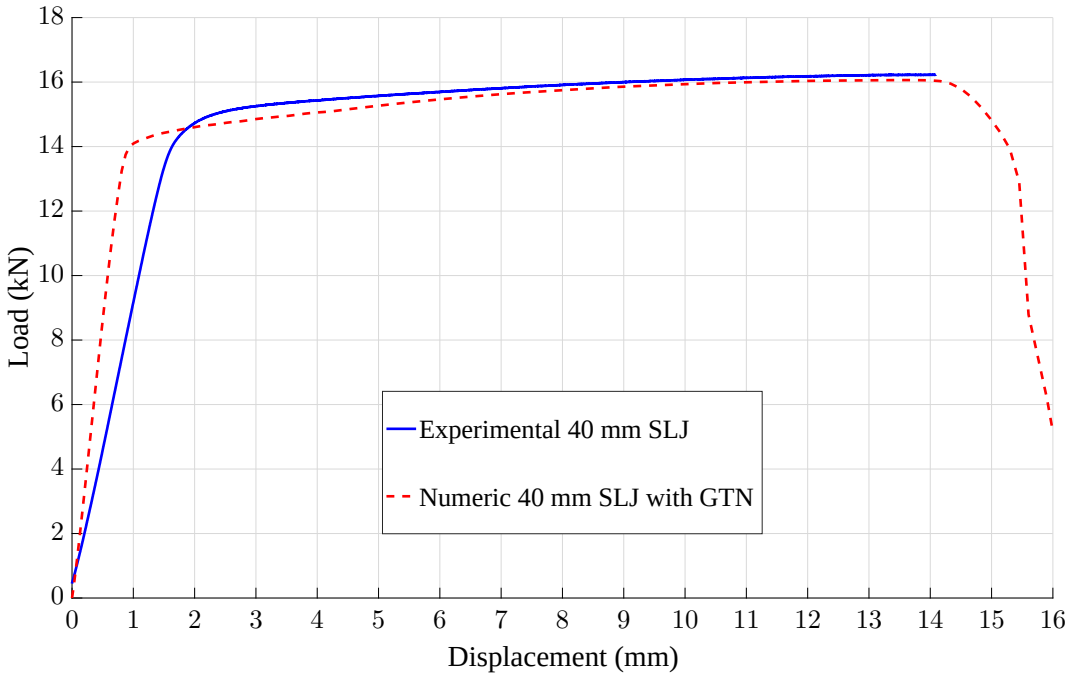

Figure 4.50: Load versus displacement of explicit numeric 40 mm overlap joint with ductile damage and experimental curve.

4.3.2 FSW Joints Models

As a simplified approach to modeling the complex stress-strain behavior within the weld, the same GTN model parameters use previously for the base material were employed on all the weld material regions, differing only the equivalent plastic strain, stress relation in the isotropic hardening behavior. The resulting stress strain behavior of the tensile dogbone welded specimen model is presented in Fig. 4.51.

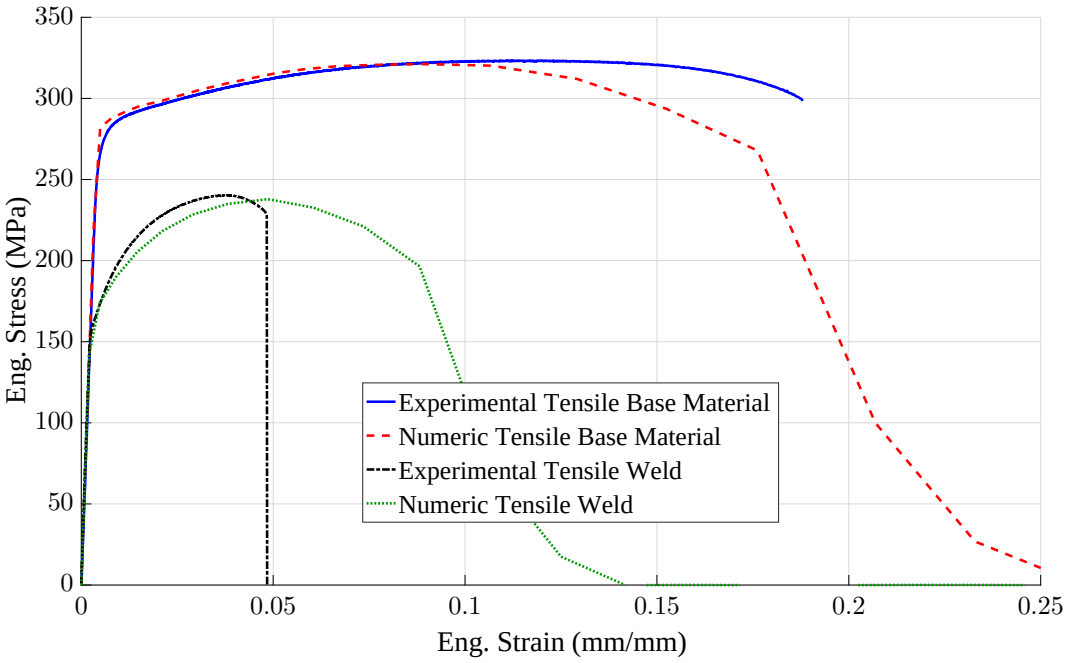

a)

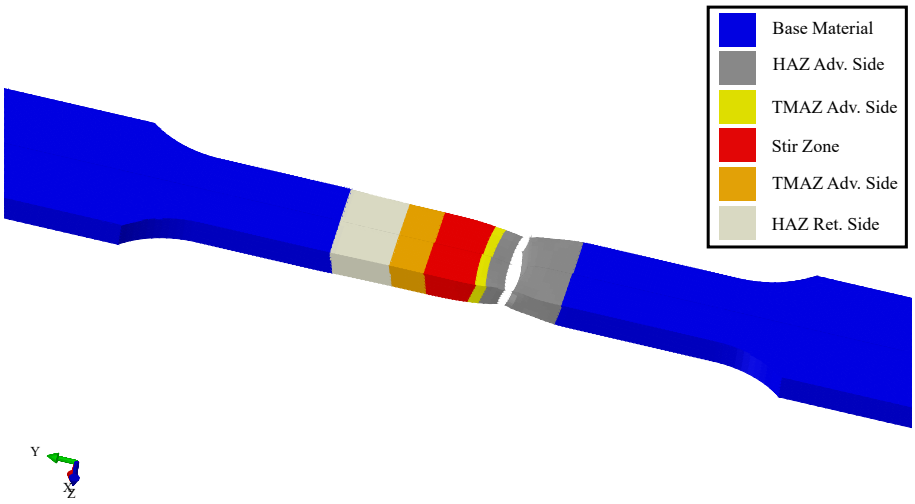

b)

Figure 4.51: a) Engineering stress versus engineering strain of both experimental and numerical dogbone tensile tests and b) failure location.

The failure location was in the advancing side heat affected zone, in accordance to the experimental result. Yield and ultimate strength correlated well with the experimental tensile tests, although the model overestimated the ductility. As the material microstructure varies considerably within the weld, with varying yielding throughout the specimen, large anisotropies arise [131]. The effect of residual stress resultant from the welding operation is also not taken into consideration, and eventhough heat input in FSW is lower than in conventional welding procedures, the rapid and localized heating leads to residual stress and distortion in these joints [132]. The combination of these factor lead to a complex stress-strain behavior, that is challenging to model and requires more complex approaches. Nevertheless given the good strength prediction, the approach was adopted to model the FSW overlap

joints.

A FSW overlap joint model was made based on cross section and micro hardness measurements, taking into consideration the hook shape and length. The resulting load versus displacement curve is shown in Fig. 4.52, as well as the failure location which corresponded to the experimental one.

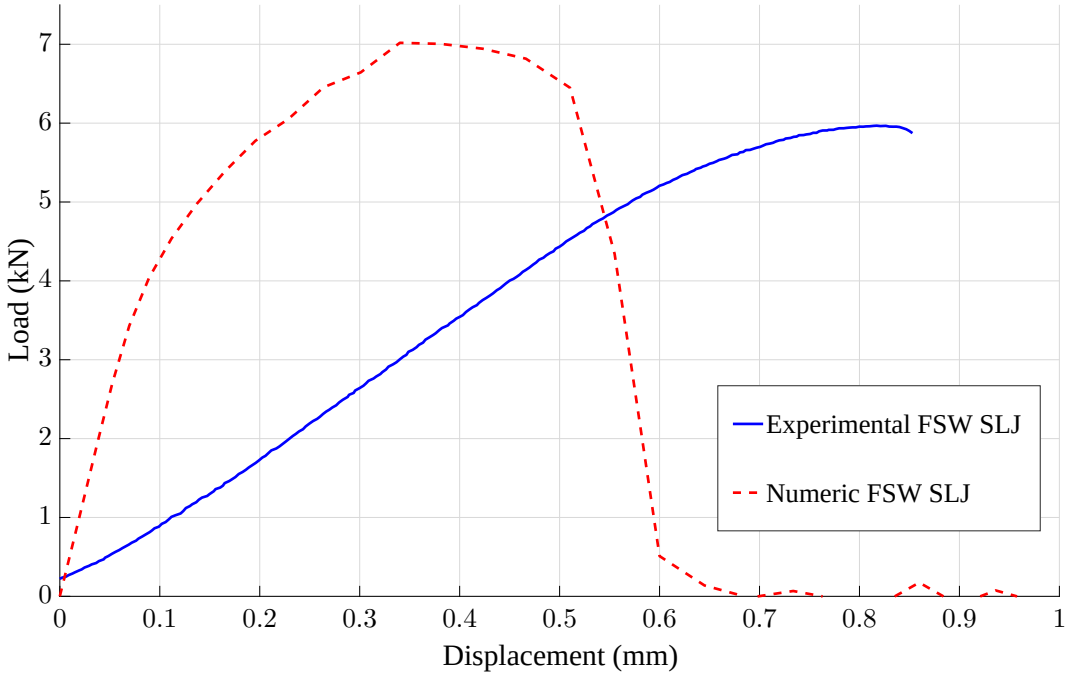

a)

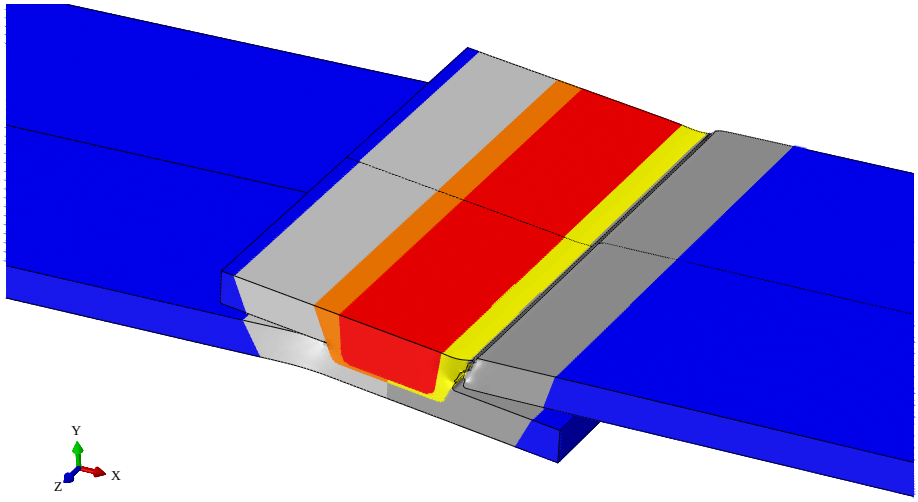

b)

Figure 4.52: Load versus displacement curve of experimental and numeric FSW SLJ a) and failure location in FEM model b).

A significant difference in stiffness is apparent which is mostly due to the way that the displacement is measured experimentally. As in the adhesive bonded SLJs, displacement is taken from the cross-head LVDT. Also, the model lacks the effect of residual stress, which may affect the stress-strain behavior. Another point to consider is that although in the numeric model the material regions are rigidly set, in reality the micro structural transforma-

tions are more gradual, especially between TMAZ and HAZ and between HAZ and base material. The hard boundaries between regions with different hardening behavior leads to stress gradients that are not completely realistic.

4.3.3 Hybrid Joints Models

The hybrid single lap joint combined both the aspects of the 40 mm overlap adhesive bonded model and the FSW single lap joint model. Failure location, as shown in Fig. 4.53, was consistent with the one obtained experimentally. Failure occurred suddenly in the adhesive immediately followed by failure in the transition between TMAZ and HAZ in the top loaded sheet. The non-dimensional stiffness degradation variable increased through both adhesive overlaps starting at the edges and hit 1 (cohesive element failure or 0 stiffness) in the majority of the overlap simultaneous, followed by failure in the substrate through void growth and nucleation.

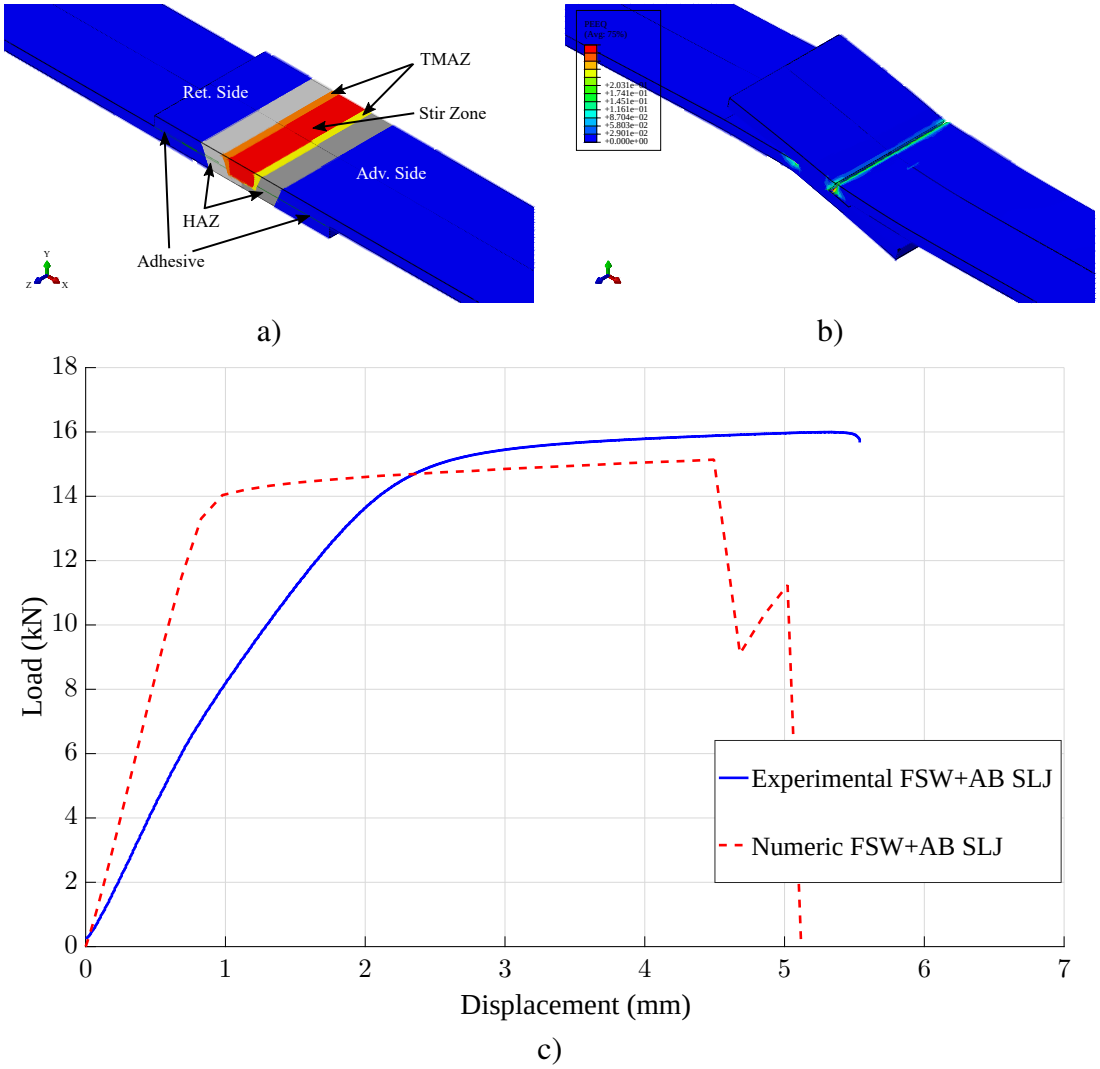

Figure 4.53: FEM model definition a) failure location and equivalent plastic strain after failure b) and load versus displacement curves c).

In Fig. 4.54 shows the load versus displacement curve of all SLJ numeric models. It

is observable that they follow the same trend as observed experimentally, with the 40 mm adhesive joint having the highest strength and ductility and the SLJ FSW having the lowest strength and ductility. From the 40 mm adhesive joint to the 40 mm hybrid one, there is a small reduction in maximum strength, but even more significant reduction occurs in the ductility of the joint. This loss of mechanical properties is mainly due to the high ductility of the epoxy adhesive, which results in higher deformation up to failure in adhesive bonded joints than in the welded ones. As such, the weld bead restricts the shear deformation of the adhesive in the overlap and when the adhesive fails, the loads at the boundary of the weld bead are sufficient to cause failure in the weld.

A significant improvement was achieved when introducing the adhesive in the overlap of FSW joints, as it increased the effective overlap, combined with the high, ductility, strength and toughness, resulted in more than double the strength and an increase of $10\times$ in displacement at failure. The use of the adhesive in the overlap distributed shear stress through the overlap in a more uniform way. The adhesive also unloaded the edge of the weld bead which is the failure initiation location, as due to its geometric features acts as a pre-crack close to mode I.

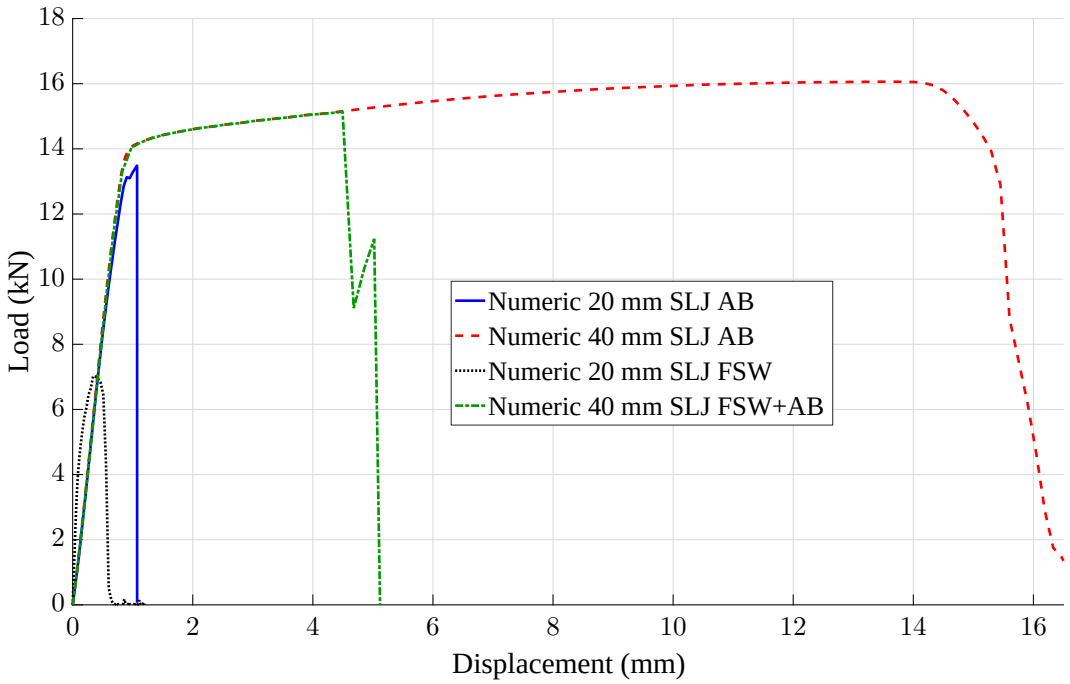

Figure 4.54: All numeric SLJ load versus displacement curves.

4.4 Chapter Summary

In this chapter the hybrid joining process was developed. The materials involved were characterized and parametric studies regarding process parameters and procedure order were made. The established process consists on phosphoric acid annodization of the aluminum surfaces to bond, bonding a continuous layer through the overlap with 0.2 mm and weld through the overlap with one weld pass with the adhesive in a non-cured form. Joints were

evaluated for their quasi-static strength and ductility as well as distortion levels and fatigue strength.

PAUT was analyzed as a potential NDT quality assurance method. It showed to be capable of detecting adhesive incursions within the weld due to poor parameter choice, but lacked the ability to detect other relevant defects in these types of joints.

Numeric models were also developed in order to model maximum load and failure location in these joints.

Having developed some degree of confidence in the process itself the application may now be studied in following chapters.

Chapter 5

Friction Stir Weld-Bonding in Aeronautical Structures

Given the development of the friction stir weld-bonding joining method presented in the previous chapter, this chapter will study its implementation in aeronautical structures. The emphasis is on joints for major component assembly (MCA) of metallic fuselages. For this purpose, joints of a typical aeronautical fuselage material were studied. Aluminum alloy AA2024 is a commonly used aluminum copper magnesium alloy in metallic fuselages for its high fatigue strength. Although newer alloys are being proposed to replace AA2024 in these applications, such as aluminum lithium and aluminum magnesium scandium alloys, aluminum alloy AA2024 is still the standard material used for new manufacturing and assembly concepts in aerostructures, due to its lower cost and easier procurement. Taking this into account, as well as the early development point of the proposed technology for the intended purpose, the study of aluminum copper magnesium friction stir weld-bonded joints was the following step. Quasi-static mechanical performance, along with fatigue and exfoliation corrosion resistance was assessed in single lap joints. A final joint configuration was proposed and benchmarked against riveted and FSW butt welded joints.

5.1 Friction Stir Weld-Bonding of Aluminum Copper Magnesium Alloys (AA2024)

Considering the different chemical composition and mechanical properties of the aluminum alloy AA2024 regarding the previously studied aluminum alloy AA6082, a small welding parameter study is required to guarantee sound, defect free welds. As the aluminum alloy AA2024 is less chemically stable than the aluminum alloy AA6082, and as such more prone to corrosion, the alloy is usually supplied with a clad layer on the exposed surfaces of the sheet. This clad layer when friction stir welded will remain in the inside of the joint and, as it is more brittle than the aluminum alloy, will lead to a premature failure of the joint. As such, it was opted to used a non-claded aluminum alloy AA2024-T3 sheet for all the joint to be manufactured. Since fuselage shells required chemical milling to introduce local

reinforcements, the removal of the clad layer selectively in the area to be welded could be easily achieved without disruptive changes to the current manufacturing processes. The chemical composition of the alloys is presented in Table 5.1, as according to the supplier certificate.

Table 5.1: Chemical composition of aluminum alloy AA2024-T3 (% mass).

	Si	Fe	Cu	Mn	Mg	Cr
min	-	-	3.8	0.3	1.2	-
max	0.5	0.5	4.9	0.9	1.8	0.1
actual	0.08	0.13	4.5	0.48	1.5	0.03

	Zn	Ti	Ti+Zr	Others (Total)	Al
min	-	-	-	-	Balance
max	0.25	0.15	0.2	0.15	
actual	0.2	0.04	0.04	0.03	

All aluminum alloy AA2024-T3 welds were performed on a FSW portal system, showed in Fig. 5.1 a). The tool used was a threaded conic 5 mm diameter tool attached to a 13 mm diameter grooved shoulder, as shown in Fig. 5.1 b) and c). The parameter window chosen was based on published results, such as [42] and past experience within the work group. The tool dimensions and geometry, as well as, rotation speed and tilt angle were kept constant while welding speed and axial loading was varied. The rotational speed used was 1000 RPM and the tilt angle was 0.5º. Welding speed was varied between 3 and 9 mm/s and axial load between 7 and 10 kN. In the case of the hybrid weld-bonding joints, the surface treatment employed was changed from the previously mentioned in chapter 3.3. Instead of the phosphoric acid anodization, the 3M^{TM} AC130 surface pre-treatment was used. This product is an anodization replacement surface preparation product for the aeronautical industry and was used in this experimental procedure due to the very large joints to be manufactured. The large dimensions of the joints to be produced, especially in the case of the longitudinal fuselage joints that will be discussed further ahead, impeded the use of anodization procedures.

a)

b)

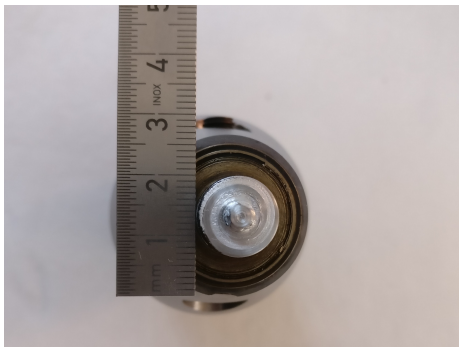

c)

Figure 5.1: FSW portal system at HZG a) and tool set-up b), c) used for aluminum aloy AA2024-T3 welds.

All welding trials were subjected to single overlap tensile testing and cross-section microscopic observation to assess for defects and measure the hook sizes. The joint with 7 kN and 7 mm/s resulted in higher strength, with an average joint efficiency of 76.19%, as shown in Fig. 5.2 a). The increase in strength was also accompanied by an increase in ductility, with the best performing joint having more than 9x higher displacement at failure than the worst performing joint as seen in Fig. 5.2 b). Joint strength and ductility increased with welding speed and was higher for the lower level of plunging force, except at 9 mm/s where voids were observed in the advancing side weld. Both, the increasing welding speed and the decreasing plunging force will result in lower heat input. Given that the AA2024-T3 is an age hardened aluminum alloy, higher welding temperatures, resulting from higher heat inputs will lead to phase transformation and lower mechanical properties [133]. Along with a thermal input consideration, the complex effect of the process parameters in material flow will result in different shape and sizes of the unwelded tips (hook defect).

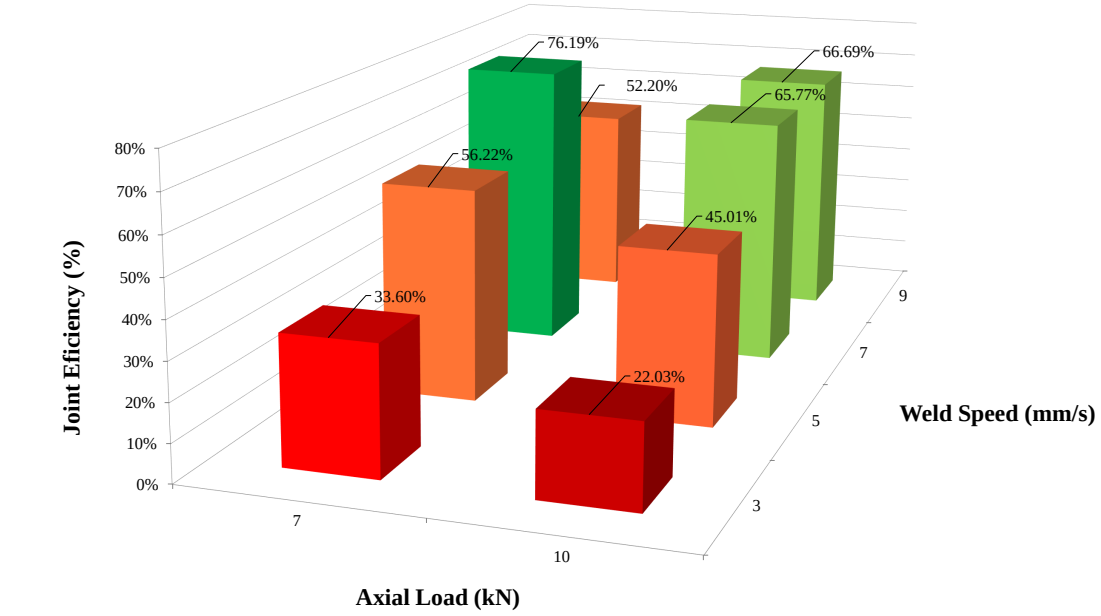

a)

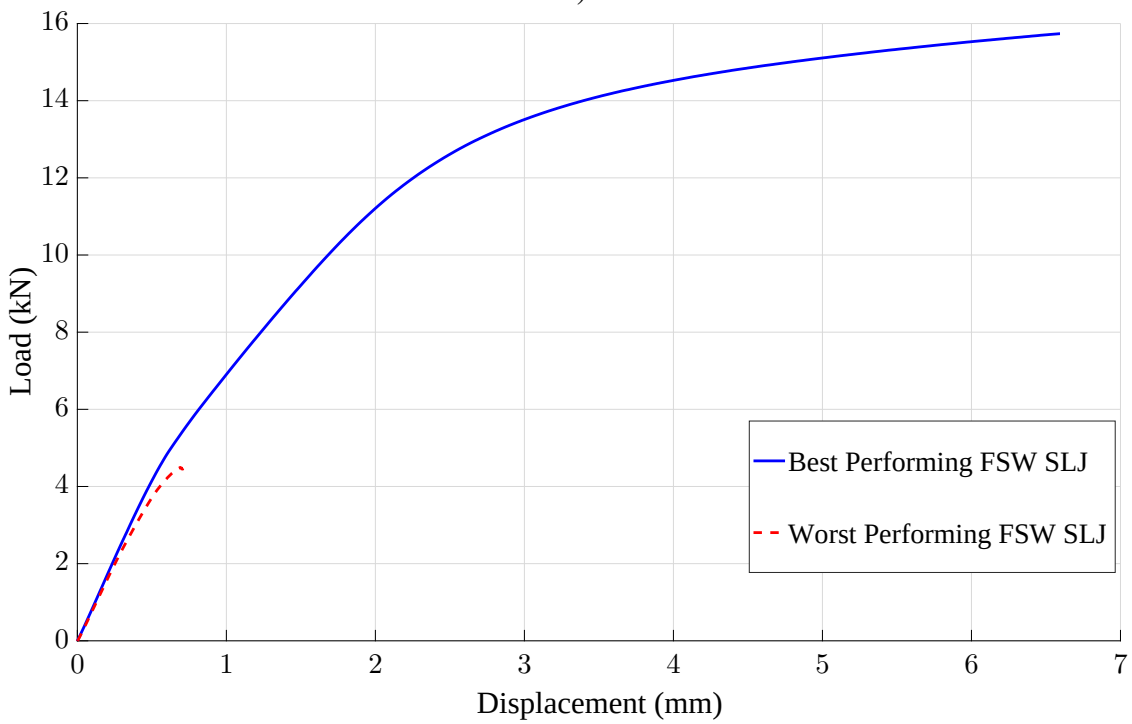

b)

Figure 5.2: a) FSW overlap joint efficiencies and b) load versus displacement curves of best and worst performing joints.

The effect of the process parameters on the shape of the weld bead edges is clearly observed in the cross sections of the worst performing joint (10 kN and 3 mm/s) and the best performing joint (7 kN and 7 mm/s), shown in Fig. 5.3 a) and b), respectively. Not only did the length of the unwelded edges decrease, but the advancing side hook changed from an upward direction to a downward one. This is particularly relevant, considering the geometry of the overlap joint the load path. As the joint tensile load and constrain are applied in the

top advancing side and bottom retreating side, the shape and size of this geometric feature will affect the effective resistant area at the center of the joint.

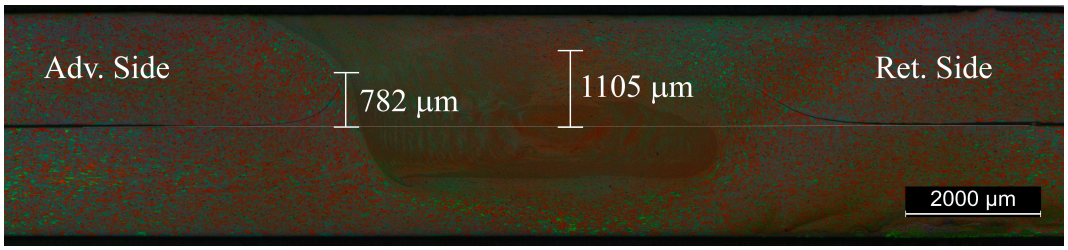

a)

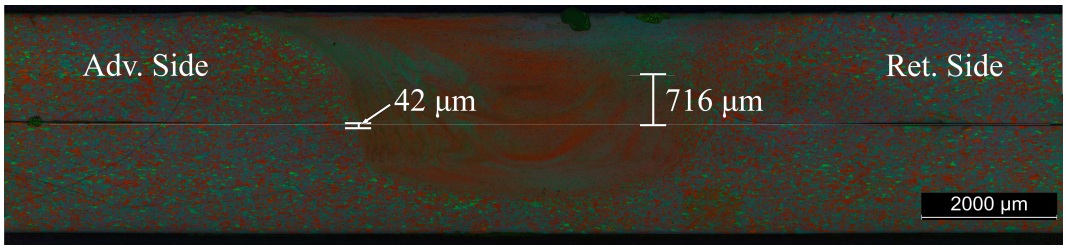

b)

Figure 5.3: Highest a) and lowest b) performing SLJs cross sections.

A similar process parameter study was performed for the hybrid FSW and adhesive bonding joints, as the adhesive interlayer is expected to affect both heat transfer and load transfer between top and bottom plates. As demonstrated before in chapter 3.3, the addition of an adhesive interlayer in the FSW overlap joint results in an overall increase in mechanical strength and ductility. All process parameters combinations resulted in joint efficiencies superior to 85%, with the higher performing joints being within the margin error of each other. Fig. 5.4, presents the average joint efficiencies in SLJ tensile testing with all combinations. Unlike the FSW overlap joints, the SLJ tensile testing alone did allow to select the best parameter combination tested. The only trend observed was that higher welding speed (9 mm/s) resulted in the highest strength. The less clear trend may be related to the procedures used in the adhesive bonding and surface treatment, as these experimental procedures were made manually, some variation may be attributed to the operator and procedure. Nevertheless the consistent high strength joints obtained and the small dispersion within each process parameter combination provide confidence in the experimental procedure.

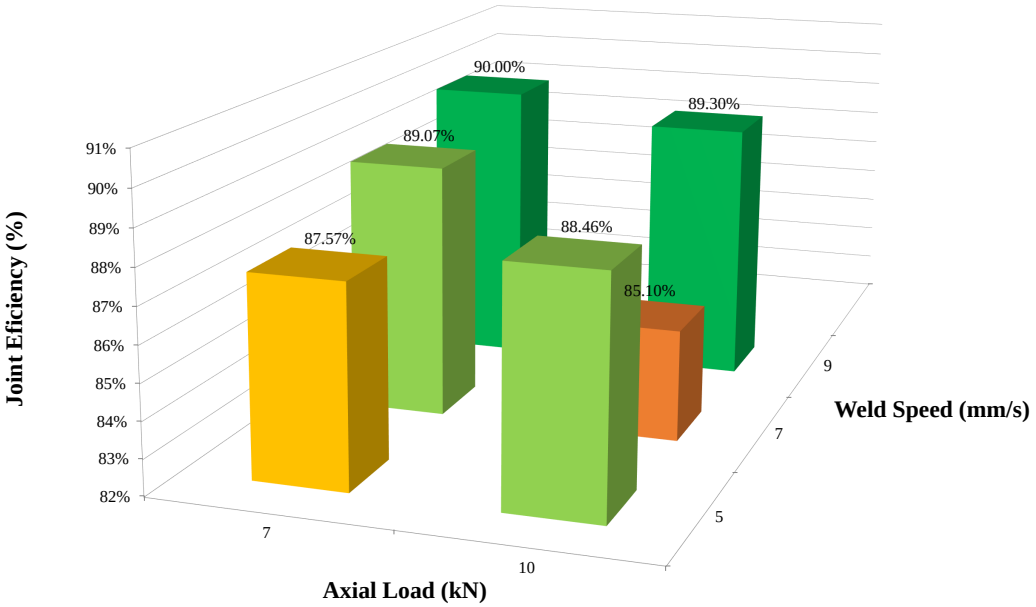

Figure 5.4: Hybrid FSW+AB SLJ efficiencies.

When analyzing the cross sections of the 9 mm/s joints, shown in Fig. 5.5, it was possible to observe the lower plunging force led to some adhesive inclusions within the weld bead. Although these inclusions appeared to have negligible effect in the average strength in quasi-static tensile loading, it would be expected that when cyclic loading the joints, performance would degrade, as the inclusions could serve as crack initiators. The introduction of these adhesive inclusions may be due to the lower plunging force, as higher axial loads may result in a more effective expulsion of the adhesive from the area to be welded. As in the best performing FSW overlap joints, the unwelded edge in the advancing side showed a downward direction.

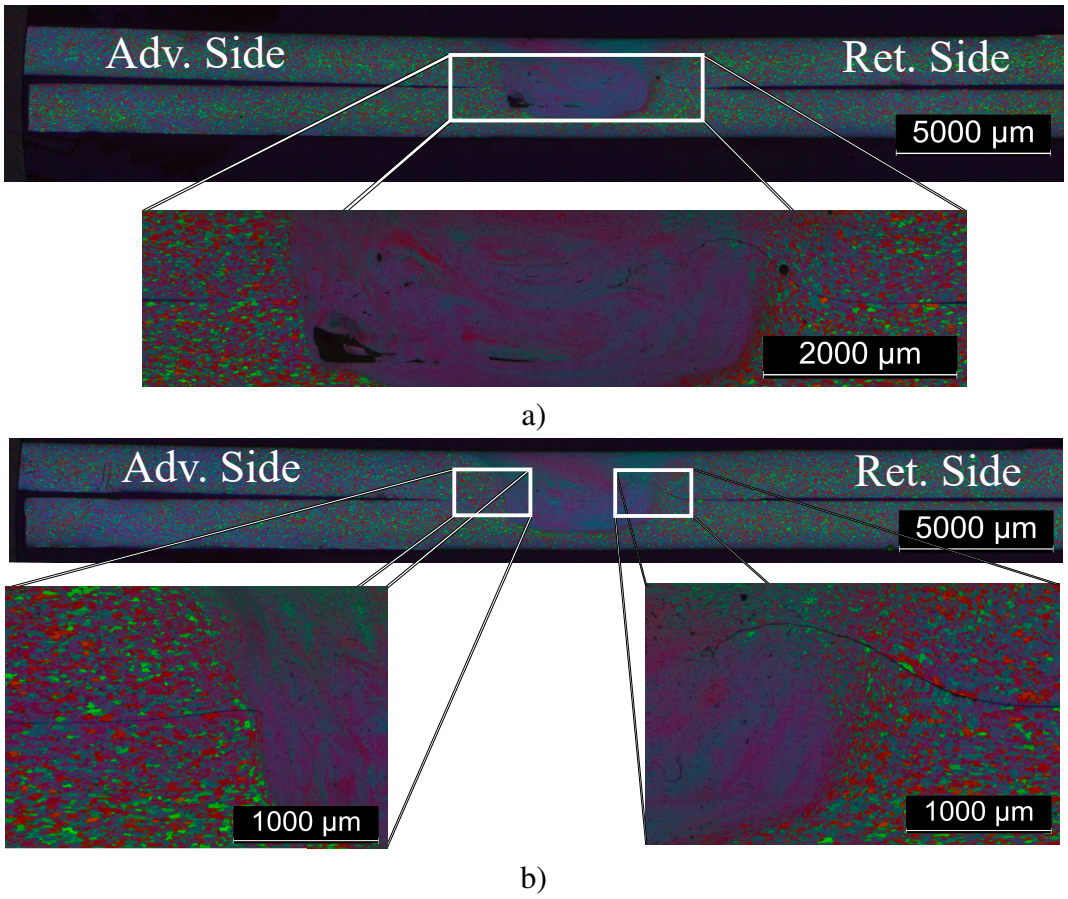

Figure 5.5: Cross sections of a 7 kN and 9 mm/s joint a) and a 10 kN and 9 mm/s joint b).

For fatigue and corrosion benchmarking which will be discussed further ahead, the process parameter combination to be used will be the 1000 RPM, 9 mm/s and 10 kN for the friction stir weld-bonded joints. Eventhough the addition of the adhesive interlayer significantly improved mechanical performance of the overlap joints, the failure mechanism showed to be mixed cohesive close to the interface and adhesive. Fig. 5.6 shows scanning electronic microscopy analysis of the failure surfaces in a hybrid joint. It may be observed that close to the overlap edges, where higher peel forces are exerted, lower remains of carbon (i.e. adhesive) may be observed. This leads to the conclusion that in these areas, the failure is mainly adhesive. During single lap joint tensile testing it was possible to observe on some of the tests that the failure of the adhesive was closely followed be the failure of the weld, through the transition zone between the advancing side themo-mechanically affected zone and heat affected zone. This area corresponds to the transition between elongated plasticized grains and larger equiaxed grains. In this region it is also present the unwelded tip, which will serve as the failure initiation for the weld failure.

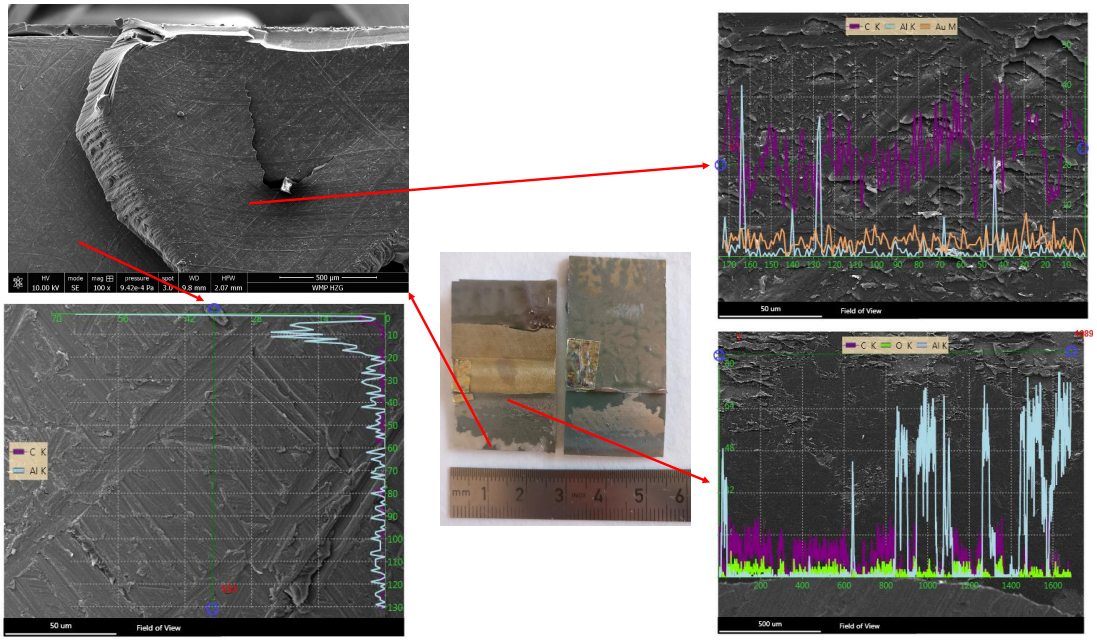

Figure 5.6: SEM and EDS analysis of the failure surface of a friction stir weld-bonded joint.

5.1.1 Fatigue Performance

Due to pressurization and depressurization cycles, longitudinal fuselage joints are subjected to cyclic loading and must be resistant to fatigue. This is in fact one of the reasons aluminum copper magnesium alloys are used in these structures. The existence of non welded tips at the weld edges in FSW overlap joints are highly detrimental for the joints fatigue strength. The addition of the adhesive interlayer at the overlap aims to overcome this challenge. To assess the effect of the use of friction stir weld-bonding technique in fatigue strength, cyclic loading of single lap joints at R=0.1 was performed. Weibull cumulative distribution function was used to plot the probabilistic S-N field for all three types of joints. As example, Fig. 5.7 shows the probabilistic S-N field along with the cumulative distribution for the hybrid FSW with adhesive bonding joints.

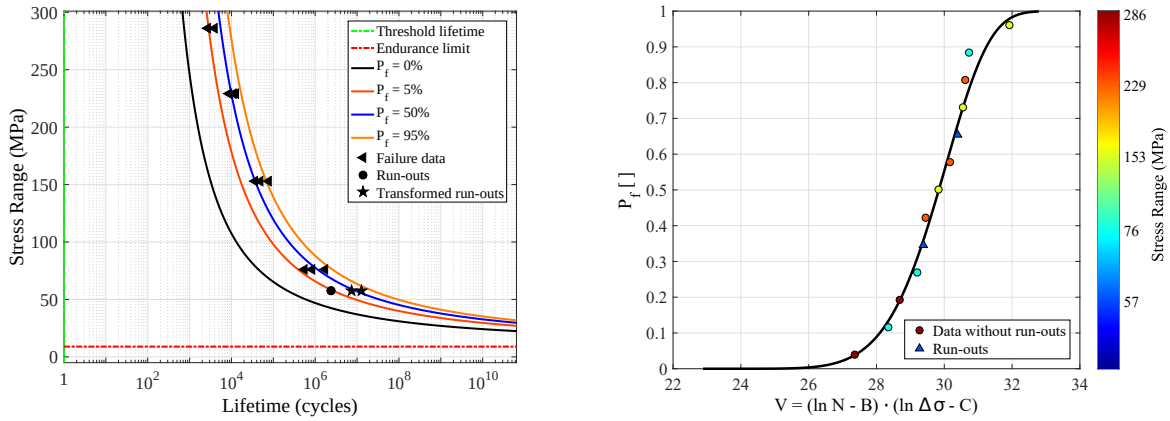

a) b)

Figure 5.7: Probabilistic S-N field of the friction stir weld-bonded joints a) and Weibull cumulative distribution b).

The resulting Weibull model parameters for the three types of joints are presented in Table 5.2.

Table 5.2: Weibull distribution parameters of the three joints tested.

	β	B	C	δ	λ
FSW overlap	1.3	0 (1 cycle)	1.7 (5.50 MPa)	2.20	24.27
Adhesive bonded	1.34	0 (1 cycle)	2.12 (8.36 MPa)	1.00	34.23
FSW + AB	6.54	0 (1 cycle)	2.3 (9.94 MPa)	7.36	22.88

Fig. 5.8 shows the median curves of FSW overlap, friction stir weld-bonded and adhesive bonded joints. As expected FSW joints had the lowest strength. The addition of the adhesive interlayer led to an increase in fatigue strength, although it did not match the fatigue strength of the adhesive bonded joints. The high ductility and as such energy absorption of the adhesive, as well as the continuous layer (no stress concentrations in the inside of the overlap) are the reason for this high strength. The limiting factors in fatigue strength of the adhesive overlap joints are related to the geometry of the joint, as the edges of the overlaps lead to peel stress and stress concentration. These edges are the failure initiation location. The failure however is sudden in these joints, as the adhesive fails without apparent fatigue cracks.

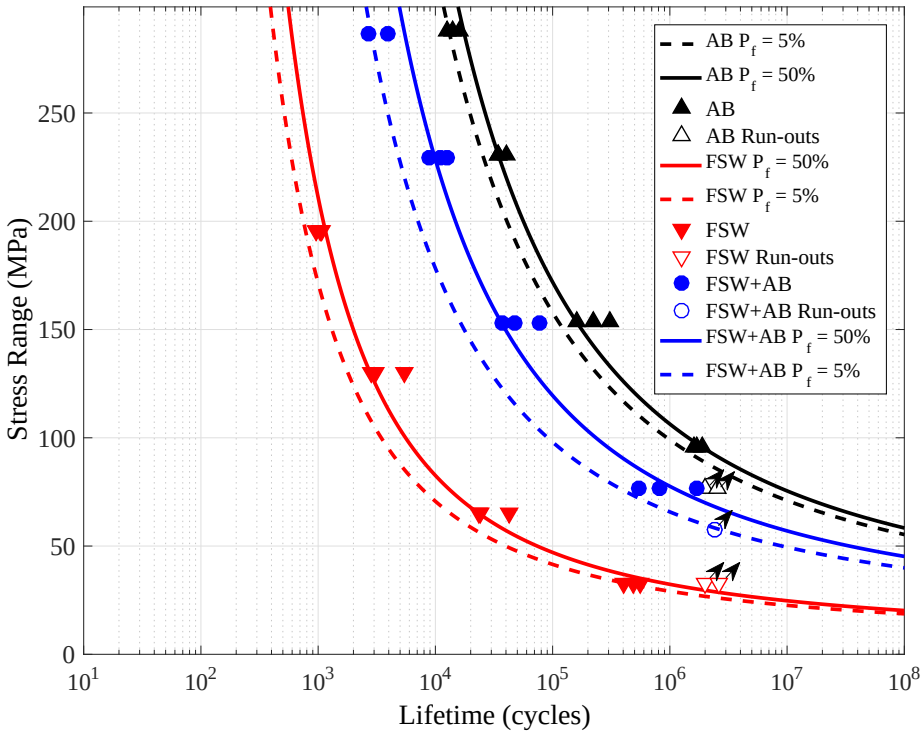

Figure 5.8: Median S-N curves of all three joint types.

5.1.2 Corrosion Performance

Although aluminum copper magnesium alloys are know for their high fatigue strength, they are more prone to corrosion than 5XXX and 6XXX aluminum alloys. For this reason this alloys are usually supplied with a high purity aluminum surface (Alclad), in order to protect the shells made with these materials. In areas where this protection layer may be removed, such as the case of riveted joints, due to hole drilling, etc., the use of sealants are required. The combined use of Alclad layers, sealants and primers and paints protect the metallic structures from environmental effects. In order to assure high strength welds, it is required to remove the Alclad from the overlap to be welded and bonded. With the aluminum sheet exposed in these areas, the adhesive layer must also act as a sealant, safeguarding this sensible area from the elements.

Before assessing the performance of the friction stir weld-bonded joints and friction stir welded overlap joints, when exposed to corrosion, the effect of corrosion exposure on the base material was studied. For this purpose tensile specimens were cut from the AA2024-T3 non-Alclad sheet with 1.6 mm thickness, parallel to the longitudinal (L) rolling direction, according to the ASTM E8 specification. The surfaces were prepared by sanding up to 1200 grit and masked with insulating material in order to be expose only at the reduced cross-section of the specimen. The surfaces were then cleaned with alcohol according to ASTM G1 specification and then exposed to exfoliation corrosion solution (EXCO), according to ASTM G34 specification. After the corrosion exposure, the specimens were immediately

cleaned according to ASTM G34 specification and then subjected to mechanical testing. The corrosive solution consisted of the following chemicals diluted in 1 l distilled water; sodium chloride (4.0 M NaCl), potassium nitrate (0.5 M KNO_3) and nitric acid (0.1 M HNO_3), as in [134]. Tensile tests were carried out in a servo-hydraulic Instron 100 kN testing machine according to the ASTM E8 specification and the crosshead displacement rate was kept constant and equal to 0.7 mm/min. Strain measurement within the reduced cross-section of the specimen was made through an extrenal Instrom extensometer with 50 mm ± 10 mm maximum travel. Seven exposure times, shown in Table 5.3, along with the reference, non corroded specimens were used.

Table 5.3: Exposure times and number of tensile specimens used for each exposure.

Exposure hours	Reference (0 h)	2 h	6 h	12 h	24 h	48 h	72 h	96 h
Number of specimens	3	3	3	3	3	3	3	3

The corrosion exposure of AA2024 specimens resulted in surface deterioration of the sheet due to the nucleation of corrosion induced surface pits, Fig. 5.9. For short corrosion exposure times and up to 2 h, pitting formation on the corroded surfaces remains limited, e.g. Fig. 5.9 a). With increasing exposure time, the pitting density and size tend to increase, Fig. 5.9 b) to g). Additionally, a transition from pitting to exfoliation corrosion mechanism takes place after 24 h exposure time; thus, the corrosion exposure times arbitrarily selected as short exposure times ($\leq$ 24 h) and long exposure times (> 24h),where accumulated corrosion damage (exfoliation) on the large surfaces is evident.

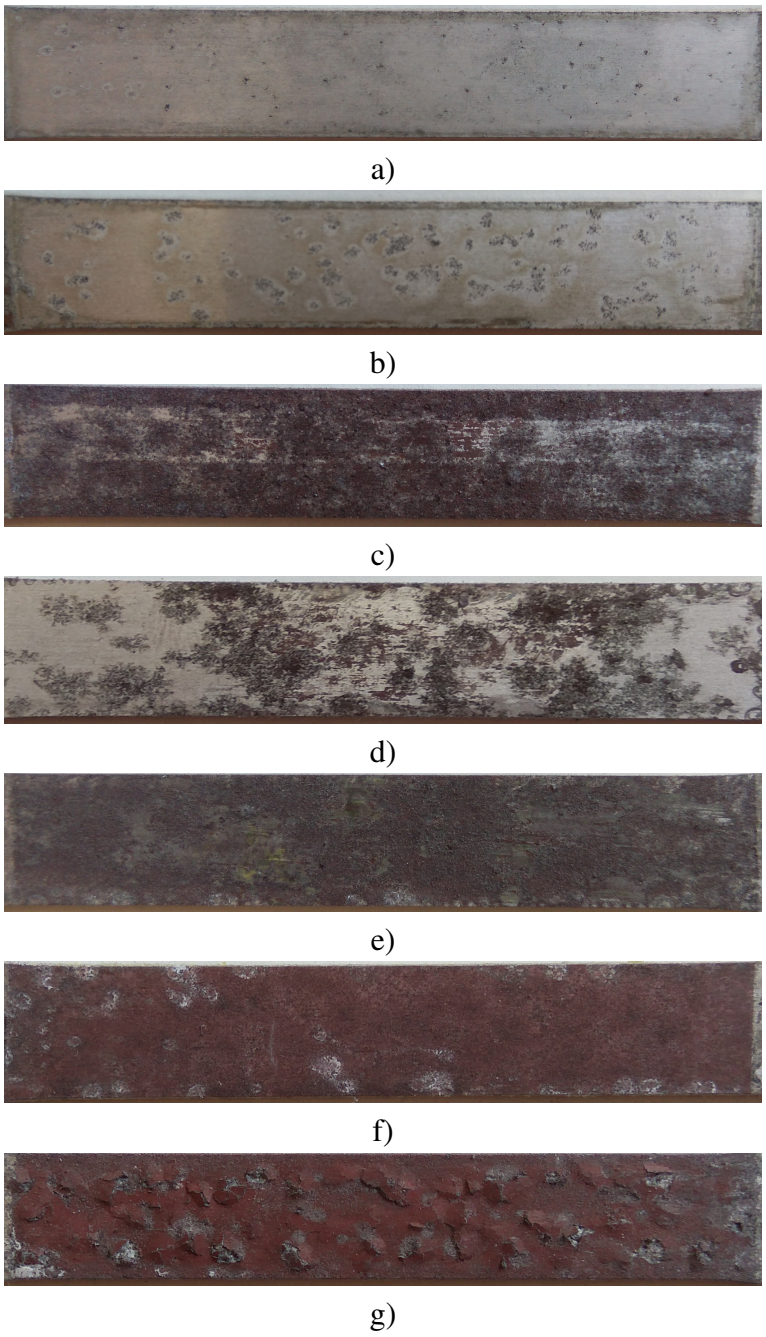

Figure 5.9: Cross-section of pre-corroded specimens for 2 h a), 6 h b), 12 h c), 24 h d), 48 h e), 72 h f) and 96 h g) corrosion exposure time.

Fig. 5.10 presents the effect of exposure time on stress-strain behavior of the AA2024-T3 base material. It is observable a reduction in yield and ultimate strength, even for small exposure times, e.g. 2 h, where no significant surface attack is evident. The reduction in ductility was however more pronounced than the reduction in strength, with exposure time having a significant effect in elongation at failure. A considerable strength drop was observed after 2 h corrosion exposure time, which was attributed to the reduction of the effective thickness of the specimens.

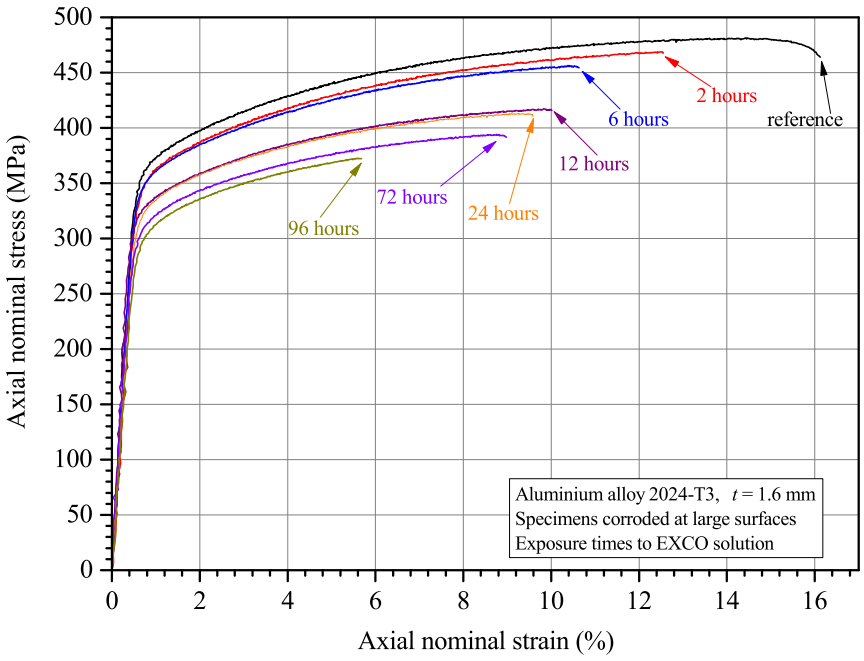

Figure 5.10: Tensile curves of AA2024-T3 non-Alclad with varying exposure time to EXCO solution.

The effect of exposure time in the mechanical properties of the base material is clearly shown in Fig. 5.11. Corrosion exposure does not essentially affect the conventional yield stress σ_{yield} as well as ultimate tensile strength σ_u values either for the short or long corrosion exposure times. They maintain approximately 85% of their initial values even after 24 h corrosion exposure time. Additionally, at the highest corrosion exposure time e.g. 96 h, where excessive exfoliation corrosion is evident, the normalized mechanical properties of σ_{yield} and σ_u are almost 80 % of the reference values.

Opposite to this, elongation at fracture A_f was essentially decreased even for the short corrosion exposure times (<24 h) where pitting corrosion is the dominant corrosion-induced degradation mechanism; approximately 50% decrease from the initial A_f value is evident after 24 h exposure time. For the long corrosion exposure times the A_f decrease exceeds 50%.

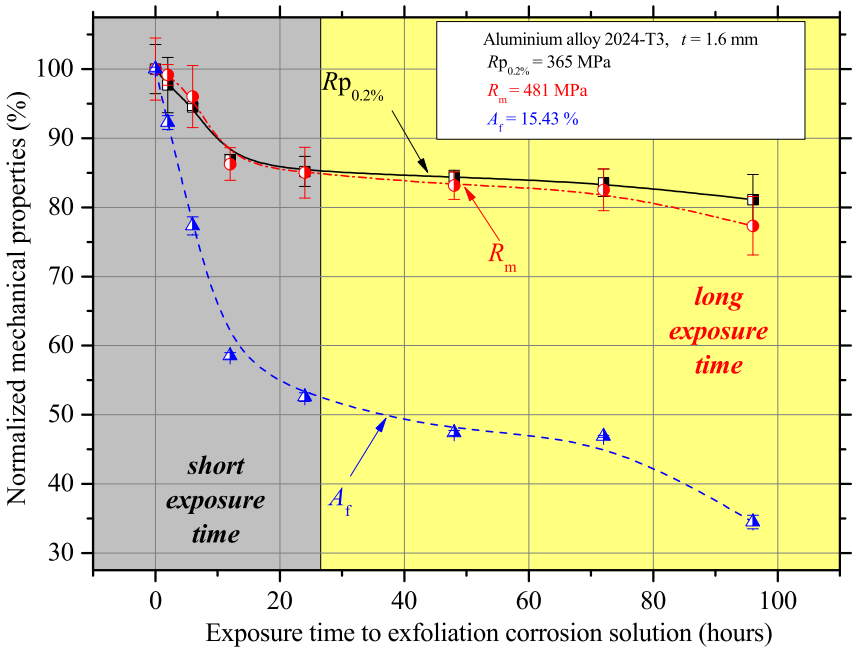

Figure 5.11: Normalized mechanical properties of AA2024-T3 non-Alclad with EXCO exposure time.

Having demonstrated the detrimental effect of exfoliation corrosion in the base alloy, FSW and FS Weld-bonded joints were then subjected to the same conditions in order to assess and compare the strength and ductility of these joints. Joints subjected to 24 h and 76 h exposure were tested at 1 mm/min cross-head speed. In the case of 24 h exposure, one sample of each joint type was also tensile loaded while displacement was measured through 3D DIC, as to assess the out of plane bending in both joint types. For these specimens, the top oxide layer was removed through mechanical means, by way of metal brush, as this oxide layer is composed of corroded aggregated particles which due not deform. Upon this, a white base layer was painted on the specimens, followed by a random black spot speckle, painted with and airbrush.

Fig. 5.12, shows the single lap joints specimens subjected to 24 h exfoliation corrosion exposure. It is possible to observe in both, that the majority of the oxidation occurred within the weld, which is due to the finer microstructure, with more intregranular boundaries in this region. No discoloration or obvious sign of degradation of the epoxy adhesive is observed in these joints.

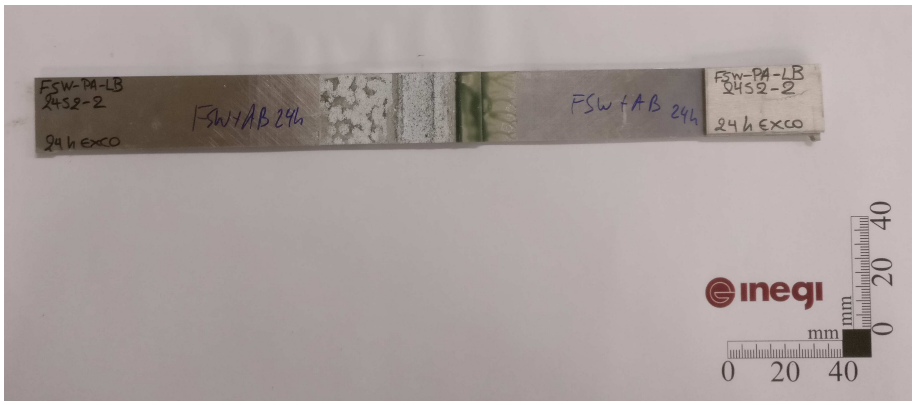

a)

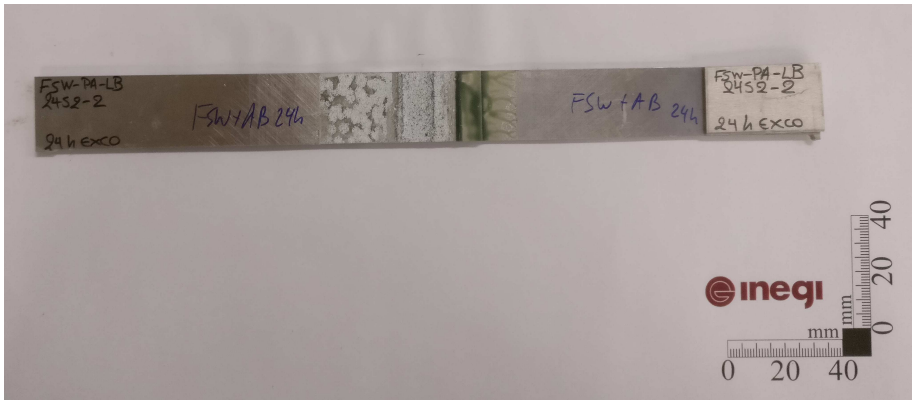

b)

Figure 5.12: FSW a) and FS Weld-bonded b) joints subjected to exfoliation corrosion for 24 h

As expected from the deterioration of the mechanical properties of the base alloy shown above and the effect of recrystallization in the joint weld, the joint strength and ductility of FSW overlap joints is highly effected by exposure time, as shown in Fig. 5.13. However, the hybrid joints did not show the same trend, as maximum load kept constant between 0 and 24 h and only reduced slightly at 76 h. This demonstrates that the epoxy adhesive did not degrade in the corrosive environment it was subjected to. As such, even though the weld in these joints loses strength, the adhesive layer keeps most of its strength.

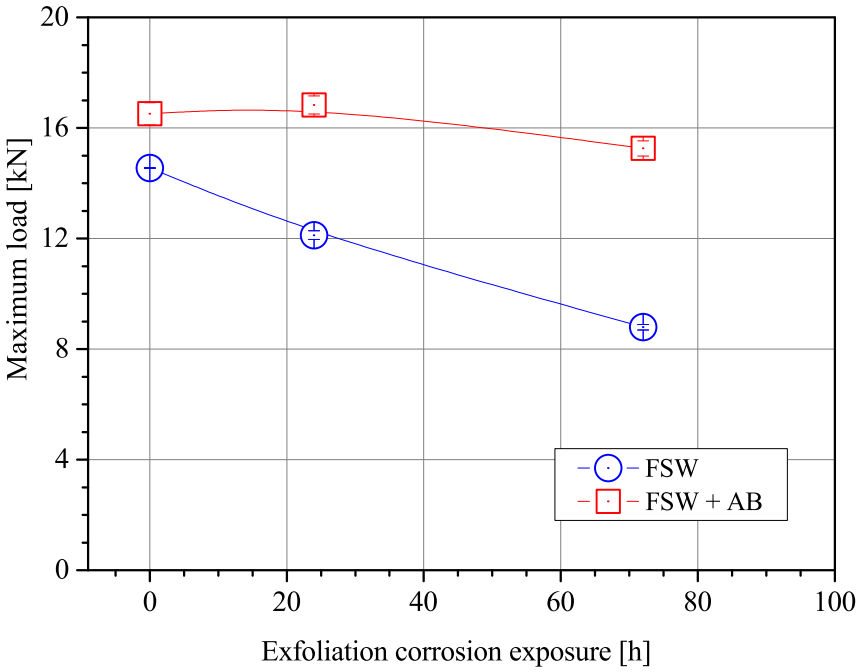

Figure 5.13: Maximum achieved load versus exposure time of FSW and FS Weld-bonded joints

Comparing the stress displacement curves for the 24 h exposure FSW and hybrid joints, shown in Fig. 5.14, it is observable not only the lower strength, but also the reduced ductility. A reduction in ductility was to be expected given that the corrosion analysis of the base material showed a more significant effect on ductility than in strength. Analyzing the out of plane deformation, it is possible to observe that the adhesive layer in the hybrid joints reduces the out of plane bending, explaining the higher strength observed. It also demonstrates that this adhesive layer did not degrade in this corrosive environment and exposure time, as it restrained the overlap out of plane bending.

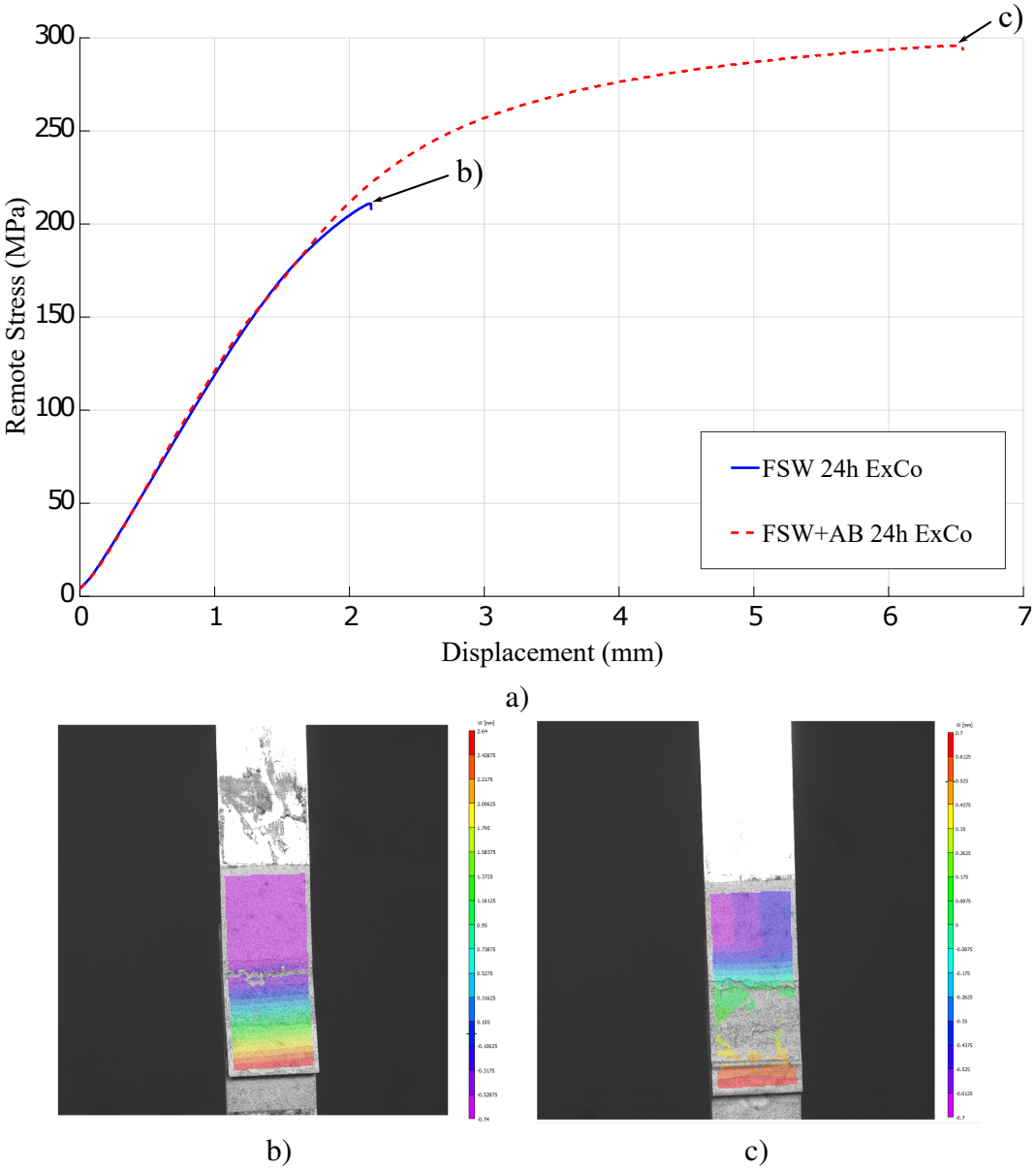

Figure 5.14: Comparison of stress-displacement behavior of FSW and hybrid joints with 24 h exfoliation corrosion exposure a) and out of plane deformation in FSW b) and FS Weld-bonded specimens c)

Upon failure FSW joints showed oxidation at the overlap edges (see Fig. 5.15), as these are exposed, while in the hybrid joints this was not the case as this region was filled with adhesive.

a)

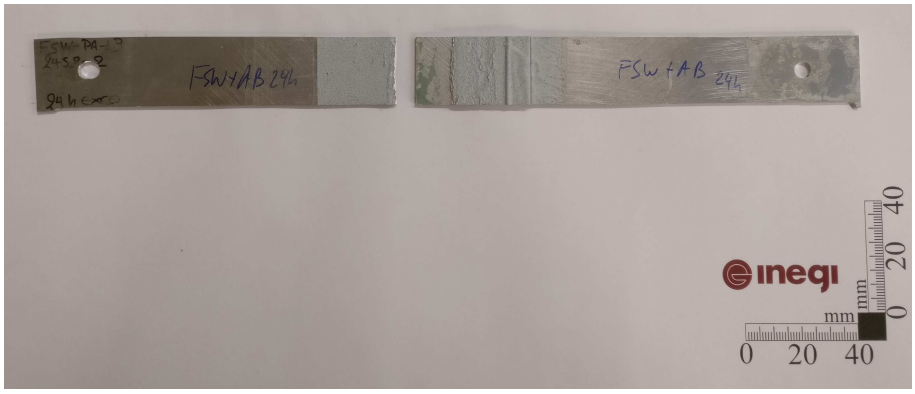

b)

Figure 5.15: FSW a) and hybrid b) specimens subjected to 24 h exposure and tensile tested

Although further testing is required to assess the corrosion protection effect of the adhesive layer in hybrid joints, it is demonstrated that these joints can still perform even with considerable corrosion of the weld bead. As such, the use of such joints could allow repair of joints that demonstrate signs of corrosion before structural integrity is significantly affected.

5.2 Major Component Assembly with Friction Stir Weld-Bonding

5.2.1 Weight and Cost Assessment

Notwithstanding all the major drivers of the aeronautical industry, aircraft manufacturing is a highly cost-driven sector. Cost may be considered a transversal target, as many other drivers, such as performance or environmental footprint may be converted to costs. Costs must also be contemplated in all product stages, from development to disposal. As such, cost reduction in aircraft may include optimization in development, manufacturing, operational and disposal costs. For instance, in the development of a new aircraft, it is a common option for the constructors to try to share the design and characteristics of parts in order to reduce development costs, [135]. This is achieved through aircraft families, who share common parts and characteristics, such as platforms and systems, but with each aircraft satisfying

different mission requirements. One example of such is the Airbus A320 family of aircraft, which includes smaller aircraft's A318 and A319 and longer haul aircraft such as the A321. Given the importance of costs in the lifetime of an aircraft, decision processes require cost analyses to be performed. Cost analyses can be done through different techniques, each one with its own specific characteristics, advantages and disadvantages. A review of these techniques was made by Curran *et al*. in [136] based in four major groups:

Analogous cost estimation Is based on comparison with similar products. Taking into account technical differences between the product of which the cost is to be estimated and similar products that provide the analogous data can refine the cost estimation;

Parametric cost estimation Cost of a product is linked to technical parameters such as weight, size or part count. To link cost to the technical parameters, relations are developed based on historical data, using statistical techniques;

Bottom-up cost estimation Requires a work breakdown structure of the product, which them is used to sum the cost of all entities; for instance, the cost of producing a joint based on all actions and materials involved in the process of producing the joint. The main disadvantage of this method is that it is very information intensive;

Generic causal estimation The genetic causal cost modeling methodology imposes a breakdown of the cost into a number of cost elements, including material cost, fabrication cost and assembly cost, so that cost can be formulated into semi-empirical equations to be linked to the same design variables as considered in the structural analysis.

Along with cost, weight is an important design driver for the aeronautical industry, as it has a direct detrimental impact in most of the variables in the aircraft design goals.

Fuselages account for the largest structure cost in percentage terms of an aircraft, with structures by themselves accounting for 35-40% of the recurring production costs [137], as shown in Fig. 5.17. Consequently, optimization in the manufacturing of these structures has large repercussions in the total operating costs of the final aircraft. Adding this to the fact that aircraft may stay in production for many decades (as is the case of the Airbus A320 and the Boeing 737), with only limited and far between revisions to fuselage design and manufacturing processes, leads aircraft manufacturers to very carefully study and decide the design and manufacturing processes to implement in this structure. One of the reasons for the high costs of fuselages is related to the large amount of manual labor time required for riveting due to the complexity involved in the automation of some of the procedures.

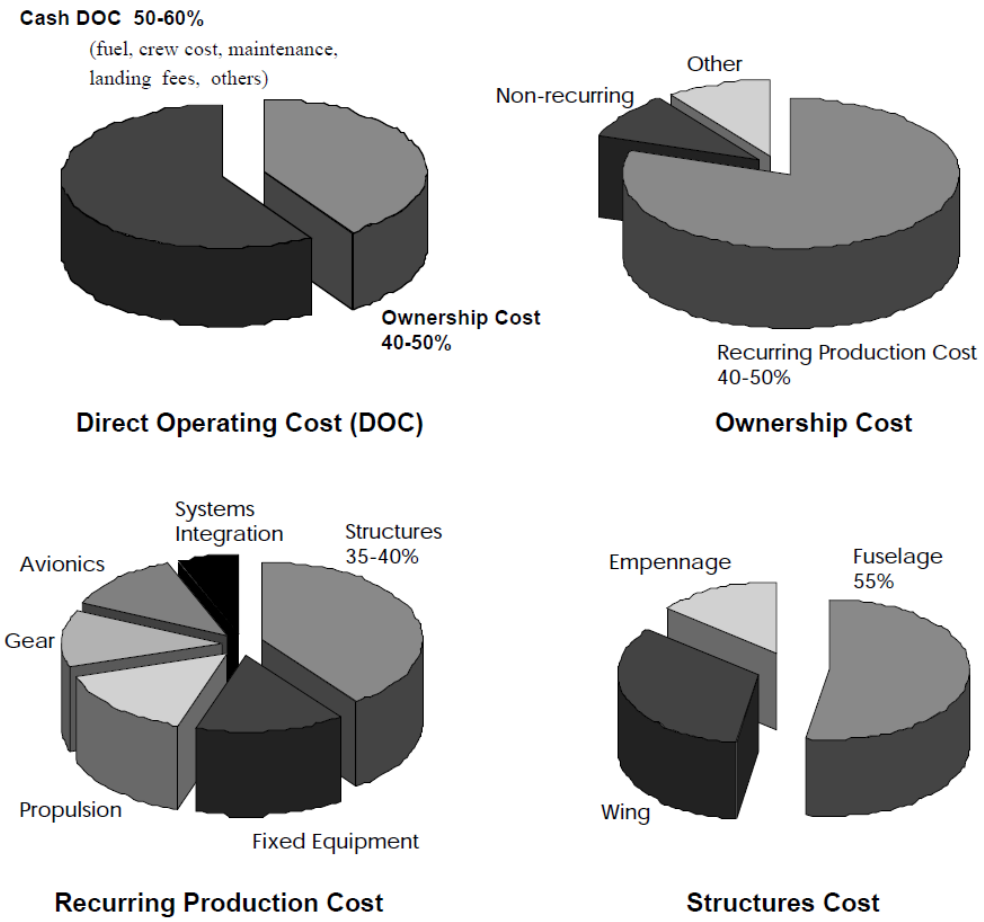

Figure 5.16: Direct operating cost breakup in a typical commercial airliner [137].

Simultaneous reduction of weight and cost in a fuselage design is challenging, as most new materials, adopted for weight reduction, are usually more expensive and require new designs and manufacturing processes, increasing the final cost. One example of such, is the adoption of carbon reinforced polymers, where weight reductions are expected, albeit with higher manufacturing costs than current state-of-the-art aluminum solutions [138]. As such, a tradeoff is required between these two variables, for a successful product development. As the Manufacturer's Empty Weight (MEW) impacts the entire lifetime of the aircraft, relations are established between structure weight and cost for design and optimization purposes. Kaufmann *et al.* considered costs of weight in [139], through a Direct Operation Cost (DOC) objective function, based on the manufacturing and assembly costs - C_{man}, the costs of lifetime fuel burnt per each kg of aircraft - p and the part weight - W:

$$DOC = C_{man} + pW \tag{5.1}$$

Although many other costs arise during the aircraft lifetime, such as service, maintenance, repair and disposal, it is assumed that manufacturing and fuel costs are the predominant costs considered in the design design of new parts and can be used for structural optimization in order to achieve the best tradeoff between weight and cost.

Weight reduction in aluminum aircraft fuselages has been pursued through the adop-

tion of new lighter alloys and new structural concepts, such as integral structures produced through new welding techniques. These new structural concepts have been developed in multiple directions, with the new machining operations (as high speed machining) or with diverse treatments (as shot peening) or with new joining processes to create integral structures without fasteners. One example of the latter is LBW, a more mature fusion welding process than FSW, that has been applied by Airbus to join stringers in fuselage panels in three models of aircraft: A318 (2 panels, corresponding to more than 50 m of welds in each aircraft), A340 (14 panels, corresponding to more than 400 m of welds in each aircraft) and A380 (8 panels, corresponding to more than 300 m of welds), [140]. In [18] Pacchione and Telgkamp, state a saving of 0.18 kg per meter from laser beam welding stringers instead of riveting at Airbus. This resulted in savings of 9 kg in the A318, 72 kg in the A340 and 54 kg in the A380. FSW is expected to yield similar savings as the same joint geometry as in LBW can be achieved. Higher weight savings may potentially be achieved in the longitudinal joints, as these are made with 2 or 3 rows of rivets. A longitudinal joint with 3 rows of rivets requires 75 mm of overlap and as such, the replacement of riveting for FSW butt-joining would potentially save 0.8 kg per meter of joint [18]. However, the use of FSW butt-joining alone for the longitudinal joints might be unfeasible due to tolerance management in MCA panel fitment.

In a fuselage, the pressure load in the fuselage is carried by hoop tension in the skin with additional support from the frames. Besides the pressure loading, in flight loads cause additional shear, compression and tensile stresses in the skin. The longitudinal joints in a pressurized fuselage are responsible for transferring the loads (hoop tension and shear stress) as well as maintaining air tightness. A typical single aisle fuselage section, shown schematically in Fig. 5.17 is assembled at MCA level by joining three previously manufactured shells and a floor frame. Each of these components are them self's assembled out of site, shipped to the assembly line before MCA and joined together in purpose made jigs. At state-of-the-art, the longitudinal joints connecting the shells are made with multi row riveted joints.

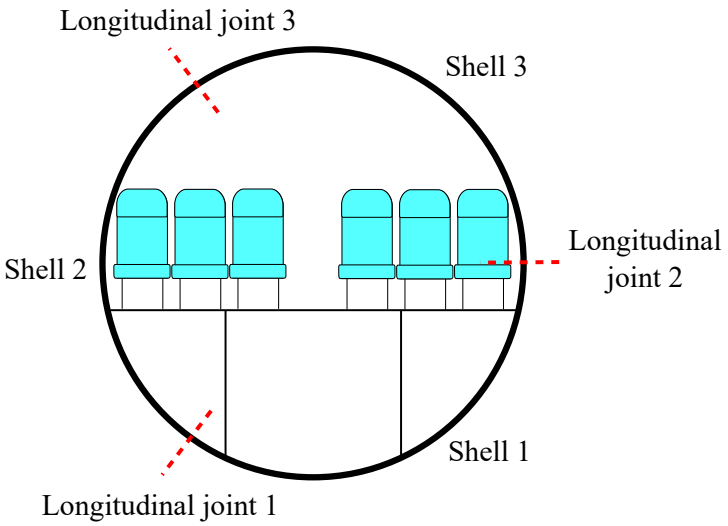

Figure 5.17: Cut through scheme of single aisle fuselage.

Even though FSW butt-joining has a high potential for weight reduction at MCA level, given the weight of overlapping material and of the fasteners, challenges in its application has hinder its adoption. Given the geometric dimensions, manufacturing methods and varying location of fabrication of the different shells that compose a fuselage section, the tolerance management required to achieve sound welds may be extremely challenging. Overlap FSW with adhesive bonding intends to generate more modest weight savings when compared with butt-joining FSW but with lower impact on alignments and tolerancing regarding the SoA. As such, overlap FSW with adhesive bonding does not compete with FSW butt joining, but complements it. In order to estimate the weight savings generated by this new joining method compared with a SoA joint, 3 changes have to be considered, the overlap length reduction, the change in overthickness and the weight of fasteners. For this analysis a typical joint with 60 mm of overlap and 3 rivet rows [141] was considered. Current riveted longitudinal joints make use of titanium (density 4506 kg/m^3) crack stoppers at frame intersections, as mention in [142], to divert the crack propagation through the joint in order to achieve damage tolerance. When butt-joining with FSW these can be disregarded, as a the issue of cracks initiating and propagating in the inside of the overlaps is avoided, no rivet holes are present in the joint to initiate cracks, and local reinforcement is achieved through the use of overthicknesses. Overlap FSW with adhesive bonding joints are most likely to require crack stoppers as cracks may initiate or propagate in the inside of the overlap, where they are not visible. The mass of the crack stoppers was set at 200 g/m. The majority of the rivets used in these joints are made of aluminum, with flush head on the outside of the joint for aerodynamic purposes, as shown in Fig. 3.3. To account for the weight added by the rivets, a 20 mm pitch and 3 rows were considered and only the volume of the fastener sticking out from the overlap was accounted as a simplified approach. The resulting weight addition due to the fasteners was 46.5 g/m.

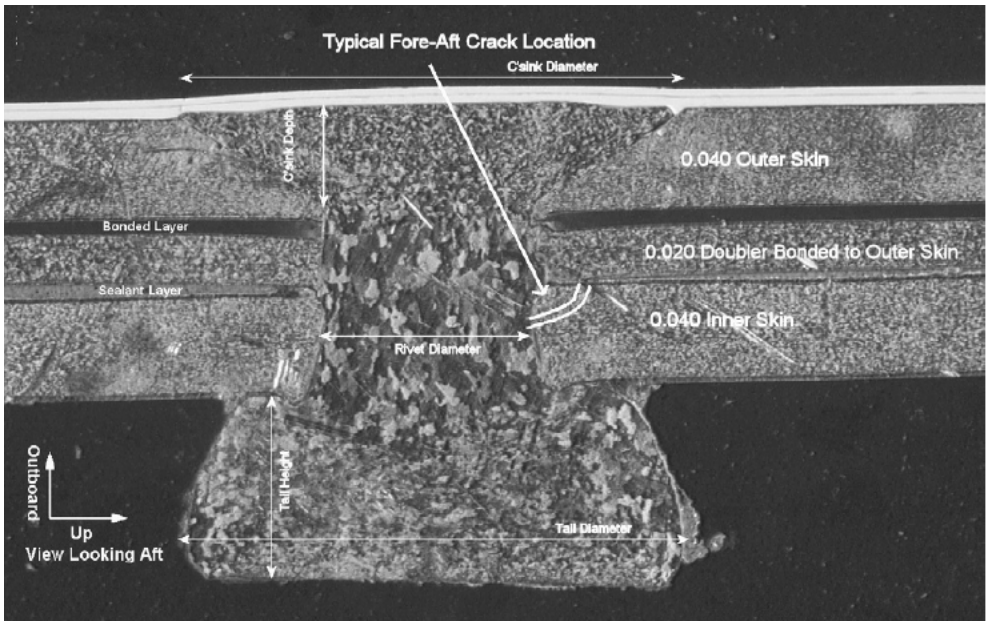

Figure 5.18: Cross-section of rivet in a retired fuselage joint [143].

A typical shell thickness of 1.2 mm was used for mass calculations. Considering a reduction in overlap from 60 to 40 mm and maintaining a 20% width of overthickness (72 mm and 48 mm respectively), an estimation on weight savings may be made. For mass calculation, the aluminum alloy AA2024-T3 with a density of 2700 kg/m^3, and a typical epoxy adhesive with a density of 1250 kg/m^3 were used. The adhesive was assumed to have the same density and thickness as the sealant already used in these joints and as such, only the difference in bonded overlap is considered. An overthickness of 1/3 was assumed for both riveted and overlap FSW with adhesive while this was considered to be 0.5 for the butt joined FSW, to account for the undermatch condition of the weld.

The mass due to geometric change in the joint can be described as:

$$mass_{Riveted} = \rho \times (width \times thickness + 2 \times width_{overthickness} \times t_{overthickness}) =$$
$$= 0.0027 \times \left(60 \times 1.2 + 2 \times 72 \times \left(\frac{1}{3} \times 1.2\right)\right) \approx 0.350\, g/mm \Rightarrow 350\, g/m$$

$$mass_{ButtFSW} = \rho \times width_{overthickness} \times t_{overthickness} =$$
$$= 0.0027 \times 72 \times (0.5 \times 1.2) \approx 0.117\, g/mm \Rightarrow 117\, g/m$$

$$mass_{OverlapFSW} = \rho \times (width \times thickness + 2 \times width_{overthickness} \times t_{overthickness}) =$$
$$= 0.0027 \times \left(40 \times 1.2 + 2 \times 48 \times \left(\frac{1}{3} \times 1.2\right)\right) \approx 0.233\, g/mm \Rightarrow 233\, g/m$$

The resulting weight loss when compared with SoA from geometric change in the joint is:

$$\Delta m_{ButtFSW} = mass_{ButtFSW} - mass_{Riveted} = 350 - 117 = 233\, g/m$$

$$\Delta m_{OverlapFSW} = mass_{OverlapFSW} - mass_{Riveted} = 350 - 233 = 117\, g/m$$

Adding the mass of the rivets and crack stoppers the mass change is:

$$\Delta m_{ButtFSW} = 233 + 46.5 + 200 = 479.5\, g/m$$

$$\Delta m_{OverlapFSW} = 117 + 46.5 = 163.5\, g/m$$

The weight reduction estimated is quite significant, more so in the case of butt joined FSW, than overlap joints, but scenarios combining both technologies are possible. To assess the potential impact in manufacturing of the adoption of overlap FSW with adhesive bonding, 3 scenarios were developed and compared against a SoA and a hypothetical full FSW butt-joined fuselage section. The first scenario, all 3 longitudinal joints in a fuselage section are joined through overlap FSW with adhesive bonding. The second scenario uses both butt welding FSW and overlap FSW with adhesive bonding, with the latter being used in the last 2 joint, to accommodate the geometric mismatches and ease tolerance management. The 3 scenario was envisioned as quick entry into service scenario where the first joint is made as SoA and the last two, as in scenario 2, were made with overlap FSW with adhesive bonding. In the last scenario the first joint was selected to be kept the same since the fuselage section is built from bottom to top, changes in the joining process in this joint result in radical changes in jigs and setups. Assuming the adhesive bonding process to be as labor intensive as the current sealant deposition at SoA and considering that the adhesive curing occurs partially during the welding procedure, it is not expected that it will delay the following manufacturing steps. Fig. 5.19 presents the estimated changes to labor time between scenarios. The most labor consuming tasks in all three scenarios explored are related with assembly of structural details, such as crack stoppers. In all scenarios a welding speed of 5 mm/min was assumed.

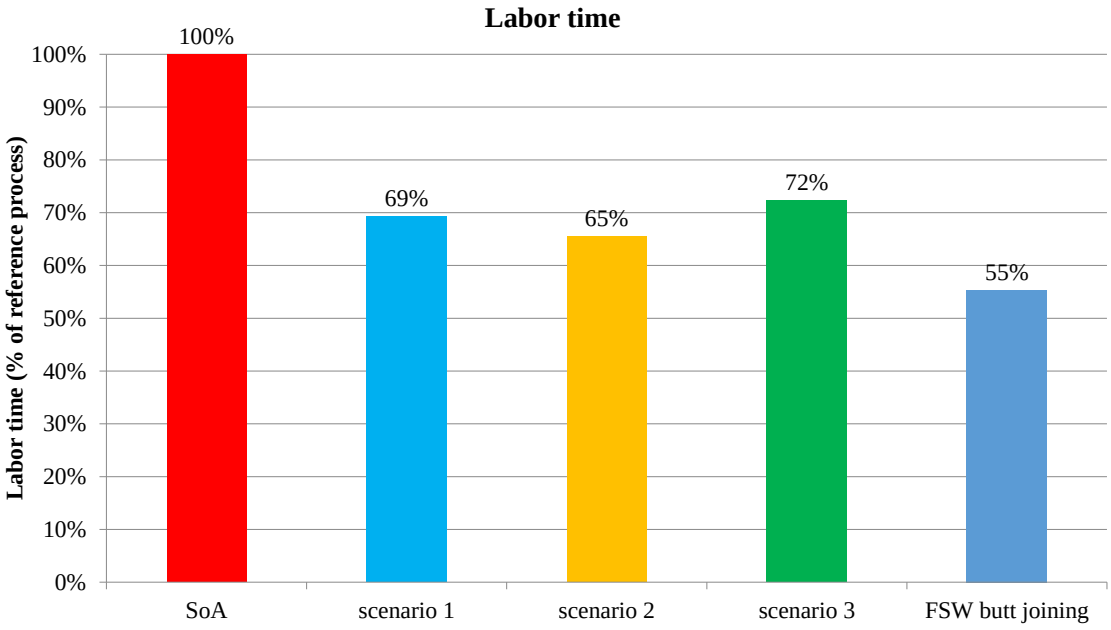

Figure 5.19: Labor time change regarding SoA process.

These estimations involve many assumptions and to improve the accuracy of the labor intensity and cost estimations, larger and more complex demonstrators will be required. Given the early development of the joining technology, it was not the purpose of this PhD research project to achieve higher TRLs which will require the creation and testing of these larger and more complex demonstrators. However, the disruptive potential of the technology was shown and a possible technology integration in the current product is explored.

5.2.2 Fuselage Butt-Joints Mechanical Performance

The mechanical performance of fuselage butt-joints was assessed through quasi-static and cyclic loading at R=0.1. In [144], Chaves and Fernandez studied the behavior of riveted and friction stir welded fuselage butt joints, using the specimens shown in Fig. 5.20 a) and b). In this study specimens with a similar geometry, presented in Fig. 5.20 c), were cyclically loaded at constant amplitude R=0.1, similarly to [144]. The overlap of the friction stir weld-bonded joints was reduced from 70 to 62 mm, regarding the riveted joints. In this joint configuration, a small gap exists between the “shells” (in this case it was set to 2 mm for consistency purposes) allowing for an easier geometric tolerance management.

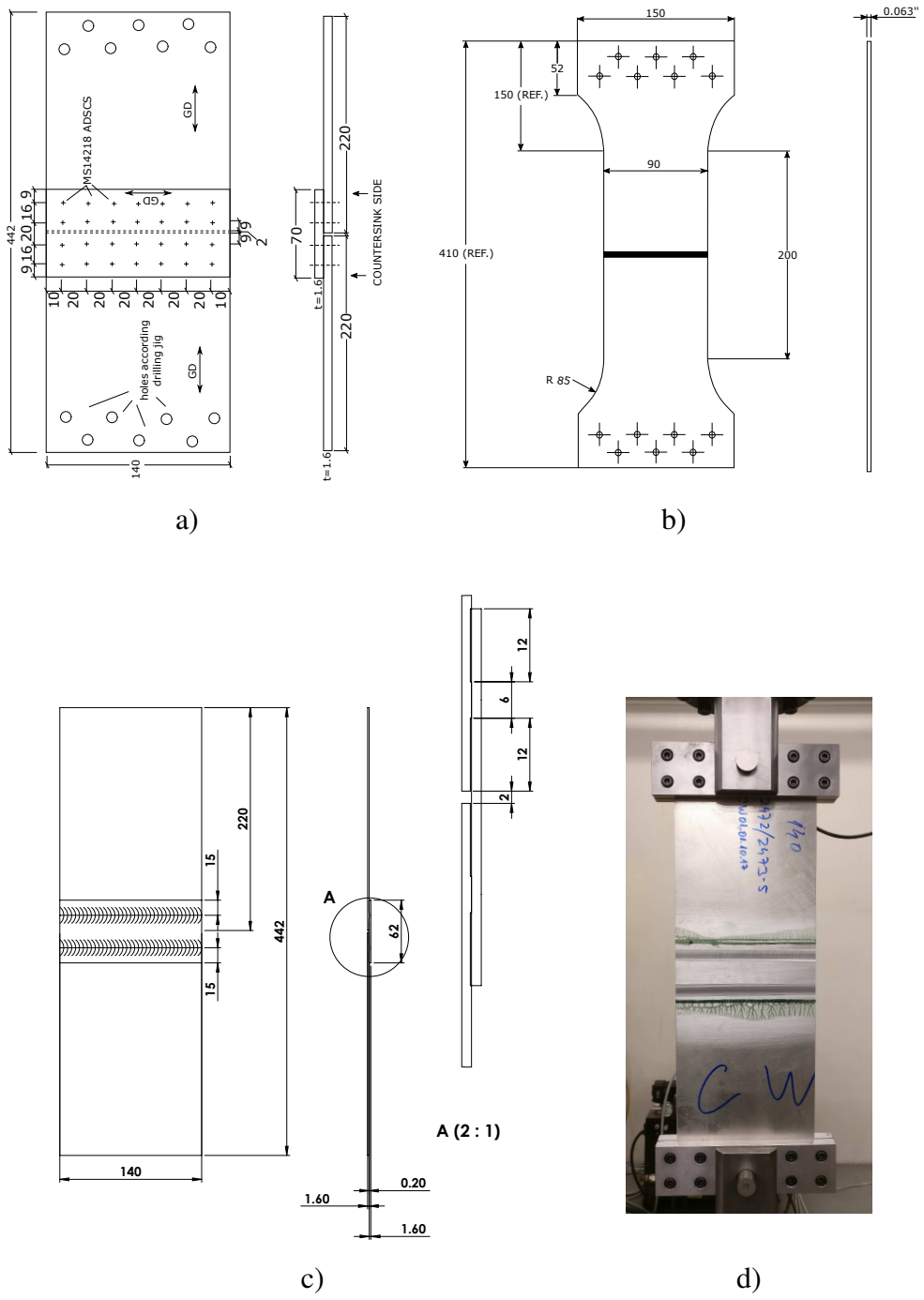

Figure 5.20: Longitudinal joints specimens geometry: riveted a), FSW b), FSW+AB c) and specimen photo d).

Two weld beads were made so that the advancing sides were facing outwards. Since the load is to be carried from one “shell” to the other through the reinforcement patch, the outside of the welds will loaded the most. In the single overlap study discussed above the joints with the top advancing side loaded resulted in higher strength and ductility than the ones with the top retreating side. This was justified by the inversion of the hook defect in the advancing side. As the process parameters were kept the same between the best performing single lap joints and the longitudinal joints, the same behavior was expected and as such the advancing sides of both welds were made to face the outsides of the overlap.

In order to define the load levels for the cyclic loading, quasi-static tensile testing of similar joints were made. The quasi-static tensile specimens had the same geometry as the ones used in fatigue testing, only differing the width. This was reduced from 140 mm to 25 mm, in order to save material for the remaining specimens. The large width used in the fatigue specimens was to guarantee comparability to the results presented in [144] and also to assure homogenization of the joint. This is to assure that small localized defects don't alter the conclusions of the study. The 25 mm width joints tested in quasi-static conditions showed little dispersion. This shows that the increase in manufacturing scale (from 300 mm long welds to more than 1 meter long welds), did not alter the consistency within the joints. Fig. 5.21 presents the remote stress, calculated according to the remote specimen cross-section, as well as the failure location. The failure location was always on the bottom sheet, in the transition between the TMAZ and HAZ, and varied only the side of the overlap, as the joint is symmetric. Upon failure of the adhesive layer, the weld failed through the unwelded tip next to the weld bead.

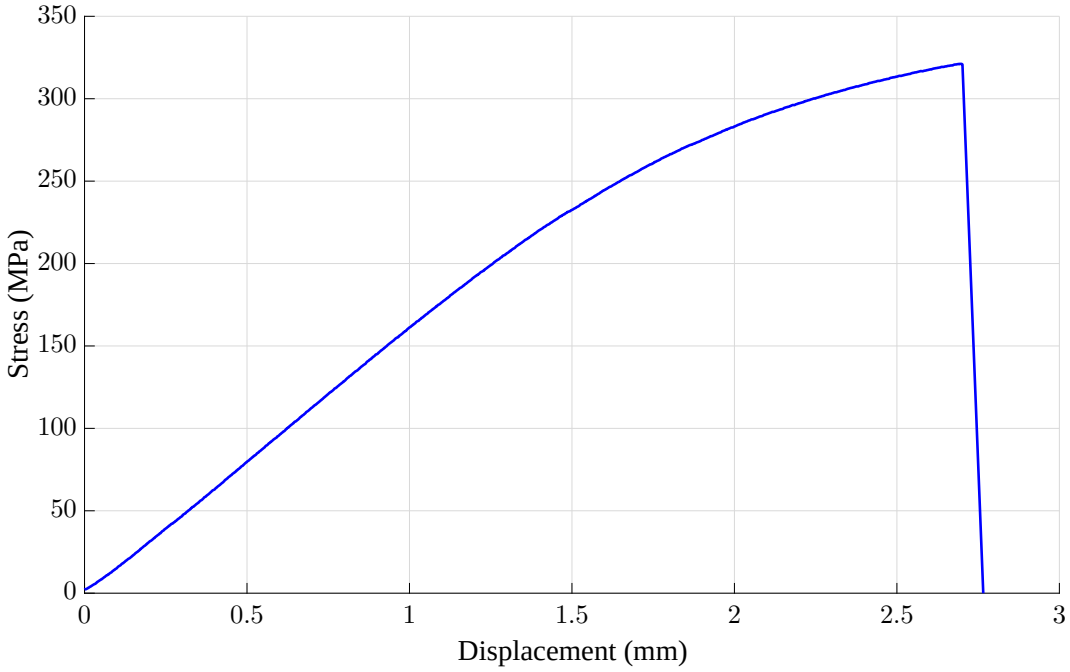

a)

Figure 5.21: Remote stress versus displacement curve a) and failure location b).

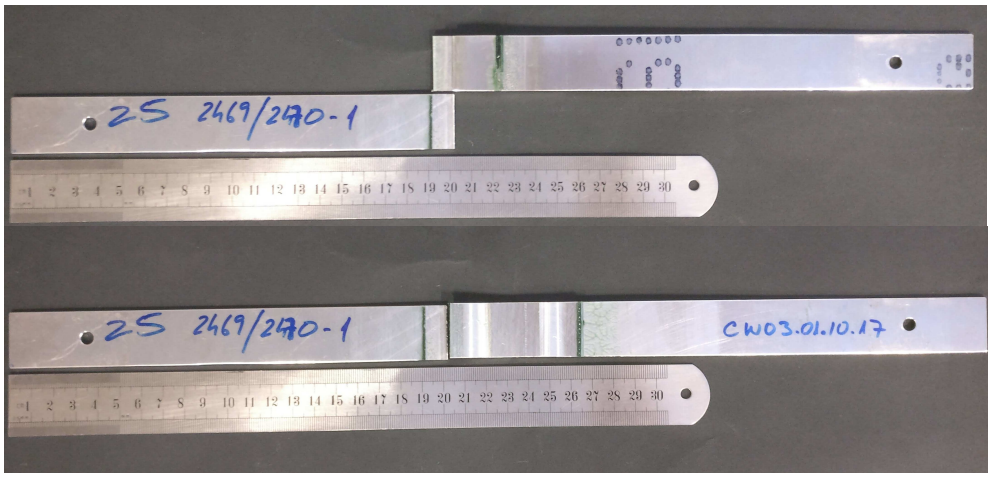

b)

Fig. 5.21 (cont.): Remote stress versus displacement curve a) and failure location b).

The resulting Wöhler curves of the friction stir weld-bonded longitudinal joints, along with the FSW and riveted joints from [144] are presented in Fig. 5.22.

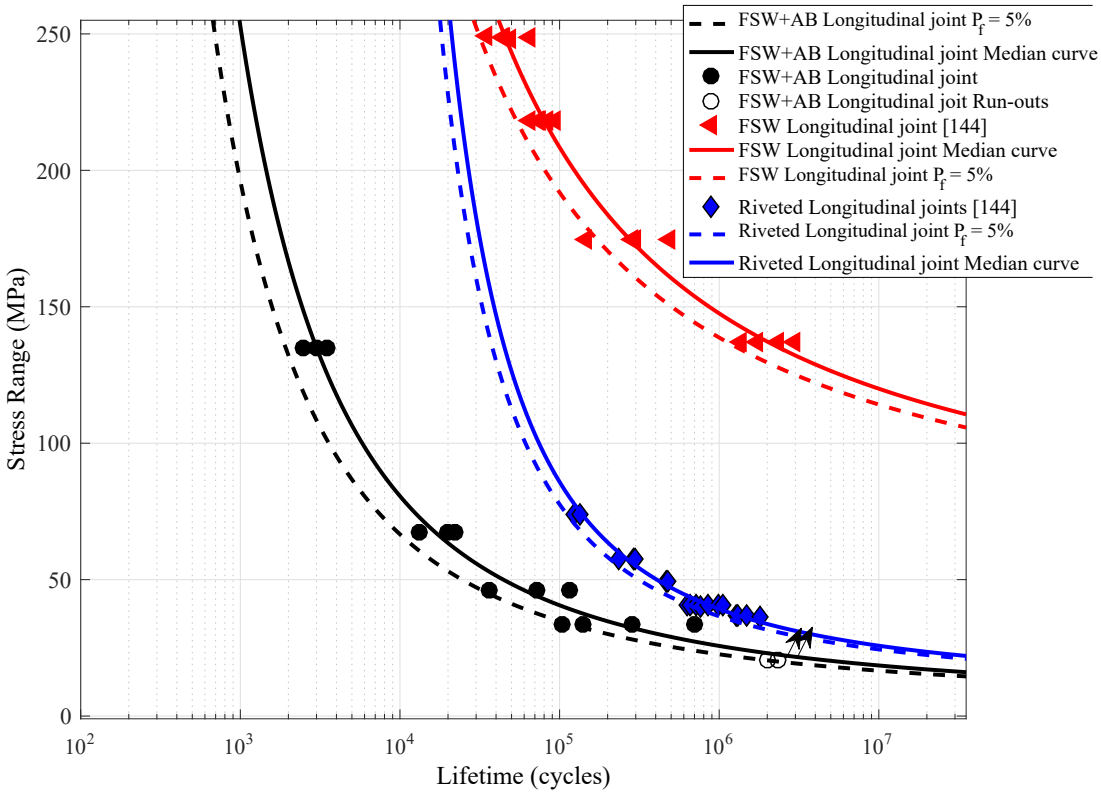

Figure 5.22: Medial S-N curves of friction stir weld-bonded longitudinal joints along with FSW and Riveted joints.

The fatigue life of the friction stir weld-bonded fuselage joints was lower than riveted joints. Fatigue strength was also lower, but the difference was smaller with the increase in

number of cycles. This indicates, that the joint design is a limiting factor, as out of plane bending occurs due to misalignment of the joint neutral axis and load axis, as well as stress concentrations in the geometric transitions. As expected the friction stir welding butt joints had much higher fatigue strength, as they are not limited by stress concentrations inherent to the geometry of the joints. In the riveted joints, the rivet holes act as stress concentration points, leading to premature failure. In the case of friction stir weld-bonded joints stress concentrations occur at the ends of the overalps where the adhesive is subjected to not only shear but also peel stress, as well as in the unwelded tips of the friction stir weld upon failure of the adhesive layer. The failure location in these tests was different from the one that occurred in quasi-static tensile loading, as although the failure occured on the underside of the weld, it was on the inside of the overlap (weld retreating side). Fig. 5.23, shows an example of specimen tested up to failure. There was adhesive remains on both surfaces and similarly to the quasi-static tests the failure of the adhesive bond was mixed adhesive-cohesive.

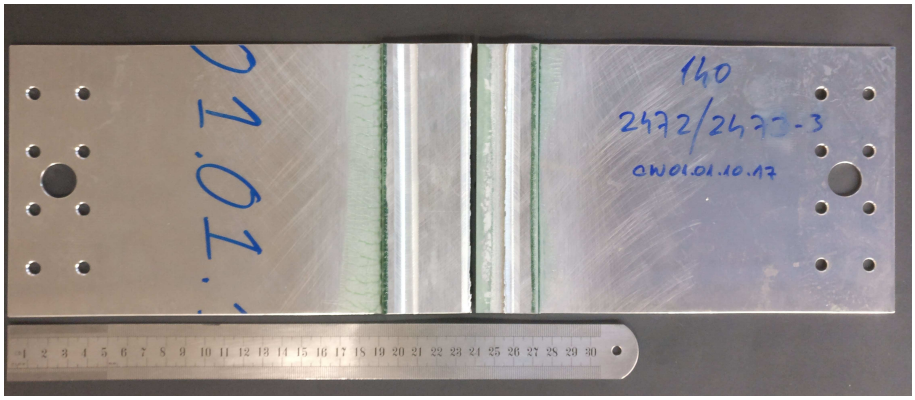

Figure 5.23: Typical failure surface of cyclic load friction stir weld-bonding fuselage butt joint.

5.3 Chapter Summary

Following the development of the joining process in the previous chapter, in this chapter the process was a conventionally used fuselage skin material, an Al-Cu-Mg alloy. Fatigue and exfoliation corrosion was assessed in single lap joints. An improvement was found in hybrid regarding FSW overlap, as the higher effective overlap, the high fracture toughness of the adhesive and the relative insensitivity of the adhesive to the corrosive environment, improve the behavior of the hybrid joints in these conditions.

A conceptual study of technology application was made in this chapter showing weight and labor time savings with the adoption of FS Weld-bonding. Fatigue performance of fuselage joints made with FS Weld-bonding was assessed and compared with riveted and butt joined FSW fuselage longitudinal joints found in the literature. Joints were made with smaller overlaps, which combined with the lack of fastners and other related details, results in weight savings. However the fatigue strength of the FS Weld-bonded joints did not match

the SoA joints, requiring still further improvement in joint design and joining methodology (especially concerning long length joints).

Chapter 6

Conclusions and Future Works

6.1 Concluding Remarks

A multi subject research was performed to develop an innovative joining technology and assess its potential to replace current SoA assembly processes in aircraft primary structures. More specifically, the research was over fuselage longitudinal joints at MCA level. The new joining process combined both friction stir welding and adhesive bonding, creating better joint efficiencies and capability to join all aluminum aeronautical alloys. As such, this joining method arouses the interest of aircraft manufactures, albeit new design concepts are required to adopt it. To ensure structural integrity, full understanding of the joint behavior and requirements along the complete service life of these structures are required. This structural integrity is fundamental, in complex safety critical structures, which should endure the multiple environmental service conditions. For these reasons, the aeronautical industry tends to be very conservative, creating a challenging design environment. To ensure the successful adoption of new materials and technologies, structured product and process development is imperative.

An important driver in development of new aircraft, has been the adoption of new materials in aeronautical primary structures, leading to higher structural efficiencies in terms of weight and cost reduction. One example of such, is the adoption in large scale of composite materials in the newer generation of twin aisle long range aircraft. However, initial estimations of weight savings at early stages of these projects could be underestimated or overestimated since the behavior of new materials under aircraft service conditions were not yet completely understood, namely from the environmental, scale and aging points of view. Along with the introduction of new materials in fuselage, alternative manufacturing processes have been adopted or considered for these structures. The research presented in this thesis focus mainly on the latter development, by studying the replacement of conventional riveting by a hybrid friction stir welding and adhesive bonding joining technology.

Riveting has been the main assembly process in fuselage structures, as it is a very flexible joining process, allows easy repairs, and ensures a damage tolerant design through the use of crack arrest features. However, riveting requires the use of sealants, large overlaps and fasteners, which add considerable weight. Also, the holes required for riveting are stress con-

centration and corrosion points where cracks usually initiate. Full automation of the process is also extremely challenging, making the process highly labor intensive. FSW in butt-joint configuration has been pointed as possible replacement for these joints, has it allows for high performing joints without most of the drawbacks associated with the SoA process. The use of FSW in fuselages would result in integral structures with large weight reductions and high potential for automation. As FSW is a solid state joining method it adds the benefit of allowing the use of newer metal alloys which cannot be welded by fusion welding processes.

Even though FSW butt joints arouse much interest as possible replacement for riveting in fuselages, many challenges have hindered the generalized adoption in these safety critical structures. Unlike riveted fuselages, the adoption of FSW requires a shift from differential to integral structures. This radical transformation will require very exhaustive studies on the behavior of this structures in service conditions, as to prevent unexpected behaviors. In the particular case of MCA, the large dimensions of the components to be assembled and the components complexity, makes the adoption of FSW butt-joints extremely challenging. Strict geometric tolerances required to achieve sound welds may be incompatible with the scale of the operation. One possible alternative to overcome these challenges is FSW in overlap configuration, but as shown throughout this thesis and in previous works, the mechanical performance of such joints do not match the requirements. To overcome the limitations of this joint configuration a hybrid technology is proposed in this thesis, combining FSW in overlap configuration and adhesive bonding. The use of an overlap configuration results in a less radical design solution when comparing with the SoA riveting and as such benefits from an easier geometric tolerance management.

In the course of this research project hybrid friction stir-weldbonded joints were studied and benchmark against FSW and adhesive bonded joints. It was shown that the increase in effective joined overlap combined with the high strength, ductility and toughness of the adhesive used, resulted in large improvements in mechanical performance. Adhesive characterization and temperature measurements during the welding process, along with post weld testing showed that the amount of adhesive degraded due to high temperatures of the welding process was negligible. The adhesive in the overlap also was shown to not affect negatively the quality of the weld itself significantly. The improvement of quasi-static mechanical performance translated well to constant amplitude cyclic loading, where the hybrid joints showed much higher fatigue strength. Even though friction stir weld-bonding joints performed much better than FSW overlap joints, they did not improve the mechanical performance of adhesive bonded joints, as a continuous adhesive layer results in a more uniform stress distribution. However in order for the adhesive to perform well and consistently, curing procedures are required, which may be nonviable or undesirable. Through the hybrid method, partial curing occurs during the welding procedure, with the remaining cure taking place after the weld, without any special care required. Another benefit of this method when compared with adhesive bonding in terms of manufacturing process is the fact that upon welding the joint has residual strength and may not require special clamping devices. These would be required in adhesive bonded joints to ensure the geometric features of the joints while the adhesive cures.

Some preliminary studies on the adoption of the proposed technology for longitudinal fuselage joints, considering several adoption scenarios were done. The potential for weight reduction in these joints was demonstrated, albeit not as high as FSW butt joining. As the potential assembly process has some resemblances to current SoA methods, but with the replacement of some of the manufacturing stages, labor times were estimated for all scenarios considered. Significant labor time reductions were calculated, although further research would be required, considering technology demonstrators of larger scales, as to refine this early estimations. Fatigue performance of longitudinal fuselage joints, using the proposed technology in a safe-life methodology were assessed. Probabilistic fatigue curves were compared with data available in the literature, and friction stir weld-bonded joints were shown to have lower fatigue strength and life than SoA joints, albeit with reduced weight. However, the overlap configuration causes stress concentrations at the ends of the overlaps and as such, these joints will always perform worse than butt welded FSW as it was shown. A more detailed joint design may overcome this challenge leading to higher fatigue strength in the hybrid joints as shown for single lap joints.

Concerning the research questions set in Chapter 1, it may be concluded that all three secondary research questions were addressed. In the first research question "*How do the mechanical properties of Friction Stir Weld-Bonding compare with other conventional joining methods, such as riveting, Friction Stir Welding and adhesive bonding?*", the subject was addressed by comparing quasi-static, fatigue and exfoliation corrosion of small coupons, showing consistent improved performance in FS Weld-bonded regarding overlap FSW. Even though, larger specimens of fuselage joints made through FS Weld-bonding showed to not yet match the performance of SoA joints, although with lower weight, the performance shown in smaller coupons leads to the belief that performance of these types of joints may improve significantly with improved design and manufacturing methodology, such as the adoption of more adequate clamping systems and bobbin tool for FSW. The second research question "*How to manufacture these hybrid joints and how does the welding temperature affect the behavior of the adhesive? Also, how does the adhesive affect the quality of the weld?*" was addressed by mechanical characterization of the adhesive, including DSC and TGA analysis, as well as microscopic observation of the joints cross-section. The third research question, "*What does the adoption of the hybrid joining process affect structural weight and manufacturing lead time?*" was addressed through conceptual application scenarios, showing the weight and labor time savings due to the adoption of FS Weld-bonding in fuselage joints. The main research question was addressed throughout the development of the PhD research project, but given the multidisciplinary nature of the question will still require further work to provide conclusive and definitive answer. However, the research performed and documented in this thesis serves as a significant development in the attempt to solve the question at end. During this thesis the process was developed, and as such the technology was at a TRL level 2 or 3 (research to prove feasibility stage) and at the conclusion of this research project the same joining technology is at a TRL 3 or 4 (technology development stage).

Through the research presented in this PhD thesis, a new joining method for aeronautic

fuselages was developed and early studies demonstrate its potential for the particular application. The transition from current assembly processes to newer ones, will demand the adoption of new structural designs. Given the complex and safety critical nature of these structures, the adoption of new technologies must be comprehensively studied for its impacts, mitigating the associated risks. As such, further development is expected before this technology becomes market ready, but its potential was demonstrated here.

6.2 Future Works

Considering that most of the development work in this PhD research project was done at low technology readiness level, as it was to be expected given that new technologies must first be proven at this level, much work is still required before the adoption of the technology in market transactional products. There are two main future development paths for friction stir weld-bonding. The first relates to the adoption of friction stir weld-bonding to fuselage joints as studied in this thesis, improving on the outcomes of this work in terms of manufacturing process, mechanical properties, etc. and directing the study to more specific design considerations. For this purpose more realistic and larger scale prototypes and technology demonstrators will be required. The other path is the expansion of the work developed in this thesis to other engineering fields.

One recurring concern throughout the development of this research was the quality of the bonding between the adhesive and the aluminum substrates. This topic should be addressed in future works, by studying different surface treatments and preparation, as well as other structural adhesives. Environmental concerns should be addressed in tandem, as new European directives and regulations aim to rule out dangerous chemicals commonly used for these purposes. Adhesives in film form should be studied, as their application may simplify some of the procedures in the manufacturing of the hybrid joints. The incorporation of sensors within the adhesive in order to achieve self-sensing and/or smart joints may be a future field of development especially for more demanding high performing structures, such as in military aviation. Optical sensors, like Fiber Bragg Gratings are a possibility for such applications, for their reduced size, versatility and insusceptible to electron-magnetic interference.

Some effort was made to model numerically the joints behavior in this thesis, however more detailed models would allow more efficient design of new joined structures with lower risks. For this approach models encompassing more detailed and realistic failure would be required, encompassing the physical transformations the materials and joints are subjected to during service. The use of global-local modeling would allow the more detailed discretizations to be extrapolated to larger and more complex structures.

Quality assurance is imperious for the successful adoption of friction stir weld-bonding joints in fuselage design. As such, new robust non destructive inspection methods are required. Considering the multi-material nature of these joints, this topic is broad and complex, as inspection procedures to be developed must detect many different nonconformities.

As for the second approach mentioned for future development of this work, new joint

design variants should be studied focusing on different applications. The use of friction stir weld-bonding to manufacture T-joints for skin and stringer or skin frame joints is an obvious extension of the current work, as it may allow new multi-objective designs (e.g. longitudinal joint and skin to frame joint in one). Adapting friction stir weld-bonding to friction stir spot and refill friction stir spot welding in combination with high toughness, impact resistant adhesives would expand the application to the automotive industry. In this case, new design methodologies and procedures should be studied, along with physical properties relevant to this application. Performance under impact and noise vibration and harshness would be two topics of study for such application.

References

[1] Tolga Dursun and Costas Soutis. Recent developments in advanced aircraft aluminium alloys. *Materials & Design*, 56:862 – 871, 2014.

[2] Airbus Group. Official airbus website of the A320 aircraft family. http://www.airbus.com/aircraftfamilies/passengeraircraft/a320family/, 2015. Accessed: 2018-03-20.

[3] E.M. Rogers. Diffusion of innovations. *New York: Free Press.*, 1962.

[4] Rudolf Smaling and Olivier de Weck. Assessing risks and opportunities of technology infusion in system design. *Systems Engineering*, 10(1):1–25, 2007.

[5] K. Tomabechi, J.R. Gilleland, Yu.A. Sokolov, R. Toschi, and ITER Team. Iter conceptual design. *Nuclear Fusion*, 31(6):1135, 1991.

[6] John C. Mankins. Technology readiness assessments: A retrospective. *Acta Astronautica*, 65(9-10):1216 – 1223, 2009.

[7] John C. Mankins. Technology readiness levels. *White Paper, April*, 6, 1995.

[8] European Space Agency. Technology readiness levels handbook for space applications, 2008.

[9] Eun Suk Suh, Michael R. Furst, Kenneth J. Mihalyov, and Olivier de Weck. Technology infusion for complex systems: A framework and case study. *Systems Engineering*, 13(2):186–203, 2010.

[10] Christopher Magee and Olivier de Weck. Complex system classification. 2004.

[11] Trent A. Greenwell. Design of repair of battle-damaged fixed-wing aircraft. Technical report, Air Force Academy Colorado Springs CO Dept of Engineering Mechanics, 2010.

[12] ICAO International Civil Aviation Organization. The convention on international civil aviation - annexes 1 to 18, 2007.

[13] European Aviation Safety Agency. Certification specifications for large aeroplanes CS-25 amendment 3, 2007.

[14] Filippo de Florio. *Airworthiness: An introduction to aircraft certification and operations*. Butterworth-Heinemann, 2016.

[15] Konstantinos Dalamagkidis, Kimon P Valavanis, and Les A Piegl. Current manned aviation regulation. *On Integrating Unmanned Aircraft Systems into the National Airspace System*, pages 43–56, 2012.

[16] Michael Kupke and Tobias Gerngross. 3.8 production technology in aeronautics: Upscaling technologies from lab to shop floor. Elsevier, 2018.

[17] R. Henke. Managing innovative technology development in aeronautics: technology assessment (ta) techniques. In *Innovation in Aeronautics*, pages 214–224. Elsevier, 2012.

[18] M. Pacchione and J. Telgkamp. Challenges of the metallic fuselage. In *Proceedings of the 25th International Congress of the Aeronautical Sciences-ICAS*, pages 451–1, 2006.

[19] S.M.O. Tavares and Paulo M.S.T. de Castro. Impact of integral structures in the design for manufacture and assembly of airframes. In *Key Engineering Materials*, volume 450, pages 279–282. Trans Tech Publ, 2011.

[20] N. Cross. *Engineering Design Methods: strategies for product Design*. J. Wiley, 2008.

[21] M. Koçak, B. Petrovski, and V. Uz. In *Workshop WEL-AIR*, 2007.

[22] Brijesh Kumar, Christian Widener, Adam Jahn, Bryan Tweedy, Dale Cope, and Ryan Lee. Review of the applicability of fsw processing to aircraft applications. In *46th AIAA SDM Conference*, 2005.

[23] R.S. Mishra and Z.Y. Ma. Friction stir welding and processing. *Materials Science and Engineering: R: Reports*, 50(1):1–78, 2005.

[24] R. Nandan, T. DebRoy, and H. Bhadeshia. Recent advances in friction-stir welding–process, weldment structure and properties. *Progress in Materials Science*, 53(6):980–1023, 2008.

[25] G.K. Padhy, C.S. Wu, and S. Gao. Friction stir based welding and processing technologies-processes, parameters, microstructures and applications: A review. *Journal of Materials Science & Technology*, 2017.

[26] V. M. Magalhães, C. Leitão, and D. M. Rodrigues. Friction stir welding industrialisation and research status. *Science and Technology of Welding and Joining*, 0(0):1–10, 2017.

[27] Ana C.F. Silva, Daniel F.O. Braga, M.A.V. de Figueiredo, and Pedro M.G.P. Moreira. Ultimate tensile strength optimization of different fsw aluminium alloy joints. *The International Journal of Advanced Manufacturing Technology*, 79(5):805–814, Jul 2015.

[28] G. Buffa, G. Campanile, L. Fratini, and A. Prisco. Friction stir welding of lap joints: Influence of process parameters on the metallurgical and mechanical properties. *Materials Science and Engineering: A*, 519(1):19–26, 2009.

[29] L. Fratini, G. Buffa, L. Filice, and F. Gagliardi. Friction stir welding of AA6082-T6 T-joints: Process engineering and performance measurement. *Proceedings of the Institution of Mechanical Engineers, Part B: Journal of Engineering Manufacture*, 220(5):669, 2006.

[30] D. Fersini and A. Pirondi. Analysis and modelling of fatigue failure of friction stir welded aluminum alloy single-lap joints. *Engineering Fracture Mechanics*, 75(3-4):790–803, 2008.

[31] Edward F. Shultz, Edward G. Cole, Christopher B. Smith, Michael R. Zinn, Nicola J. Ferrier, and Frank E. Pfefferkorn. Effect of compliance and travel angle on friction stir welding with gaps. *Journal of Manufacturing Science and Engineering*, 132(4):041010–041010–9, July 2010.

[32] V. Richter-Trummer, E. Suzano, M. Beltrão, A. Roos, J.F. dos Santos, and Paulo M.S.T. de Castro. Influence of the fsw clamping force on the final distortion and residual stress field. *Materials Science and Engineering: A*, 538:81–88, 2012.

[33] P. Wanjara, B. Monsarrat, and S. Larose. Gap tolerance allowance and robotic operational window for friction stir butt welding of AA6061. *Journal of Materials Processing Technology*, 213(4):631 – 640, 2013.

[34] S. Schulze, G. Göbel, E. Beyer, U. Füssel, and V. Richter-Trummer. *The influence of gaps and misalignment on friction stir welded butt joints of medium-sized parts*, volume 783-786 of *Materials Science Forum*. Trans Tech Publications Ltd, Elan-Ausy, 2014.

[35] M. Ericsson, L.Z. Jin, and R. Sandström. Fatigue properties of friction stir overlap welds. *International Journal of Fatigue*, 29(1):57–68, 2007.

[36] D. Fersini and A. Pirondi. Fatigue behaviour of Al2024-T3 friction stir welded lap joints. *Engineering fracture mechanics*, 74(4):468–480, 2007.

[37] M. Ericsonn and R. Sandstrom. Fatigue of fsw overlap joints in aluminium welded with different tool designs. In *Fifth international symposium on friction stir welding, Metz, France*, volume 14, page 16, 2004.

[38] CEN ENV. Eurocode 9: design of aluminium structures - part 2: structures susceptible to fatigue. *European Committee for Standardisation*, 1998.

[39] E. Lertora. Comparison of AA 2024 T3 friction stir welded and riveted overlap joints with the addition of a pressurization test. *Materials & Design*, 49:259–266, 2013.

[40] L. Dubourg, A. Merati, and M. Jahazi. Process optimisation and mechanical properties of friction stir lap welds of 7075-T6 stringers on 2024-T3 skin. *Materials & Design*, 31(7):3324–3330, 2010.

[41] D. He, K. Yang, M. Li, H. Guo, N. Li, R. Lai, and S. Ye. Comparison of single and double pass friction stir welding of skin–stringer aviation aluminium alloy. *Science and Technology of Welding and Joining*, 18(7):610–615, 2013.

[42] Michael Papadopoulos, S.M.O. Tavares, M. Pacchione, and Sp.G. Pantelakis. Mechanical behaviour of AA 2024 friction stir overlap welds. *International Journal of Structural Integrity*, 4(1):108–120, 2013.

[43] C. Leitao, E. Arruti, E. Aldanondo, and D.M. Rodrigues. Aluminium-steel lap joining by multipass friction stir welding. *Materials & Design*, 106(Supplement C):153 – 160, 2016.

[44] W.M. Thomas, E.D. Nicholas, J.C. Needham, M.G. Murch, P. Templesmith, and C. J. Dawes. Improvements relating to friction welding, 1993. WO1993010935A1.

[45] Craig L. Campbell, Mark S. Fullen, and Michael J. Skinner. Welding head, March 13 2001. US Patent 6,199,745.

[46] Alexander Von Strombeck and J.F. dos Santos. Device for joining workpieces by friction stir welding, October 5 2004. US Patent 6,799,708.

[47] Philip L. Threadgill, M.M.Z. Ahmed, Jonathan P. Martin, Jonathan G. Perrett, and Bradley P. Wynne. The use of bobbin tools for friction stir welding of aluminium alloys. In *Materials Science Forum*, volume 638, pages 1179–1184. Trans Tech Publ, 2010.

[48] Y.X. Huang, L. Wan, S.X. Lv, and J.C. Feng. Novel design of tool for joining hollow extrusion by friction stir welding. *Science and Technology of Welding and Joining*, 18(3):239–246, 2013.

[49] J. Hilgert, H.N.B. Schmidt, J.F. dos Santos, and N. Huber. Thermal models for bobbin tool friction stir welding. *Journal of Materials Processing Technology*, 211(2):197 – 204, 2011.

[50] Rajesh Talwar and Richard Lederich. Joining fuselage skins using friction stir welding, 2009. US 2009/0184201 A1.

[51] S. Schulze, V. Richter-Trummer, Jürgen Silvanus, M. Pacchione, Andreas Grimm, Gunther Göbel, Jens Standfuß, and Eckhard Beyer. Konzept zum fügen von 3d-schalen in der luftfahrt. In *7. FSW-Workshop Rührreibschweißen und verwandte Verfahren, Geesthacht*, 2016.

[52] R.D. Adams. *Adhesive bonding: science, technology and applications*. Elsevier, 2005.

[53] John D. Russell. Composites affordability initiative: Successes, failures-where do we go from here? *SAMPE journal*, 43(2):26–36, 2007.

[54] M.D. Banea and Lucas F.M. da Silva. Adhesively bonded joints in composite materials: an overview. *Proceedings of the Institution of Mechanical Engineers, Part L: Journal of Materials Design and Applications*, 223(1):1–18, 2009.

[55] Abdelaziz A. Taib, Rachid Boukhili, Said Achiou, Sebastien Gordon, and Hychem Boukehili. Bonded joints with composite adherends. part i. effect of specimen configuration, adhesive thickness, spew fillet and adherend stiffness on fracture. *International Journal of Adhesion and Adhesives*, 26(4):226 – 236, 2006.

[56] D.N. Markatos, K.I. Tserpes, E. Rau, S. Markus, B. Ehrhart, and Sp.G. Pantelakis. The effects of manufacturing-induced and in-service related bonding quality reduction on the mode-i fracture toughness of composite bonded joints for aeronautical use. *Composites Part B: Engineering*, 45(1):556 – 564, 2013.

[57] W. Steven Johnson and Lawrence M. Butkus. Designing for the durability of bonded structures. In *FAA-NASA Symposium on the Continued Airworthiness of Aircraft Structures, Atlanta, GA, Proceedings.*, volume 1, pages 147–160, 1996.

[58] Murat Demir Aydın, Şemsettın Temiz, and Adnan Özel. Effect of curing pressure on the strength of adhesively bonded joints. *Journal of Adhesion*, 83(6):553–571, 2007.

[59] Choothum Jeenjitkaew, Zofia Luklinska, and Felicity Guild. Morphology and surface chemistry of kissing bonds in adhesive joints produced by surface contamination. *International Journal of Adhesion and Adhesives*, 30(7):643–653, 2010.

[60] Choothum Jeenjitkaew, Zofia Luklinska, and Felicity Guild. Morphology and surface chemistry of kissing bonds in adhesive joints produced by using electrelease adhesive. *The Journal of Adhesion*, 87(4):291–312, 2011.

[61] E.A.S. Marques, Lucas F.M. da Silva, M.D. Banea, and R.J.C. Carbas. Adhesive joints for low-and high-temperature use: An overview. *The Journal of Adhesion*, 91(7):556–585, 2015.

[62] Ernest W. Flick. *Epoxy resins, curing agents, compounds, and modifiers: an industrial guide*. William Andrew, 2012.

[63] G. Viana, M. Costa, M.D. Banea, and Lucas F.M. da Silva. A review on the temperature and moisture degradation of adhesive joints. *Proceedings of the Institution of Mechanical Engineers, Part L: Journal of Materials: Design and Applications*, 231(5):488–501, 2017.

[64] G. Viana, M. Costa, M.D. Banea, and Lucas F.M. da Silva. Behaviour of environmentally degraded epoxy adhesives as a function of temperature. *The Journal of Adhesion*, 93(1-2):95–112, 2017.

[65] M. Costa, G. Viana, Lucas F.M. da Silva, and Raul D.S.G. Campilho. Environmental effect on the fatigue degradation of adhesive joints: A review. *The Journal of Adhesion*, 93(1-2):127–146, 2017.

[66] M. Costa, G. Viana, Lucas F.M. da Silva, and Raul D.S.G. Campilho. Effect of humidity on the fatigue behaviour of adhesively bonded aluminium joints. *Latin American Journal of Solids and Structures*, 14(1):174–187, 2017.

[67] Bernt B. Johnsen, Fabrice Lapique, Astrid Bjørgum, John Walmsley, Bjørn Steinar Tanem, and Tomas Luksepp. The effect of pre-bond moisture on epoxy-bonded sulphuric acid anodised aluminium. *International Journal of Adhesion and Adhesives*, 24(3):183 – 191, 2004.

[68] Gerald Doyle and Richard A. Pethrick. Environmental effects on the ageing of epoxy adhesive joints. *International Journal of Adhesion and Adhesives*, 29(1):77 – 90, 2009.

[69] Yoshino Sugita, Charles Winkelmann, and Valeria La Saponara. Environmental and chemical degradation of carbon/epoxy lap joints for aerospace applications, and effects on their mechanical performance. *Composites Science and Technology*, 70(5):829 – 839, 2010.

[70] L.J. Hart-Smith. Aerospace. In R.D. Adams, editor, *Adhesive Bonding: Science, Technolohy and Applications*, pages 489–527. 2005.

[71] Christian Tornow, Mareike Schlag, Luiz Cezar Miranda Lima Junior, Dorothea Stübing, Michael Hoffmann, Paul-Ludwig Michael Noeske, Kai Brune, and Stefan Dieckhoff. Quality assurance concepts for adhesive bonding of composite aircraft structures - characterisation of adherent surfaces by extended ndt. *Journal of Adhesion Science and Technology*, 29(21):2281–2294, 2015.

[72] Toshiyuki Sawa and Takashi Kobayashi. The strength of joints combining an adhesive with a bolt. *The Journal of Adhesion*, 25(4):269–280, 1988.

[73] Annn. *Guide to the Structural Use of Adhesives*. Institution of Structural Engineers, 1999.

[74] J.R. Weitzenböck and D. McGeorge. Science and technology of bolt-adhesive joints. *Hybrid Adhesive Joints*, pages 177–199, 2011.

[75] Mel M. Schwartz. Metals joining manual.(book). *McGraw-Hill Book Co., Chapters paged separately, 1979*, 1979.

[76] S.M.H. Darwish and A. Ghanya. Critical assessment of weld-bonded technologies. *Journal of Materials Processing Technology*, 105(3):221 – 229, 2000.

[77] Holger Gaul and Gert Weber. Technology of weld-adhesive joints. In *Hybrid Adhesive Joints*, pages 37–77. Springer, 2011.

[78] F. Moroni, A. Pirondi, and F. Kleiner. Experimental analysis and comparison of the strength of simple and hybrid structural joints. *International Journal of Adhesion and Adhesives*, 30(5):367 – 379, 2010. Special Issue on Joint Design.

[79] Raul D.S.G. Campilho, A.M.G. Pinto, M.D. Banea, and Lucas F.M. da Silva. Optimization study of hybrid spot-welded/bonded single-lap joints. *International Journal of Adhesion and Adhesives*, 37(0):86 – 95, 2012. Special Issue on Joint Design 3.

[80] G. Casalino. Statistical analysis of mig-laser CO_2 hybrid welding of Al–Mg alloy. *Journal of Materials Processing Technology*, 191(1):106–110, 2007.

[81] Liming Liu and Daxin Ren. A novel weld-bonding hybrid process for joining Mg alloy and Al alloy. *Materials & Design*, 32(7):3730–3735, 2011.

[82] Hongyang Wang and Gang Song. Influence of adhesive and Ni on the interface between Mg and Fe in the laser-TIG-adhesive hybrid welding joint. *International Journal of Precision Engineering and Manufacturing*, 17(6):823–827, 2016.

[83] L.M. Liu, H.Y. Wang, and Z.D. Zhang. The analysis of laser weld bonding of Al alloy to Mg alloy. *Scripta Materialia*, 56(6):473 – 476, 2007.

[84] H.Y. Wang, L.M. Liu, M.L. Zhu, and H. Wang. Laser weld bonding of A6061Al alloy to AZ31B Mg alloy. *Science and Technology of Welding and Joining*, 12(3):261–265, 2007.

[85] Liming Liu, Daxin Ren, and Yongfei Li. Static mechanics analyses of different laser weld bonding structures in joining AZ61 Mg alloy. *International Journal of Adhesion and Adhesives*, 31(7):660 – 665, 2011.

[86] H.Y. Wang, L.M. Liu, and Z.Y. Jia. The influence of adhesive on the Al alloy in laser weld bonding Mg–Al process. *Journal of materials science*, 46(16):5534, 2011.

[87] Yinan Ma, Wang Tao, Liqun Li, Mingmao Wang, Yanbin Chen, and Yang Wang. Laser spot weld bonding of mild steel. *International Journal of Adhesion and Adhesives*, 34(0):1 – 5, 2012.

[88] Francesca Lionetto, Frank Balle, and Alfonso Maffezzoli. Hybrid ultrasonic spot welding of aluminum to carbon fiber reinforced epoxy composites. *Journal of Materials Processing Technology*, 247:289–295, 2017.

[89] S.H. Chowdhury, D.L. Chen, S.D. Bhole, X. Cao, and P. Wanjara. Lap shear strength and fatigue behavior of friction stir spot welded dissimilar magnesium-to-aluminum joints with adhesive. *Materials Science and Engineering: A*, (0):–, 2012.

[90] Natália M. André, Seyed M. Goushegir, J.F. dos Santos, Leonardo B. Canto, and Sergio T. Amancio-Filho. Friction spot joining of aluminum alloy 2024-T3 and carbon-fiber-reinforced poly (phenylene sulfide) laminate with additional PPS film interlayer: Microstructure, mechanical strength and failure mechanisms. *Composites Part B: Engineering*, 94:197–208, 2016.

[91] Daniel J. Franke, Justin D. Morrow, Neil A. Duffie, Michael Zinn, and Frank E. Pfefferkorn. Towards improved hybrid joining of aluminum alloys to carbon fiber composites with friction stir welding. In *ASME 2016 11th International Manufacturing Science and Engineering Conference*, pages V001T02A058–V001T02A058. American Society of Mechanical Engineers, 2016.

[92] Brent Christner. Welded joints with polymer sealant, 2007. US 7225966 B2.

[93] Jeremy Micah Brown. The effects of sealants and surface treatments on the faying surface of swept friction stir spot welds. Master's thesis, 2008. Wichita State University, College of Engineering, Dept. of Aerospace Engineering.

[94] Rajesh Talwar. Friction stir welding method of joining at least two adjoining work-pieces with application of an adhesive between the at least two workpieces, 2008. EP 2008751 A2.

[95] Pei-Chung Wang, Samuel P. Marin, Sheila A. Marin, and Peter C. Sun. Method to reduce thermal degradation of adhesive in weldbonding, 2011. US 20110073572 A1.

[96] Aditya R. Prabhukhot and Kaushal Prasad. Effect of heat treatment on hardness and corrosion behavior of 6082-T6 aluminium alloy in artificial sea water. *International Journal of Materials Science and Engineering*, 3:287–294, 2015.

[97] Matweb. http://www.matweb.com. Accessed: 2017-12.

[98] Carlos M.S Canto. Strength and fracture energy of adhesives for the automotive industry. Master's thesis, Faculdade de Engenharia da Universidade do Porto, Portugal, 2013.

[99] Pedro M.G.P. Moreira. *Lightweight Stiffened Panels: Mechanical Characterization of Emerging Fabrication Technologies*. PhD thesis, Faculdade de Engenharia Universidade do Porto, 2008.

[100] ASTM International. Standard test methods for tension testing of metallic materials. Standard ASTM E8 / E8M-16a, West Conshohocken, PA, 2016.

[101] A.C.F. Silva, Daniel F.O. Braga, M.A.V. de Figueiredo, and Pedro M.G.P. Moreira. Friction stir welded butt joints optimization. *Materialwissenschaft und Werkstofftechnik*, 45(11):1010–1017, 2014.

[102] J.W. Yoon and F. Barlat. Modeling and simulation of the forming of aluminum sheet alloys. 2013.

[103] R.J.C. Carbas, E.A.S. Marques, Lucas F.M. da Silva, and A.M. Lopes. Effect of cure temperature on the glass transition temperature and mechanical properties of epoxy adhesives. *The Journal of Adhesion*, 90(1):104–119, 2014.

[104] R.J.C. Carbas, Lucas F.M. da Silva, E.A.S. Marques, and A.M. Lopes. Effect of post-cure on the glass transition temperature and mechanical properties of epoxy adhesives. *Journal of Adhesion Science and Technology*, 27(23):2542–2557, 2013.

[105] Y. Zhang, R.D. Adams, and Lucas F.M. da Silva. A rapid method of measuring the glass transition temperature using a novel dynamic mechanical analysis method. *The Journal of Adhesion*, 89(10):785–806, 2013.

[106] ASTM International. Standard test method for tensile properties of plastics. Standard ASTM D638-14, West Conshohocken, PA, 2014.

[107] ISO International Organization for Standardization. Adhesives – determination of shear behaviour of structural adhesives – part 2: Tensile test method using thick adherends. Standard ISO 11003-2:2001, West Conshohocken, PA, 2001.

[108] ASTM International. Standard test method for thick-adherend metal lap-shear joints for determination of the stress-strain behavior of adhesives in shear by tension loading. Standard ASTM D5656-10(2017), West Conshohocken, PA, 2017.

[109] Jean-Yves Cognard, Peter Davies, B Gineste, and L Sohier. Development of an improved adhesive test method for composite assembly design. *Composites Science and Technology*, 65(3-4):359–368, 2005.

[110] Jean-Yves Cognard, Romain Créac'hcadec, Laurent Sohier, and Peter Davies. Analysis of the nonlinear behavior of adhesives in bonded assemblies-comparison of tast and arcan tests. *International Journal of Adhesion and Adhesives*, 28(8):393–404, 2008.

[111] ASTM International. Standard test method for poisson's ratio at room temperature. Standard ASTM E132-17, West Conshohocken, PA, 2017.

[112] M.F.S.F. de Moura, J.J.L. Morais, and N. Dourado. A new data reduction scheme for mode i wood fracture characterization using the double cantilever beam test. *Engineering Fracture Mechanics*, 75(13):3852–3865, 2008.

[113] M.F.S.F. de Moura, M.A.L. Silva, A.B. de Morais, and J.J.L. Morais. Equivalent crack based mode ii fracture characterization of wood. *Engineering Fracture Mechanics*, 73(8):978–993, 2006.

[114] ASTM International. Standard test method for apparent shear strength of single-lap-joint adhesively bonded metal specimens by tension loading (metal-to-metal). Standard ASTM D1002-10, West Conshohocken, PA, 2010.

[115] ASTM International. Standard guide for preparation of aluminum surfaces for structural adhesives bonding (phosphoric acid anodizing). Standard ASTM D3933-98(2017), West Conshohocken, PA, 2017.

[116] Pierre Descamps, Jean Iker, and Andreas T Wolf. Effects of anodized aluminium surface parameters on the long-term adhesion of silicone structural glazing sealants. *Construction and Building Materials*, 10(7):527–538, 1996.

[117] C.R. Bird. Ultrasonic phased array inspection technology for the evaluation of friction stir welds. *Insight-Non-Destructive Testing and Condition Monitoring*, 46(1):31–36, 2004.

[118] G. Viana, M. Costa, M.D. Banea, and Lucas F.M. da Silva. A review on the temperature and moisture degradation of adhesive joints. *Proceedings of the Institution of Mechanical Engineers, Part L: Journal of Materials: Design and Applications*, page 1464420716671503, 2016.

[119] Enrique Castillo and Alfonso Fernandez-Canteli. *A unified statistical methodology for modeling fatigue damage*. Springer Science & Business Media, 2009.

[120] Raul D.S.G. Campilho, M.D. Banea, J.A.B.P. Neto, and Lucas F.M. da Silva. Modelling of single-lap joints using cohesive zone models: effect of the cohesive parameters on the output of the simulations. *The Journal of Adhesion*, 88(4-6):513–533, 2012.

[121] Raul D.S.G. Campilho, M.F.S.F. de Moura, A.M.G. Pinto, J.J.L. Morais, and J.J.M.S. Domingues. Modelling the tensile fracture behaviour of CFRP scarf repairs. *Composites Part B: Engineering*, 40(2):149–157, 2009.

[122] Arthur L. Gurson. Continuum theory of ductile rupture by void nucleation and growth: Part i - yield criteria and flow rules for porous ductile media. *Journal of engineering materials and technology*, 99(1):2–15, 1977.

[123] Viggo Tvergaard. Material failure by void coalescence in localized shear bands. *International Journal of Solids and Structures*, 18(8):659–672, 1982.

[124] Viggo Tvergaard and Alan Needleman. Analysis of the cup-cone fracture in a round tensile bar. *Acta metallurgica*, 32(1):157–169, 1984.

[125] M. Hval, C. Thaulow, J.H. Lange, S.H. Hoydal, and Z.L. Zhang. Numerical modeling of ductile fracture behavior in aluminum weldments. *Welding Journal-New York-*, 77:208–s, 1998.

[126] Abaqus Inc. Abaqus quasi-static analysis. http://imechanica.org/files/l5-quasi-static.pdf, 2005. Online; accessed 28-February-2018.

[127] Xiaosheng Gao, Tingting Zhang, Jun Zhou, Stephen M. Graham, Matthew Hayden, and Charles Roe. On stress-state dependent plasticity modeling: Significance of the hydrostatic stress, the third invariant of stress deviator and the non-associated flow rule. *International Journal of Plasticity*, 27(2):217 – 231, 2011.

[128] Ken Nahshon and Zhenyu Xue. A modified gurson model and its application to punch-out experiments. *Engineering Fracture Mechanics*, 76(8):997 – 1009, 2009.

[129] J. Jackiewicz. Use of a modified gurson model approach for the simulation of ductile fracture by growth and coalescence of microvoids under low, medium and high stress triaxiality loadings. *Engineering Fracture Mechanics*, 78(3):487 – 502, 2011. Meso-Mechanical Modelling of Fatigue and Fracture.

[130] L. Malcher, F.M. Andrade Pires, and J.M.A. César de Sá. An extended gtn model for ductile fracture under high and low stress triaxiality. *International Journal of Plasticity*, 54:193 – 228, 2014.

[131] Z.H. Zhang, W.Y. Li, Y. Feng, J.L. Li, and Y.J. Chao. Global anisotropic response of friction stir welded 2024 aluminum sheets. *Acta Materialia*, 92:117 – 125, 2015.

[132] Marcel Bachmann, Jan Carstensen, Luciano Bergmann, J.F. dos Santos, Chuan Song Wu, and Michael Rethmeier. Numerical simulation of thermally induced residual stresses in friction stir welding of aluminum alloy 2024-T3 at different welding speeds. *The International Journal of Advanced Manufacturing Technology*, 91(1):1443–1452, Jul 2017.

[133] Jose I. Rojas and Daniel Crespo. Modeling of the effect of temperature, frequency, and phase transformations on the viscoelastic properties of AA7075-T6 and AA2024-T3 aluminum alloys. *Metallurgical and Materials Transactions A*, 43(12):4633–4646, Dec 2012.

[134] N.D. Alexopoulos and P. Papanikos. Experimental and theoretical studies of corrosion-induced mechanical properties degradation of aircraft 2024 aluminum alloy. *Materials Science and Engineering: A*, 498(1-2):248–257, 2008.

[135] E. Murman. A value perspective on aerospace innovation. In *Proceedings of the 24th International Congress of the Aeronautical Sciences-ICAS*, 2004.

[136] Richard Curran, Srinivasan Raghunathan, and Mark Price. Review of aerospace engineering cost modelling: The genetic causal approach. *Progress in aerospace sciences*, 40(8):487–534, 2004.

[137] J. Munroe, K. Wilkins, and M. Gruber. Integral airframe structures (ias)—validated feasibility study of integrally stiffened metallic fuselage panels for reducing manufacturing costs. 2000.

[138] Jens Hinrichsen and Cesar Bautista. The challenge of reducing both airframe weight and manufacturing cost. *Air & Space Europe*, 3(3):119–121, 2001.

[139] Markus Kaufmann, Thomas Czumanski, and Dan Zenkert. Manufacturing process adaptation for integrated cost/weight optimisation of aircraft structures. *Plastics, Rubber and Composites*, 38(2-4):162–166, 2009.

[140] J. Schumacher. Laserstrahlschweien im flugzeugbau. In *Neueste Entwicklungen der Industriellen Lasertechnik* (Wofsburg, Germany, October 2005).

[141] Andrzej Skorupa and Małgorzata Skorupa. Differences between the fatigue behaviour of longitudinal lap joints in a pressurized fuselage and laboratory lap joint specimens. In *Riveted Lap Joints in Aircraft Fuselage*, pages 11–26. Springer, 2012.

[142] Jaap Schijve. Fatigue damage in aircraft structures, not wanted, but tolerated? *International Journal of Fatigue*, 31(6):998 – 1011, 2009. Damage Tolerance of Aircraft Structures.

[143] J.C. Newman and R. Ramakrishnan. Fatigue and crack-growth analyses of riveted lap-joints in a retired aircraft. *International Journal of Fatigue*, 82:342 – 349, 2016.

[144] Carlos Eduardo Chaves and Fernando Ferreira Fernandez. A review on aircraft joints design. *Aircraft Engineering and Aerospace Technology*, 88(3):411–419, 2016.